THE UNIVERSITY
of EDINBURGH

The impact of two autism related genes on amygdala physiology

Anna Karina Hugger Toft B.Sc. M.Sc.

THE UNIVERSITY *of* EDINBURGH

Doctor of Philosophy

Biomedical Sciences

School of Medicine and Veterinary Medicine

University of Edinburgh

April 2019

Abstract

Intellectual disability (ID) and autism spectrum disorder (ASD) are two of the most common developmental disorders affecting 3–5% of the population. These disorders have a high burden on society with no efficient treatment options. This is complicated further by the high comorbidity between ID and ASD, as well as epilepsy. Understanding the aetiology and pathophysiology of ID and ASD is of vital importance in order to find better treatment options for the patients and their families. Recent genomic studies have identified hundreds of genetic variants contributing to the incidence of ID and ASD. Many of these genes are important for synaptogenesis and maintenance of synaptic function, such as the neuroligins (*NLGN1-4*), neurexin 1 (*NRXN1*), fragile x mental retardation 1 (*FMR1*), Synaptic Ras GTPase-activating protein 1 (*SYNGAP1*), and SH3 And Multiple Ankyrin Repeat Domains 3 (*SHANK3*). Understanding how the proteins of these genes operate, and how they influence synaptic development and function will increase our understanding of what goes wrong in their absence.

In this thesis, the role of two synaptic proteins across development were examined in principal cells of the amygdala: NLGN3 and SynGAP. Neuroligins are postsynaptic cell adhesion molecules that bind to presynaptic neurexins, and are required for both excitatory and inhibitory synapse maturation and function. The *Nlgn3*$^{-/y}$ rat model was utilised to study the role of the NLGN3 isoform in this study. SynGAP is one of the major constituents of the postsynaptic density (PSD). However, there are contrasting hypotheses as to how SynGAP mediates its effects on synaptic morphology and function. One hypothesis suggests that SynGAP plays a key role in regulating the structural composition of the PSD by sequestering PSD-95, and thereby modulating synaptic function. The alternative hypothesis suggests that SynGAP regulates synaptic structure/function through its GTPase activating activity of Ras/Rap and their downstream signalling pathways. To test the relative roles of SynGAPs scaffolding and signaling functions in disease pathophysiology, two genetically modified Syngap rat models were used; one with a heterozygous deletion of the GAP-domain (*Syngap*$^{+/\Delta GAP}$); and one with a null-mutation (*Syngap*$^{+/-}$).

It was found that *Nlgn3*$^{-/y}$ displayed an age-dependent increase in intrinsic excitability compared to WT littermates, as well as an age-dependent increase in miniature inhibitory postsynaptic currents (mIPSCs) amplitude. No change was observed on excitatory postsynaptic currents in *Nlgn3*$^{-/y}$. Furthermore, a deficit in long term potentiation

(LTP) at thalamic inputs to the lateral amygdala (LA) was found using a 30Hz induction protocol.

No difference was found in intrinsic properties in either of the two SynGAP models at two weeks of age, but at four weeks divergence were found between the two. In the LA, *Syngap*$^{+/-}$ displayed an increase in excitability, whereas *Syngap*$^{+/\Delta GAP}$ was comparable to WT. Conversely in the basal amygdala (BA), *Syngap*$^{+/-}$ did not present with any changes in intrinsic properties, in opposition to *Syngap*$^{+/\Delta GAP}$, which exhibited a decreased firing rate compared to WT. Both models had a deficit in LTP from thalamic input into the LA, but only *Syngap*$^{+/-}$ demonstrated a decrease in paired-pulse facilitation. Taken together, this work shows that NLGN3 is important for development of normal cellular and synaptic functions. Furthermore, this work helps to highlight the different roles exerted by the functional domains of SynGAP.

Lay Summary

The brain is a complex network composed of billions of nerve cells, called neurons, forming intricate connections with each other. The neurons must communicate with each other in order to maintain everyday activities, such as retaining information, speaking, and processing emotions. In order to communicate, neurons use tiny connections between each other, called synapses, to send electrochemical signals. When synapses are working correctly, the neurons are able to communicate, and your brain can function normally. When your synapses are not working properly, the communication is disrupted or altered, and your brain cannot function the way it should. This can result in disorders such as intellectual disabilities (ID) or autism spectrum disorder (ASD). At the moment, there are no good treatment options for people with these disorders, and in order to develop them, we must get a better understanding of how the synapses work and how neurons communicate.

One way synapses can be disrupted is if they are missing a protein or a protein is dysfunctional. My thesis concerns the function of two such proteins that are important for normal synaptic function and that are associated with ID and ASD. People with ASD often have altered emotional processing, functions relying on the brain region called the amygdala. To assess how the synapses function in the amygdala, electrical activity was recorded from individual neurons in this brain area. One of the proteins investigated is involved in the physical scaffolding process across the synapse. The key findings from this work are that when this scaffolding protein is missing from the synapse, the neurons are in a state of hyperactivity when receiving signals from other neurons. Furthermore, the synapses are not able to strengthen and learn as well in the absence of this protein.

The other protein also has a function in the physical scaffold of the synapse, but one part of the protein is also important for relaying the electrochemical signal coming to the synapse from another neuron. The key findings from this work are that the scaffolding function of the protein is important for determining how a neuron responds to the signal it receives, whereas the relaying part of the protein is important for the synapses to strengthen and learn from the signals.

Altogether this research has given us a better understanding of how neurons communicate, and thus how the brain works. This helps us better understand disorders like ID and ASD, and how we can develop treatment for these disorders.

Acknowledgement

First and foremost, I would like to thank my two supervisors Prof. Peter Kind and Prof. David Wyllie for giving me the great opportunity of working in the Kind/Wyllie lab, for giving me academic support, and for their guidance for the past 4 years. I want to thank Prof. Sumantra Chattarji for welcoming me in Bangalore and to all his lab members who shared their expertise and made it a rewarding experience.

I want to thank all past and present members of the Kind/Wyllie lab who helped me throughout my PhD, provided support, valuable feedback, and a fantastic work environment filled with laughter. A special thanks to Dr Sam Booker, who taught me how to patch, and Dr Adam Jackson for the endless help you have provided throughout. Thank you, Shinjini Basu for being my PhD companion, for helping my out on the 4th floor, and all our adventures together. Thank you Natasha Anstey for all your help, for always being joyful, and all our trips up North. Farhana Yasmin, thank you for always offering advice when needed, an ear to speak to, and for allowing me to drag you up hills.

Finally, I would like to thank my family for always supporting me. Most importantly, a very special thank you to Colin — you have been my rock for the last four years, without you it would have been a lot harder to get through.

Declaration

I declare that this thesis was composed by myself and that the work contained herein is my own, unless otherwise states and with exception of the following:

- Mr. Zrinko Kozic performed the GLMM on a selection of the data
- Ms Natasha Anstey contributed to the data collection of $Nlgn3^{-/y}$ 30 Hz LTP in Chapter 3

No part of the work contained in this thesis has been submitted for any other degree or professional qualification.

Signed: ---------- Date: ----------

Contents

List of Abbreviations

AChE	Acetylcholinesterase-homology
ACSF	Artificial cerebral spinal fluid
ADP	Afterdepolarisation
AHP	Afterhyperpolarisation
AM	Acetoxymethyl
AMPARs	α-amino-3-hydroxy-5-methyl-4-isoxazolepropionic acid receptors
AP	Action potential
ASD	Austism Spectrum Disorder
BA	Basal amygdala
BLA	Basolateral amygdala
CC	Coiled-coil
CDC	Centers of Disease Control and Prevention
CeA	Central amygdala
CeL	Lateral central amygdala
CeM	Medial central amygdala
CNV	Copy number variants
CS	Conditioned stimulus
FXS	Fragile X Syndrome
GABA	Gamma-Aminobutyric acid
GAPs	GTPase-activating proteins
GEFs	Guanine nucleotide exchange factor
GLMM	Generalised linear mixed model
GUK	Degenerate guanylate kinase
HVA	High-voltage activated
ICM	Intercalated cell masses
ID	Intellectual disability
IL	Infralimbic
KI	Knock-in
KO	Knock-out
LA	Lateral amygdala
LRRC	Leucine-rich repeat containing
LRRTMS	Leucine-rich repeat transmembrane neuronal

LTD	Long-term depression
LTP	Long-term potentiation
MAGUKs	Membrane-associated guanylate kinases
mAHP	Medium afterhyperpolarisation
mEPSCs	Miniature excitatory postsynaptic currents
mGluRs	Metabotropic glutamate receptors
mIPSCs	Miniature inhibitory postsynaptic currents
MRD5	Mental retardation type 5
NDDs	Neurodevelopmental disorders
NLGNs	Neuroligins
NMDA	N-Methyl-D-aspartic acid
NRXNs	Neurexins
PCR	Polymerase chain reaction
PH	Pleckstrin Homology
PL	Prelimbic
PSD	Post-synaptic density
PTX	Picrotoxin
PV	Parvalbumin
RMP	Resting membrane potential
sAHP	Slow afterhyperpolarisation
SH3	Src Homology 3
SOM	Somatostatin
SynCAMs	Synaptic cell adhesion molecules
SynGAP	Synaptic Ras GTPase activating protein
TARPs	Transmembrane AMPA receptor regulatory proteins
TTX	Tetrodotoxin
US	Unconditioned stimulus
VGCCs	Voltage gated calcium channels

List of Figures

List of Tables

Chapter 1

Introduction

1.1 ID/ASD

Intellectual disability (ID) and Autism Spectrum Disorders (ASDs) are two debilitating neurodevelopmental disorders (NDDs) that can have a severe impact on affected individuals, their families, and society. Both conditions are heterogeneous, thereby creating an immense challenge both for clinicians searching for a diagnosis, but also in terms of therapeutic interventions, of which there are none that significantly improve quality of life.

Intellectual Disability is a disorder with onset during development and include intellectual and adaptive functioning deficits. ID is highly prevalent and affect 1% of the world-wide population (Maulik et al. (2011)). ID is characterized by deficits in general mental abilities, such as reasoning, problem solving, planning, judgment, and learning from experience. This results in impairments in adaptive behaviours. ID is defined by three criteria: an intelligence quotient (IQ) of less than 70; limitations in two or more adaptive behaviours; and onset before the age of 18 (Van Bokhoven (2011)). ID can present alone or in combination with congenital malformations or other neurological features such as epilepsy, ASD, anxiety, depression, and schizophrenia. (Cherry et al. (1997); Matson et al. (1997); McGillivray et al. (2008))

Autism Spectrum Disorder comprises a group of disorders that includes autistic disorders, Asperger syndrome, and pervasive development disorder not otherwise specified (American Psychiatric Association (2013)). The Centers of Disease Control and Prevention (CDC) has recently reported the prevalence of ASD to be between 1-3% (CDC (2018)). Affected individuals show deficits in reciprocal social communication and

social interactions, including abnormal non-verbal communication like gaze-avoidance, and restrictive, repetitive interests and behaviours (Murphy et al. (2016)). ASD has widely varied behavioural manifestations, severity, and comorbid conditions, such as attention deficit hyperactivity disorder, anxiety, ID, and epilepsy (Simonoff et al. (2008); McCarthy (2007)).

Considerable overlap between ID and ASD is often seen (Matson and Shoemaker (2009)) hinting at a related aetiology. ID is observed in about 30–50% of ASD patients, and at least 10–30% of individuals with ID have ASDs (Srivastava and Schwartz (2014)).

1.1.1 Causes of ID/ASD

ID and ASD can be caused by numerous exogenous factors, such as intrauterine infections, birth complications, and traumatic brain damage (Cooper and Van Der Speck (2009); Lai et al. (2014)). Genetic variants are known to have an important role in the aetiology and recent large-scale genetic studies have highlighted several hundred genes as risk factors for ID and ASD (De Rubeis et al. (2014); Iossifov et al. (2014); Sanders et al. (2015); Vissers et al. (2016)). Single gene mutations, as well as copy number variants (CNVs), are associated with both conditions with multiple large effect single-gene mutations identified. Furthermore, monogenic causes account for about 60% of undiagnosed cases of individuals with severe NDDs, making the genetic risk for severe NDD presentation very high (Deciphering Developmental Disorders (2015)). The most common single-gene disorders of ID and ASD are Fragile X Syndrome (FXS; *FMR1*), Tuberous Sclerosis (*TSC1*, *TSC2*), Rett syndrome (*MECP2*), Phelan-McDermid syndrome (*SHANK3*), Autosomal mental retardation type 5 (MRD5; *SYNGAP1*), and Neurexin (*NRXN1*). More rare single-gene mutations or CNVs include the genes encoding for Neuroligins (*NLGN1–4*).

There are few if any effective treatment options for the most serious symptoms associated with these disorders. In order to improve the lives of patients with ID/ASD, an understanding of the underlying aetiology is needed in order to develop therapeutic strategies. This is made difficult by the heterogeneity of ID and ASD, both clinically and genetically. The identification of high-risk monogenetic causes (Ogden et al. (2016)), has enabled the generation of many animal models of these disorders with face and construct validity. This allows research into the underlying disease-relevant phenotypes.

The significant co-occurrence in genetically caused ID and ASD, suggests the possibility of a common underlying pathophysiology. In the last decade, several proteins involved in synaptic development, maintenance, and function have been associated with ID, ASD, schizophrenia, and epilepsy (Zoghbi and Bear (2012); De Rubeis et al. (2014); Bourgeron (2015)). These includes cell adhesion proteins (*NRXN1, NLGN1–4, SynCAM*), scaffolding proteins (*SHANK2, SHANK3*), ion channels and receptors (*SCN2A, GABRB3, GRIN2B*), and synaptic signalling proteins (*SYNGAP1, PTEN, TSC1–2*). This points towards commonalities in the pathological scenarios at the synapses and in neuronal circuit formation (Chechlacz and Gleeson (2003); Kroon et al. (2013)). Therefore in depth study of synaptic function in monogenetic ID/ASD models could provide important insight into the pathophysiology of a range of disorders.

The focus of this thesis is the two synaptic proteins, Neuroligin-3 (NLGN3) and Synaptic Ras GTPase-activating protein (SynGAP). *NLGN3* and *SYNGAP1* are both candidate genes for ID/ASD. NLGN3 is a synaptic adhesion protein, whereas SynGAP is an abundant PSD signalling and scaffolding protein. Both proteins have been shown to play an important role in synaptic function — as will be described in more detail below — but much is still to be determined about their functional role in the synapse, and how mutations in these genes contribute to disease-relevant phenotypes.

1.2 The Synapse

Most synapses between excitatory neurons are located on spines, where the synaptic contact is generally found at the tip of the spine. It is made up of three compartments: the presynaptic active zone, which is the site for synaptic vesicle fusion and neurotransmitter release; the synaptic cleft; and the postsynaptic density. Spines vary in both shape and size, usually with larger spines containing stronger synapses. A stronger synapse is able to elicited a larger depolarisation upon activation, and thus is more likely to generate an action potential (Harris and Stevens (1989); Matsuzaki et al. (2001)).

1.2.1 The postsynaptic density

Within a glutamatergic synapse resides the post-synaptic density (PSD), a structure about 1 μm in diameter. It is a fibrous cytoskeletal specialisation attached to the postsynaptic membrane (Kennedy (1997)). The PSD is composed of hundreds of proteins

including adhesion proteins, receptors, and enzymes, but the "core" of PSD proteins is more likely to be between 30 and 60 proteins that are present at nearly all PSD structures (Kennedy (2018)). Proper assembly into multiprotein complexes is required for normal synaptic function, which is enabled by an organised scaffold of proteins. The central scaffold is comprised of four major classes of scaffolding proteins: the PSD-95 family (also called MAGUKs; membrane-associated guanylate kinases); SAPAPs (also called GKAPs), the SHANKs; and the Homer family. PSD-95 and its related proteins SAP97, SAP102, and PSD-93 link glutamate receptors in the membrane to the PSD structure and to adjacent signalling proteins. Each **MAGUK** has several domains that act as protein-docking sites: three PDZ domains; a SH3 domain; and a carboxy-terminal degenerate guanylate kinase (GUK) domain. The PDZ domains binds to a variety of synaptic proteins containing PDZ-binding motifs in their C-terminal, such as N-Methyl-D-aspartic acid receptors (NMDARs), transmembrane AMPAR regulatory proteins (TARPs), NLGNs, and Synaptic Ras GTPase-activating protein (SynGAP). The GUK domain directly link **GKAPs** to the SHANKs. The **SHANKs** act as a "scaffold of scaffolds" within the PSD, forming an interacting network to which more proximal scaffold proteins are anchored. The **Homers** form rod shaped multimers that link metabotropic glutamate receptors (mGluRs), IP3 receptors, and TRP channels to the SHANK scaffold (Kennedy (2016)).

This highly dynamic scaffold provides the spatial organisation for the neuronal events that modulate synaptic strength by coupling glutamatergic receptors to downstream signalling effectors, which organise the regulation of a cellular response (Frank et al. (2016, 2017)). Formation and specification of synapses is immensely important for appropriate neural-circuit function. The development of appropriate synaptic connections requires a series of steps: axonal pathway guidance; selection of appropriate targets; the formation of organised and specific projections within the target; and synapse stabilization and modulation.

1.2.2 Synapse development and maintenance

The formation of functional synapses involves a host of proteins to mediate co-ordinated pre- and postsynaptic growth. The synapse is an asymmetric structure, and thus requires heterotypic transsynaptic signaling to mediate synaptogenesis, and to specifically and differentially recruit pre- and postsynaptic proteins to their corresponding

subcellular compartments. The presynaptic-postsynaptic coordination is the result of regulated assembly of specific molecules on both sides of the synaptic cleft. Adding the diversity of synapses, it is likely that a panoply of mechanisms exists for their formation, which are still largely unknown. A general model for what is currently known about the sequence of events that happen during synaptogenesis follows below.

There is evidence demonstrating both intrinsic assembly and partner-induced synaptic assembly. Prior to synapse formation, pre- and postsynaptic proteins are already expressed. The axon growth cone contains synaptic vesicles and neurotransmitters, while the dendritic arbors express functional neurotransmitter receptors (Garner et al. (2002)). The interaction between the axon growth cone with the soma or the dendritic arbors of their target is what initiates the concentration and juxtaposition of the pre- and postsynaptic elements, and is thought to be initiated by a diverse set of membrane proteins and pathways, as well as astrocyte-secreted factors (Baldwin and Eroglu (2017)). The initial contact often happens between filopodia extending from both the axon and the dendrites, which are then thought to transform into synaptic structures. Synaptogenic cues after initial contact are needed to guide further synapse assembly (Burden and Scheiffele (2013)).

Target-derived retrograde signals, such as Wnts and fibroblast growth factors, are believed to recruit pre-assembled units containing presynaptic components, like synaptic vesicles, voltage-gated calcium channels (VGCCs), and syntaxin. Subsequently, the axon releases anterograde signals, such as Pentraxins, driving accumulation of neurotransmitter receptors at the postsynaptic site with NMDARs being recruited first, and α-amino-3-hydroxy-5-methyl-4-isoxazolepropionic acid receptors (AMPARs) subsequently. At the same time, several adhesion and signalling complexes are formed across the synaptic cleft, which cooperate in the organisation of pre- and postsynaptic components (Burden and Scheiffele (2013)). Among the many adhesion molecules in the synapse that is thought to have synaptogenic activity, is a pair of transmembrane proteins, the neurexins (NRXNs) and the NLGNs. Together they form a trans-synaptic adhesion complex across the synaptic cleft, thereby directly connecting the pre- and postsynapse (Südhof (2008)). Exogenous expression of NLGN in non-neuronal cells is enough to induce accumulation of NRXN and presynaptic differentiation in contacting axons (Scheiffele et al. (2000)). The synaptogenic activity of transsynaptic adhesion

molecules, such as NLGN, is thought to be mediated through the synaptic scaffolding complexes (Burden and Scheiffele (2013)). Postsynaptically, NLGN aggregation results in the recruitment of PSD-95 and SAP102, as well as clustering of NMDARs (Graf et al. (2004); Chih et al. (2005)).

At inhibitory synapses, scaffolding molecules play a similar role. The best studied example is the scaffolding protein gephyrin, which recruits inhibitory glycine receptors and gamma-Aminobutyric acid $(GABA)_A$ receptors to developing postsynaptic sites, and links them to the cytoskeleton (Kneussel and Betz (2000)). NLGN2 is another adhesion molecule, which localises to GABAergic synapses. It tethers gephyrin at the postsynapse by activating the cytoskeletal protein, collybistin. Gephyrn in turn retains glycine and $GABA_A$-receptors at the postsynaptic site (Poulopoulos et al. (2009)).

Even though there is evidence showing the synaptogenic effect of scaffolding and trans-synaptic protein, like gephyrin and NLGNs, whether these proteins are necessary for initiating the pre- and postsynaptic specialisations *in vivo* is uncertain. Knock-out mouse models of neurexin or neuroligin show only mild effects on synaptic formation (Missler et al. (2003); Varoqueaux et al. (2006); Kim et al. (2008); Chen et al. (2017)), and in *C. elegans* when neurexin is absent synapses are still present, but are smaller and fail to recruit vesicles and active zone proteins (Kurshan et al. (2018)). This could suggests that multiple proteins have synaptogentic effects at each synapse creating a functional overlap between them, or that synaptic cell adhesion molecules promote the process of maturation and specificity rather than initiating synapse formation and assembly (Kurshan and Shen (2019)).

The exact mechanism for synaptic specification is still not clear. NLGNs are part of a larger superfamily of post-synaptic adhesion molecules, which includes proteins such as cadherins, synaptic cell adhesion molecules (SynCAMs), leucine-rich repeat transmembrane neuronal proteins (LRRTMs), and NGLs/LRRC proteins (leucine-rich repeat containing) (Bemben et al. (2015b)). Presynaptically, the primary adhesion partner of NLGNs is the NRXN family. It is comprised of more than 1000 isoforms created through alternative splicing (Ullrich et al. (1995)), contributing to the diversity of adhesion proteins. The diversity of synaptic adhesion molecules suggests that they act as molecular markers in the formation and specification of synapses.

Formation of new synapses can happen throughout the lifetime of an organism and

can be induced by a range of experience-driven memory and learning, such as fearful learning conditioning (Dalzell et al. (2011)). Though dendritic arbors and spines are highly dynamic structures showing frequent additions and retractions, a subset of arbors and dendritic spines are stable for long periods of time. Thus, mechanisms must exist to maintain synapses and dendrites.

Like synapse development, synaptic maintenance relies on the structural support and synaptic signalling provided by adhesion molecules and scaffolding proteins (Lin and Koleske (2010)). The actin cytoskeleton provides essential structural support for the long-term synapse maintenance. Actin undergoes continuous action polymerisation/depolymerisation, which requires tight regulation in order to maintain spine stability. A number of proteins are known to regulate actin structure, and thus synapse stability.

One such protein is cofilin. Cofilin, an F-actin severing protein, controls the ratio of G-actins (soluble monumers) to F-actin (actin filaments) by increasing the turnover rate, and thereby works to control the dynamics and the length of actin filaments in spines (Carlier et al. (1997)). Cofilin is inactivated by phosphorylation, a process that is attenuated by SynGAP. A reduction in SynGAP causes increased phosphorylation of cofilin and increased actin polymerisation, leading to spine head enlargement (Carlisle et al. (2008)). Additionally, scaffolding proteins and adhesion molecules, such as PSD-95, SHANK, and NLGN, have also been shown to be important for long-term maintenance of synapses (Lin and Koleske (2010)). For example, knockdown of PSD-95 results in reduction in spine density and size, and causes activity-dependent spine destabilization (Ehrlich et al. (2007)).

1.2.3 Synaptic Plasticity

The ability for synapses to respond to neuronal activity by changing their strength and size is as important for memory encoding, as the ability for synaptic structures to maintain their stability. Glutamatergic signal transduction is highly controlled by physical interactions amongst proteins within the PSD, and respond to distinct signal input by controlling these interactions and initiating molecular programs that change its future responsiveness, i.e. functional and structural changes of the synapse (Maletic-Savatic et al. (1999); Malinow and Malenka (2002); Matsuzaki et al. (2004)). This process is known as synaptic plasticity, and is believed to be the principal mechanism

for memory formation in the brain (Lüscher et al. (2000)). Two well known models of synaptic changes are long-term potentiation (LTP; strengthening of synapses) and long-term depression (LTD; weakening of synapses).

Synaptic strengthening and weakening depend, in part, on exocytosis and endocytosis of glutamatergic AMPARs, respectively (Malinow and Malenka (2002)). Three steps are involved in trafficking AMPARs to and from the synaptic membrane in response to activity: (1) exocytosis at extra- and perisynaptic sites of AMPARs that are tightly bound to TARPs; (2) lateral diffusion into synapses; and (3) diffusional trapping in the PSD through phosphorylation and subsequent binding of TARPs to PDZ domains on PSD-95. During removal of AMPAR from the synapse the reverse order of events likely takes place with (1) destabilisation of AMPARs from PSD-95 via dephosphorylation, (2) followed by diffusion out of the synapse (3) where they undergo endocytosis (Opazo and Choquet (2011)).

Exocytosis and endocytosis of AMPARs is regulated by the Ras and Rho families of small GTPases (Zhu et al. (2002)). They regulate both homeostatic maintenance of the synaptic structure, as well as activity-induced changes (Kennedy (2016)). The Ras-MEK-ERK1/2 signalling pathway is important for the activity-induced increase in synaptic AMPARs, whereas Rap activation of MAPK p38 facilitates endocytosis of AMPARs (Zhu et al. (2002)). Ras GTPases are regulated by cycling between an inactive GDP-bound state and an active GTP-bound state, which is facilitated by GTPase-activating proteins (GAPs) or guanine nucleotide exchange factors (GEFs). Several mechanisms exists for regulating Ras GTPases in spines (reviewed by Kennedy et al. (2005)). One example of a negative regulator of Ras and Rap is SynGAP. Its GAP activity targets both Ras and Rap, which is increased upon phosphorylation by CaMKII (Oh et al. (2004); Krapivinsky et al. (2004)). How SynGAP regulates AMPAR trafficking through small GTPases is discussed further later in this chapter.

1.3 Neuroligins

Neuroligins (NLGNs) are single-pass transmembrane proteins located in the post-synaptic membrane of both glutamatergic and GABAergic synapses, where they act as adhesion molecules bridging the synaptic cleft by binding to neurexins (NRXNs) on the presynaptic side. They were originally discovered as binding partners to the

presynaptic proteins β-neurexins (Ichtchenko et al. (1995)), and since then 5 human genes have been identified encoding neuroligins (*NLGN1*, *NLGN2*, *NLGN3*, *NLGN4X*, and *NLGN4Y*). *NLGN1* and *NLGN2* are located on autocomal chromosomes, while *NLGN3*[1] and *NLGN4X* are located on the X chromosome, and *NLGN4Y* on the Y chromosome.

NLGN1, *NLGN2*, and *NLGN3* are highly conserved in rodents, but no homologs of *NLGN4X* or *NLGN4Y* has been found. A distant *NLGN4* variant have been identified in mice, *Nlgn4l* (Bolliger et al. (2008)).

1.3.1 Structure of the protein

The overall domain structure is well conserved between the NLGNs, and there is substantial conservation in amino acid sequence. All neuroligin proteins have an acetylcholinesterase-homology (AChE) domain in its extracellular domain lacking in amino acids important for catalysis, and thus has no esterase activity. NLGNs have a short cytoplasmic tail containing a class I PDZ binding sequence at the C-terminal, which interacts with the N-terminal of PSD-95 and other PDZ containing proteins. Furthermore, the NLGNs have a single transmembrane domain. (Ichtchenko et al. (1995); Irie et al. (1997); Bolliger et al. (2001); Dean et al. (2003)).

NLGNs are further diversified by two alternative splice sites in their ectodomain, site A and B, incorporating short alternative exons (20 and 9 amino acids in length). All NLGNs are spliced at splice site A, while *NLGN1* is spliced at both of these sites (Ichtchenko et al. (1996); Scheiffele et al. (2000); Boucard et al. (2005); Chih et al. (2006)). Alternative splicing of both NLGNs and NRXNs plays a central role in the functional regulation of the NLGN-NRXN complex at glutamatergic and GABAergic synapses. For NLGN, having the B splice site insertion restrict its function to glutamatergic synapses, whereas isoforms containing no insertion or only the A insert are found at GABAergic synapses (Chih et al. (2006); Boucard et al. (2005)).

1.3.2 Expression and localisation of Neuroligins

NLGNs are found exclusively in the brain and are expressed in most neuronal populations and astrocytes (Ichtchenko et al. (1995); Scheiffele et al. (2000); Varoqueaux et al. (2004, 2006); Liu et al. (2017)). Expression of neuroligins are detected at low

[1] https://www.ncbi.nlm.nih.gov/gene/54413

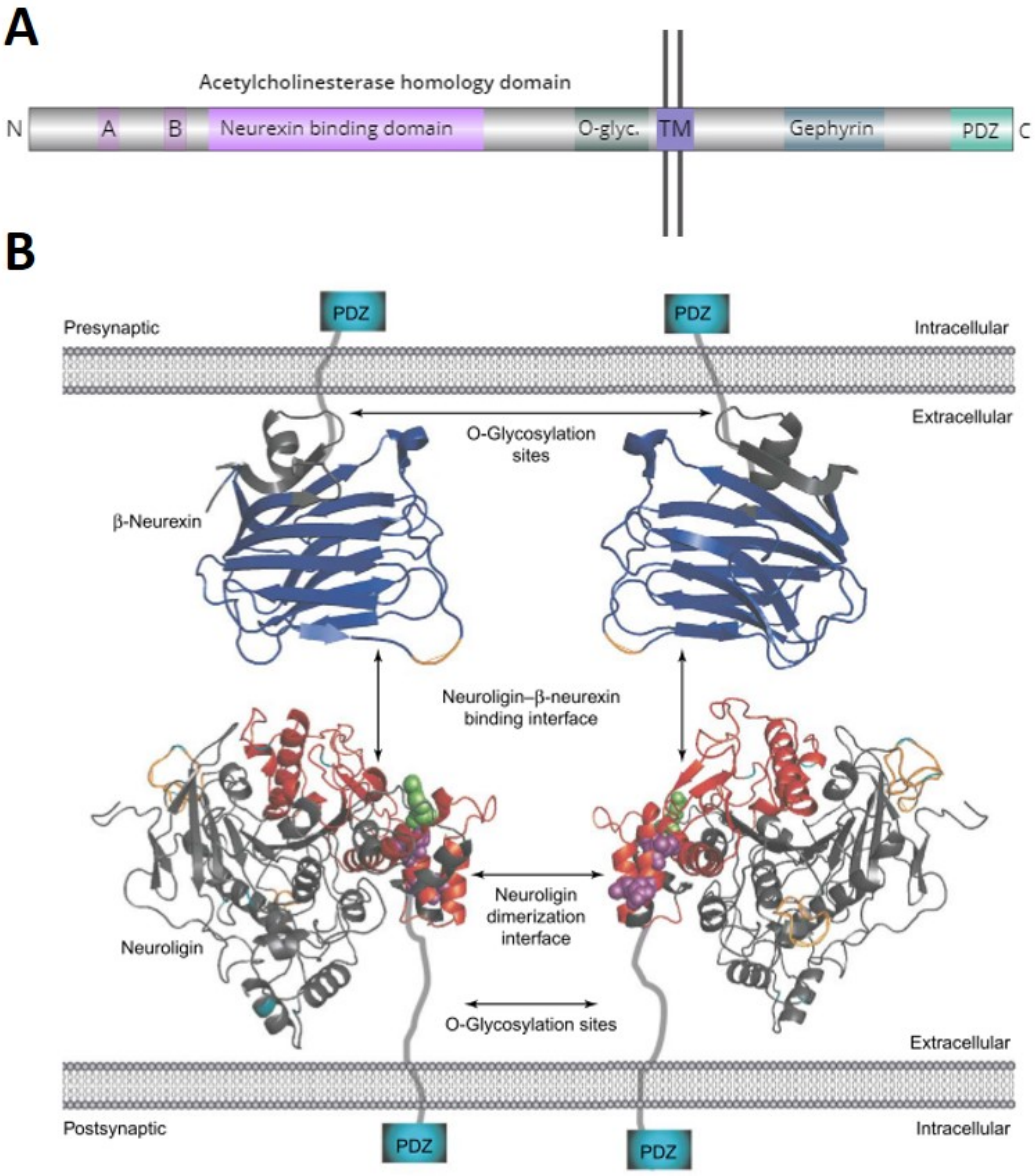

Figure 1.1: Structure of Neuroligins (A) NLGNs contain several functional domains: an Acetylcholinesterase homology domain, which contains the portion necessary for NRXN binding; an O-glycosylation region; a transmembrane domain; a cytoplasmic C-tail domain containing a PDZ-interaction site and a gephyrin interacting domain. A and B are the NLGN splice sites. (B) The structure of NLGNs and β-NRXNs showing their interaction domains and the NLGN dimerisation interfaces. Green residue corresponds to residue 451 in NLGN3 (mutated in ASD). Red residues are part of the AChE domain needed for binding to NRXN. Purple residues represent the NLGN dimerisation interface. Splice sites are in yellow. Adapted from Dean and Dresbach (2006)

levels at an early postnatal age and increase through development and into adulthood (Scheiffele et al. (2000); Song et al. (1999); Varoqueaux et al. (2006)).

NLGN isoforms have unique subcellular localisation: NLGN1 is mainly concentrated at glutamatergic synapses (Song et al. (1999)); NLGN2 are preferentially located in GABAergic synapses (Chih et al. (2005); Graf et al. (2004); Varoqueaux et al. (2004)); NLGN3 are expressed in both glutamatergic and GABAergic synapses (Budreck and Scheiffele (2007)); and NLGN4 is seemingly only expressed in the adult, and is localised to GABAergic and glycinergic synapses (Varoqueaux et al. (2006); Hoon et al. (2011)).

1.3.3 Binding partners

NLGNs are associated as homo- or heterodimers via their AChE domain (Comoletti et al. (2003); Araç et al. (2007); Poulopoulos et al. (2012)), and form a heterotetrameric complex together with neurexin across the synaptic cleft (Araç et al. (2007)). NLGN dimerisation is important for NLGNs to regulate synaptic function (Ko et al. (2009)). In addition, dimerisation has been shown to be necessary for NLGN trafficking (Poulopoulos et al. (2012)), though there is also evidence to the contrary (Shipman and Nicoll (2012b)). The recognised association between NLGNs follow their expression pattern. The three NLGNs 1–3 have each been shown to homodimerise, and NLGN3 to form heterodimers with both NLGN1 and NLGN2 (Budreck and Scheiffele (2007); Shipman et al. (2011); Poulopoulos et al. (2012)).

NLGN1 and NLGN2 bind to both α- and β-NRXN, whereas NLGN3 only binds to β-NRXN (Boucard et al. (2005)). The distinction in NRXN binding partner is regulated by alternative splicing of both NLGNs and NRXNs (Boucard et al. (2005)), thus NLGN–NRXN binding depends on which principal isoforms are expressed and which splice variants are used. Furthermore, binding of NLGN–NRXN is dependent on presence of Ca^{2+} (Comoletti et al. (2003); Dean et al. (2003)). Apart from binding to NRXNs, the extracellular domain in NLGN1, specifically, was shown to recruit and retain NMDARs at glutamatergic synapses through extracellular coupling (Budreck et al. (2013)).

The PDZ ligand in the cytoplasmic tail of NLGNs is conserved between all isoforms. It binds to the third PDZ domain of PSD-95 (Irie et al. (1997)), as well as other MAGUKs (Meyer et al. (2004)). NLGNs also bind to synaptic scaffolding molecule (S-SCAM)(Meyer et al. (2004)), which is involved in synaptic clustering of NLGNs at

both excitatory and inhibitory synapses (Iida et al. (2004); Sumita et al. (2007)). At GABAergic synapses, NLGN2 has been shown to directly bind to gephyrin (Graf et al. (2004); Varoqueaux et al. (2004)). As with the PDZ ligand motif, the gephyrin-binding domain is conserved between all isoforms (Poulopoulos et al. (2009)). All NLGNs are able to bind gephyrin and PSD-95, indicating that these binding domains do not dictate differential localisation of NLGN subtypes (Irie et al. (1997); Poulopoulos et al. (2009)). NLGN2 and NLGN4 has been shown to bind to collybistin, another important inhibitory synapse molecule, possible through unique binding domains in these subtypes (Poulopoulos et al. (2009); Hoon et al. (2011); Soykan et al. (2014)).

While the extracellular domain of NLGNs is important for the trans-synaptic binding to NRXNs, the cytoplasmic tail is thought to regulate synaptic specification and transmission through association with other postsynaptic proteins. NLGN1 was shown to strongly promote the recruitment of PSD-95 and NMDARs, and to a lesser extent AMPARs to the postsynapse, which was perturbed when the cytolasmic tail was truncated (Chih et al. (2005)). A mutation in the cytoplasmic tail of NLGN3 selectively impaired AMPAR mediated synaptic transmission (Etherton et al. (2011b)), but the same mutation in NLGN4 lead to increases in AMPAR- and NMDAR-mediated responses by enhancing their surface expression (Chanda et al. (2016)). In addition, NLGNs form several small clusters within the synapse that co-localises closely with AMPAR nanodomains and through binding to PSD-95 via its C-terminal PDZ motif arranges these in close contiguity to the pre-synaptic release sites (Haas et al. (2018)). These findings suggest that the cytoplasmic tail of NLGNs has a central role in synaptic function.

1.3.4 Synaptic specification

NLGN subtypes show distinct subcellular localisation, but share the same protein-interacting domains with similar binding affinity. Therefore, another mechanism must exist to determine synaptic localisation and for NLGN promotion of synaptic specificity. The exact mechanisms are still uncertain, but phosphorylation has been implicated in isoform-specific regulation (Bemben et al. (2015b)). Phosphorylation of the C-terminal region through Trk tyrosine kinases prevented binding of NLGN1 to gephyrin, allowing it to assemble with excitatory molecules (Letellier et al. (2018)). Similarly, a proline-directed phosphorylation of NLGN2 negatively regulated its binding to gephyrin

(Antonelli et al. (2014)). These phosphorylation sites are present on all NLGN subtypes, and could thus serve as a regulation site for determining which postsynaptic machinery to recruit. This could be directed through NLGN-NRXN specific binding, which was shown to be the case for NLGN1 tyrosine phosphorylation (Giannone et al. (2013)). In addition to phosphorylation, differential glycosylation has been proposed to regulate NLGN activity (Bemben et al. (2015b)), but still more research is needed on this subject.

1.3.5 Functions of Neuroligins

Despite much effort, the roles of NLGNs in synapse formation and function still remain uncertain. The general picture emerging from overexpression and knockdown studies both *in vitro* and *in vivo*, is that NLGNs are synaptogenic and play an important role in synapse formation. Initially, NLGNs were linked to a role in synaptogenesis from experiments showing that NLGNs expressed in non-neuronal cells were capable of inducing presynaptic specialisation in co-cultured neurons (Scheiffele et al. (2000); Dean et al. (2003)), and direct overexpression or downregulation of NLGNs in neurons increased or decreased the number of synapses, respectively (Chih et al. (2004, 2005)). Complimenting this, were findings showing that NRXNs could promote the formation of postsynaptic specialisations in co-cultured neurons when expressed in non-neuronal cells (Graf et al. (2004)). Several studies following these, have demonstrated similar synaptogenic effects of NLGNs (Boucard et al. (2005); Dahlhaus et al. (2010); Shipman et al. (2011); Shipman and Nicoll (2012a); Jiang et al. (2016)).

Genetic knock-out experiments, however, have suggested NLGNs to be implicated in synaptic function, rather than formation (Varoqueaux et al. (2006); Chubykin et al. (2007); Chanda et al. (2017)). These studies showed that *NLGN1-3* knockout mice showed severe impairments of excitatory and inhibitory synaptic transmission, but displayed no alterations in synapse numbers or structure. Another more recent study, found that NLGNs were not required for formation of excitatory synapses or functions of AMPARs, but were necessary for normal NMDAR-mediated synaptic transmission. However, this study also found that NLGNs, more specifically NLGN2, were needed for typical inhibitory synaptic formation and transmission (Jiang et al. (2016)). It is possible that NLGN isoforms have distinct roles in formation and function at excitatory and inhibitory synapses. It is furthermore possible that alternative splicing of NLGNs could help determine their synaptic function. Alternative splicing has been shown to

affect synaptic formation in cultures (Boucard et al. (2005); Chih et al. (2006)), but much less is known about the effect of splice variants *in vivo*.

To help identify what the core function of neruoligins is, species-to-species translatability can be utilised, as you would expect the core functions of homologous genes to be preserved across species. Most studies have been carried out in cultures and mice with very little research on neuroligin function having been done in rat models. The model used in this thesis, $Nlgn3^{-/y}$, could help shed a light on key functions of this protein.

1.3.6 Regulation of NLGNs

NLGNs are negatively modulated by the Ig superfamily (IgSF)MDGA (meprin, A-5 protein, and receptor protein-tyrosine phosphatase mu [MAM] domain-containing glycosylphosphatidylinositol anchor). MDGAs can bind to all NLGNs, but with higher affinity for NLGN1 and NLGN2 with splice site B weakening the affinity (Connor et al. (2016); Clayton et al. (2017)). MDGA1 blocks the interaction between NLGN2 and NRXN and supresses inhibitory synapse development in cultures (Pettem et al. (2013)), while MDGA2 blocks the interaction of NLGN1 and NLGN2 with NRXN and can suppress both excitatory and inhibitory synaptic development (Connor et al. (2016)).

NLGN3 undergoes isoform-specific cleavage on the cell surface by MMPs following PKC activation, which reduces synaptic strength. Passive basal cleavage of NLGN3 is led by ADAM10, and heterodimerization of NLGN1 or NLGN2 with NLGN3 renders them sensitive to the same proteolytic cleavage as NLGN3 (Bemben et al. (2015a)).

1.3.7 Neuroligin mutations in humans with ASD

NLGN3 and NLGN4 were the first NLGNs to be described as candidate genes for ASD (Jamain et al. (2003)), but since then all NLGN genes have been associated with ASD. Clinical interest in NLGNs began when mutations in *NLGN3* and *NLGN4* were reported in two Swedish families (Jamain et al. (2003)). The mutation in *NLGN4* was a *de novo* frameshift mutation resulting in a premature stop codon and was identified in two affected brothers, one with typical autism and one with Aspergers. Another two affected brothers, one with typical autism and the other with Aspergers, were found to have a point mutation in *NLGN3*, causing a change to a highly conserved arginine residue to a cysteine (R451C) within the esterase-homology domain of NLGN3. This mutation resulted in intracellular retention of mutant protein, causing loss of synaptic

function (Chih et al. (2004)). Since then several gene variants (frameshifts, missense mutations, internal deletions, and microduplication) in *NLGN3* and *NLGN4* in humans have been linked to autism (Laumonnier et al. (2004); Yan et al. (2005); Talebizadeh et al. (2006); Sanders et al. (2011); Gumus (2019)).

In *NLGN1*, five mutations (a substitution and four missense) have been identified in individuals with ASD. Three of these five mutations were predicted to be high-risk. One of these variants were analysed in a mouse model (Nlgn1-P89L) and showed several ASD-like phenotypes (Nakanishi et al. (2017)).

NLGN2-overlapping CNVs have been associated with a wide range of phenotypic consequences, including autism, ID, and dysmorphic features (Deciphering Developmental Disorders (2015)), and a nonsense variant was identified in a human patient with anxiety, autism, ID, hyperphagia, and obesity (Parente et al. (2017)).

Not all NLGN variants are pathogenic mutations. 4 missense mutations (one *NLGN3* and three *NLGN4X* variants) in the extracellular noncatalytic acetylcholinesterase homology domain essential for neurexin binding and triggering of synaptic activity were investigated and found to not have any effect on protein expression levels or interaction with NRXN. (Xu et al. (2017))

1.3.8 Animal models of *NLGN3*

Several knock-in (KI) mouse models of *NLGN* mutations have been created (Tabuchi et al. (2007); Chadman et al. (2008); Etherton et al. (2011a,b); Jiang et al. (2018)). In addition, knock-out (KO) rodent models of *Nlgn1*, *Nlgn2*, *Nlgn3*, and *Nlgn4* as single KOs or combinations of two of three genes have been generated (Varoqueaux et al. (2006); Jamain et al. (2008); Hamilton et al. (2014); Tabuchi et al. (2007); Etherton et al. (2011a)).

A higher number of studies have looked at the effect of the *Nlgn3* missense mutation, R451C, in mice compared to the *Nlgn3* KO. The R451C KI mice and *Nlgn3* KO animals are viable and fertile, and exhibit no obvious abnormalities or premature mortality (Tabuchi et al. (2007)), unlike *Nlgn1-3* homozygous KO mice that die shortly after birth (Varoqueaux et al. (2006)). The R451C consistently display divergent phenotypes between brain regions (Tabuchi et al. (2007); Etherton et al. (2011a); Speed et al. (2015); Hosie et al. (2018)). Moreover, The R451C KI causes gain of function effects not observed in *Nlgn3* (Tabuchi et al. (2007); Etherton et al. (2011a); Földy et al. (2013)).

This is exemplified by an increase of excitatory synaptic strength, but no change in inhibitory synaptic strength in the hippocampus of R451C KI mice, while the opposite is observed in somatosensory cortex. Meanwhile, the *Nlgn3* KO mice display a decrease in excitatory synaptic strength but an increase in inhibitory synaptic strength in the hippocampus.

The R451C KI mice show impaired social interaction, and enhanced spatial learning and memory (Tabuchi et al. (2007); Etherton et al. (2011a); but see Chadman et al. (2008)), whereas *Nlgn3* KO mice exhibit impaired social memory (Radyushkin et al. (2009)). Both models demonstrate enhanced formation of repetitive motor routines, owing to an increased excitatory/inhibitory balance in the nucleus accumbens (Rothwell et al. (2014)). The *Nlgn3* KO rats display aberrant juvenile play, but otherwise normal social interaction. Furthermore, the *Nlgn3* KO rats show reduced anxiety, perseverative behaviour, hyperactivity, and exhibit less prepulse inhibition to an auditory startle stimulus (Hamilton et al. (2014); Thomas et al. (2017)).

1.4 SynGAP

SYNGAP, located on chromosome 6p21.3[2], encodes the 140 kDa protein, Synaptic Ras GTPase activating protein (SYNGAP). SYNGAP is one of the most numerous proteins in the PSD, and is a major regulator of synaptic strength and size.

1.4.1 *Syngap* structure, isoforms, and expression

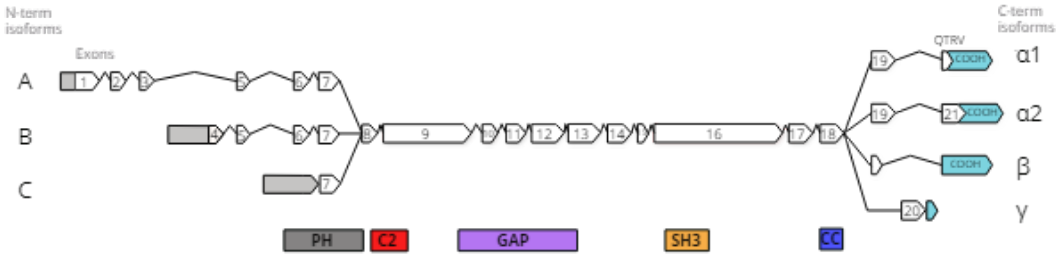

Figure 1.2: Alternative splicing and protein domains of SynGAP. Map showing alternative use of exons in the N- and C-terminal isoforms. Schematic below depicts the protein domains: PH domain only found in isoform A and B; C2, GAP, SH3, and the CC domain are shared between all isoforms; in the C-terminal, the α1 isoform contains a QTRV motif which is a PDZ ligand. Figure adapted from Kilinc et al. (2018)

SynGAP is expressed exclusively in the brain (Chen et al. (1998); Kim et al. (1998)),

[2]https://www.ncbi.nlm.nih.gov/gene/8831

more specifically in forebrain structures (Porter et al. (2005)). It localises mainly to excitatory neurons (Chen et al. (1998); Kim et al. (1998); Moon et al. (2008)), but can also be found at GABAergic neurons (Zhang et al. (1999); Moon et al. (2008)). SynGAP reaches peak expression in neurons within the first two postnatal weeks, after which the expression levels gradually decrease into adulthood (Porter et al. (2005); Clement et al. (2012)). *SynGAP* is a complex gene generating multiple N- and C-terminal isoforms each containing numerous functional protein domains, some isoform unique and some shared by all (Fig. 1.2). N-terminal variants (A, B, and C) result from use of different start codons located in exon 1, 4, or 7. Exon 4 is present only in isoform B. **The pleckstrin homology (PH)** domain is found in all N-terminus isoforms bar SynGAP C, where the domain is truncated. The PH domain is thought to act as signal-dependent membrane adaptor important for membrane trafficking and protein-protein interactions (Lemmon (2008)). C-terminal isoforms (α1, α2, β, and γ) arise from use of alternative splice sites in exon 19 and 21, with exon 20 only being included in isoform γ. The α1 isoforms contains a **QTRV motif**, which is the PDZ-binding domain that mediates binding to scaffolding proteins in the PSD, such as SAP102 and PSD-95 (Kim et al. (1998)). Even though only α1 contains a PDZ-binding domain, α1, α2, and β are all found in the PSD, suggesting multiple ways for SynGAP to get localised in the PSD (Li et al. (2001); McMahon et al. (2012); Yang et al. (2013)). One way that has been proposed is that SynGAP α2 gets to the PSD by forming heterotrimers with α1 via the coiled-coil domain (Zeng et al. (2017)).

The core SynGAP domains shared by all isoforms include the C2, GAP, Src Homology 3 (SH3), and coiled-coil (CC) domains. In addition, multiple phosphorylation sites are present downstream of the GAP domain. (Chen et al. (1998); Kim et al. (1998); Zeng et al. (2016)). **The C2 domain** is thought to mediate binding of Ca^{2+} in a phospholipid-dependent manner. Furthermore, the C2 domain is necessary for SynGAP's role as a RapGAP (Pena et al. (2008)). Additionally, **The Ras-GAP domain** negatively regulates small GTPases by enhancing the intrinsic rate of GTP to GDP hydrolysis of the small G proteins Ras, Rap, and Rab (Walkup et al. (2015); Pena et al. (2008); Krapivinsky et al. (2004)). **The Coiled coil (CC) domain** in the C-terminal half of SynGAP, has been proposed to facilitate SynGAP trimer formation that mediates binding to PSD-95 (Zeng et al. (2016)).

Transcriptional regulation of *SYNGAP1* is dependent upon neuronal activity. During

increased network activity, *SYNGAP1* isoforms B and C are upregulated, while isoform A is downregulated (McMahon et al. (2012)).

1.4.2 Function of SynGAP

SynGAP is one of the most abundant proteins in the PSD (Sheng and Hoogenraad (2007)). It binds strongly to all three PDZ domains of PSD-95 (Chen et al. (1998); Kim et al. (1998); Walkup et al. (2016); Zeng et al. (2016)), putting it in close proximity to NMDA- and AMPA-receptors. SynGAP regulates synaptic strength, size and plasticity, which is evident from a number of studies (Kim et al. (2003); Vazquez et al. (2004); Rumbaugh et al. (2006); McMahon et al. (2012)), but how SynGAP does this is under debate. It has long been thought that the main mechanism was through its negative regulation of small GTPases via the GAP domain, but it was recently proposed that another important mechanism of SynGAP in regulating the postsynaptic membrane composition is through its binding to PSD-95 (Walkup et al. (2016)).

The GAP domain model for SynGAP regulation

Ras and Rap are integral in the regulation of exocytosis and endocytosis of AMPARs near the synapse. They have opposing regulatory effects on AMPAR trafficking, with active Ras increasing exocytosis of AMPARs, while active Rap stimulates the endocytosis of AMPARs (Zhu et al. (2002)). The activity of these GTPases is determined by the balance of their activation by exchange of GDP for GTP and their inactivation by hydrolysis of GTP to GDP. SynGAP promotes the intrinsic GTPase activity of Rap and Ras, and thereby their inactivation (Walkup et al. (2015); Pena et al. (2008); Krapivinsky et al. (2004)). Thus, SynGAP is in a position to finely control synaptic strength by altering the ratio of Ras/Rap inactivation. Evidence suggests that the activity of the GAP domain of SynGAP and its primary choice of small GTPase is regulated by the phosphorylation of SynGAP. Phosphorylation by CaMKII accelerates the rate of inactivation of Rap-GTPases more than that of Ras, whereas phosphorylation by CDK5 and/or Plk2 increases the GAP inactivation of Ras-GTPases more than that of Rap (Walkup et al. (2015, 2018)). CaMKII is activated rapidly when Ca^{2+} flows through NMDA receptors during induction of LTP, whereas both Plk2 and CDK5 are induced by activity-driven protein synthesis over a longer time scale, consistent with a homeostatic role (Walkup et al. (2018)). The distinct phosphorylation of SynGAP by

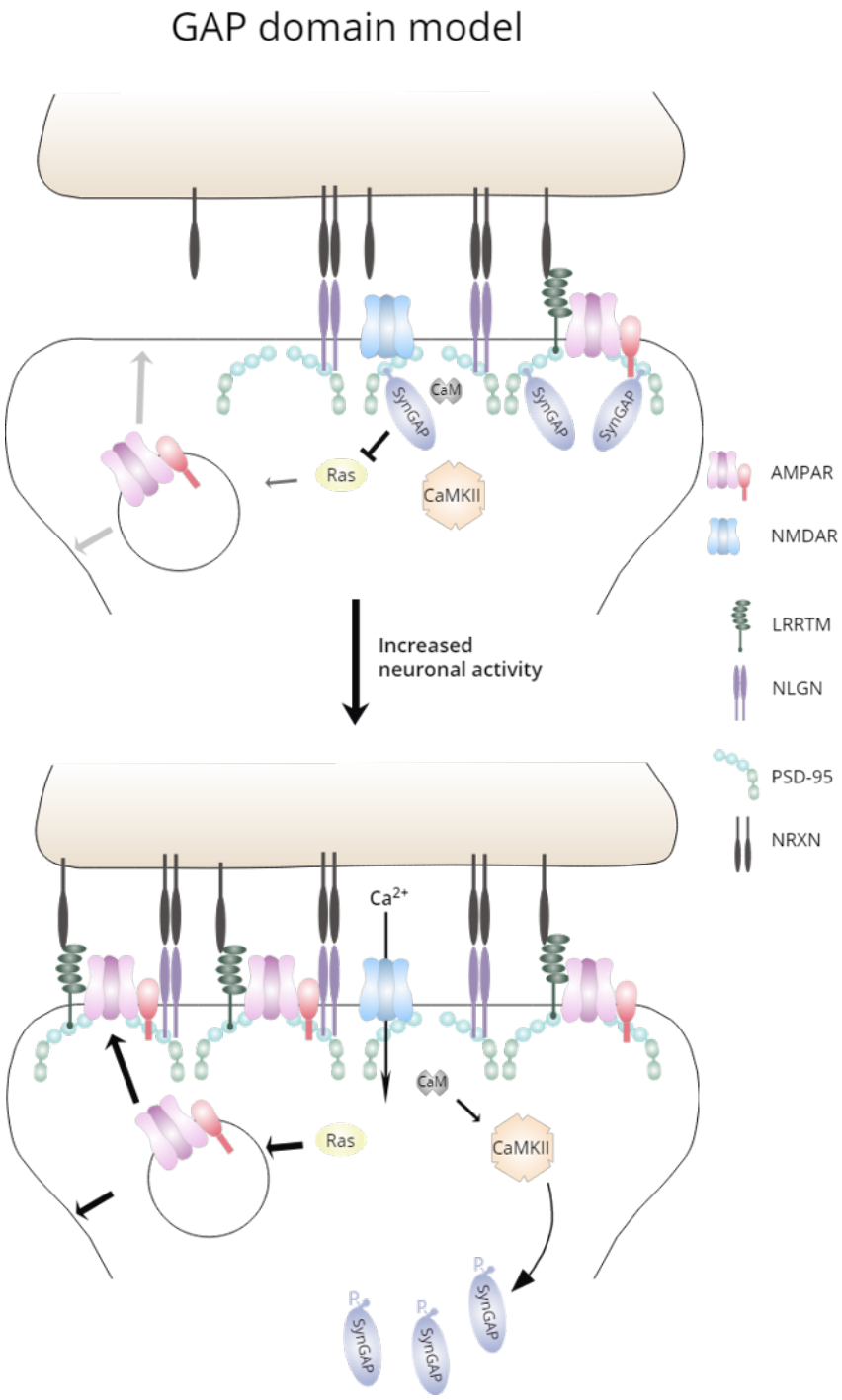

Figure 1.3: GAP domain model. Schematic diagram of how GAP domain model regulates synaptic strength of the postsynaptic compartment during basal states (TOP) and the cellular changes after increased neuronal activity (BOTTOM). Figure adapted from Araki et al. (2015)

a combination of kinases could act like a rheostat by tightly controlling the number of surface AMPARs depending on the type of synaptic input received.

The importance of the GAP domain for synaptic function was demonstrated by the inability to decrease synaptic strength by overexpression of a SynGAP construct with a non-functional GAP domain in cultured neurons in contrast to the decrease in synaptic strength observed when overexpressing a functional GAP containing SynGAP (Rumbaugh et al. (2006)). Furthermore, mutated GAP SynGAP was not able to rescue dendritic spine abnormalities in SynGAP KO cultured neurons (Vazquez et al. (2004)).

The basic model for how SynGAP modulates synaptic strength through its GAP domain is as follows (Fig. 1.3): At basal activity, SynGAP is present in the PSD. Here it attenuates small GTPases, like Ras, and limits the trafficking of AMPARs to the postsynaptic membrane. Upon increased neuronal activation, Ca^{2+} influx through NMDARs triggers phosphorylation of SynGAP by CaMKII (Carlisle et al. (2008); Yang et al. (2013)). This results in dispersion of SynGAP away from the PSD (Yang et al. (2013); Araki et al. (2015)), relieving the Ras/ERK1 pathway from attenuation. As a result, AMPAR exocytosis is expected to be enhanced (Zhu et al. (2002)) and synaptic strength increased (Araki et al. (2015)).

The GAP domain model is complicated by SynGAPs GAP activity not being exclusive to Ras. In fact, SynGAP produces a larger increase in GTPase activity of Rap than of Ras (Krapivinsky et al. (2004); Walkup et al. (2015)). Upon a reduction of SynGAP, you would therefore expect the activity of Rap to increase more than the activity of Ras. This would result in a relative increase in endocytosis of AMPARs compared to exocytosis (Zhu et al. (2002)), and hence fewer AMPARs at the synapse not more, as observed in $Syngap^{+/-}$ (Kim et al. (2003); Vazquez et al. (2004)). This could indicate that SynGAP has more than one way of regulating synaptic function, either acting in conjunction with or independently of the GAP domain.

The PDZ 'slot' model for SynGAP regulation

A new model has been proposed for an additional way for SynGAP to regulate synaptic strength and size that is distinct from its function as a Ras/Rap GAP (Walkup et al. (2016)). The model suggests that SynGAP plays an important role in limiting the

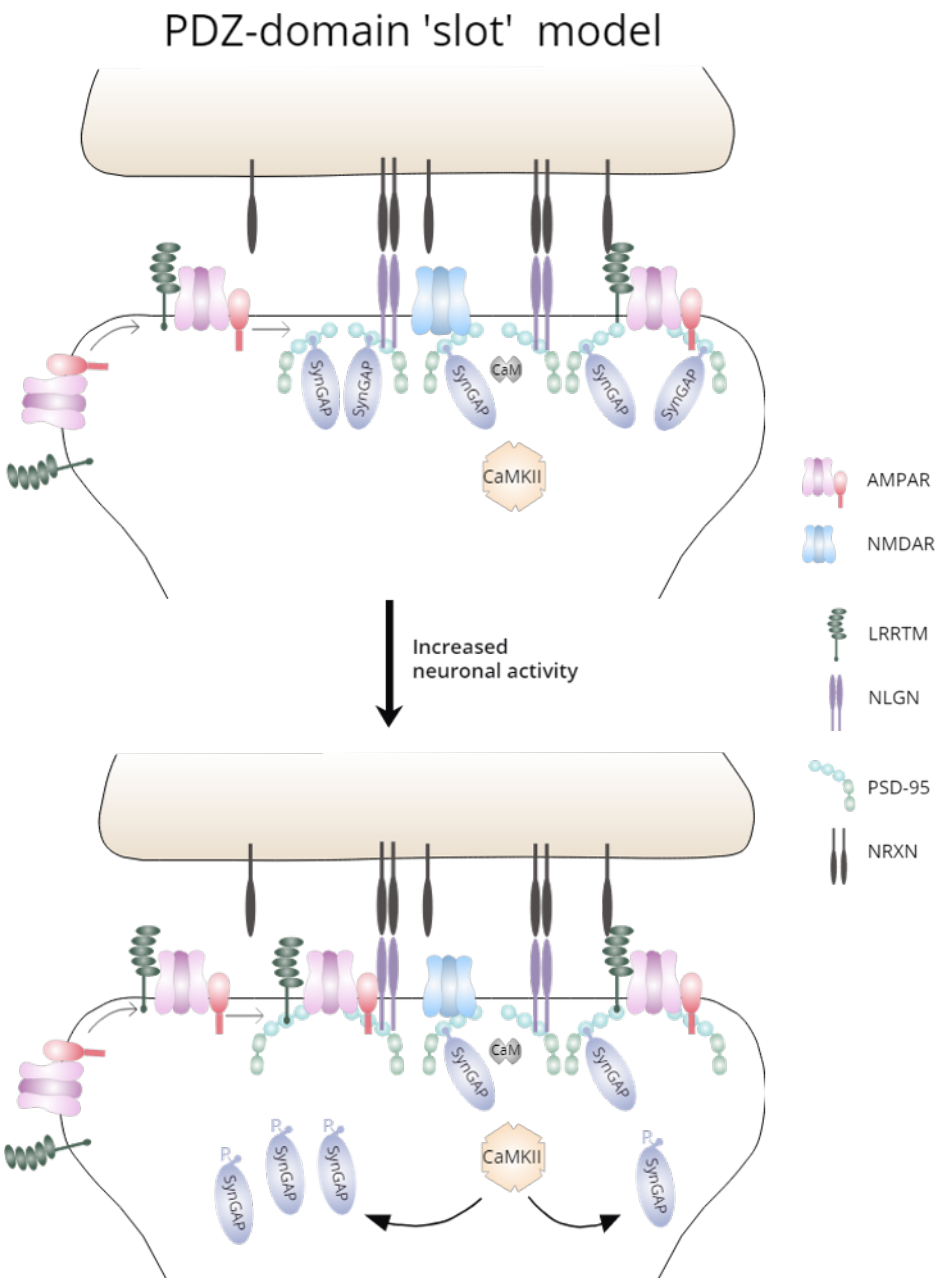

Figure 1.4: PDZ 'slot' model. Schematic diagram of the PDZ-domain 'slot' model and how SynGAP's sequestering of PDZ domains stops other proteins, such as AMPARs/TARPs from trapping in the PSD during steady state (TOP). After increase neuronal activity, SynGAP disassociates with PSD-95 allowing for other proteins to bind (BOTTOM). Figure adapted from Walkup et al. (2016)

size and strength of excitatory synapses by restricting the available PDZ domain 'slots' on PSD-95 that can bind AMPAR complexes, thereby regulating the overall protein composition of the PSD. Activation of NMDARs and CaMKII leads to phosphorylation of SynGAP, followed by its dispersion from the PSD. This renders it incapable of competing with other proteins for binding to PSD-95, thereby freeing up PDZ 'slots' for AMPARs to bind to, leading to an increase in synaptic strength (Fig. 1.4).

During activity-induced AMPAR trafficking to the postsynaptic membrane, AMPARs from the perisynapse laterally diffuse and become trapped in the postsynaptic density by binding to 'slots' that are believed to consist mainly of PDZ domains on PSD-95 (Opazo and Choquet (2011); Opazo et al. (2012)). The rate of trapping is rapid (Makino and Malinow (2009)), and matches the rate of SynGAP dispersal from the PSD after CaMKII phosphorylation (Yang et al. (2013); Araki et al. (2015)), aligning with the notion that activity-induced reduction of SynGAP–PSD-95 association opens up binding slots for AMPAR complexes. Exocytosis of AMPARs on the other hand, does not contribute to the increased trapping of AMPARs after synaptic stimulation (Makino and Malinow (2009)). Exocytosis restores AMPARs surface expression in dendrites and perisynaptically, and at a slower rate than AMPAR trapping, suggesting that SynGAP–PSD-95 dissociation and AMPAR trapping is the method used for initial increase of synaptic strength.

A SynGAPα1 construct with its PDZ motif missing, failed to rescue aberrant spine morphology in SynGAPα1 KO hippocampal cultures (Vazquez et al. (2004)). In addition, the PDZ binding motif was found to be necessary for SynGAP to decrease synaptic strength when overexpressed in cultured neurons (Rumbaugh et al. (2006)). This supports the model that SynGAPs ability to compete for binding of PSD-95 is important for regulating the composition of the PSD.

Furthermore, SynGAP isoforms have been shown to have opposing effects when expressed in primary forebrain cultures. SynGAPα1 expression caused the neurons to be silent i.e. with the postsynaptic density containing no AMPA-type glutamate receptors, whereas SynGAPα2, which lacks the PDZ binding motif, had no effect on the proportion of silent neurons (McMahon et al. (2012)). The differences exerted by these isoforms could be explained by the PDZ 'slot' model in that SynGAPα1 overexpression stops the trapping of AMPARs at the PSD, resulting in silent synapses.

Walkup et al. (2016) supported their model by demonstrating that phosphorylation by CaMKII and PLK2 of several sites on SynGAP reduces the affinity of the PDZ-binding domain to all three PDZ-domains on PSD-95. In addition, they showed that in *Syngap*$^{+/-}$ mice less SynGAP was associated per molecule PSD-95, and more copies of other proteins that bind PSD-95. Supporting this, a recent study found that following NMDAR activation, SynGAP dissociates from the PSD-95 synaptic complex, followed by an increase in association between PSD-95 and AMPARs (Lautz et al. (2018)).

1.4.3 *SYNGAP* in neurodevelopmental disorders

SYNGAP is a high-risk locus for several neuropsychiatric disorders, including ID, ASD, epilepsy, and schizophrenia (Hamdan et al. (2009, 2011); Carvill et al. (2013); Purcell et al. (2014); Deciphering Developmental Disorders (2015, 2017)). *SYNGAP* haploinsufficiency causes a genetically defined form of ID termed autosomal mental retardation type 5 (MRD5[3]). Common phenotypes include early developmental delay, cognitive impairment, severely impaired expressive and receptive language, sensory processing impairments, behavioural deficits, and epilepsy (Berryer et al. (2013); Parker et al. (2015); Mignot et al. (2016); Weldon et al. (2018)). In addition, ASD is often co-diagnosed in MRD5 individuals (Pinto et al. (2010); De Rubeis et al. (2014); Iossifov et al. (2014)). *SYNGAP* variants are amongst the most commonly found in ID patients, causing 0.5–1.0% of all ID cases (Berryer et al. (2013); Deciphering Developmental Disorders (2015, 2017)).

Most of the identified mutations associated with MRD5 are frameshift deletions and nonsense mutations. Pathogenic mutations are distributed throughout the gene, especially in exon 5, 8, and 15 (Mignot et al. (2016)). Almost all reported cases have resulted from de novo mutations, except one inherited case from a mildly affected father, who was found to be mosaic for the mutation (Berryer et al. (2013)).

1.4.4 Rodent models of *Syngap1*

Several rodent models of *SYNGAP* haploinsufficiency have been created (Komiyama et al. (2002); Kim et al. (2003); Vazquez et al. (2004); Muhia et al. (2010)). Homozygous mutants appear normal at birth but do not survive for more than a week. (Komiyama

[3]https://www.omim.org/entry/612621

et al. (2002); Kim et al. (2003); Barnett et al. (2006)). *SynGAP*$^{+/-}$ animals appear normal and survive into adulthood, and display no gross brain abnormalities (Komiyama et al. (2002)). *SynGAP*$^{+/-}$ have higher average numbers of AMPARs at their synapses (Kim et al. (2003); Vazquez et al. (2004)), and accelerated excitatory synapse formation (Vazquez et al. (2004); Clement et al. (2012)), resulting in a shift in excitatory/inhibitory balance, thereby restricting critical developmental period efficacy (Clement et al. (2013)). Examination of spine morphology has suggested abnormal spines, but more recent findings have found the alterations in spine morphology to be minimal (Vazquez et al. (2004); Carlisle et al. (2008); Barnes et al. (2015))

Behaviourally, *SynGAP*$^{+/-}$ mutant mice display hyperactivity, learning and memory deficits, altered social interaction, impaired cued fear conditioning, enhanced startle response, and impaired sensory motor gating (Komiyama et al. (2002); Guo et al. (2009); Muhia et al. (2010)). However, because *SynGAP*$^{+/-}$ mice display hyperactivity, caution should be made when interpreting behavioural data, as altered behaviours could be confounded by the hyperactivity, i.e. the mice might be able to distinguish between a familiar and novel object or mouse, but the hyperactivity could mask preference. Furthermore, *SynGAP*$^{+/-}$ mice are susceptible to audiogenic seizures and have reduced seizure threshold (Clement et al. (2012); Ozkan et al. (2014)), resembling the prominent clinical epilepsy feature observed in *SYNGAP1* human patients.

1.5 Amygdala

The amygdala is an essential brain structure in emotional processing and learning of both positive and negative valence, including negative emotions such as fear and anxiety (LeDoux (2003)). The amygdala has long been a region of interest investigating the pathology of ID and ASD, given its role in modulating anxiety, social behaviour, and emotional states. Individuals with ASD have difficulties interpreting the social behaviours of other people, interaction in complex social groups, to empathize with others, and to predict how people will think and act, i.e. impaired social intelligence. The neural basis of social intelligence has been proposed to involve three brain regions: the amygdala, the orbito-frontal cortex (OFC), and the superior temporal sulcus and gyrus (STG) (Kling and Brothers (1992); Adolphs (2010)). This prompted the amygdala theory of autism which "...proposes that the amygdala is one of several neural regions

that are necessarily abnormal in autism" (Baron-Cohen et al. (2000)).

There is a range of evidence of abnormal amygdala function in ASD from humans supporting this theory. Anatomical abnormalities have been observed in ASD individuals, where the volume of the amygdala in children with ASD is larger, but then does not undergo the same age-dependent increase in volume as seen in normally developing children (Schumann et al. (2011)). Cognitively, amygdala abnormalities are associated with alterations in familiar and unfamilar face processing. Individuals with autism show gaze avoidance, combined with hyperactive amygdala response to face processing and gaze fixation (Pierce et al. (2001); Dalton et al. (2005); Nacewicz et al. (2006); Kleinhans et al. (2009)). This could suggest that ASD patients perceive social interactions as fearful or anxiety inducing given the role of amygdala in fear and anxiety (Schumann et al. (2011)).

One way to measure fear states in rodents is by using fear conditioning — a conditioned learning paradigm — which has served as a model for emotional learning in animals for decades. The circuitries involved in fear and anxiety related behaviours are complex, and it is beyond the scope of this thesis to go into the details of them all. A brief description will follow from an amygdalo-centric view.

1.5.1 Anatomy

The amygdala is a complex collection of heterologous nuclei and cortex-like structures. Most of these structures have been divided into two or more subnuclei each exhibiting distinct cytoarchitecture, histochemistry, and connections. This section will only detail the components thought to be involved in conditioned fear acquisition and extinction; the basolateral complex (BLA), a cortical like structure; the central amygdala (CeA); a nuclei reminiscent to striatum; and the intercalated cell masses (ICM) (Mahanty and Sah (1999)).

Basolateral complex

The basolateral complex, BLA, can be further divided into the lateral (LA) and the basal (BA) amygdala. The BLA consist of 80% spiny glutamatergic (principal) neurons and 20% sparsely spiny GABAergic interneurons with most of the latter being local-circuit cells. Morphologically, principal neurons in the BLA have pyramidal-like somata with three to seven dendrites arising from the soma into large dendritic arbors.

In general, neurons in the BA are larger than in the LA, but otherwise no clear morphological distinctions exist. Principal neurons are randomly organised within the BLA, particularly close to the nuclei borders (McDonald and Augustine (1993); Sah et al. (2003); Spampanato et al. (2011)).

In the LA principal neurons fire broad action potentials, and show a continuum of spike frequency adaptation. Action potentials are followed by a prolonged (1–5 s) afterhyperpolarisation (AHP). Principal neurons in the BA can be divided into two main groups, burst firing and repetitive firing. Burst firing cells fire one or two action potentials, while repetitive firing neurons fire throughout a current injection with little accommodation. Repetitive firing neurons diverge from LA principal neurons by a delay in firing during depolarising current injections. Burst firing cells have significantly larger AHP than repetitively firing neurons. Principal neurons in the BLA receive both cortical and thalamic inputs, which form asymmetrical glutamatergic synapses. AMPA- and NMDA- receptors are present at both these synapses, but it has been suggested that NMDARs at thalamic inputs have lower levels of Mg^{2+}, and thus are active at resting membrane potentials. In addition, the principal neurons also express kainate receptors and metabotropic glutamate receptors (mGluRs) (Sah et al. (2003); Duvarci and Pare (2014)).

Two main classes of interneurons exist in BLA, parvalbumin (PV^+) and somatostatin (SOM^+). They show fast spiking in response to current injection with short duration action potentials and little frequency adaptation. PV^+ and SOM^+ are involved in feedback and feedforward inhibition, respectively (Sah et al. (2003); Duvarci and Pare (2014)).

Central Amygdala

The central amygdala is commonly divided into two nuclei, lateral (CeL) and medial (CeM), each having one main GABAergic cell type. CeL neurons resemble striatal medium spiny neurons, whereas CeM neurons are larger with sparing dendritic branching and low spine density. CeA neurons can be grouped into three types; regular spiking cells with firing throughout a prolonged current injection with little frequency adaptation; late firing displaying large outward rectification; and bursting cells giving rise to low-threshold spike bursts. CeA neurons exhibit both medium and slow AHP (Sah et al. (2003); Duvarci and Pare (2014)).

Intercalated cell masses

The ICM form small densely packed clusters of neurons found in fibre bundles around the amygdala. The ICM in the external capsule project to the BLA, whereas the ICM in the intermediate capsule project to CeL or CeM depending on location. Intercalated neurons are mostly GABAergic that display a regular firing pattern and modest frequency adaptation (Duvarci and Pare (2014)).

1.5.2 Amygdala circuitry

Extrinsic connectivity of the Amygdala

Afferents to the amygdala are distinguished by their origin. Cortical and thalamic inputs bring sensory and memory information of every modality, while brain stem and hypothalamic afferents bring information from behavioural and autonomic systems. Whereas the LA is the main recipient of sensory input coming from the sensory cortices, thalamic and prethalamic inputs reach LA, BA, and CeA with some pathways completely bypassing the LA (Turner and Herkenham (1991); Mcdonald (1998)). The sensory input received is generally not direct, but has undergone a cascade of processing elsewhere first (Pape and Pare (2010)).

The outputs from the amygdala are very diverse with extensive connections to the cortical, striatal, thalamic, and hypothalamic nuclei, as well as brain stem areas and various mid brain areas (Sah et al. (2003)). The CeM is considered the main output of the amygdala, but projections arise in all subnuclei. BLA and CeA generally project to different regions. The projections to the striatum, thalamus, and cerebral cortices originate from the BLA, while the CeA supplies the brainstem nuclei with most of the efferents from the amygdala. Here behavioural and visceral correlates of fear are generated. However, BLA and CeA send overlapping projections to the lateral hypothalamus, basal forebrain regions, and to bed nucleus of the stria terminalis (BNST) (Sah et al. (2003); Pape and Pare (2010)). The BLA is reciprocally connected to both the ventral hippocampus and the medial prefrontal cortex (mPFC) (Sah et al. (2003)).

Intrinsic Connectivity of the Amygdala

In the original model of the amygdala intranuclear circuitry of fear conditioning, LA was contemplated as the main input nuclei of the amygdala, and the CeA as the

main output for fear responses with direct connections between the two (Davis (1993); LeDoux (1993)). While the reality is a bit more complex, such as no direct connection existing between LA and CeM, the basic idea still holds true.

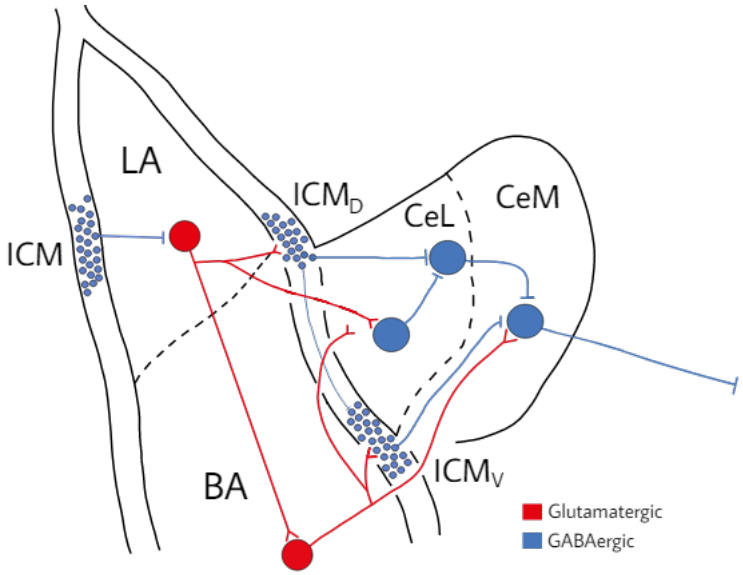

Figure 1.5: Intrinsic connectivity of the amygdala Simplified schematic of the local microcircuit of the amygdala. The major internuclear connections are colour coded: Red depicts glutamatergic neurons; blue depicts GABAergic. ICM$_D$: Dorsal ICM; ICM$_V$: Ventral ICM. Figure adapted from Duvarci and Pare (2014)

The amygdala has extensive intra- and internuclear connectivity (Mahanty and Sah (1999)). Principal neurons preferentially target interneurons in their near proximity and other principal cells at a distance. This avoids runaway excitation locally while still allowing connections to neurons further away. The internuclear projections are mostly one directional with not many reciprocal connections (Duvarci and Pare (2014)). Figure 1.5 shows a simple schematic of the amygdala microcircuit: within the BLA, LA projects to the BA. From here, BLA has two ways of regulating the CeA: via direct connections from LA and BA to the CeL, and from the BA nuclei to CeM (Note there is no direct connection between the main input and the main output of the amygdala); or indirectly from LA and BA by forming glutamatergic synapses onto intercalated cells in the dorsal and ventral mass, respectively, generating feedforward inhibition in CeA neurons. It has been proposed that learned fear is regulated by altering the efficacy of the direct versus the indirect branches of this microcircuit. Within an ICM, neurons form non-reciprocal inhibitory synapses with other intercalated neurons. The dorsal most ICM in the intermediate capsule sends connections to the ventral intermediate capsule.

The ICM in the external capsule projects to the BLA, while the dorsal and ventral intermediate capsule ICM sends connections to the CeL and the CeM, respectively (Pare and Duvarci (2012); Duvarci and Pare (2014); Tovote et al. (2015)).

1.5.3 Associative fear conditioning

The standard paradigm for assessing learned fear behaviour in rodents is Pavlovian fear conditioning and extinction. It involves repeated presentations of a previously innocuous stimulus (conditioned stimulus; CS), such as a tone or flashing light, paired with an aversive unconditioned stimulus (unconditioned stimulus; US) like a foot shock. After repeated pairings, the CS when presented alone will come to elicit a fearful response. Over time if the CS no longer predicts a US, extinction learning occurs and the fearful response will diminish.

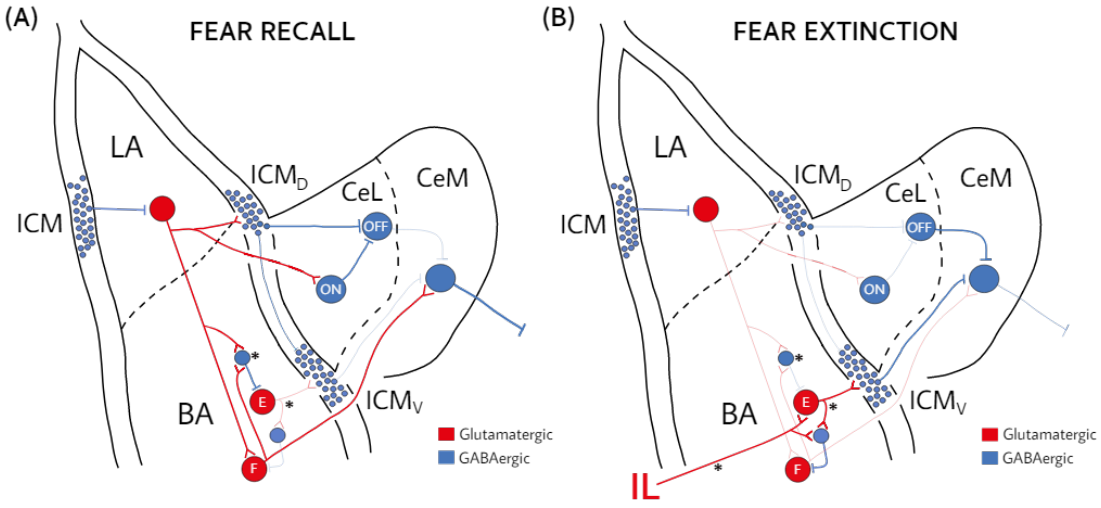

Figure 1.6: Amygdala fear circuits. Simplified models of the intra-amygdala circuit involved in fear recall (A) and fear extinction (B). The asterisk denote hypothetical connections. Figure adapted from Pare and Duvarci (2012).

The CS and US has multiple routes into the amygdala: direct subcortical routes, through dorsal thalamus, and via the cerebral cortex. Upon convergence of synaptic CS and US inputs in LA (Romanski et al. (1993)), synapses transmitting CS undergo potentiation (Quirk et al. (1995); McKernan and Shinnick-Gallagher (1997); Rogan et al. (1997)). Only about 20% of LA neurons show increased responsiveness to the CS after fear conditioning (Han et al. (2007)), suggesting a competitive recruitment of neurons to the fear memory trace, thought to be preferential towards neurons with

higher intrinsic excitability (Han et al. (2007, 2009); Kim et al. (2013); Duvarci and Pare (2014)). From the LA there are two main ways of transmitting CS information to the fear output neurons in CeM; through facilitation of CeM via the BA; or through disinhibition of CeM via ICM and CeL. Once recruited to the fear circuit, BA neurons are necessary for relaying the CS-evoked LA response to CeM, but without the BA, CS information reaching the CeM through the CeL is enough to elicit fear responses (Duvarci and Pare (2014)).

In the BA, during fear conditioning two types of neurons develop with activity oppositely correlated with high ('Fear' neurons) and low ('Extinction' neurons) fear states. 'Fear' neurons exhibit a selective increase in CS evoked activity during and after fear conditioning, which is reversed by extinction (Herry et al. (2008); Amano et al. (2011)). The activity of 'fear' neurons are required for eliciting normal fear responses during fear recall (Amano et al. (2011)). 'Extinction' neurons are switched on during extinction training in response to CS. A rapid switch between the balance of 'fear' and 'extinction' neuron activity is essential for behavioural transitions during extinction and context-dependent fear renewal (Herry et al. (2008)). Similarly, two populations of cells are found in the CeL with opposing responsiveness to the CS. CeL-ON neurons display excitatory responses to the CS, whereas CeL-OFF neurons display inhibitory responses (Ciocchi et al. (2010)).

In the BLA a type of principal neurons exists with a unique relationship to inhibitory interneurons. Their activation results in recruitment of interneurons and the consequent inhibition of principal neurons in the BA (Popescu and Paré (2011)). The target of the local-circuit interneurons has been hypothesised to be the 'exctinction' neurons, and this help regulate the behavioural transition during recall and extinction (Pare and Duvarci (2012)).

Amygdala microcircuit in fear recall

The level of fear expressed during fear recall is associated with the responsiveness of the CeM to the CS (Pare and Duvarci (2012)). CeM neurons exhibit a continuous increase in firing during CS presentations (Ciocchi et al. (2010)). During low fear states the CeM is under tonic inhibition from the CeL and the ICM_V, thus disinhibition from these is needed to elicit a fear response. The potentiation of LA neurons by the CS leads to an increased recruitment of ICM_V and CeL-ON neurons, which inhibits CeL-OFF

neurons. Together with inhibition of ICM_D by ICM_V cells, this result in disinhibition of the CeM and elevation of CeM output. Additionally, the CeM output is facilitated further by excitation from BA 'fear' neurons (Fig. 1.6A).

Amygdala microcircuit in fear extinction

Extinction is considered a new type of learning. The circuit involved in extinction overlaps with the one involved in fear conditioning. The conditioned-stimulus-recruited networks in the amygdala are reduced during extinction, likely through recruitment of local interneurons by a distinct extinction-specific circuit (Tovote et al. (2015)).

To extinguish the fear expression, the reduced CeM responsiveness to the CS would depend on increased feedforward inhibition and CeM disfacilitation. During extinction, the responsiveness of the LA to CS rapidly decreases. This results in reduced recruitment of BA 'fear' neurons and disfacilitation of CeM. Additionally, it is thought to lead to a reduced recruitment of interneurons inhibiting BA 'extinction' neurons. This in turn, causes an increase in inhibition of 'fear' neurons diminishing their response to the CS. Furthermore, an increase in feedforward inhibition to the CeM happens as a result of reduced LA responsiveness causing a disfacilitation of the ICM_D cells. Consequently, disinhibition of ICM_V and CeL-OFF neurons occurs. This ultimately leads to the increased feedforward inhibition of CeM, and the decreased CeM responsiveness to the CS (Fig. 1.6B).

Amygdala microcircuit in anxiety

Fear and anxiety are two distinct evoked defensive behavioural responses. Fear is elicited upon actual, acute sensory input. Anxiety, on the other hand, can be elicited by hidden, incidental, and anticipated threats. Many areas of the brain are involved in fear and anxiety responses. Evidence is emerging that the circuitries involved in processing fear and anxiety are overlapping, but separate (Tovote et al. (2015)). However much less is known about the circuitry involved in anxiety and how it distinguishes from that involved in fear. BLA-CeL specific projections have been shown to bidirectionally affect acute anxiety (Tye et al. (2011)). General activation of BLA neurons elevated anxiety-like behaviour. However, selective activation of BLA–CeL had acute anxiolytic effects, whereas inhibiting these projections increased anxiety-related behaviours, suggesting that specific BLA-CeL connections are critical for acute anxiety control (Tye et al. (2011)).

The target neurons in the CeL were later identified as CeL-OFF (Cai et al. (2014)). Another study, identified distinct neuronal populations in the LA signalling generalised versus cue-specific association during fear conditioning. Upon fear generalisation cue-specific neurons lost their specificity tilting the balance toward generalising neurons (Ghosh and Chattarji (2015)). Generalised fear was shown to also affect the CeA microcircuit. Tonic activity was seen in CeL-OFF neurons after fear condition in animals exhibiting generalised fear, while CeM neurons showed an inverse correlation (Ciocchi et al. (2010)). These findings could suggest generalised fear/anxiety has a distinct network, but it also recruits neurons involved in fear circuit.

1.5.4 Synaptic plasticity underlying associative fear learning

A necessity for learning and memory encoding is activity-dependent plasticity. For conditioned fear learning, the LA is believed to be the site of associative plasticity (Pape and Pare (2010)).

LA is the major hub for sensory input, and it is where afferents carrying CS and US information converge onto single neurons (Romanski et al. (1993)). Transmission of the CS through thalamic afferents into the LA is a key segment of the fear conditioning circuit. The ability of this pathway to support LTP implicates it as a potential site for associative plasticity. Early studies showed that fear conditioning increased the magnitude of CS evoked responses in the LA similarly to electrical LTP induction, which prevented electrically induced synaptic plasticity (Quirk et al. (1995); Rogan and LeDoux (1995); Rogan et al. (1997); McKernan and Shinnick-Gallagher (1997); Tsvetkov et al. (2002)). This demonstrates that fear conditioning induces changes in efficacy of sensory afferent input. However, LA as a driver of conditioned fear behaviour was demonstrated by showing that conditioning-induced plasticity preceded increases in responsiveness in the cortex and thalamus; it developed faster than the behavioural response; and optogenetic activation of LA can instruct associative fear learning (Quirk et al. (1997); Repa et al. (2001); Johansen et al. (2010)). LTP at sensory inputs to the amygdala has been shown to share a common set of molecular mechanisms with fear conditioning. Pharmacological infusion of NMDAR antagonist blocks the acquisition of conditioned fear *in vivo* and induction of LTP *in vitro* (Miserendino et al. (1990); Kim et al. (1991); Huang and Kandel (1998); Bauer et al. (2002)). Furthermore, voltage-gated Ca^{2+} activation has been suggested to contribute to fear conditioning during

stronger induction protocols (Bauer et al. (2002); Schroeder and Shinnick-Gallagher (2004); Humeau et al. (2005)).

Together these findings indicate that LTP at sensory efferents is the cellular correlate of associative plasticity. Recording LTP at thalamic afferents *in vitro* has therefore often been used to assess the cellular function of fear conditioning and how it might be affected during disease.

1.6 Aims of this thesis

The overarching aim of this thesis is to further our understanding of the two synaptic proteins, NLGN3 and SynGAP, and how they contribute to the aetiology of ID and ASD. This will not only provide valuable information about the pathophysiology of the ID/ASD cases specifically associated with *NLGN3* and *SYNGAP*, but hopefully also to a range of disorders linked to synaptic dysfunction.

Both proteins were investigated at two age ranges to get a sense of the developmental effect of these proteins. To enable comparison between models and examine if they share common pathologies, a set of electrophysiological protocols were used to investigate the impact of NLGN3 (**Chapter 3**) and SynGAP (**Chapter 4**) on amygdala intrinsic and synaptic physiology. Furthermore, **Chapter 4** provides a unique opportunity to gain insight into the function of SynGAP, and the roles of its functional domain. This was enabled by the use of two new *Syngap* rat models: one with a null deletion, and one with a deletion of the GAP domain. Finally, **Chapter 5** aims to establish a methodology to study the circuit function in amygdala using optical imaging.

Chapter 2

Materials and Methods

The experiments for this thesis were done either at the Centre for Discovery Brain Sciences (CDBS, University of Edinburgh), or at the Centre for Brain Development and Repair (CBDR, InStem, NCBS, Bangalore). Great care was taken to keep the experiments done at the two sites as similar as possible. If the experimental setup differs, it will be noted under the description in the relevant section.

All experiments performed at the CDBS were done in accordance with The University of Edinburgh Animal Welfare committee and performed under a UK Home Office project license. All procedures complied with the Animals (Scientific Procedures) Act, 1986, and were approved by the Named Veterinary Surgeon. All experiments performed at CBDR were conducted in accordance with the guidelines of the CPCSEA, Government of India and approved by the Institutional Animal Ethics Committee of National Centre for Biological Sciences.

2.1 Animals

2.1.1 CDBS experiments

All animals were group housed, and colonies were maintained in facilities with a 12:12hrs light:dark cycle with food and drink *ad libitum*. All animals used for experiments were male, and littermate controls were used when possible. Experiments and analyses were performed blind to genotype.

For the preparation of rat brain slices, animals were anaesthetised using isoflurane. Decapitation were done with either sharp scissors or with a guillotine.

2.1.2 CBDR experiments

All animals were group housed, and colonies were maintained in facilities with a 16:8hrs light:dark cycle with food and drink *ad libitum*. All experimental animals were male, and littermate controls were used when possible. Experiments and analyses were performed blind to genotype.

For the preparation of rat brain slices, animals were anaesthetised using halothane. Decapitation were done with either sharp scissors or with a guillotine.

All experiments done on the *Nlgn3*$^{-/y}$ rats were performed at CBDR. mEPSCs and intrinsic properties of the p14 age group of *Syngap*$^{+/\Delta GAP}$ were performed at CBDR. The AMPA/NMDA ratios and the paired pulse facilitation for *Syngap*$^{+/\Delta GAP}$ were collected at both CDBS and CBDR and compiled into one dataset. All other experiments were done at CDBS.

2.1.3 *Nlgn3*$^{-/y}$ deletion Sprague Dawley rat

Nlgn3$^{-/y}$ is a knockout mutation of *Nlgn3* bred on the sprague dawley background. The rat model was designed and engineered by Sigma Advanced Genetic Engineering (SAGE) Labs (A Horizon Discovery Group Company, St. Louis, Missouri, USA) using Zinc finger Technology. The Zinc finger nuclease target was within exon 5 and led to a 58bp deletion and a loss of the *Nlgn3* gene protein product.

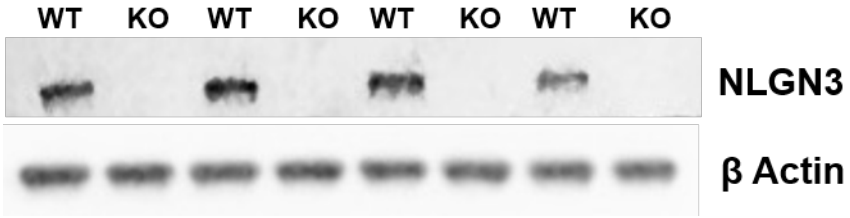

Figure 2.1: Validation of the *Nlgn3*$^{-/y}$ rat model. Western blots with homogenates from WT and *Nlgn3*$^{-/y}$ rats show absence of NLGN3 protein in the homozygous KOs (Western blots was supplied by Dr. Sarfaraz Nawaz, unpublished data).

2.1.4 *Syngap*$^{+/\Delta GAP}$ deletion Long Evans Hooded rats

Syngap$^{+/\Delta GAP}$ rats are missing the GAP domain and part of the C2 domain of SynGAP. They were designed in consultation with the Patrick Wild Centre (University of Edinburgh) and provided by Sage Labs (A Horizon Discovery Group Company, Saint-Louis, Missouri, USA), and were engineered using Zinc Finger nuclease with motifs to

delete exons 8-12. This resulted in an in-frame deletion encompassing amino acids 255 to 705. *Syngap*$^{+/\Delta GAP}$ were outbred on a Long Evans Hooded background. Reduction of SynGAP expression was confirmed through western blots and synaptosome preps of hippocampal homogenates (Fig. 2.2).

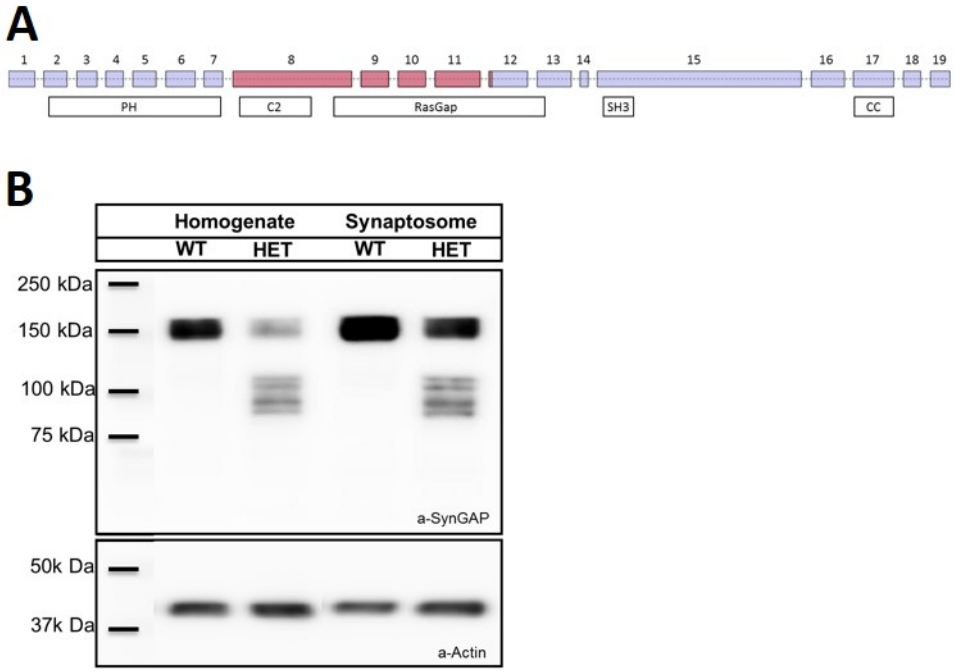

Figure 2.2: Confirmation of *Syngap*$^{+/\Delta GAP}$ rat model. (A) Schematic diagram of the *Syngap* gene with the deletion covering exon 8-12 in red. Below are the functional protein domains and their corresponding exon locations. (B) Western blot with hippocampus homogenates and synaptosome labelled with pan SynGAP antibody shows a 50% reduction in SynGAP expression in *Syngap*$^{+/\Delta GAP}$ heterozygous animals. Note that the SynGAP GAP domain deletion protein is also expressed in the heterozygous animals, and the truncated protein also reaches the synaptosome. WT band 134-140 kDA and truncated SynGAP band 95-100 kDA. (Western blots provided by Dr. Sarfaraz Nawaz, unpublished data).

2.1.5 *Syngap*$^{+/-}$ Long Evans Hooded rat

Syngap$^{+/-}$ is a null-deletion of SynGAP. It was generated by Horizon Discovery using CRISPR-Cas9 technology. A sgRNA target site was designed within exon 8 to insert 1bp at location 15589 in the genomic sequence. This resulted in several early stop codons after the insert, and no functional protein being translated. Reduction of SynGAP expression was confirmed through western blots and synaptosome preps of hippocampal homogenates (Fig. 2.3).

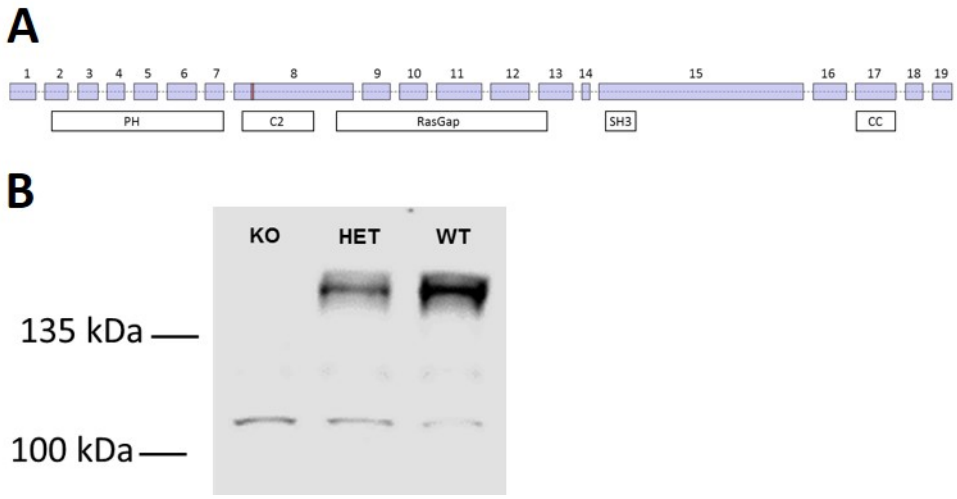

Figure 2.3: Validation of *Syngap*$^{+/-}$ rat model (A) Schematic diagram of the *SynGAP* gene with the 1bp insert shown in exon 8. (B) Western blot with hippocampus homogenates labelled with pan SynGAP antibody shows a 50% reduction in SynGAP expression in *Syngap*$^{+/-}$ heterozygous animals. WT band 134-140 kDA (Western blot provided by Shinjini Basu, unpublished data).

2.2 Genotyping

Genotyping was done either in house using the protocols described below, or sent to Transnetyx, inc., (Memphis, Tennessee, USA) who uses a real-time PCR method for genotyping.

2.2.1 DNA extraction

Tail or ear clips for genotyping were collected at weaning for animal identification or at the time of experimental culling. DNA extraction was done using the DNeasy Blood & Tissue kit (QIAGEN, Netherlands) following their provided protocol.

2.2.2 *Nlgn3*$^{-/y}$ Primers

A single assay was used for *Nlgn3*$^{-/y}$ genotyping using the following primers

***Nlgn3*$^{-/y}$ Primers**	**Sequence - 5'-3'**
Forward primer	CATCCGAGACAGTGGTGCTA
Reverse primer	AGAAAGCCCTTGGTATTCGG

2.2.3 *Syngap*$^{+/\Delta GAP}$ Primers

This genotyping protocol was designed using two assays - Assay 1 with primers on either side of the deletion to confirm the absence of the deletion (i.e. WT alleles). A positive result is only achieved in heterozygotes, since the distance between the primers is too great in the WTs; and Assay 2 with primers within the deletion giving a product in both WT and heterozygotes. The primers for the assays were as follows.

Syngap$^{+/\Delta GAP}$ **Primers**		**Sequence - 5'-3'**
Assay 1	Forward primer	GGCACCTTCCCCAAGTAAGT
	Reverse primer	TCACTTGGTGAGTGAGTGCC
Assay 2	Forward primer	ACTGCGAGTTATGCCTGGAC
	Reverse primer	CTCATTGTCTGGTAACGGGC

2.2.4 Polymerase Chain Reaction (PCR)

The PCR reaction mix for all primers were as listed in Table 2.1. The thermocycling conditions for *Nlgn3*$^{-/y}$ primers are shown in Table 2.2, and the conditions for *Syngap*$^{+/\Delta GAP}$ primers are shown in Table 2.3. The PCR products were run on a 2% agarose gel made in TBE buffer containing EtBr at 140V for 30min with a GeneRuler 100bp DNA ladder (Thermo Scientific, MA, USA).

Reagent	**Concentration (μL)**
Dream Green	6
Nuclease free water	3
10 μM Forward primer	1
10 μM Reverse primer	1
DNA	1

Table 2.1: PCR reaction mix

Cycle Step	**Temp** (°C)	**Time**	
1	95	5 min	
2	95	30 s	x 35 cycles
3	60	30 s	
4	68	45 s	
5	68	5 min	

Table 2.2: Thermocycling conditions for *Nlgn3*$^{-/y}$ primers

Cycle Step	Temp (°C)	Time	
1	95	5 min	
2	95	30 s	x 35 cycles
3	60	30 s	
4	68	60 s	
5	68	50 min	

Table 2.3: Thermocycling conditions for *Syngap*$^{+/\Delta GAP}$ primers

2.3 Electrophysiology preparation

2.3.1 Solutions

All chemicals used for electrophysiological experiments were purchased from Sigma-Aldrich (St Louis, MO, US), Abcam biochemicals (Cambridge, UK), Fisher Scientific (Hampton, NH, US), Tocris (Abingdon, UK), or HelloBio (Bristol, UK).

External solutions

	Cutting ACSF (mM)	Recording ACSF (mM)
NaCl	86	124
NaH_2PO_4	1.2	1.2
KCl	2.5	2.5
$NaHCO_3$	25	25
D-glucose	25	20
Sucrose	75	0
$CaCl_2$	0.5	2
$MgCl_2$	7	1

Table 2.4: External solutions. External solutions were continuously carbogenated with 95% O_2/5% CO_2

Intracellular solution: Cs-Gluconate (mM)	
CsOH	110
D-Gluconic Acid	110
CsCl	20
HEPES	10
NaCl	4
Mg-ATP	4
Na-GTP	0.3
EGTA	0.2
pCreatine	10

Table 2.5: Cs-Gluconate internal. Solution was adjusted to pH 7.30 with CsOH and osmolarity was ∼280-300 mOsm.L^{-1}

Intracellular solution: Cs-Cl (mM)	
CsCl	140
HEPES	10
Mg-ATP	5
Na-GTP	1
pCreatine	10
$MgCl_2$	2

Table 2.6: Cs-Cl internal. Solution was adjusted to pH 7.30 with CsOH and osmolarity was ∼280-300 mOsm.L^{-1}

Intracellular solution: K-Gluconate (mM)	
K-Gluconate	120
KCl	20
HEPES	10
NaCl	4
Mg-ATP	4
Na-GTP	0.3
pCreatine	10

Table 2.7: K-Gluconate internal. Solution was adjusted to pH 7.30 with CsOH and osmolarity was ∼280-300 mOsm.L^{-1}

2.3.2 Tissue Slicing

Animals were used at two different ages p12-p16 (p14) and p25-p32 (p28). To prepare acute coronal rat slices, rats were decapitated and the brains were rapidly dissected and placed in ice-cold carbogenated cutting artificial cerebral spinal fluid (ACSF) (Table 2.4). The cerebellum was removed before mounting the brain to the stage of the Leica VT12000S vibrating blade microtome (Leica Biosystems, Milton Keynes, UK). 400 μm thick coronal slices were prepared, while immersed in ice-cold carbogenated cutting ACSF. After slicing, the slices recovered at 34°C for 30 min after which they were stored at room temperature for at least 30 min before the start of experimentation.

2.3.3 Intracellular recordings

For whole-cell recordings, slices were transferred to a submerged recording chamber of an upright microscope (S-SCOPE-II, Scientifica, UK). Slices were continuosly perfused with carbogenated recording ACSF (Table 2.4) at a rate of 5 mL/min using a peristaltic pump. The temperature was managed using a HPT-2 inline heater (ALA Scientific, NY, US) and ranged from 24–30°C depending on the experimental design. Recordings were made using a MultiClamp 700B amplifier and a Digidata digitiser (CDBS: series 1440a; CBDR: series 1550a, Molecular Devices CA 94089 USA). Samples were digitised

at 20 kHz and low pass filtered at either 2 kHz for voltage clamp recordings or 10 kHz for current clamp recordings. Clampex Version 10 (Molecular Devices) was used as acquisition software.

Borosilicate Capillary glass with filament (OD 1.5 mm, ID 0.86 mm, Harvard Apparatus, UK) were used to pull patch pipettes (1.8-5 MΩ) on a horizontal puller (P-97 or P-1000 Flaming Brown, Sutter Instrument, US). These were then filled with the appropriate internal solution (Tabel 2.5-2.7).

Cells were visualised using IR-DIC video microscopy using a CCD camera (CDBS: SciCam Pro, Scientifica, UK; CBDR: IR-1000, Dage-MTI, US). After a principal cell was visually identified, a whole-cell recording was executed. Positive pressure was applied to the pipette, and using a micromanipulator (Patchstar, Scientifica, UK) the pipette was advanced through the tissue towards the cell. Pipette resistance was continuously monitored using the membrane test function in Clampfit (-5mV test step at 10 Hz). Positive pressure was released, when an small increase in pipette resistance was observed and a dimple on the cell could be visualised. Immediately hereafter, negative pressure was applied if necessary to form a giga-ohm seal (>1GΩ). Before breaking into the cell, pipette capacitance was compensated for. Short, sharp suctions of negative pressure were employed to rupture the cell membrane. Throughout the experiment, the access resistance was monitored, and a cell was accepted if it had a resting membrane potential lower than -55 mV and an access resistance <25 MΩ. If any of these properties changed by more than 25% during the recording, the recording was aborted.

2.3.4 Recording Paradigms

Passive membrane properties

To examine the intrinsic properties of cell (passive and active membrane properties), the following protocols were run after establishing whole-cell. The internal solution used for these experiments was a Potassium based internal (Table 2.7). A 1 minute of gap-free recording was done to measure the resting membrane potential (RMP) of the cell by switching the amplifier to the I=0 configuration. RMP was measured as the mean membrane voltage during this 1 min recording. Afterwards, the recording was switched to current clamp mode and the cell maintained at a set membrane potential at -70 mV for the remaining of the recording.

A series of small depolarising 500 ms steps of 25 pA was injected to calculate the

input resistance, capacitance, and membrane time constant of the cell. Input resistance, R_i, was calculated using Ohm's law

$$R = \frac{V}{I}$$

where V corresponds to the mean steady state voltage response during the 500 ms current injection, and I is the 25 pA current injection step. The membrane time constant, τ_M, was measured by fitting a single exponential curve between 10–90% of the rising phase of the membrane charging curve. Capacitance, C_M, was calculated using

$$C_M = \frac{\tau_M}{R_i}$$

The depolarising 'sag' potential seen at hyperpolarising currents is the result of activation of HCN channels, and is a measure of I_h. A series of -250 pA hyperpolarising steps was applied to calculate the sag ratio using the peak hyperpolarised potential and the steady-state voltage response

$$\frac{peak - steady\text{-}state}{peak} * 100$$

Active membrane properties

A series of depolarising current steps were applied in triplicate to investigate the neurons firing characteristics. The size of the steps depended on the age of the animal. For animals in the p14 age-group: 500 ms steps, 0 pA to +200 pA, 10 pA increments; For p28: 500 ms steps, 0 to +400 pA, 25 pA increments. The number of action potentials fired during the 500 ms was plotted against the injected current to get an F-I plot. The rheobase of the cell was taken as the first current step injection that evoked at least one action potential (AP). The rheobase current injection step was also used to measure AP waveform properties. AP threshold was defined as the voltage at which the derivative of the upsweep of the spike exceeded 10 $ms.mV^{-1}$. AP amplitude was determined as the maximal voltage peak measured from the threshold of the AP. AP half width was taken as the width at half the maximal spike response.

Next, post action potential currents were investigated. A train of 5 pulses of 2 nA, 2 ms at several fixed frequencies (20–100 Hz) was executed to measure the medium afte-

rhyperpolarisation (mAHP). The mAHP was quantified at the peak hyperpolarisation during the first 200 ms after the final AP. The slow afterhyperpolarisation was evoked using a train of 15 action potentials at 50 Hz elicited by 2 nA, 2 ms pulses and measured as the membrane potential deflection at 1 s after the current step. Lastly, to examine the afterdepolarisation (ADP) following an action potential, a single action potential was evoked using a 2 ms, 2 nA current pulse, and ADP was measured as the maximum depolarised potential following the AP.

Intrinsic properties were analysed using StimFit or using a custom made Matlab script (Dr. Adam Jackson, University of Edinburgh).

Synaptic events

After breakthrough and stable access was established, the cell was given 5 min to stabilise before mEPSCs/mIPSCs were acquired. During this time 300 nM Tetrodotoxin (TTX) was washed in with the recording ACSF and either 50 μM picrotoxin (PTX) for mEPSCs or 10 μM CNQX for mIPSCs. mEPSCs were recorded at a holding potential of -70 mV in voltage clamp mode using Cs-Gluconate internal (Table 2.5). mIPSCs were recorded at -70 mV using a high chloride Cs internal (Table 2.6). Stimfit was used to isolate individual mPSC events by using a template scaling matching algorithm (Guzman et al. (2014)). Events were extracted to excel, where mean amplitude and frequency was calculated. Only events with amplitudes exceeded 2×SD of baseline noise were included.

Synaptic currents

AMPA/NMDA ratios were collected by recording EPSCs in whole-cell voltage clamp mode by delivery of a single pulse. Test pulses were delivered to thalamic inputs to the LA at 0.05 Hz using a bipolar stimulating electrode placed in the internal capsule. Bipolar stimulating electrodes were made with twisted nickel/chromium (80%/20%) wire, and pulses were delivered by a DS3 Isolated Constant Current stimulator (Digitmer Ltd). First, AMPA EPSCs were recorded at -70 mV, followed by recordings at +40 mV to get the NMDA EPSCs. 15 trials for each were acquired which were averaged before analysis. The AMPA/NMDA ratios were calculated by dividing the average peak AMPA EPSC amplitude by the average NMDA amplitude measured at 50 ms after stimulation. All the recordings were done in the presence of 50 μM PTX.

Paired pulse facilitation

Paired pulse facilitation was recorded in whole-cell voltage clamp by delivering a pair of pulses with an interstimulus interval of 50 ms to the internal capsule and was recorded in the LA. The recordings were done in the presence of 50 μM PTX. The amplitude of the second EPSC was divided by the amplitude of the first to get the paired pulse ratios.

Synaptically induced LTP

5 to 6 weeks old animals were used for the LTP experiments. For synaptically induced LTP experiments were done in the lateral amygdala using high frequency stimulation consisting of two trains of 100 pulses at 30 Hz or 100 Hz with interstimulus interval of 20 s. Experiments were done in current clamp using K-Gluconate internal (Table 2.7) and with 50 μM PTX in the recording ACSF. Test pulses were delivered to thalamic inputs to the LA at 0.05 Hz using a bipolar stimulating electrode placed in the internal capsule. The baseline evoked EPSP was $\leq$10 mV to ensure that the cell did not fire action potentials during the LTP induction protocol. After the cell was broken into, a 5 min baseline was established and LTP was induced less than 11-12 min after breakthrough to avoid too much of the intracellular machinery needed for LTP to be washed out by the internal solution. LTP was quantified by normalising the slope (10–90%) of the EPSP to the average of the EPSP slopes of the 5 min baseline preceding LTP induction.

2.3.5 Data analysis and statistics

Data was analysed offline using Clampfit software (Molecular Devices, CA, US), Stimfit software 0.9.2–0.14 (Guzman et al. (2014)), GraphPad Prism 7 (GraphPad Software, CA, USA) or Excel 2013 (Microsoft).

Statistical analysis was carried out in GraphPad Prism7. Data is presented as animal mean $\pm$ SEM. Data was not tested for normality. Statistical comparison between groups was performed using unpaired two-tailed Student's t-test or two-way repeated measure ANOVA with Sidak post hoc analysis with animal numbers used as sample size. P values $<$0.05 were considered statistically significant and set as follows: *P$<$0.05; **P$<$0.01 and ***P$<$0.001. No statistical methods were used to predetermine the sample size, but the sample sizes are generally consistent with the literature. For power calculations 2-sample, 2-sided equality power analysis was performed using a power of 0.80 and Type

I error rate of 5% to calculate the sample size needed for the mean difference to be significant.

Chapter 3

Neuronal excitability and synaptic deficits across development in amygdala of *Nlgn3*$^{-/y}$ rats

3.1 Introduction

NLGNs have distinct distributions at excitatory and inhibitory synapses, barring NLGN3 that can be found at both types (Song et al. (1999); Graf et al. (2004); Varoqueaux et al. (2004); Budreck and Scheiffele (2007)). At the synapse, the neurexin-neuroligin complex forms a trans-synaptic bridge that facilitates pre–post synaptic alignment, and thus regulates synaptic efficacy by aligning pre-synaptic release sites with post-synaptic AMPAR nanodomains (Haas et al. (2018)). The role of NLGNs in synapses has been studied, since NLGN1 was first identified as a binding partner to NRXN (Ichtchenko et al. (1995)), though there are still some discrepancies regarding what that role might be. There is a large body of evidence, primarily from culture work, indicating that NLGNs has a key role in the initial formation of synapses (Scheiffele et al. (2000); Chih et al. (2004); Graf et al. (2004); Chih et al. (2005); Ko et al. (2009); Shipman et al. (2011); Kwon et al. (2012)), whereas others hypothesise that NLGNs specify and validate synapses and maintain their function after initial formation, instead of promoting synapse formation (Chubykin et al. (2007); Kim et al. (2008); Blundell et al. (2010); Liang et al. (2015); Zhang et al. (2015); Jiang et al. (2016); Chanda et al. (2017)). All of the NLGN isoforms have now been associated with ASD (Jamain et al. (2003); Deciphering Developmental Disorders (2015); Nakanishi et al. (2017); Parente et al. (2017)), and the importance of NLGNs for normal brain function is thus hard to dispute, whether that be in formation of synapses, specifying and maintaining their function, or both.

The amygdala plays a key role in fear learning, anxiety and general processing of emotional states, which are some of the characteristic behavioural measures that are altered in individuals with ASD. One way to examine emotional behaviours in animals models of ASD is by measuring fear states elicited by auditory fear conditioning. The thalamic input to the LA brings in auditory afferents involved in fear response, and synaptic plasticity at these synapses is thought to be the cellular mechanism underlying auditory fear conditioning (Pape and Pare (2010)). Given the role of NLGNs in synaptic function, you might expect their absence to have an effect on synaptic plasticity, and on the behavioural outcomes dependent on it. Knock-down or knock-out of NLGN1 in the amygdala results in an abolishment of LTP in thalamo-amygdala synapses of LA principal neurons, and a reduction in freezing during cued fear recall (Kim et al. (2008); Jung et al. (2010)), confirming that NLGNs play an important role in amygdala function and amygdala-dependent behaviour. However, how NLGN3 functions in the amygdala, and what its absence might lead to has not been studied previously. Based on the known functional role of NLGN1 in this brain area, and NLGN3's strong association with ASD, I hypothesise that a reduction in NLGN3 will result in altered basal synaptic function, and that *Nlgn3*$^{-/y}$ rats will display deficits in LTP at thalamo-amygdala synapses in LA.

To test this hypothesis, I investigated intrinsic excitability and synaptic transmission of principal neurons in developing and more mature synapses in the BLA in the *Nlgn3*$^{-/y}$ rat model. Furthermore, I explored the actions of NLGN3 on long term potentiation at thalamic synapses onto the LA.

3.2 Results

3.2.1 No changes were observed in intrinsic excitability in *Nlgn3*$^{-/y}$ LA principal neurons at p14.

Intrinsic cell properties were assessed by a range of current injection protocols in LA principal neurons at p12 to p16 (hereafter denoted as p14) in WT and *Nlgn3*$^{-/y}$ rats. Several passive membrane properties were examined (RPM, membrane time constant, input resistance, capacitance, and sag). *Nlgn3*$^{-/y}$ LA principal neurons showed comparable passive properties to that of their WT littermates on all of these parameters (Fig. 3.1).

Next, intrinsic cell excitability was examined by injecting a sequence of depolarising

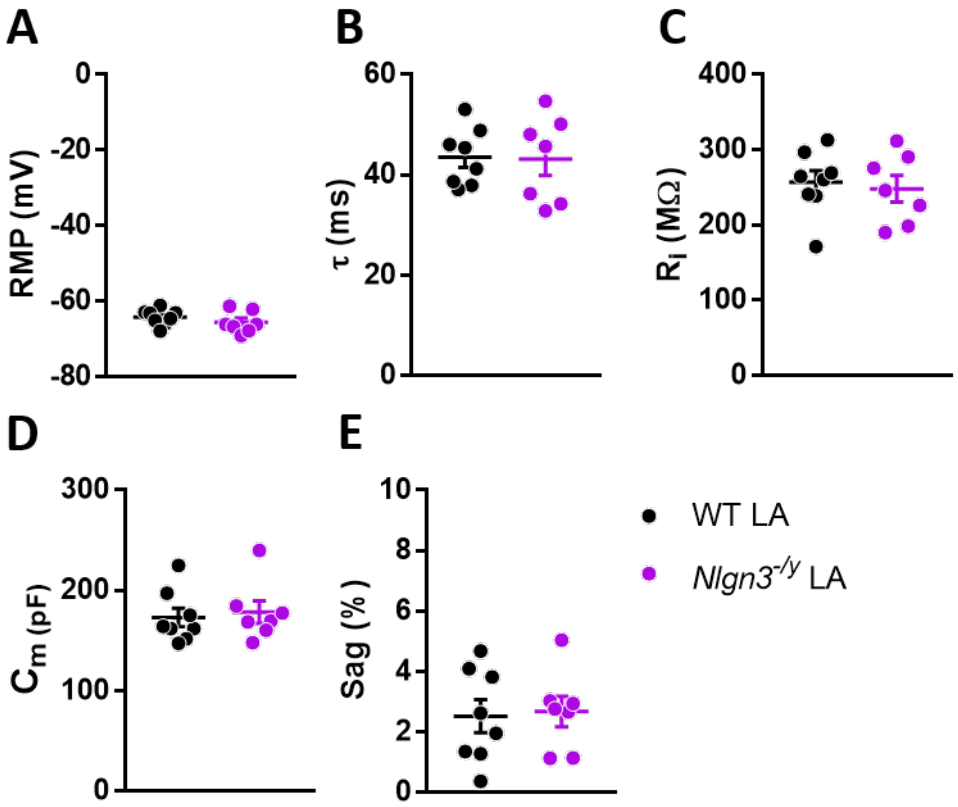

Figure 3.1: Passive membrane properties are comparable between WT and *Nlgn3*$^{-/y}$ LA principal neurons at p14. (A) Resting membrane potential measured during 1 min of I=0 shows that *Nlgn3*$^{-/y}$ LA neurons have a comparable RMP to WT (WT: -64.26 ± 0.75 mV, n=25 cells/8 animals; KO: -65.64 ± 1.08 mV, n=20 cells/7 animals; p=0.30, Student's unpaired *t*-test). (B) The membrane time constant, τ, was not significantly different between the genotypes (WT: 43.53 ± 2.03 ms, n=25 cells/8 animals; KO: 43.12 ± 3.26 ms, n=20 cells/7 animals; p=0.92, Student's unpaired *t*-test). (C) The input resistance of *Nlgn3*$^{-/y}$ LA neurons was comparable to that of WT (WT: 256.90 ± 15.18 MΩ, n=25 cells/8 animals; KO: 248.30 ± 17.51 MΩ, n=20 cells/7 animals; p=0.71, Student's unpaired *t*-test). (D) The capacitance of the cells was comparable between genotypes (WT: 173.00 ± 9.15 pF, n=25 cells/8 animals; KO: 178.40 ± 11.14 pF, n=20 cells/7 animals; p=0.71, Student's unpaired *t*-test). (E) *Nlgn3*$^{-/y}$ LA neurons showed a comparable sag to WT (WT: 2.52 ± 0.55 %, n=25 cells/8 animals; KO: 2.67 ± 0.50 %, n=20 cells/7 animals; p=0.84, Student's unpaired *t*-test).

current steps ranging from 0 to +200 pA in 10 pA increments. This revealed a similar firing frequency between WT and *Nlgn3*$^{-/y}$ LA principal neurons (Fig.3.2B). The rheobase, i.e. the amount of current needed to elicit at least one action potential during a step, was also similar between the two genotypes (Fig. 3.2C). Analysing the action potential waveforms and kinetics revealed significant differences in AP amplitude (Fig. 3.2E; WT: 73.46 ± 0.92mV, n=25 cells/8 animals; KO: 77.19 ± 1.28mV, n=20 cells/7 animals; p=0.03) and the AP maximum rise rate (Fig. 3.2H; WT: 213.70 ± 20.57mV/ms, n=25 cells/8 animals; KO: 286.70 ± 17.7mV/ms, n=20 cells/7 animals; p=0.02), however no other measurements were significantly different. Given that no changes were observed in firing frequency or other AP waveforms and kinetics, these changes were taken with reservation.

After a train of action potentials follows a hyperpolarising current, called afterhyperpolarisation (AHP), which is important in regulating cell excitability (Alger and Nicoll (1980); Hotson and Prince (1980)). AHP has two components defined by their timings, medium and slow AHP. The medium AHP (mAHP) follows immediately after the train and decays within 200 ms. The slow AHP (sAHP) peaks after the mAHP and decays within several seconds (Sah and Faber (2002)). Since mAHP can be affected by both the number of action potentials in the train and the frequency of them (Abel et al. (2004)), the mAHP was investigated by using a train of 5 pulses at several fixed frequencies covering 20–100 Hz.

The mAHP increased initially at higher frequencies before plateauing in WT with similar levels of mAHP observed in *Nlgn3*$^{-/y}$ LA principal neurons at all frequencies (Fig. 3.3B). sAHP was evoked with a train of 15 action potentials at 50 Hz and measured 1 s after the current step to ensure that the mAHP had decayed. No difference was observed in sAHP between WT and *Nlgn3*$^{-/y}$ (Fig. 3.3D). To investigate the afterdepolarisation (ADP) following an action potential, a single action potential was elicited, and the ADP measured as the peak depolarisation following an action potential. This showed no differences in ADP between the two genotypes (Fig. 3.3F). Thus, the absence of NLGN3 in LA principal neurons has no measurable effect on post action potential currents.

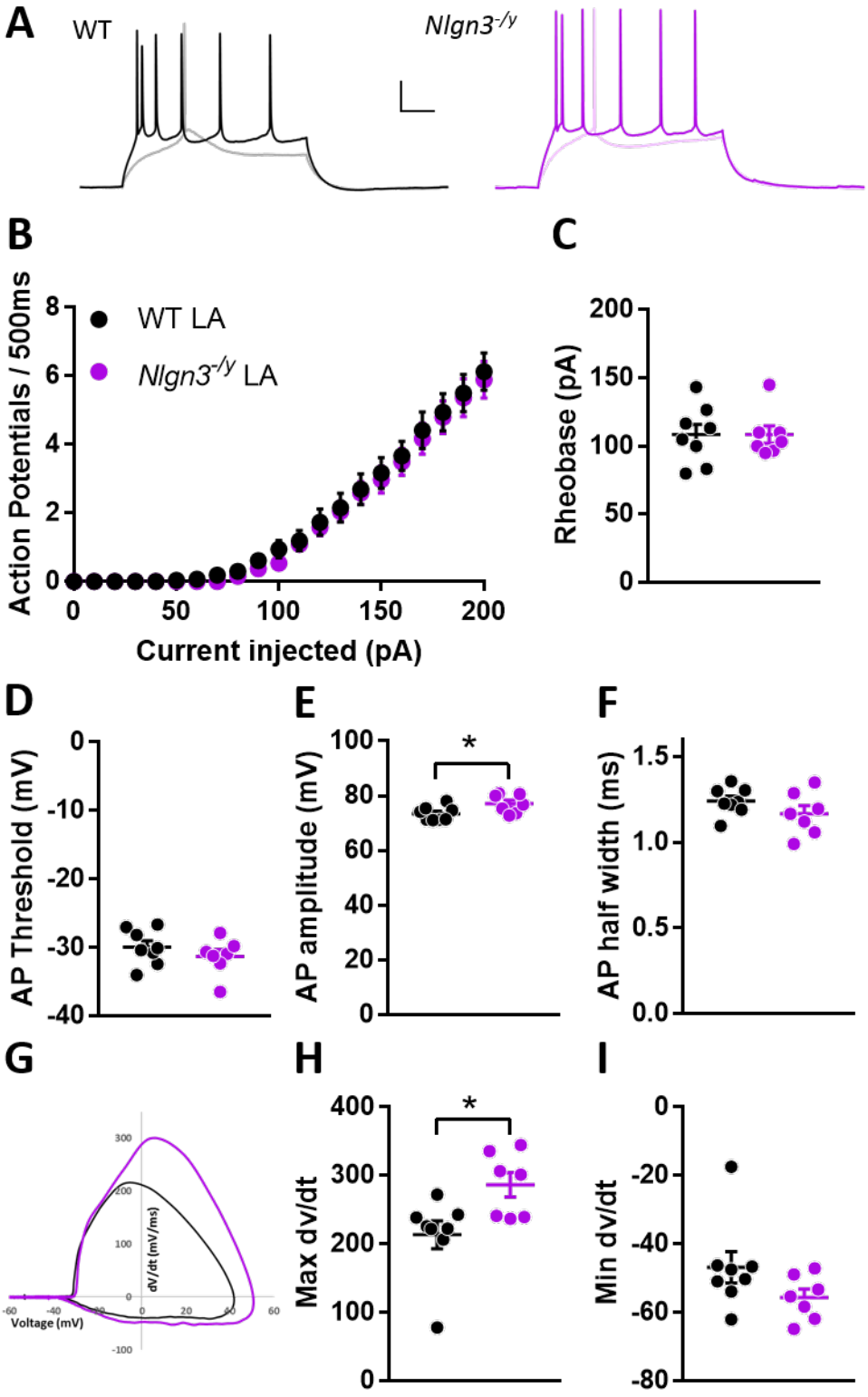

Figure 3.2: Intrinsic excitability are unaltered in *Nlgn3*$^{-/y}$ LA principal neurons at p14. (A) Example traces of WT and *Nlgn3*$^{-/y}$ neuron voltage responses to rheobase and +200 pA current steps. Scale 100ms, 20 mV. (B) LA *Nlgn3*$^{-/y}$ neurons firing frequency to a series of depolarising current injections (0-200pA) are comparable to that of WT ((F(1,13)=2.354; p=0.15, 2way RM-ANOVA). (C) Rheobase was comparable between genotypes (WT: 108.50 ± 7.52pA, n=25 *(continued on next page)*

Figure 3.2: *(continued)* cells/8 animals; KO: 108.60 ± 6.47pA, n=20 cells/7 animals; p=0.99. Student's unpaired *t*-test). (D) The AP threshold of LA neurons was not significantly changed in *Nlgn3*$^{-/y}$ compared to WT (WT: -29.92 ± 0.91 mV, n=25 cells/8 animals; KO: -31.30 ± 1.01 mV, n=20 cells/7 animals; p=0.33, Student's unpaired *t*-test). (E) *Nlgn3*$^{-/y}$ AP amplitude was significantly larger than WT (WT: 73.46 ± 0.92 mV, n=25 cells/8 animals; KO: 77.19 ± 1.28 mV, n=20 cells/7 animals; p=0.03, Student's unpaired *t*-test). (F) The AP half width was similar between genotypes (WT: 1.24 ± 0.03 ms, n=25 cells/8 animals; KO: 1.17 ± 0.05 ms, n=20 cells/7 animals; p=0.19, Student's unpaired *t*-test). (G) Phase plot of action potential in WT (black) and *Nlgn3*$^{-/y}$(purple) LA neuron. (H) Max dvdt is significantly increased in *Nlgn3*$^{-/y}$ LA neurons compared to WT (WT: 213.70 ± 20.57 mV/ms, n=25 cells/8 animals; KO: 286.70 ± 17.7 mV/ms, n=20 cells/7 animals; p=0.02, Student's unpaired *t*-test), but (I) min dvdt was similar between genotypes (WT: -46.82 ± 4.58 mV/ms, n=25 cells/8 animals; KO: -55.63 ± 2.46 mV/ms, n=20 cells/7 animals; p=0.13, Student's unpaired *t*-test).

3.2.2 LA principal neurons at p28 are hyperexcitable in *Nlgn3*$^{-/y}$

NLGNs are expressed at low levels at early postnatal age and upregulated in parallel during postnatal development (Song et al. (1999); Varoqueaux et al. (2006)). Peak expression is reached >3 weeks after birth, and it is therefore possible that changes in cellular and synaptic function will emerge later in postnatal development. I therefore repeated the experiments above at p25 to p32 (hereafter denoted as p28), to investigate what the long term effect of absence of NLGN3 would be. A slightly different protocol was used for the F/I plot. The neurons at p28 are more mature, and thus have a lower input resistance and higher capacitance. This means they need more current before firing, and you can inject more current into the cell before it goes into depolarising block. I therefore chose a set of depolarising steps going from 0 to +400 pA in 25 pA increments. This would allow me to get more information about the firing pattern of the cells, than if I had used the same protocol for the p14 neurons.

Similarly to p14, *Nlgn3*$^{-/y}$ LA neurons at p28 displayed no significant changes in any of the passive membrane properties measured (Fig. 3.4). However, when measuring the frequency of firing upon increasing depolarising current steps, a hyperexcitability was observed in these neurons (Fig. 3.5B; 2way RM-ANOVA show effect of interaction $F(16,304)=9.994$; $p<0.001$). This was not reflected in a significantly lower rheobase using Student's *t*-test (WT: 150.8 ± 13.85 pA, n=31 cells/11 animals; KO: 125 ±7.76 pA, n=29 cells/10 animals; p=0.13, Student's unpaired *t*-test).

No changes were observed in the AP waveform or kinetics (Fig.3.5D-I), indicating that changes in the active cation currents underlying the AP does not contribute to the increased firing observed in these neurons.

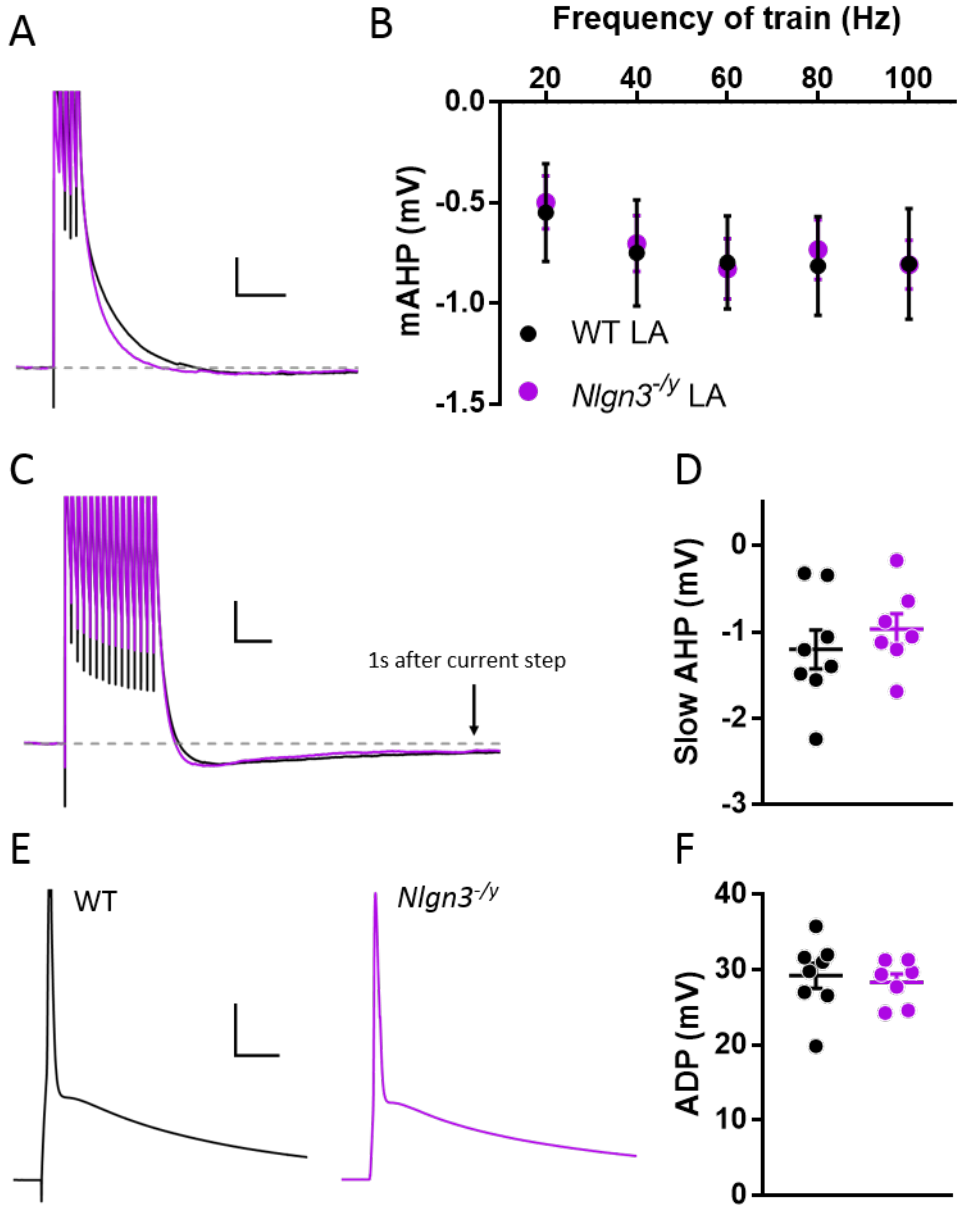

Figure 3.3: Post burst AHP are not changed in *Nlgn3*$^{-/y}$ LA principal neurons at p14. (A) Example traces of the maximum mAHP evoked by a train of 5 pulses at 100 Hz in WT (black) and *Nlgn3*$^{-/y}$ (purple) BA neurons. Scale 100 ms, 5 mV. (B) Average mAHP after a train of 5 pulses at varying frequencies shows no significant differences between genotypes ($F(1,13)=0.009$; $p=0.93$, 2way RM-ANOVA). (C) Example traces of sAHP measured 1 s after the train of 15 action potentials at 50 Hz. Scale 100 ms, 5 mV. (D) No significant difference was observed in sAHP between the two genotypes (WT: -1.20 ± 0.22 mV, n=24 cells/8 animals; KO: -0.97 ± 0.18 mV, n=20/7 animals; p=0.44, Student's unpaired *t*-test). (E) Example traces of ADP following a single action potential. Scale 10 ms, 20 mV. (F) The ADP after a single action potential is comparable between WT and *Nlgn3*$^{-/y}$ LA neurons (WT: 29.21 ± 1.70 mV, n=25 cells/8 animals; KO: 28.32 ± 1.11 mV, n=20 cells/7 animals; p=0.68, Student's unpaired *t*-test.)

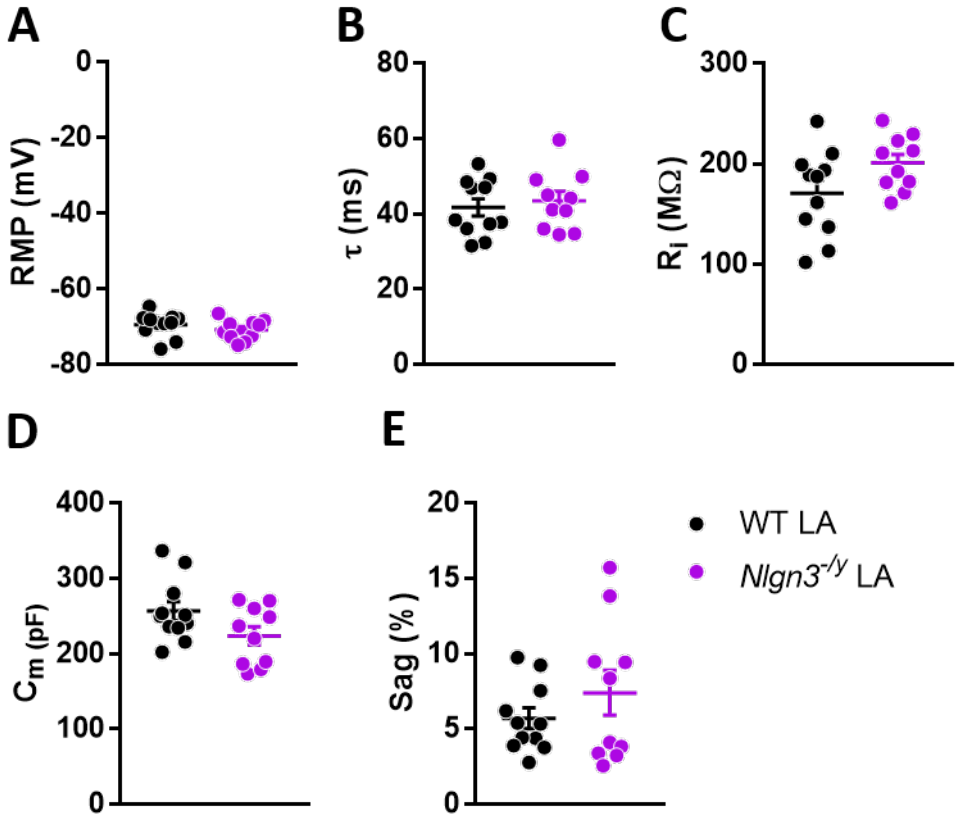

Figure 3.4: Passive membrane properties are comparable between WT and *Nlgn3*$^{-/y}$ LA principal neurons at p28. (A) Resting membrane potential measured during 1 min of I=0 shows that *Nlgn3*$^{-/y}$ LA neurons have a comparable RPM to WT (WT: -69.41 ± 0.95 mV, n=30 cells/11 animals; KO: -70.80 ± 0.86 mV, n=29 cells/10 animals; p=0.29, Student's unpaired *t*-test). (B) The membrane time constant, τ, was not significantly different between the genotypes (WT: 41.73 ± 2.26 ms, n=30 cells/11 animals; KO: 43.54 ± 2.50 ms, n=29 cells/10 animals; p=0.60, Student's unpaired *t*-test). (C) The input resistance was comparable between genotypes (WT: 170.90 ± 12.99 MΩ, n=30 cells/11 animals: KO: 200.90 ± 8.54 MΩ, n=29 cells/10 animals; p=0.08, Student's unpaired *t*-test). Power analysis revealed that a sample size of 19 WTs/21 KOs is needed to reach significance. (D) Membrane capacitance was not significantly different in *Nlgn3*$^{-/y}$ compared to WT (WT: 256.80 ± 12.45 pF, n=30 cells/11 animals: KO: 223.80 ± 12.33 pF, n=29 cells/10 animals; p=0.08, unpaired *t*-test). Power analysis revealed that a sample size of 20 WTs/23 KOs is needed to reach significance. (E) Sag, a measure of I_h, was similar between genotypes (WT: 5.72 ± 0.69%, n=30 cells/11 animals: KO: 7.41 ± 1.49%, n=29 cells/10 animals; p=0.32, unpaired Welch's *t*-test). Power analysis of the sag data revealed that a sample size of 61WTs/68 KOs is necessary for the change in I_h to be significantly increased in *Nlgn3*$^{+/-}$

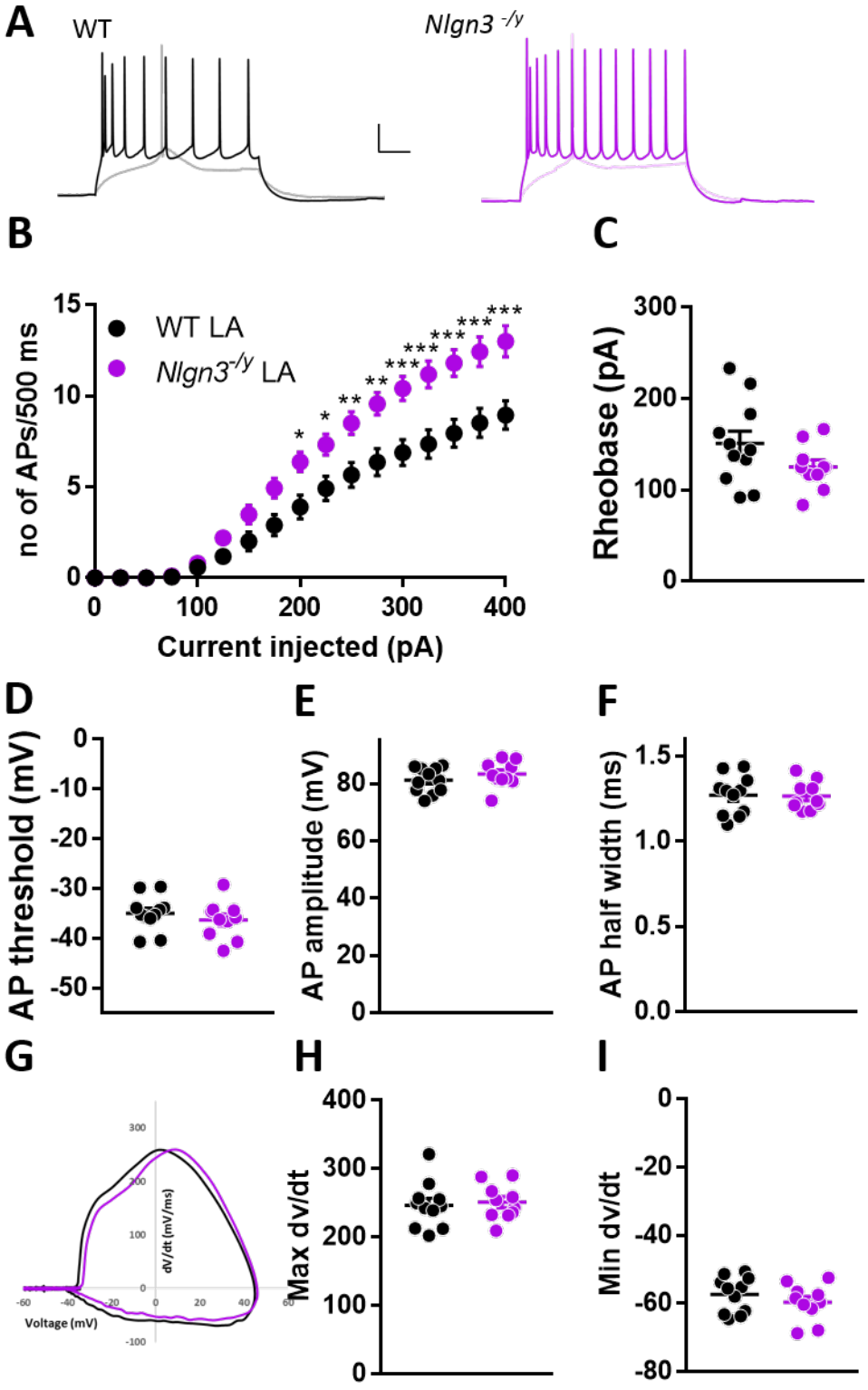

Figure 3.5: *Nlgn3*$^{-/y}$ LA principal neurons at p28 have an increased firing rate compared to WT. (A) Example traces of WT and *Nlgn3*$^{-/y}$ neuron voltage responses to rheobase and +400 pA current steps. Scale 100ms, 20 mV. (B) LA *Nlgn3*$^{-/y}$ neurons firing frequency to a series of depolarising current injections (0-400pA) are increased to that of WT (Effect of interaction: $F(16,304)=9.994$; $p<0.001$, 2way RM-ANOVA with Sidak's post hoc test). (C) Rheobase was not significantly lower in *Nlgn3*$^{-/y}$ *(continued on next page)*

Figure 3.5: *(continued)* compared to WT (WT: 150.8 ± 13.85 pA, n=31 cells/11 animals; KO: 125 ±7.76 pA, n=29 cells/10 animals; p=0.13, Student's unpaired *t*-test). Power analysis showed that 25 WTs/28 KOs are needed to reach significance. (D) AP threshold was comparable between the two genotypes (WT: -34.97 ± 1.05 mV, n=31 cells/11 animals; KO: -36.32 ± 1.19 mV, n=29/10 animals; p=0.40, Student's unpaired *t*-test). (E) AP amplitude from threshold was not different in *Nlgn3*$^{-/y}$ (WT: 81.14 ± 1.32 mV, n=31 cells/11 animals; KO: 83.23 ± 1.42 mV, n=29/10 animals; p=0.29, Student's unpaired *t*-test). (F) AP half width was similar between the two genotypes (WT: 1.27 ± 0.03 ms, n=31 cells/11 animals; KO: 1.27 ± 0.03 ms, n=29/10 animals; p=0.91, Student's unpaired *t*-test). (G) Phase plot of action potential in WT (black) and *Nlgn3*$^{-/y}$ (purple) LA neuron. (H) Max dvdt was not significantly different between WT and *Nlgn3*$^{-/y}$ (WT: 247.00 ± 10.05 mV/ms, n=31 cells/11 animals: KO: 251.30 ± 8.15 mV/ms, n=29 cells, 10 animals; p=0.75, Student's unpaired *t*-test), nor was min dvdt (I) (WT: -57.32 ± 1.58 mV/ms, n=31 cells/11 animals; KO: -59.62 ± 1.70 mV/ms, n=29 cells/10 animals; p=0.33, Student's unpaired *t*-test).

As described above, the post AP currents can affect the excitability of a cell, so these were measured to see if they were contributing to the increase in firing rate seen in the *Nlgn3*$^{-/y}$ p28 LA neurons. Neither mAHP, sAHP, or ADP (Fig. 3.6) showed an effect of genotype. Thus, the post action potential currents are not underlying the changes in firing frequency in these neurons.

3.2.3 Intrinsic properties are unaltered in BA principal neurons at p14

Despite the fact that LA and BA are often grouped together as one overall nuclei, they are two distinct nuclei exhibiting different properties and exerting different roles in fear learning and memory (Rainnie et al. (1993); Faber et al. (2001); LeDoux (2003)). Thusly, I wanted to investigate the effect the absence of NLGN3 would have on the development of the principal neurons of the BA as well.

Looking at the passive membrane properties revealed slight trends, but no significant differences between WT and *Nlgn3*$^{-/y}$ BA neurons (Fig. 3.7). The firing rate upon depolarising current steps was slightly lower in *Nlgn3*$^{-/y}$ compared to WT, but no significant genotype effect was observed (Fig. 3.8B). Rheobase was also comparable between WT and *Nlgn3*$^{-/y}$ BA principal neurons (Fig. 3.8C), as were the AP waveform and kinetics (Fig. 3.8D-I).

Next I looked at the post AP currents in the *Nlgn3*$^{-/y}$ BA principal cells at p14, and found that mAHP, sAHP, and ADP were all comparable to WT (Fig. 3.9). Thus, absence of NLGN3 has no apparent effect on intrinsic cell properties in BA principal neurons.

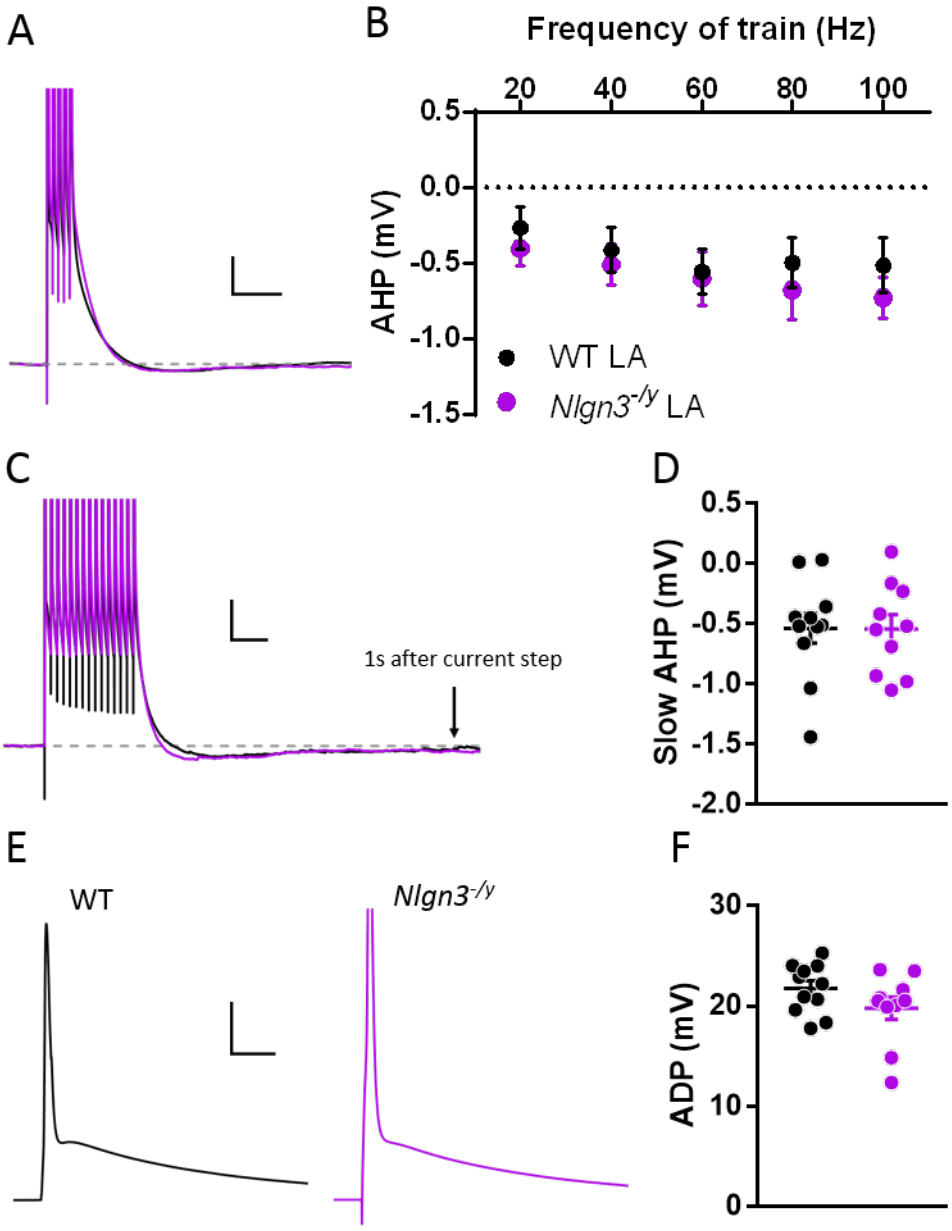

Figure 3.6: Post burst AHP are not changed in *Nlgn3*$^{-/y}$ LA principal neurons at p28. (A) Example traces of the maximum mAHP evoked by a train of 5 pulses at 100 Hz in WT (black) and *Nlgn3*$^{-/y}$ (purple) BA neurons. Scale 100ms, 5 mV. (B) Average mAHP after a train of 5 pulses at varying frequencies shows no significant differences between genotypes ($F(1,19)=0.3974$; $p=0.54$, 2way RM-ANOVA). (C) Example traces of sAHP measured 1s after the train of 15 action potentials at 50 Hz. Scale 100 ms, 5mV. (D) No significant difference was observed in sAHP between the two genotypes (WT: -0.54 ± 0.13 mV, n=30 cells/11 animals; KO: -0.54 ± 0.12 mV, n=29 cells/10 animals; p=0.97, Student's unpaired *t*-test). (E) Example traces of ADP following a single action potential. Scale 10 ms, 20 mV. (F) The ADP after a single action potential is comparable between WT and *Nlgn3*$^{-/y}$ LA neurons (WT: 21.76 ± 0.74 mV, n= 30 cells/11 animals; KO: 19.78 ± 1.12 mV, n=29 cells/10 animals; p=0.15, Student's unpaired *t*-test.). Power analysis revealed that 31 WTs/35 KOs are needed for statistical significance.

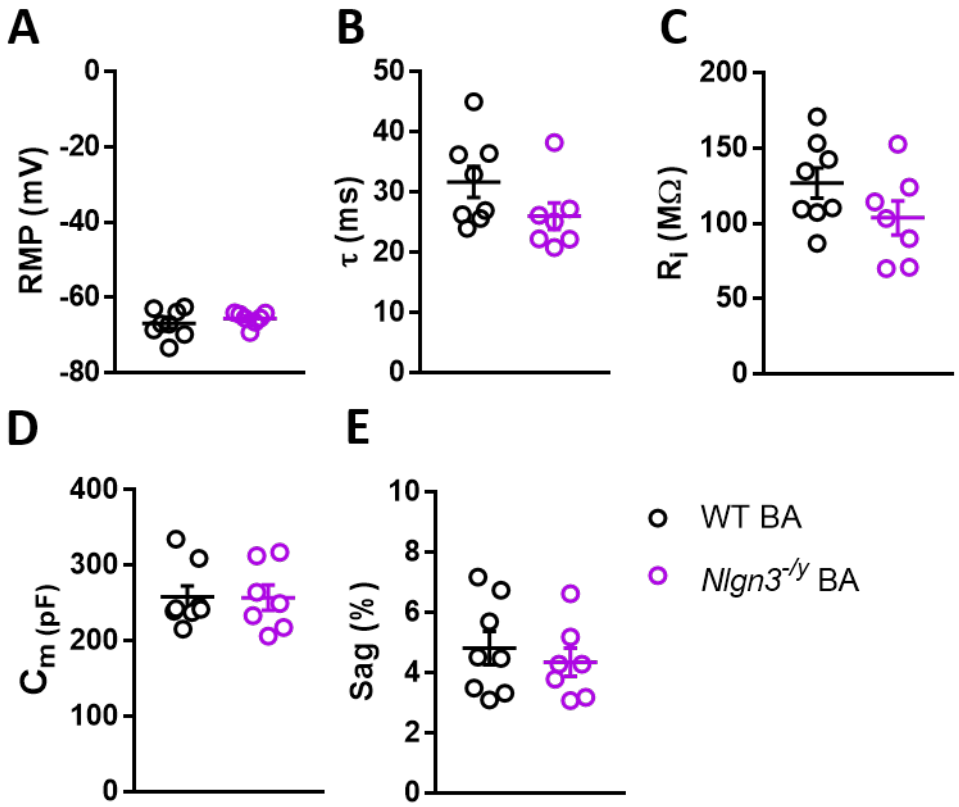

Figure 3.7: Passive membrane properties are comparable between WT and *Nlgn3*$^{-/y}$ BA principal neurons at p14. (A) Resting membrane potential measured during 1 min of I=0 shows that *Nlgn3*$^{-/y}$ BA neurons have similar RPM to WT (WT: -66.89 ± 1.32mV, n=25 cells/8 animals; KO: -65.61 ± 0.69 mV, n=22 cells/7 animals; p=0.43, Student's unpaired *t*-test). (B) The membrane time constant, τ, was comparable between the genotypes (WT: 31.72 ± 2.57 ms, n=25 cells/8 animals; KO: 26.03 ± 2.22 ms, n=22 cells/7 animals; p=0.12, Student's unpaired *t*-test). (C) The input resistance of *Nlgn3*$^{-/y}$ LA neurons was not significantly different to WT (WT: 127.10 ± 9.92 MΩ, n=25 cells/8 animals; KO: 103.80 ± 11.27 MΩ, n=22 cells/7 animals; p=0.14, Student's unpaired *t*-test). (D) The capacitance of the cells was comparable between genotypes (WT: 258.60 ± 14.43 pF, n=25 cells/8 animals; KO: 257.60 ± 16.56 pF, n=22 cells/7 animals; p=0.96). (E) *Nlgn3*$^{-/y}$ LA neurons showed similar level of sag to WT (WT: 4.82 ± 0.55 %, n=25 cells/8 animals; KO: 4.36 ± 0.47 %, n=22 cells/7 animals; p=0.54, Student's unpaired *t*-test).

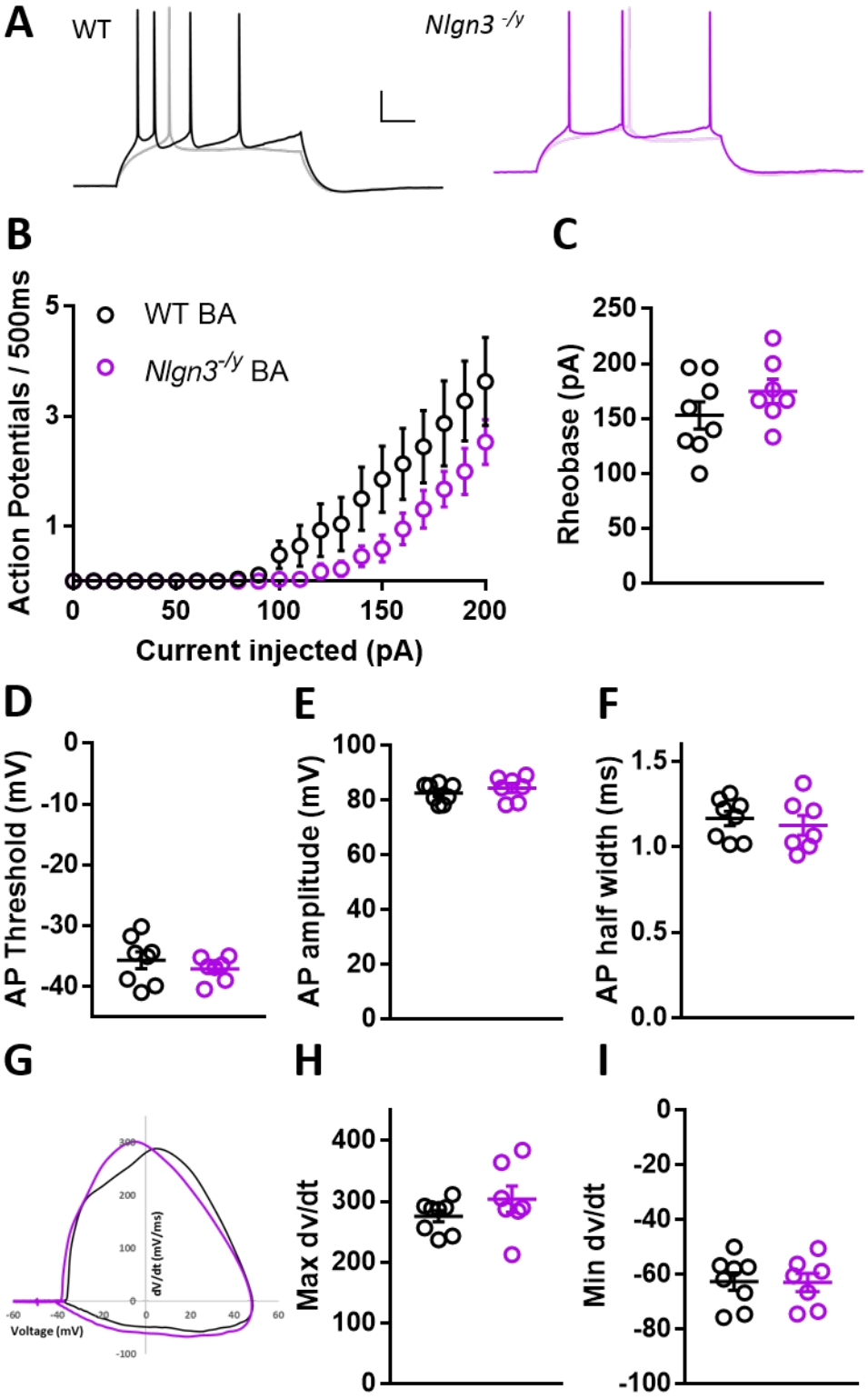

Figure 3.8: Intrinsic properties are unaltered in *Nlgn3*$^{-/y}$ BA principal neurons at p14. (A) Example traces of WT and *Nlgn3*$^{-/y}$ neuron voltage responses to rheobase and +200 pA current steps. Scale 100 ms, 20 mV. (B) BA *Nlgn3*$^{-/y}$ neurons firing frequency to a series of depolarising current injections (0-200pA) are comparable to that of WT ((F(1,13)=0.1819; p=0.68, 2way RM-ANOVA). (C) Rheobase was similar between genotypes (WT: 153.10 ± 12.35 pA, *(continued on next page)*

Figure 3.8: *(continued)* n=25 cells/8 animals; KO: 174.9 ± 11.07pA, n=22 cells/7 animals; p=0.22, Student's unpaired *t*-test). (D) The AP threshold of BA neurons was comparable between genotypes (WT: -35.68 ± 1.37 mV, n=25 cells/8 animals; KO: -37.09 ± 0.75 mV, n=22 cells/7 animals; p=0.40, Student's unpaired *t*-test). (E) *Nlgn3*$^{-/y}$ AP amplitude was not significantly different to WT (WT: 82.70 ± 1.22 mV, n=25 cells/8 animals; KO: 84.53 ± 1.2 mV, n=22 cells/7 animals; p=0.38, Student's unpaired *t*-test). (F) The AP half width was similar between genotypes (WT: 1.17 ± 0.04 ms, n=25 cells/8 animals; KO: 1.13 ± 0.06 ms, n=22 cells/7 animals; p=0.57, Student's unpaired *t*-test). (G) Phase plot of action potential in WT (black) and *Nlgn3*$^{-/y}$ (purple) BA neuron. (H) Max dvdt is comparable in *Nlgn3*$^{-/y}$ BA neurons to WT (WT: 275.90 ± 9.42 mV/ms, n=25 cells/8 animals; KO: 304.00 ± 21.39 mV/ms, n=22 cells/7 animals; p=0.23, Student's unpaired *t*-test), as is (I) min dvdt (WT: -62.57 ± 3.21 mV/ms, n=25 cells/8 animals; KO: -62.91 ± 3.38 mV/ms, n=22 cells/7 animals; p=0.94, Student's unpaired *t*-test).

3.2.4 BA principal neurons at p28 display increased firing rate in *Nlgn3*$^{-/y}$

As with the LA, I also investigated what a longer term consequence of NLGN3 absence would be on BA principal neurons. Similar to p14 BA principal neurons, no changes were observed in passive membrane properties (Fig. 3.10A-D), except for sag, which was increased in *Nlgn3*$^{-/y}$ compared to WT (Fig. 3.10E; WT: 7.28 ± 0.64%, n=27 cells/10 animals: KO: 10.04 ± 0.89%, n=30 cells/10 animals; p=0.02, Student's unpaired *t*-test).

Unlike *Nlgn3*$^{-/y}$ BA principal neurons at p14 that showed a slight, though not significant decrease in firing rate compared to WT (Fig.3.8B), *Nlgn3*$^{-/y}$ BA principal neurons at p28 displayed an increase in firing compared to WT with significance for interaction (Fig. 3.11B; F(16,288)=2.17; p<0.01, 2Way RM-ANOVA). Rheobase was comparable between the two genotypes (Fig. 3.11C), as were AP waveform and kinetics (Fig. 3.11D-I).

I_h has been found to assist in the generation of mAHP (Oswald et al. (2009)), thus one might expect to find a change in mAHP in *Nlgn3*$^{-/y}$ BA principal neurons, since a difference was observed in sag in these neurons (Fig. 3.10E). A decrease in mAHP was seen across all frequencies tested in the *Nlgn3*$^{-/y}$, but no significant effect of genotype was found with 2way ANOVA (Fig. 3.12B; F(1,18)=2.119; p=0.16, Student's unpaired *t*-test). sAHP was found to be comparable between *Nlgn3*$^{-/y}$ and WT (Fig. 3.12), as were ADP (Fig. 3.12F).

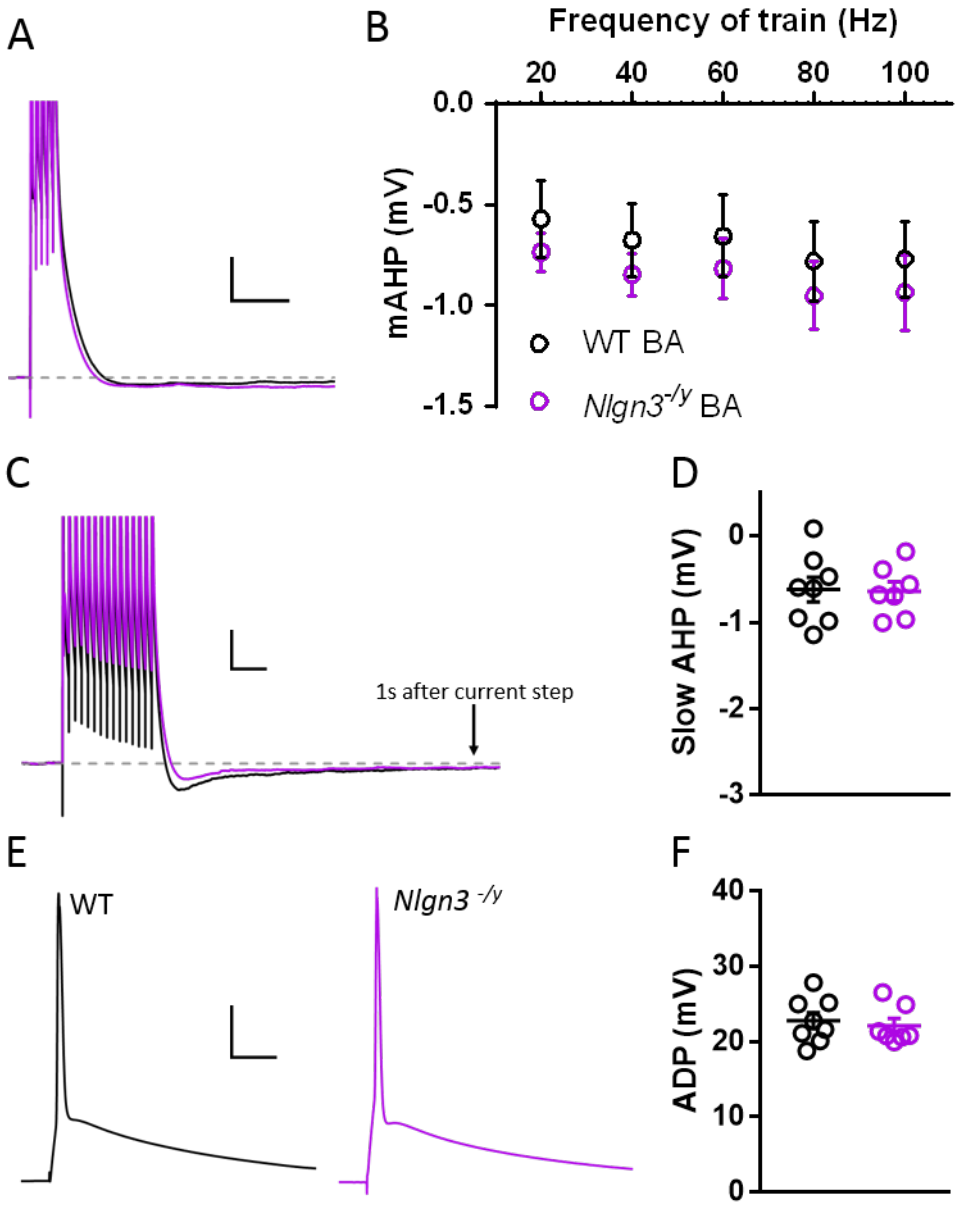

Figure 3.9: Post burst AHP are not changed in *Nlgn3*$^{-/y}$ BA principal neurons at p14. (A) Example traces of the maximum mAHP evoked by a train of 5 pulses at 100 Hz in WT (black) and *Nlgn3*$^{-/y}$ (purple) BA neurons. Scale 100 ms, 5 mV. (B) Average mAHP after a train of 5 pulses at varying frequencies. No significant difference was observed between genotypes ($F(1,13)=0.5055$; $p=0.50$, 2way RM-ANOVA). (C) Example traces of sAHP measured 1s after the train of 15 action potentials at 50 Hz. Scale 100 ms, 5 mV. (D) Average sAHP are comparable between the two genotypes (WT: -0.62 ± 0.14 mV, n=25 cells/8 animals; KO: -0.64 ± 0.18 mV, n=20/7 animals; p=0.92, Student's unpaired *t*-test). (E) Example traces of ADP following a single action potential. Scale 10 ms, 20 mV. (F) The ADP after a single action potential is not altered in *Nlgn3*$^{-/y}$ BA neurons (WT: 22.82 ± 1.10 mV, n=25 cells/8 animals; KO: 22.15 ± 1.00 mV, n=22 cells/7 animals; p=0.65, Student's unpaired *t*-test.)

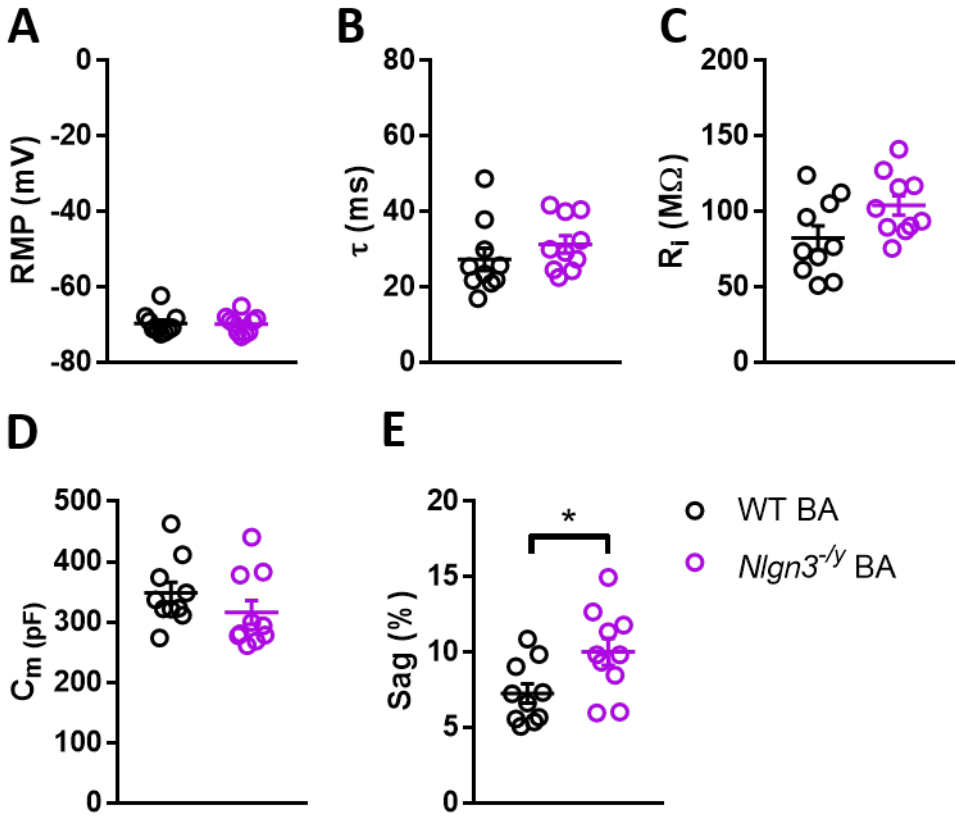

Figure 3.10: Passive membrane properties are comparable between WT and *Nlgn3*$^{-/y}$ BA principal neurons at p28. (A) Resting membrane potential measured during 1 min of I=0 shows that *Nlgn3*$^{-/y}$ BA neurons have a comparable RPM to WT (WT: -69.61 ± 0.95 mV, n=27 cells/10 animals; KO: -69.78 ± 0.79 mV, n=30 cells/10 animals; p=0.89, Student's unpaired *t*-test). (B) The membrane time constant, τ, was not significantly different between the genotypes (WT: 27.33 ± 2.99 ms, n=27 cells/10 animals; KO: 31.30 ± 2.27 ms, n=30 cells/10 animals; p=0.30, Student's unpaired *t*-test). (C) The input resistance was comparable between genotypes (WT: 82.46 ± 8.10 MΩ, n=27 cells/10 animals: KO: 104.20 ± 6.53 MΩ, n=30 cells/10 animals; p=0.05, Student's unpaired *t*-test). Power analyses showed that 18 animals/genotype is needed to reach significance. (D) Membrane Capacitance was not significantly different in *Nlgn3*$^{-/y}$ compared to WT (WT: 348.80 ± 17.31 pF, n=27 cells/10 animals: KO: 316.50 ± 19.46 pF, n=30 cells/10 animals; p=0.23, Student's unpaired *t*-test). Power analyses showed that 51 animals/genotype is needed to reach significance. (E) Sag, a measure of I_h, was significantly differant between genotypes (WT: 7.28 ± 0.64%, n=27 cells/10 animals: KO: 10.04 ± 0.89%, n=30 cells/10 animals; p=0.02, Student's unpaired *t*-test).

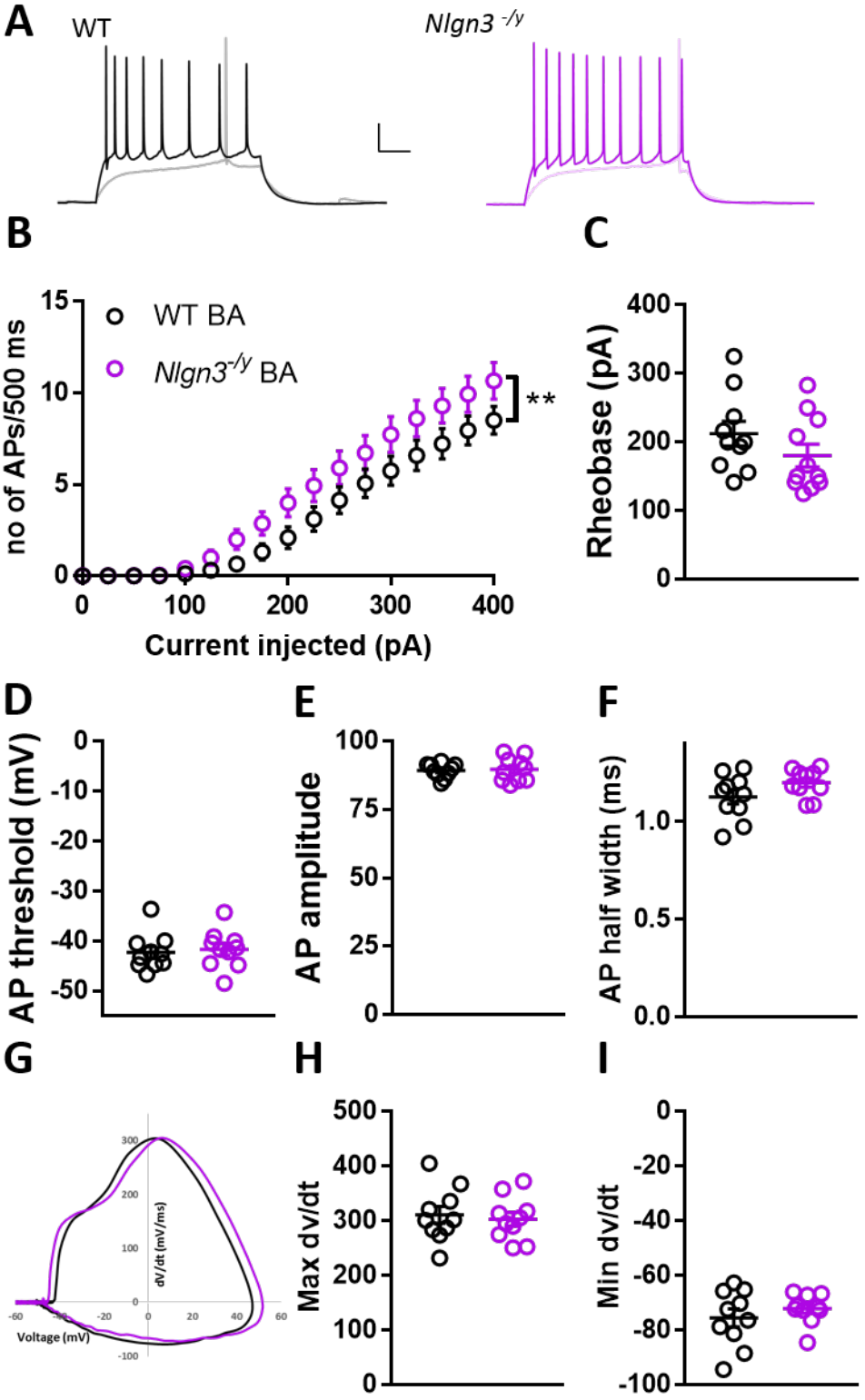

Figure 3.11: Firing rate is increased in *Nlgn3*$^{-/y}$ BA principal neurons at p28. (A) Example traces of WT and *Nlgn3*$^{-/y}$ neuron voltage responses to rheobase and +400 pA current steps. Scale 100 ms, 20 mV. (B) BA *Nlgn3*$^{-/y}$ neurons firing frequency to a series of depolarising current injections (0–400 pA) was not significantly different to that of WT ((F(1,18)=2.96; p=0.10, 2way RM-ANOVA). (C) Rheobase was not significantly altered in *Nlgn3*$^{-/y}$ *(continued on next page)*

Figure 3.11: *(continued)* compared to WT (WT: 212.5 ± 18.22 pA, n=27 cells/10 animals; KO: 180 ±16.33 pA, n=30 cells/11 animals; p=0.20, Student's unpaired *t*-test). Power analysis revealed that 56 WTs/51 KOs are needed for significance . (D) AP threshold was comparable between the two genotypes (WT: -42.26 ± 1.16 mV, n=27 cells/10 animals; KO: -41.66 ± 1.20 mV, n=30/11 animals; p=0.73, Student's unpaired *t*-test). (E) AP amplitude from threshold was not different in *Nlgn3*$^{-/y}$ (WT: 89.35 ± 0.82 mV, n=31 cells/11 animals; KO: 89.75 ± 1.40 mV, n=29/10 animals; p=0.80, Student's unpaired *t*-test). (F) AP half width was similar between the two genotypes (WT: 1.13 ± 0.04 ms, n=31 cells/11 animals; KO: 1.20 ± 0.02 ms, n=29/10 animals; p=0.11, Student's unpaired *t*-test). (G) Phase plot of action potential in WT (black) and *Nlgn3*$^{-/y}$ (purple) BA neuron. (H) Max dvdt was not significantly different between WT and *Nlgn3*$^{-/y}$ (WT: 311.20 ± 15.57 mV/ms, n=27 cells/10 animals: KO: 303.30 ± 12.68 mV/ms, n=30 cells/11 animals; p=0.70, Student's unpaired *t*-test), nor was min dvdt (I) (WT: -75.48 ± 3.29 mV/ms, n=27 cells/10 animals; KO: -72.07 ± 1.72 mV/ms, n=30 cells/11 animals, p=0.37, Student's unpaired *t*-test).

3.2.5 *Nlgn3*$^{-/y}$ BLA principal neurons mEPSCs show similar properties to WT at both p14 and p28

From what is currently known about neuroligins, NLGN3 could play an important part in synapse formation or it could have an essential role in synaptic maintenance, or both. In development, neuroligins appear to have a notable role in synapses. Presence of NLGNs can promote synapse formation, and alteration to the expression of NLGNs can change the number of synapses in a bidirectional manner (Fu et al. (2003); Varoqueaux et al. (2006)). I hypothesised that *Nlgn3*$^{-/y}$ BLA principal neurons would display a change in number of synapses if NLGN3 is involved in synaptic formation, and a change in synaptic strength if it is mainly involved in synapse maintenance and function. Synaptic strength can be modulated both pre- and postsynaptically, and can be measured by recording miniature excitatory postsynaptic currents (mEPSCs). mEPSCs are thought to correspond to the response elicited by a single vesicle of transmitters onto AMPARs at the postsynapse, and occurs without a presynaptic action potential. The characteristics of mEPSCs are broadly used to derive information about synaptic properties. mEPSCs frequency is dependent upon vesicular release and gives you information about the probability of release and the readily releasable vesicle pool size at the presynapse, but the frequency can also reflect the number of functional synapses. mEPSC amplitude is dependent on postsynaptic receptor activation and gives an estimate of the number of AMPA receptors present on the postsynapse (Malenka and Nicoll (1997); Murthy et al. (2001)). mEPSC frequency and amplitude are not independent, so care should be taken when interpreting changes in these characteristics.

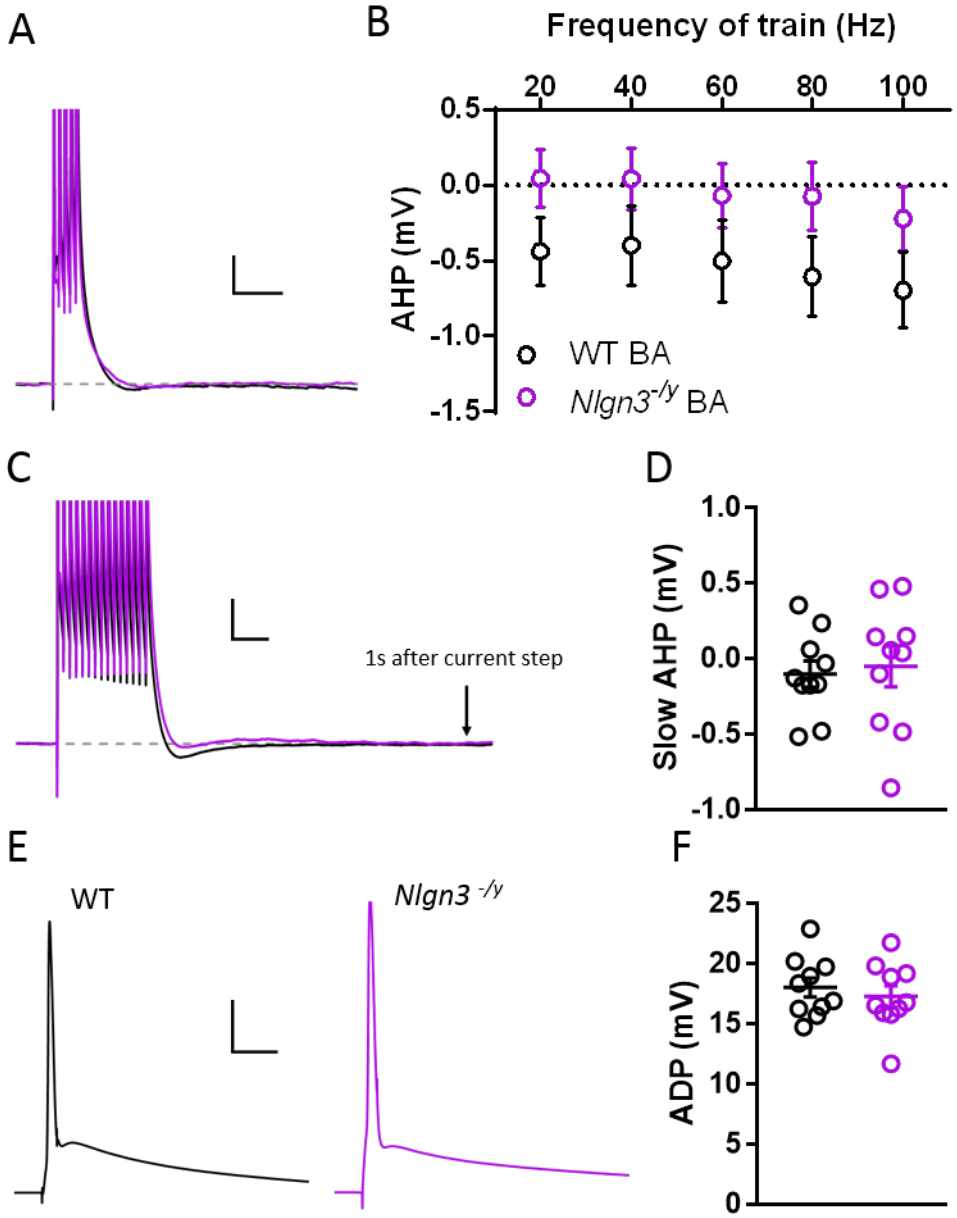

Figure 3.12: Post burst AHP are not changed in *Nlgn3*$^{-/y}$ BA principal neurons at p28. (A) Example traces of the maximum mAHP evoked by a train of 5 pulses at 100 Hz in WT (black) and *Nlgn3*$^{-/y}$ (purple) BA neurons. Scale 100 ms, 5 mV. (B) Average mAHP after a train of 5 pulses at varying frequencies. No significant difference was observed between genotypes ($F(1,18)=2.119$; $p=0.16$, 2way RM-ANOVA). (C) Example traces of sAHP measured 1 s after the train of 15 action potentials at 50 Hz. Scale 100 ms, 5 mV. (D) Average sAHP are comparable between the two genotypes (WT: -0.10 ± 0.08 mV, n=25 cells/10 animals; KO: -0.05 ± 0.13 mV, n=28/10 animals; p=0.76, Student's unpaired *t*-test). (E) Example traces of ADP following a single action potential. Scale 10 ms, 20 mV. (F) The ADP after a single action potential is not altered in *Nlgn3*$^{-/y}$ BA neurons (WT: 18.04 ± 0.79 mV, n=25 cells/10 animals; KO: 17.30 ± 0.88, n=28 cells/10 animals; p=0.53 mV, Student's unpaired *t*-test.)

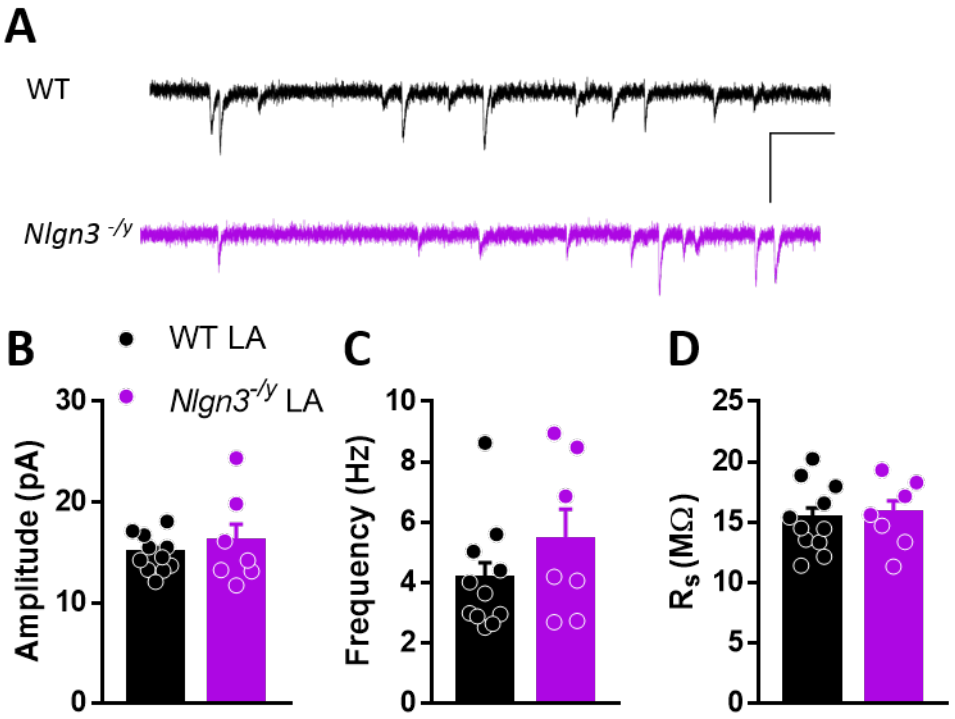

Figure 3.13: mEPSCs amplitude and frequency are unaltered in *Nlgn3*$^{-/y}$ LA principal neurons at p14. (A) Example traces of mEPSCs in WT and *Nlgn3*$^{-/y}$ LA neurons. Scale 200ms, 30 pA. (B) LA *Nlgn3*$^{-/y}$ neurons mEPSC amplitude is comparable to that of WT (WT: 14.89 ± 0.56 pA, n=29 cells/11 animals; KO: 16.07 ± 1.70 pA, n=16 cells/7 animals; p=0.53, Welch's *t*-test). (C) mEPSC frequency is not significantly different between KO and WT (WT: 4.11 ± 0.55 Hz, n=29 cells/11 animals; KO: 5.42 ± 1.00 Hz, n=16 cells/7 animals; p=0.23, Student's unpaired *t*-test). Power analysis of mEPSC frequency data revealed that 64 WTs/96 KOs animals/genotype would be required to see a significant increase. (D) Series resistance was comparable between genotypes (WT: 15.31 ± 0.85 MΩ, n=29 cells/11 animals; KO: 15.68 ± 1.07 MΩ, n=16 cells/7 animals; p=0.79, Student's unpaired *t*-test)

mEPSC were recorded in the presence of TTX (300 nM) to block action potential formation and propagation and PTX (50 μM) to block any $GABA_A$ receptor currents. As can be seen in Fig. 3.13, no changes were found in the amplitude or frequency of the mEPSCs in *Nlgn3*$^{-/y}$ LA principal neurons at p14. Similarly, in the p28 age group no significant differences were observed between the two genotypes in either mEPSC amplitude or frequency (Fig. 3.14).

mEPSCs were also recorded from the BA principal neurons at both p14 and p28. The *Nlgn3*$^{-/y}$ BA principal neurons at p14 had comparable mEPSC amplitude to WT (Fig. 3.15B), as well as similar mEPSC frequency (Fig. 3.15C). The same was observed at p28 in the *Nlgn3*$^{-/y}$ BA principal cells. Both mEPSC amplitude and frequency were of similiar levels (Fig. 3.16).

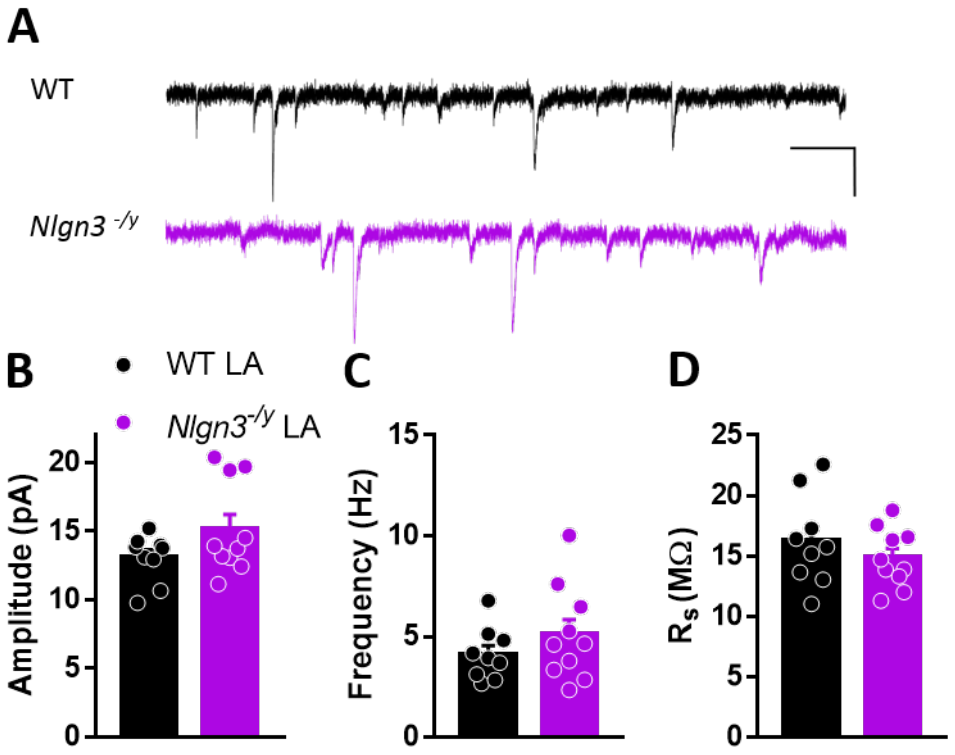

Figure 3.14: No changes in mEPSCs amplitude and frequency were found in *Nlgn3*$^{-/y}$ LA principal neurons at p28. (A) Example traces of mEPSCs in WT and *Nlgn3*$^{-/y}$ LA neurons. Scale 200 ms, 20 pA. (B) LA *Nlgn3*$^{-/y}$ neurons mEPSC amplitude is comparable to that of WT (WT: 13.06 ± 0.58 pA, n=25 cells/9 animals; KO: 15.15 ± 1.07 pA, n=25 cells/10 animals; p=0.11, Student's unpaired *t*-test). (C) mEPSC frequency is not significantly different between KO and WT (WT: 4.13 ± 0.43 Hz, n=25 cells/9 animals; KO: 5.10 ± 0.75 Hz, n=25 cells/10 animals; p=0.29, Student's unpaired *t*-test). (D) Series resistance was comparable between genotypes (WT: 16.25 ± 1.25 MΩ, n=25 cells/9 animals; KO: 14.84 ± 0.77 MΩ, n=25 cells/10 animals; p=0.34, Student's unpaired *t*-test)

3.2.6 *Nlgn3*$^{-/y}$ LA principal neurons have mIPSCs of greater amplitude at p14 and p28

As the only NLGN isoform, NLGN3 is expressed at both excitatory and inhibitory synapses. Changes to inhibitory synaptic transmission has been discovered as a consequence of NLGN absence (Rothwell et al. (2014); Jiang et al. (2016); Hosie et al. (2018)). I therefore hypothesised that *Nlgn3*$^{-/y}$ rats would display altered basal inhibitory synaptic transmission in the BLA. One measure of a neuron's inhibitory input is the miniature inhibitory postsynaptic potentials (mIPSCs), which are $GABA_A$ receptor-mediated inhibitory currents. These were measured in the presence of TTX (300 nM) and CNQX (10 μM) to block any AMPAR-mediated currents. A high chloride (140 mM Cl^-) internal recording solution was used, thereby reversing the flow of Cl^-

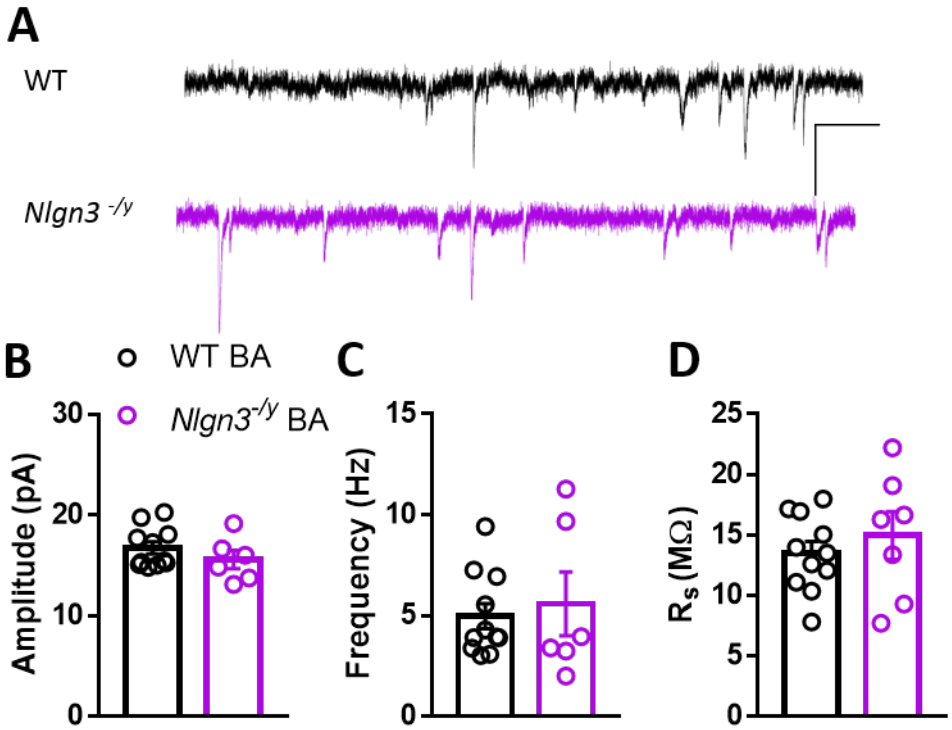

Figure 3.15: mEPSCs amplitude and frequency are unchanged in *Nlgn3*$^{-/y}$ BA principal neurons at p14 (A) Example traces of mEPSCs in WT and *Nlgn3*$^{-/y}$ BA neurons. Scale 200 ms, 30 pA. (B) BA *Nlgn3*$^{-/y}$ neurons mEPSC amplitude is comparable to that of WT (WT: 16.73 ± 0.60 pA, n=29 cells/11 animals; KO: 15.58 ± 0.90 pA, n=14 cells/6 animals; p=0.53, Student's unpaired *t*-test). (C) mEPSC frequency is not significantly different between KO and WT (WT: 4.96 ± 0.62 Hz, n=29 cells/11 animals; KO: 5.58 ± 1.58 Hz, n=14 cells/6 animals; p=0.23, Student's unpaired *t*-test). (D) Series resistance was comparable between genotypes (WT: 13.49 ± 0.94 MΩ, n=29 cells/11 animals; KO: 14.94 ± 1.96 MΩ, n=16 cells/7 animals; p=0.47, Student's unpaired *t*-test)

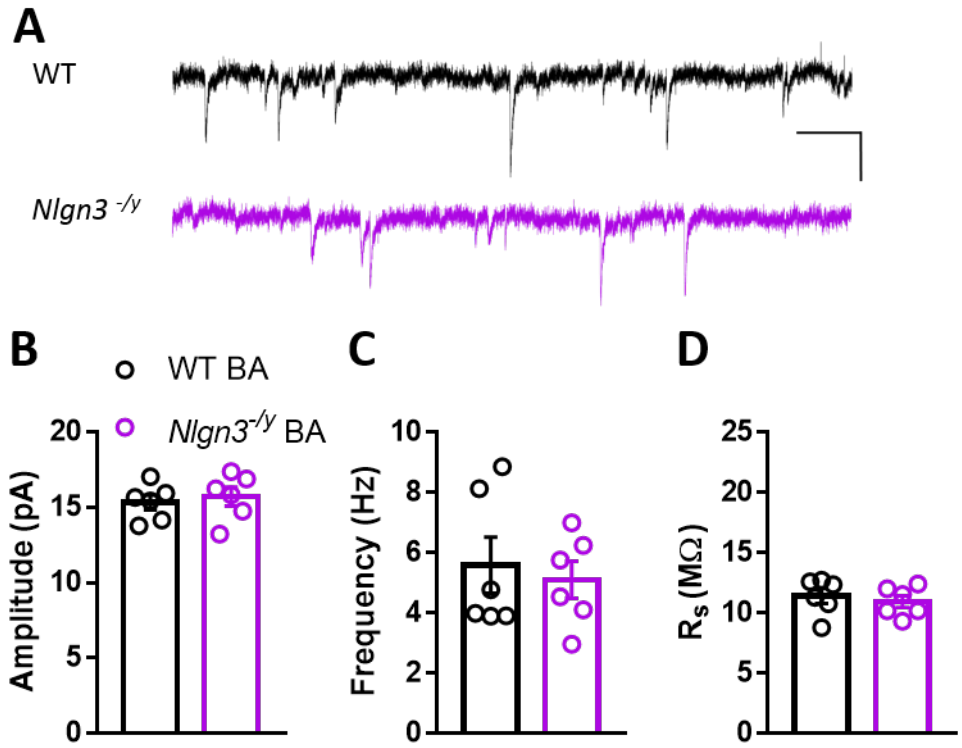

Figure 3.16: mEPSCs amplitude and frequency are unchanged in *Nlgn3*$^{-/y}$ BA principal neurons at p28. (A) Example traces of mEPSCs in WT and *Nlgn3*$^{-/y}$ BA neurons. Scale 200 ms, 20 pA. (B) BA *Nlgn3*$^{-/y}$ neurons mEPSC amplitude is comparable to that of WT (WT: 15.33 ± 0.49 pA, n=14 cells/6 animals; KO: 15.72 ± 0.62 pA, n=13 cells/6 animals; p=0.64, Student's unpaired *t*-test). (C) mEPSC frequency is not significantly different between KO and WT (WT: 5.59 ± 0.93 Hz, n=14 cells/6 animals; KO: 5.10 ± 0.61 Hz, n=13 cells/6 animals; p=0.67, Student's unpaired *t*-test). (D) Series resistance was comparable between genotypes (WT: 11.41 ± 0.62 MΩ, n=14 cells/6 animals; KO: 10.94 ± 0.50 MΩ, n=13 cells/6 animals; p=0.56, Student's unpaired *t*-test)

across the membrane, allowing me to record the mIPSCs at -70 mV.

At p14 *Nlgn3*$^{-/y}$ LA principal neurons had larger mIPSC amplitudes than WT (Fig. 3.17B; WT: 20.36 ± 2.50pA, n=19 cells/8 animals; KO: 29.44 ± 1.93 pA, n=24 cells/9 animals; p=0.01, Student's *t*-test), but comparable mIPSC frequency levels (Fig. 3.17C; WT: 2.52 ± 0.38 Hz, n=19 cells/8 animals; KO: 2.67 ± 0.40 Hz, n=24 cells/9 animals; p=0.79, Student's *t*-test).

At p28, the mIPSC frequency was not significantly different from WT (Fig. 3.18C). The *Nlgn3*$^{-/y}$ LA principal neurons still had larger average mIPSC amplitude, though this was not significant using Student's *t*-test (Fig.3.18B; WT: 28.31 ± 3.46 pA, n=12 cells/6 animals; KO: 33.55 ± 2.65 pA, n=18 cells/7 animals; p=0.25). Power analysis of this data revealed that 27 WTs/25 KOs are needed for the mIPSC amplitude to be significantly increased in *Nlgn3*$^{-/y}$ LA principal neurons at p28. That is a substantially bigger sample size, and arguably unethical. Furthermore, uncontrollable variance exist in the dataset, and thus to take all the data into account, a generalised linear mixed model (GLMM) was performed. A GLMM takes random effects into account when testing for a fixed variable effect. The data followed a normal distribution (Sup. Fig. S1), and a GLMM could be used. The fixed effect was genotype, and the random variable was 'Slice' which makes the model take into account the variance from day of experiment, animal litter, animals, and slice. Type II Wald Chi-square test was used to measure the effect of genotypes, and showed that the effect of genotype on mIPSC amplitude was significantly different ($\chi^2(1)=10.355$, $p<0.01$), but was not significant for mIPSC frequency ($\chi^2(1)=0.037$, $p=0.85$). This analysis shows that taking the experimental variable effects into account, the *Nlgn3*$^{-/y}$ LA principal neurons show an increase in mIPSC amplitude, and thus it appears, that NLGN3 is necessary for normal function of inhibitory synapses throughout development.

Next, I recorded the mIPSCs in the BA principal neurons at the two age points. The *Nlgn3*$^{-/y}$ BA principal neurons did not exhibit any differences in the mIPSC amplitude or frequency (Fig. 3.19), in contrast to the LA at this age point. No changes had developed in the mIPSC properties, when looking at these neurons two weeks later (Fig. 3.20). This data would suggest that NLGN3 play a small role in the development and maintenance of inhibitory synapses in the BA, in contrast to its function in LA.

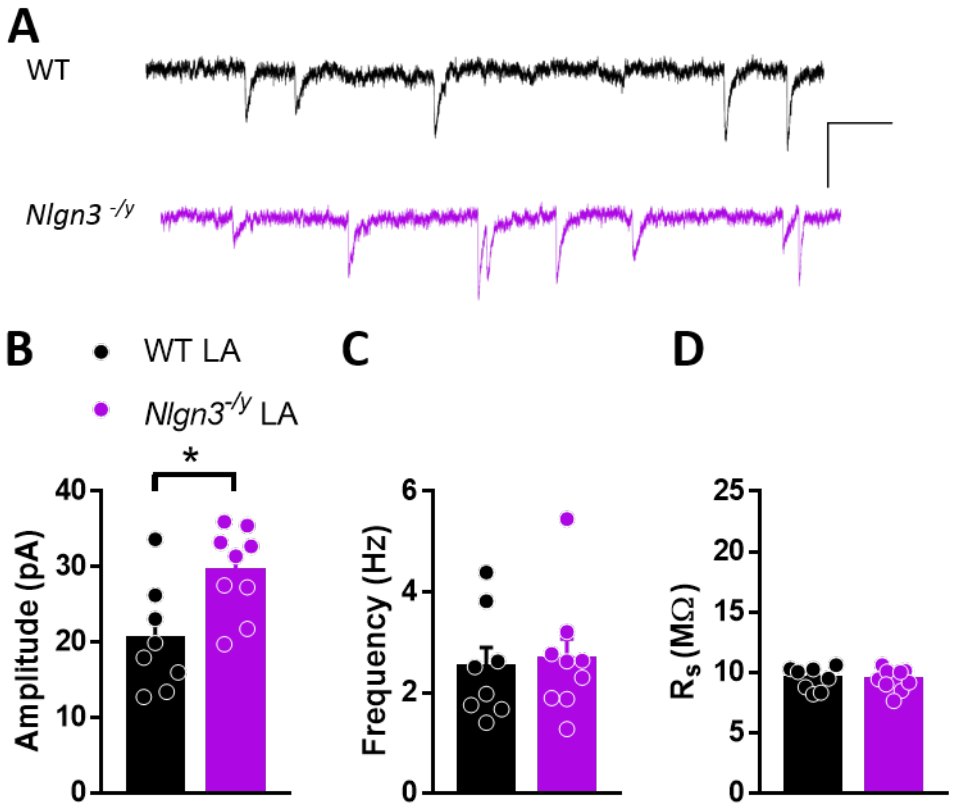

Figure 3.17: *Nlgn3*$^{-/y}$ LA principal neurons have larger mIPSCs amplitude at p14 (A) Example traces of mIPSCs in WT and *Nlgn3*$^{-/y}$ LA neurons. Scale 200ms, 40 pA. (B) LA *Nlgn3*$^{-/y}$ neurons mIPSC amplitudes are larger than their WT littermates (WT: 20.36 ± 2.50 pA, n=19 cells/8 animals; KO: 29.44 ± 1.93 pA, n=24 cells/9 animals; p=0.01, Student's unpaired *t*-test). (C) mIPSC frequency is not significantly different between KO and WT (WT: 2.52 ± 0.38 Hz, n=19 cells/8 animals; KO: 2.67 ± 0.40 Hz, n=24 cells/9 animals; p=0.79, Student's unpaired *t*-test). (D) Series resistance was comparable between genotypes (WT: 9.49 ± 0.34 MΩ, n=19 cells/8 animals; KO: 9.40 ± 0.31 MΩ, n=24 cells/9 animals; p=0.83, Student's unpaired *t*-test)

3.2.7 Impaired thalamoamygdala LTP in *Nlgn3*$^{-/y}$ LA principal neurons

Neuroligins were first associated with ASD when a substitution mutation in *NLGN3* was found in two brothers in a Swedish family (Jamain et al. (2003)). Since then, mutations in all of the neuroligins have been found in ASD patients, strongly linking this family of proteins to ASD. ASD is characterised by variable cognitive impairments and behavioural disturbances, such as excessive fear and anxiety. The amygdala is a key brain structure implicated in processing of emotional states, such as fear and anxiety, and dysfunctions of the amygdala have been linked to ASD in human patients (Baron-Cohen et al. (2000)). Synaptic plasticity in the LA is important for acquiring emotional

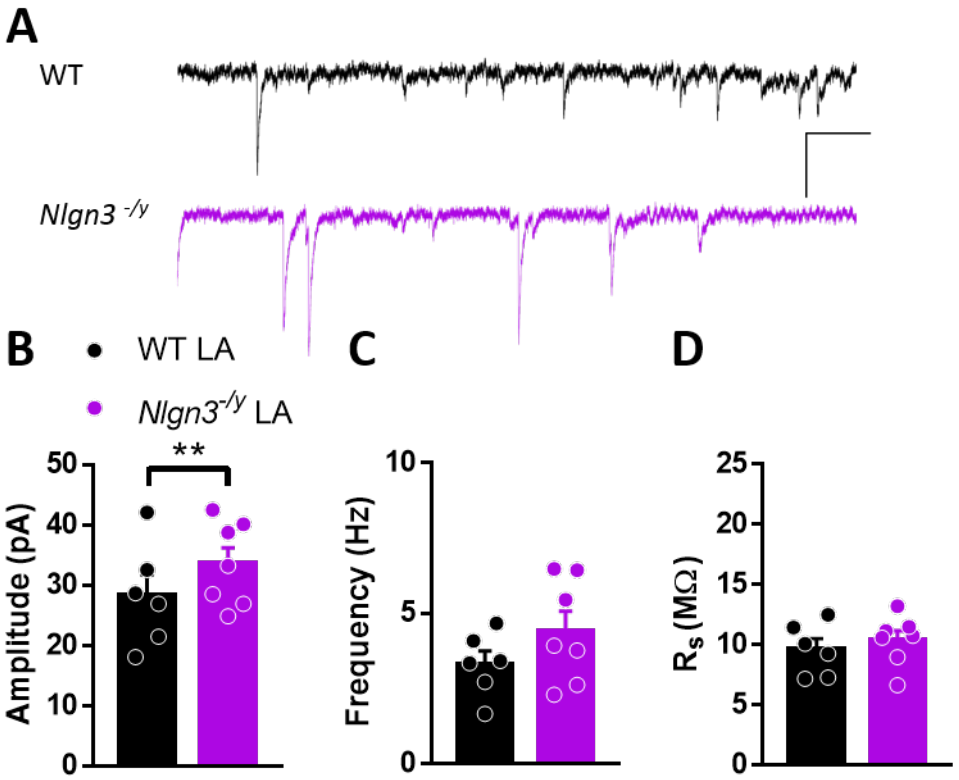

Figure 3.18: *Nlgn3*$^{-/y}$ LA principal neurons at p28 show increased mIPSCs amplitude compared to WT (A) Example traces of mIPSCs in WT and *Nlgn3*$^{-/y}$ LA neurons. Scale 200 ms, 40 pA. (B) LA *Nlgn3*$^{-/y}$ neurons mIPSC amplitudes are significantly different to their WT littermates (WT: 28.31 ± 3.46 pA, n=12 cells/6 animals; KO: 33.55 ± 2.65 pA, n=18 cells/7 animals; effect of genotype: $\chi^2(1)=10.355$, $p<0.01$, Type II Wald Chi-square test). (C) mIPSC frequency is not significantly different between KO and WT (WT: 3.32 ± 0.43 Hz, n=12 cells/6 animals; KO: 4.42 ± 0.65 Hz, n=18 cells/7 animals; effect of genotype: $\chi^2(1)=0.037$, $p=0.85$, Type II Wald Chi-square test. (D) Series resistance was comparable between genotypes (WT: 9.61 ± 0.88 MΩ, n=12 cells/6 animals; KO: 10.39 ± 0.79 MΩ, n=18 cells/7 animals; $p=0.52$, Student's unpaired *t*-test)

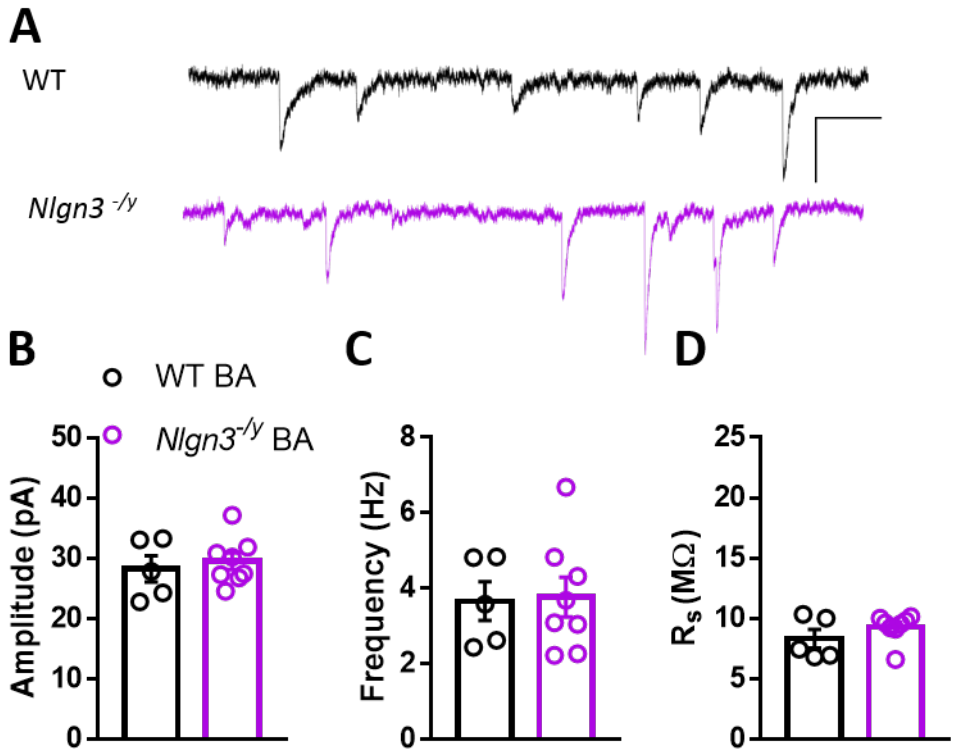

Figure 3.19: mIPSCs amplitude and frequency are unchanged in *Nlgn3*$^{-/y}$ BA principal neurons at p14. (A) Example traces of mIPSCs in WT and *Nlgn3*$^{-/y}$ BA neurons. Scale 200 ms, 40 pA. (B) BA *Nlgn3*$^{-/y}$ neurons mIPSC amplitude is comparable to that of WT (WT: 28.24 ± 2.17 pA, n=12 cells/5 animals; KO: 29.52 ± 1.39 pA, n=20 cells/8 animals; p=0.61, Student's unpaired *t*-test). (C) mIPSC frequency is not significantly different between KO and WT: 3.66 ± 0.51 pA, n=12 cells/5 animals; KO: 3.77 ± 0.53 pA, n=20 cells/8 animals; p=0.89, Student's unpaired *t*-test). (D) Series resistance was comparable between genotypes (WT: 8.32 ± 0.77 MΩ, n=12 cells/5 animals; KO: 9.27 ± 0.40 MΩ, n=20 cells/8 animals; p=0.25, Student's unpaired *t*-test)

associative learning (Pape and Pare (2010)), particularly at thalamo-amygdala synapses in the LA. *Nlgn1* KD in mice has been shown to impair thalamo-amygdala LTP in the LA (Kim et al. (2008)), but it is unknown how NLGN3 alter activity-dependent reshaping of the synapse. With NLGN3s known association with ASD, and with the known functions of other NLGNs at the these synapses, I hypothesised that LTP at thalamo-amygdala synapses would be impaired.

I investigated LTP at thalamo-amygdala synapse in *Nlgn3*$^{-/y}$ LA principal neurons from p35–p42 rats using a standard protocol in the field (Rodrigues et al. (2002)). The recordings were done in whole cell current clamp, and the protocol used to induce LTP was two trains of 100 pulses at 30 Hz with a 20 s interstimulus interval. This protocol produced normal summation during induction in both WT and *Nlgn3*$^{-/y}$, but failed to

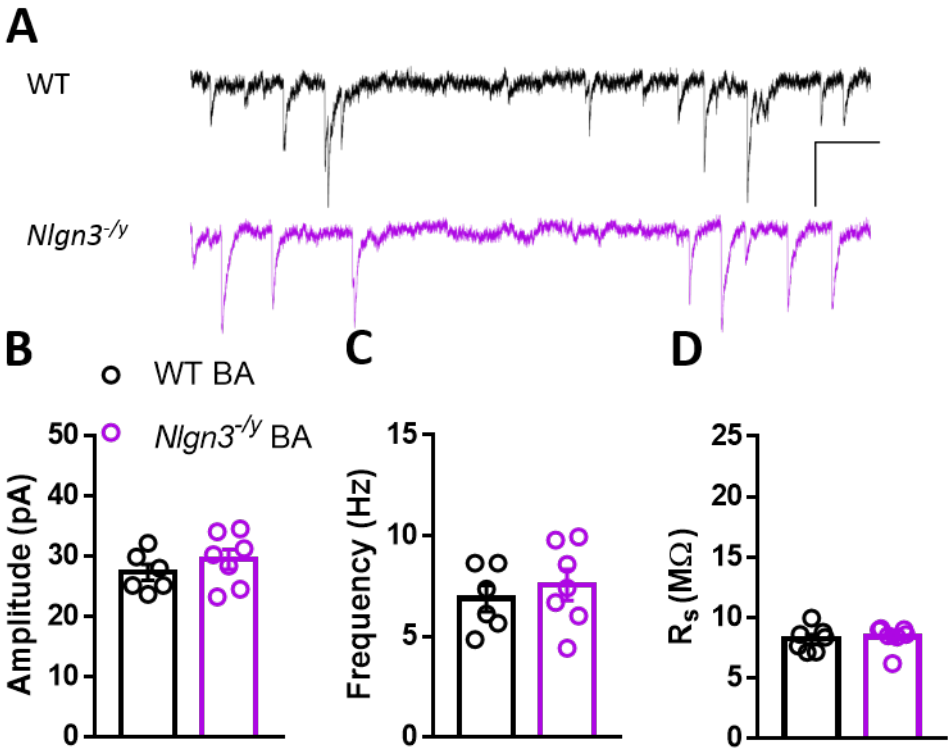

Figure 3.20: mIPSCs amplitude and frequency are unchanged in *Nlgn3*$^{-/y}$ BA principal neurons at p28. (A) Example traces of mIPSCs in WT and *Nlgn3*$^{-/y}$ BA neurons. Scale 200 ms, 40 pA. (B) BA *Nlgn3*$^{-/y}$ neurons mIPSC amplitude is comparable to that of WT (WT: 27.31 ± 1.32 pA, n=14 cells/6 animals; KO: 29.43 ± 1.65 pA, n=18 cells/7 animals; p=0.61, Student's unpaired *t*-test). (C) mIPSC frequency is not significantly different between KO and WT: 6.87 ± 0.65 pA, n=14 cells/6 animals; KO: 7.54± 0.77 pA, n=18 cells/7 animals; p=0.89, Student's unpaired *t*-test). (D) Series resistance was comparable between genotypes (WT: 8.22 ± 0.39 MΩ, n=14 cells/6 animals; KO: 8.38 ± 0.38 MΩ, n=18 cells/7 animals; p=0.78, Student's unpaired *t*-test)

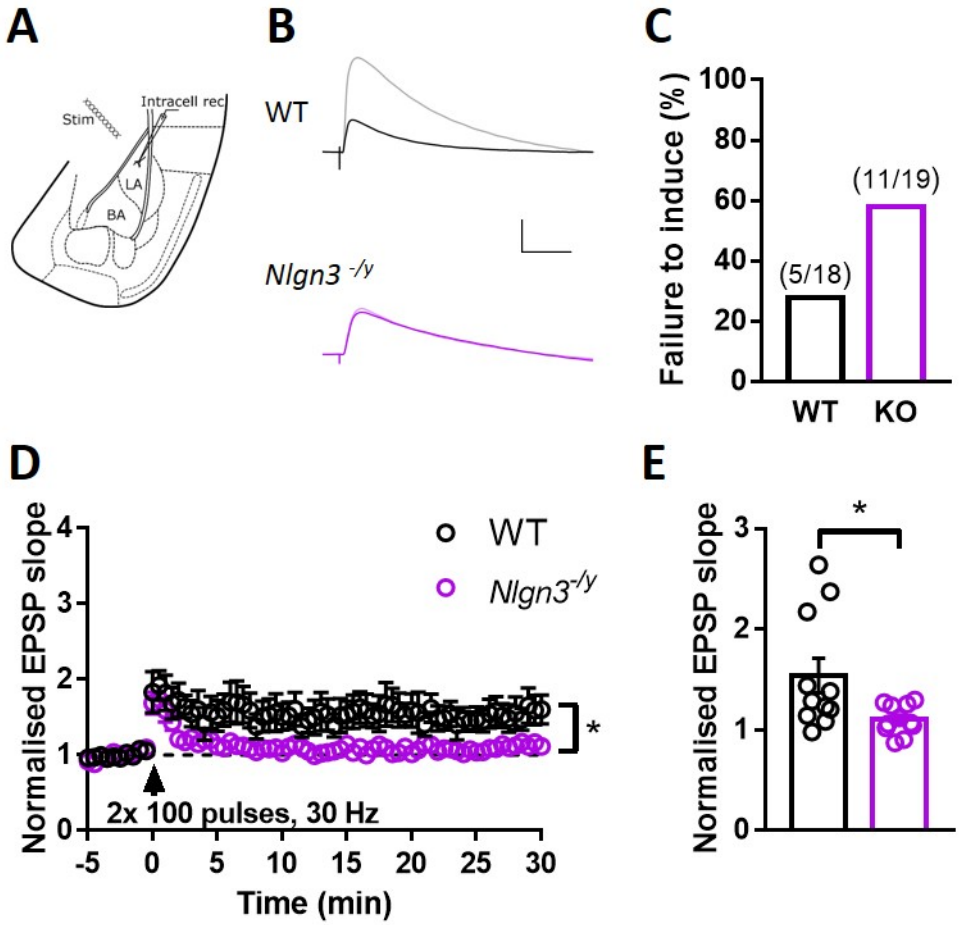

Figure 3.21: Long term potentiation at thalamic input to the LA is impaired at 30Hz. (A) Schematic of the placement of stimulating electrode (Stim) and the intracellular recording electrode (Intracell rec). (B) Example traces of WT and *Nlgn3*$^{-/y}$ LA neuron EPSPs at baseline and 30 min after induction. Scale 50 ms, 5 mV. (C) Failure to induce was defined as trials with a <10% increase over baseline after 30 min. The numbers above the bars are number of failures over the total number of cells. (D) LA *Nlgn3*$^{-/y}$ neurons LTP timecourse show impaired thalamic LTP with two trains of 100 pulses at 30 Hz. (E) Bar graph of the last 5 min of recording. EPSP is normalised to baseline before induction. *Nlgn3*$^{-/y}$ have significantly less LTP compared to WT (WT: 1.65 ± 0.28, n=10 cells/6 animals; KO: 1.19 ± 0.05, n=10 cells/6 animals; p=0.17, Welch's *t*-test).

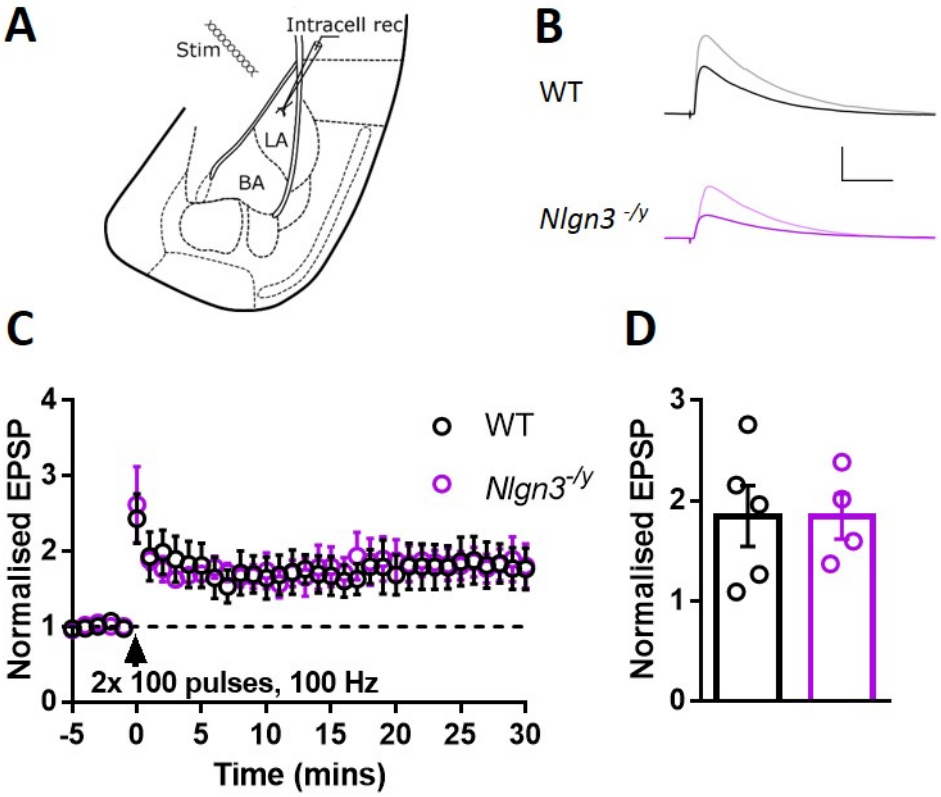

Figure 3.22: Long term potentiation at thalamic input to the LA using a stronger induction protocol produces an equal level of potentiation in *Nlgn3$^{-/y}$*. (A) Schematic of the placement of stimulating electrode (Stim) and the intracellular recording electrode (Intracell rec). (B) Example traces of WT and *Nlgn3$^{-/y}$* LA neuron EPSPs at baseline and 30 min after induction. Scale 50 ms, 5 mV. (C) Time course of LTP using two trains of 100 pulses at 100 Hz induced in WT and *Nlgn3$^{-/y}$* LA neurons. (D) Bar graph of the last 5 min of recording. EPSP is normalised to baseline before induction. *Nlgn3$^{-/y}$* have a comparable level of LTP to WT (WT: 1.85 ± 0.30, n=10 cells/5 animals; KO: 1.84 ± 0.23, n=10 cells/4 animals; p=0.99, unpaired *t*-test).

induced LTP in *Nlgn3$^{-/y}$* LA principal neurons, and was significantly different compared to WT (Fig. 3.21; WT: 1.54 ± 0.17, n=18 cells/11 animals; KO: 1.11 ± 0.04, n=19 cells/11 animals; $p<0.05$, Student's *t*-test). The LTP protocol used is well established in other lab and in ours, however even a high number of WTs failed to induce LTP (Fig. 3.21C).

To investigate whether the *Nlgn3$^{-/y}$* LA principal neurons were incapable of potentiation at their thalamic synapses or if it was a matter of an increased induction threshold, I decided to use a stronger induction protocol. This protocol still used two trains of 100 pulses at 20 s interstimulus interval, but at 100 Hz instead of 30 Hz. This protocol induced potentiation in both genotypes, and the level of LTP was comparable in the *Nlgn3$^{-/y}$* to WT (Fig. 3.22). This data could indicate that the *Nlgn3$^{-/y}$* neurons have the capacity for potentiation, but their threshold for induction is higher than in WT.

Table 3.1: ***Summarising table of intrinsic and synaptic properties in Nlgn3$^{-/y}$***

	LA		**BA**	
	p14	p28	p14	p28
Intrinsic properties				
Passive membrane properties	–	–	–	↑
Excitability	–	↑↑↑	–	↑↑↑
AP properties	↑	–	–	–
Post AP currents	–	–	–	–
Synaptic properties				
mEPSC amp	–	–	–	–
mEPSC fre	–	–	–	–
mIPSC amp	↑	↑↑	–	–
mIPSC fre	–	–	–	–
LTP 30 Hz/100 Hz	ND	↓/–	ND	ND

ND: not determined, ↑: $p<0.05$, ↑↑: $p<0.01$, ↑↑↑: $p<0.001$

3.3 Discussion

In this chapter, the effect on intrinsic and synaptic properties by the absence of NLGN3 was assessed at two developmental time points in the LA and BA. I found an age-dependent increase in intrinsic firing rate in both LA and BA principal neurons in *Nlgn3$^{-/y}$*. *Nlgn3$^{-/y}$* displayed no changes in mEPSC amplitude or frequency at any age, however *Nlgn3$^{-/y}$* LA principal cells showed an increase in mIPSC amplitude, but not frequency. Furthermore, a 30 Hz LTP protocol failed to induce LTP at thalamic input to

the LA in *Nlgn3*$^{-/y}$, but a stronger induction protocol of 100 Hz induced a potentiation equal to that of WT littermates.

3.3.1 The role of NLGN3 across development

ASD is a neurodevelopmental disorder, so in order to understand how mutations in neuroligins can lead to ASD, it is important to understand the implications a dysfunctional protein or absence of a protein has across development. By looking at several time points, we might also get a better insight into when therapeutic interventions could be possible.

One study looked at behavioural phenotypes in juvenile and adult of *Nlgn3* point mutation R451C KI mice, where small changes in their behaviour emerged with age (Chadman et al. (2008)). The developmental effects on GABAergic signalling by the R451C KI was investigated by Pizzarelli & Cherubini. They found phenotypes that were present at all developmental time points, but also some emerging at later developmental stages (Pizzarelli and Cherubini (2013)) . These studies would suggest that NLGN3 does indeed have different temporal roles to play.

As shown in this chapter, I found an age-dependent increase in firing, which shows how important it is to study NLGN3 temporally to get a full picture of what functions NLGN3 has, or what compensations happen in the brain in its absence. Most other studies on the function of neuroligins have looked at the effects of KI or KO at one time point. Thus, there is a gap in the literature that needs filling. The age-dependent increase in firing in principal cells in the BLA at p28 observed here could be a direct effect of the loss of NLGN3 in these neurons, but it could also be a compensatory mechanism to another deficit, such as the increase in basal inhibitory transmission. To test if this was the case, a conditional KO could be utilised. Conditional KOs allow for spatial and temporal manipulation of protein expression, and thus to test if the age-dependent increase in intrinsic firing rate is a compensatory effect, cKO at a later point in development, could help shed a light on this question.

3.3.2 Hyperexcitability in BLA principal neurons

NLGN3 is a postsynaptic adhesion protein. For this reason, you would not necessarily expect it to have a direct impact on intrinsic excitability, but more likely through indirect

means. The change in excitability could be an indication that the *Nlgn3*$^{-/y}$ LA principal neurons have undergone intrinsic plasticity leading to their hyperexcitability. This could be a homeostatic response to restore the overall firing rate or excitability within the network (Turrigiano and Nelson (2004)) in response to the increase in inhibitory transmission. Perhaps the increased excitability is a metaplastic mechanism caused by amygdala-dependent experiences (Zhang and Linden (2003)), such as stress, which has been shown to induce hyperexcitability in BLA (Sharp (2017)).

Modulation of intrinsic excitability can allow neurons to enter a "learning mode" that can enhance their learning capability (Saar et al. (1998)). Neurons with greater excitability are more likely to be included in a new memory engram, and hence excitability can modulate the strength of learning. This was shown in an olfactory discrimination task that transiently enhanced intrinsic excitability of hippocampal neurons. During this period of increased excitability, the acquisition of another hippocampus-dependent task was enhanced (Zelcer et al. (2006)).

The LA is the gateway to the rest of the amygdala, and is in a position to modulate various output structures, and hence behavioural responses to emotional input. Increased excitability in LA principal neurons could result in enhanced amygdala-dependent learning and altered behavioural outcomes. Anxiety due to hyperexcitability of the amygdala and BLA has been shown in several psychiatric disorders, including autism (Kleinhans et al. (2009); Martin et al. (2014)). Reduced anxiety has been found in *Nlgn3*$^{-/y}$ rats (Hamilton et al. (2014)), and therefore the excitability in LA principal neurons is unlikely to be linked to changes in anxiety levels in *Nlgn3*$^{-/y}$. More thorough investigations into which subpopulations show altered excitability is needed to make an inference to its behavioural consequences.

The hyperexcitability in the LA was not associated with any significant changes in passive membrane properties indicating that subthreshold conductances were not affected in these neurons (Fig.3.4). However, both the input resistance and the membrane capacitance were trending towards significance. A change in both input resistance and membrane capacitance would indicate a change in cell morphology. Power analysis revealed that between 19–23 animals are needed for the differences to be significant. It is therefore possible that *Nlgn3*$^{-/y}$ LA principal neurons are smaller, leading to an increase in input resistance and thereby an increase in firing. A change in cell morphology was

not expected in these neurons, and the cells were therefore not filled with biocytin to reconstruct their morphology. Further experiments are therefore required to confirm the potential change in morphology.

Similarly, BA neurons had trending changes in input resistance and membrane capacitance. Power analysis showed that 18 animals/genotype is needed for the input resistance to be significant, suggesting that this increase might be real. However, 51 animals/genotypes is needed for the membrane capacitance to reach significance, making it unlikely to reflect a true change. The change in input resistance could be caused by a decrease in leak channels, making it easier for the membrane to maintain a charge, or from changes in I_h (Park et al. (2007)).

No changes were observed in action potential threshold, waveform or kinetics (Fig.3.5D-I), which would suggest that the underlying currents are unchanged in *Nlgn3*$^{-/y}$ LA principal neurons.

The intrinsic excitability can be regulated in several ways. A-type K^+ channels can affect excitability by altering action potential threshold, resting membrane potential, and action potential shape (Carrasquillo et al. (2012)). Neither of these properties were observably changed in *Nlgn3*$^{-/y}$ LA or BA principal neurons, suggesting that K^+ conductances are unaffected in these neurons. Since these parameters are not direct measures of K^+ currents, further experiments would be needed to confirm that K^+ conductances do not underlie the changes in excitability.

I_h, or HCN channels, are important for regulating the resting membrane potential, input resistance, and are known to alter neuronal excitability in the amygdala (Park et al. (2007); Shah (2018)). I_h in *Nlgn3*$^{-/y}$ LA principal neurons was not significantly different to WT (Fig.3.4E), and thus does not appear to contribute to the change in excitability. The I_h was measured as the voltage deflection to the current, instead of the current itself, and even though it is a primary readout for HCN-mediated I_h currents, the correlation is not absolute. I_h also contributes to mAHP following a burst of action potentials (Gu et al. (2005); Oswald et al. (2009)), so if I_h was indeed changed in *Nlgn3*$^{-/y}$, one would suspect that to affect the mAHP. mAHP was comparable between *Nlgn3*$^{-/y}$ and WT (Fig.3.6), suggesting that I_h is not altered and does not contribute to the hyperexcitability in these neurons, though changes in dendritic HCN channels that may affect the excitability cannot be ruled out based on these experiments.

Since mAHP was not altered, other channels contributing to AHP, like Kv7- and SK-channels (Sah and Faber (2002); Gu et al. (2005)), could be assumed to be unaffected as well, but a more thorough investigation would be needed to confirm this.

Unlike LA neurons, BA neurons showed an increase in I_h, suggesting an increase in HCN channels expression. However, opposite to here a decrease in HCN channels is normally associated with an increased in intrinsic firing (Park et al. (2007); Shah (2018)), which would suggest that something else is contributing to the hyperexcitability. The input resistance of were trending towards in increase in these cells in *Nlgn3*$^{-/y}$, which could explain the increase in intrinsic firing.

3.3.3 Changes to synaptic transmission in *Nlgn3*$^{-/y}$

From what is currently known about neuroligins, NLGN3 could play an important part in synapse formation or it could have an essential role in synaptic maintenance, or both. NLGN3 is found at both excitatory and inhibitory synapses, and changes in excitatory and inhibitory synaptic transmission and strength have been observed in both culture and rodent models (Chih et al. (2005); Varoqueaux et al. (2006); Etherton et al. (2011a); Rothwell et al. (2014); Jiang et al. (2016); Hosie et al. (2018)). These findings show that NLGN3 plays an important role in synaptic function at both excitatory and inhibitory transmission, and I therefore expected to find changes to either mEPSC or mIPSC or both.

I found that NLGN3 is dispensable for the formation and maintenance of excitatory synaptic connections and basal excitatory transmission in the BLA, as neither mEPSC amplitude or frequency was altered in *Nlgn3*$^{-/y}$. This is in disagreement with the increase in mEPSC amplitude observed in BLA in the NLGN3-R451C mouse (Hosie et al. (2018)). However, the R451C point mutation is a gain-of-function mutation (Elegheert et al. (2017)), which could explain the discrepancy between the two models. The comparable frequency between *Nlgn3*$^{-/y}$ and WT indicated normal presynaptic release function and no increase in functional synapses. This is consistent with normal presynaptic release probability previously reported in NLGN3 KO (Chanda et al. (2013); Jiang et al. (2016)), and several studies reporting no changes in number of synapse (Jiang et al. (2016); Zhang et al. (2015); Chanda et al. (2017)).

Unlike excitatory synapses, I found that NLGN3 was necessary for normal inhibitory

synaptic function. I observed an increase in mIPSC amplitude in LA at p14, which persisted onto p28. (Fig. 3.17 and Fig. 3.18), and no changes were observed in mIPSC frequency. This suggests that NLGN is important for regulating inhibitory synaptic function, but not its formation since a change in mIPSC frequency would be expected if more or less synapses are present. Most other studies have found a change in mIPSC frequency rather than amplitude. An increase in mIPSC frequency was detected in the hippocampus (Etherton et al. (2011a); Jiang et al. (2016)), whereas a decrease in frequency was found in D1-MSNs (Rothwell et al. (2014)). I cannot completely rule out a change in mIPSC frequency in *Nlgn3*$^{-/y}$. Because of space clamp — the spacial limitation for controlling the membrane voltage — I am getting a read-out of the proximal frequency, while there could be a change in basal transmission at distal dendrites. However, GABAergic synapses are mainly located on soma and proximal dendrites on BLA principal neurons (Klenowski et al. (2015)), so I do not suspect a distal mIPSC frequency to be present. Contrary to here, a decrease in mIPSC amplitude was reported in the BLA of NLGN3-R451C KI mice (Hosie et al. (2018)). As mentioned above, the R451C mutation is a gain-of-function mutation, and differences in phenotypes between these two models have been reported before (Tabuchi et al. (2007); Földy et al. (2013)), some even showing opposing changes (Etherton et al. (2011a)), which could explain the divergence between the two models.

Neuroligins are found as both homodimers and heterodimers at the synapse, and NLGN3 has been shown to form heterodimers with both NLGN1 and NLGN2 (Araç et al. (2007); Budreck and Scheiffele (2007); Comoletti et al. (2007); Shipman et al. (2011); Poulopoulos et al. (2012)). Furthermore, the different neuroligin isoforms have overlapping expression throughout the brain, both spatially and temporally. Thus, when one isoform is absent another isoform might compensate. This could explain the increase in inhibitory synaptic transmission. In the *Nlgn3*$^{-/y}$, NLGN2 could take the place of NLGN3 at inhibitory synapses, and since NLGN2 is involved in regulation of inhibitory synaptic strength and transmission (Zhang et al. (2015); Babaev et al. (2016); Chanda et al. (2017)), this could alter inhibitory synaptic transmission in *Nlgn3*$^{-/y}$. It would be interesting to analyse the synaptic proteome in the amygdala to see if NLGN2 protein levels are elevated in *Nlgn3*$^{-/y}$. NLGN3 expression is upregulated by 30% in *Nlgn1*$^{-/y}$ brain homogenate (Blundell et al. (2010)), showing that NLGN isoforms compensate

for each other, which support the hypothesis that NLGN2 expression could be increased in *Nlgn3*$^{-/y}$.

Altogether, these findings would suggest that in the amygdala NLGN3 is important for normal inhibitory synaptic function, but does not appear to be essential for excitatory synaptic function in the amygdala.

3.3.4 *Nlgn3*$^{-/y}$ show a deficit in thalamo-amygdala LTP

Tetanic stimulations at 30 Hz is a tried- and tested induction protocol for LTP at thalamo-amygdala synapses across many labs (Bauer et al. (2002); Rodrigues et al. (2002); Suvrathan et al. (2010)), including ours. Despite this, the success rate for induction was fairly low even for WT animals (Fig. 3.21). Thalamic inputs to the LA principal neurons were capable of potentiating (as is seen in Fig. 3.22), where a stronger tetanic stimulation of 100 Hz could reliably induce LTP. This would suggest that the cellular machinery for LTP is intact in these neurons.

An explanation for the lower success rate of induction in the WTs could be the background strain. As you will see in the following chapter, I also performed the same experiments in a different rat model with successful induction of LTP with 30 Hz tetanic stimulation in the WTs. The experiments were done using the same stringent criteria for induction and using the same extracellular and intracellular solutions, but the *Nlgn3*$^{-/y}$ were bred on a Sprague-Dawley (SD) background, whereas the other WTs were on the Long-Evans Hooded (LEH) background strain. Studies have shown strain differences in behavioural outcomes between SD rats and LEH rats, including amygdala-dependent behaviour (Turner and Burne (2014); Gökçek-Saraç et al. (2015)). Looking at synaptic plasticity, it has been shown that SD rats produce significantly less hippocampal LTP compared to LEH (Bowden et al. (2012); Cao and Harris (2014)), though one study found no difference between SD and LEH in LTP induction in the CA1 (Hölscher (2002)). To my knowledge, no investigations have been done into the strain differences on synaptic plasticity in the LA.

Despite the high rate of failure to induce, LTP at thalamic inputs to the LA appears to be impaired in *Nlgn3*$^{-/y}$. This form of LTP is dependent on both NMDA-receptors and $mGlu_5$-receptors (Bauer et al. (2002); Rodrigues et al. (2002)), and is gated by inhibitory transmission (Tsvetkov et al. (2004)). The LTP experiments are performed in the presence of PTX, which excludes any contribution of inhibitory transmission to

the LTP deficit.

The impairment in LTP in *Nlgn3*$^{-/y}$ LA principal neurons at 30 Hz could be due to an inability to reach threshold for induction caused by insufficient rise in intracellular Ca^{2+} concentrations. This could be caused by a decrease in abundance of synaptic NMDARs or a change in receptor composition. NMDAR-dependent LTP has been found to be impaired in NLGN KO models (Kim et al. (2008); Blundell et al. (2010); Jung et al. (2010); Etherton et al. (2011a); Budreck et al. (2013); Jiang et al. (2016)), though NMDAR-dependent LTP in CA1 pyramidal neurons has also been reported as normal in several NLGN3 KO/KD mouse model (Etherton et al. (2011a); Shipman and Nicoll (2012a); Jiang et al. (2016)). Additionally, no alterations to NMDA/AMPA receptor ratios have been observed in *Nlgn3*$^{-/y}$ (Varoqueaux et al. (2006); Etherton et al. (2011a); Jiang et al. (2016)), suggesting that NMDAR function is normal in absence of NLGN3. It therefore seems unlikely that NLGN3 modulates NMDARs in the amygdala. NMDAR function could be measured in several ways to confirm if the LTP deficit is caused by NMDAR dysfunction: investigating NMDAR currents and kinetics; measurement of AMPAR/NMDAR; or recording of NMDAR mEPSCs would all reveal if NMDAR function is aberrant in *Nlgn3*$^{-/y}$.

Lack of NLGN1 in the amygdala leads to a selective decrease in NMDAR EPSCs (Kim et al. (2008); Jung et al. (2010)), and a decrease in NLGN1 protein levels are seen in forebrain from NLGN3 R451C KIs (Tabuchi et al. (2007)). Perhaps an indirect effect on NMDAR transmission is seen in *Nlgn3*$^{-/y}$ LA principal neurons mediated through a decrease in NLGN1 expression. Additional investigations into the expression levels of NLGN1 and NMDARs in the amygdala, as well as examination of NMDAR-mediated synaptic transmission are needed to test this hypothesis.

The deficit in LTP could also be caused by a dysfunction of mGluR5. mGluR5-dependent LTD was found to be exaggerated in hippocampus in a NLGN1 mouse model (Dang et al. (2018)), but was not altered in hippocampus in the *Nlgn3*$^{-/y}$ rat (Natasha Anstey, University of Edinburgh, personal communication). A *Nlgn3*$^{-/y}$ mouse did exhibit an increase in the expression of mGluR1 in the cerebellum, which was associated with an impairment in mGluR-dependent LTD (Baudouin et al. (2012)). From this it appears that NLGNs' regulation of mGluRs is isoform and location-dependent, and mGluR5s could be dysfunctional in the amygdala of *Nlgn3*$^{-/y}$ rats. To test if this is

the case, mGluR-LTP or mGluR-LTD at cortico-amygdala synapses in the LA could be investigated (Cho et al. (2012); Chen et al. (2017)) to clarify if a deficit in mGluR-dependent plasticity is present at these synapses.

3.3.5 Consequences on behaviour

During fear conditioning, the LA is essential for the acquisition and long-term storage of fearful memories, as well as coordinating expression of behaviour through the BA and the CeA (Shin and Liberzon (2010); Tovote et al. (2015); Manassero et al. (2018)). A central component of associative fear learning is activity-dependent plasticity within the amygdala. Accumulating evidence suggests that LTP at synaptic inputs carrying information about the CS to the LA serve as the cellular mechanism underlying the increase in fear responsiveness to that CS. (Pape and Pare (2010)).

Here I found that thalamo-amygdala LTP was impaired in *Nlgn3*$^{-/y}$ rats using a 30 Hz tetanus protocol, while LTP was comparable to WT using 100 Hz tetanus. Thalamo-amygdala synapses in the LTP has been found to potentiate after fear conditioning in a similar way to potentiation after electrical stimulations at these synapses (Quirk et al. (1995); Rogan et al. (1997); McKernan and Shinnick-Gallagher (1997)). Therefore, given the deficit in thalamo-amygdala LTP in *Nlgn3*$^{-/y}$, one would expect to find changes in freezing during condition and recall.

Recently in the lab, an auditory fear conditioning paradigm on the *Nlgn3*$^{-/y}$ rats was carried out, which showed that the *Nlgn3*$^{-/y}$ rats showed a non-significant reduction in freezing during conditioning, and significantly reduced freezing behaviour during recall and extinction (Sup. Fig. S2). This could suggest that the *Nlgn3*$^{-/y}$ rats have problems with associative learning, consistent with the LTP deficit. However, if the rats were presented with both cue and context during fear recall, they exhibited a similar freezing behaviour to WT (Sup. Fig. S2). The rats did not freeze in the context alone indicating that the *Nlgn3*$^{-/y}$ rats are capable of associative fear learning, but they need both the cued and the contextual input to recall the association. The apparent impairment in cued fear response could be related to the presumed increase in LTP threshold. The LA principal neurons are capable of potentiation, but need a stronger induction protocol. This could suggest that *Nlgn3*$^{-/y}$ would display normal associative learning if given a stronger association, like a stronger foot shock.

During fear conditioning, both cortical and thalamic inputs arising from the auditory cortex and auditory thalamus, respectively, deliver CS information to the LA. Either pathway alone has been shown to be sufficient as CS transmission routes to facilitate fear association (Romanski and Ledoux (1992)). It is therefore possible that deficit in thalamo-amygdala LTP does not translate to a decrease in freezing during conditioning, because the cortico-amygdala pathway is unaffected in *Nlgn3*$^{-/y}$. Futhermore, coactivation of thalamic and cortical pathways induces input-timing dependent plasticity at cortical-amygdala synapses (Cho et al. (2012)). So even though the thalamo-amygdala pathway has a reduced ability for potentiation, it is still able to facilitate the potentiation at cortico-amygdala synapses, and hence acquire the associative fear learning. This hypothesis could easily be tested by doing paired stimulation of thalamic and cortical inputs with the thalamic stimulation being delivered 15 ms earlier than the cortical stimulation. This mimics the temporal pattern of activation in behaving animals during auditory fear conditioning (Cho et al. (2012)). The expectation would be that cortico-amygdala potentiation *Nlgn3*$^{-/y}$ is inducible and comparable to that of WT.

The BA is important for fear avoidance behaviour (Manassero et al. (2018)). Interestingly, subsequent fear behaviour experiments have uncovered that *Nlgn3*$^{-/y}$ rats express their fear through flight rather than freezing, i.e. the animals will try to escape from the fear inducing context by running and jumping out the box if able (N. Anstey, University of Edinburgh, personal communication). The BA principal neurons exhibit increased firing in the *Nlgn3*$^{-/y}$, which could alter their fear expression, leading to rats trying to avoid the danger instead of freezing. It would be interesting to investigate if optogenetic inactivation of BA neurons during fear recall would change the *Nlgn3*$^{-/y}$'s behaviour from avoidance to freezing.

3.4 Summary

In summary, the findings in this chapter show that NLGN3 is important for normal amygdala function demonstrated through a variety of experiments. The loss of NLGN3 results in age-dependent increase in intrinsic excitability of BLA principal neurons. Whereas NLGN3 displays no involvement in basal excitatory synapse function, it is important for regulating inhibitory synaptic function in the LA. These findings support the theory that NLGNs are involved in regulating synapse maintenance, rather than

formation. Interestingly, the change in inhibitory transmission was restricted to the LA showing that NLGN3 loss can have distinct effects on closely associated brain regions. Finally, the loss of NLGN3 results in failure to induce LTP at a major sensory input associated with the formation of fear memories.

Chapter 4

Bridging the GAP

4.1 Introduction

SynGAP is well known for its role in regulating glutamatergic synapses through modulation of GTPase signaling in the PSD (Chen et al. (1998); Kim et al. (1998); Vazquez et al. (2004); Rumbaugh et al. (2006); Ozkan et al. (2014); Araki et al. (2015)), however it has been proposed by Walkup et al. (2016) that an important function of SynGAP is its ability to regulate the composition of the PSD, and thereby synaptic strength, through its association with PSD-95 — a role that is independent of the GTPase activity. The 'slot' hypothesis proposed by Walkup et al. (2016) suggests that SynGAP binds to and sequesters PDZ slots in the PSD-95, and that this sequestering is essential for structural and functional organisation of the PSD. Synaptic strength is then enhanced when SynGAP is reduced, either genetically or during activity-induced dispersion, and the PDZ binding slots become available. Other PDZ binding proteins are allowed to take the place of SynGAP, proteins that may stabilize and/or recruit AMPARs at the synapse, resulting in strengthening of the synapse.

A reduction in SynGAP expression results in an increased number of AMPARs at the synapse (Kim et al. (2003); Vazquez et al. (2004)) and accelerated synapse formation (Vazquez et al. (2004); Clement et al. (2012)) leading to a shift in excitatory/inhibitory balance (Clement et al. (2013)). Furthermore, aberrant synaptic plasticity is observed in *Syngap* haploinsufficiency (Komiyama et al. (2002); Kim et al. (2003); Carlisle et al. (2008); Ozkan et al. (2014); Barnes et al. (2015)). Moreover, *Syngap* haploinsufficient rats display enhanced fear recall after fear conditioning (Sup. Fig. S3; Dr. Sally Till, University of Edinburgh, unpublished).

It is likely that the reduction in SynGAP and the resulting decrease in its ability to compete for PDZ domains contribute to disease-relevant phenotypes as significantly as the reduction in synaptic Ras/Rap GAP activity. Dissecting the distinct molecular functions of SynGAP, and how they contribute to individual phenotypes, is necessary to further our understanding of this critical neurodevelopmental gene. Until now, the effects of a reduction of SynGAP in animal models has been restricted to null-mutations. It is therefore unclear how the distinct functions of SynGAP influence the phenotypes associated with *Syngap* loss-of-function. This thesis is the first study seeking to dissect the distinct molecular functions of SynGAP, and how they contribute to disease-relevant phenotypes by dissociating phenotypes observed in a null mutation and GAP deletion model of SynGAP haploinsufficiency.

In this chapter, I will seek to decipher the relative contributions of the two functional roles of SynGAP to the cellular physiology of principal neurons in amygdala. Two rats models have been developed for this purpose; a heterozygous null deletion of *Syngap*, $Syngap^{+/-}$; and a heterozygous *Syngap* with its GAP domain deleted, $Syngap^{+/\Delta GAP}$. The $Syngap^{+/\Delta GAP}$ rat model has an in-frame deletion in exon 8–12 — the exons partly encoding the GAP domain — thereby creating a SynGAP protein without a functional GAP domain. This truncated protein still gets transported to the postsynaptic compartment (Fig. 2.2), where it can potentially execute its GAP-independent functions. $Syngap^{+/-}$, on the other hand, is a null allele resulting in a 50% reduction of functional SynGAP protein. These two models can be used in unison to elucidate what roles the functional domains play in the synapse.

Based on the presumed functional roles of SynGAP, and studies in culture and $Syngap^{+/-}$ mice models, I hypothesised that a reduction in SynGAP would lead to increased excitability and excitatory synaptic transmission in $Syngap^{+/-}$, and that $Syngap^{+/\Delta GAP}$ would display the same phenotypes if the GAP domain is necessary and not only sufficient for the increase in synaptic strength. I postulated that the changes could be restricted to an earlier post-natal developmental stage, as studies indicate that SynGAP controls the trajectory of synapse maturation during development (Clement et al. (2012, 2013)). To test this, I investigated the intrinsic excitability of BLA principal neurons in p14 and p28 in the two *Syngap* rat models. Moreover, I examined the effect on basal excitatory and inhibitory synaptic transmission, in addition

to measuring activity-induced synaptic transmission at thalamo-amygdala synapses.

4.2 Results

The *Syngap*$^{+/-}$ and *Syngap*$^{+/\Delta GAP}$ rats were bred in separate colonies, and therefore each have their own WT control groups. The WTs are both denoted as *Syngap*$^{+/+}$, but with distinct colours: *Syngap*$^{+/-}$ WTs are light grey; whereas *Syngap*$^{+/\Delta GAP}$ WTs are black. To make comparison between models easier, a similar set of protocols to those done in *Nlgn3*$^{-/y}$ were performed in the two SynGAP models.

4.2.1 Comparable intrinsic properties of principal neurons of the BLA in *Syngap* haploinsufficiency models

SynGAP expression in the amygdala is very strong from p4–p14 (Porter et al. (2005)), suggesting that this period of brain development can be sensitive to reduced SynGAP protein expression. In agreement with this, an increased intrinsic excitability phenotype in hippocampus was observed in *Syngap*$^{+/-}$ mice at p8–9, though this had normalised by p14–16 (Clement et al. (2012)). I hypothesised that principal neurons in LA and BA would display an increase in intrinsic excitability at p14 as a consequence of SynGAP reduction.

To investigate the role of SynGAP on intrinsic cell physiology, a range of intrinsic properties were measured. Passive membrane properties (RMP, membrane time constant (τ), input resistance (R_i), membrane capacitance (C_M), and sag) were examined in p14 LA principal neurons and were found to be comparable between *Syngap*$^{+/-}$, *Syngap*$^{+/\Delta GAP}$, and their respective WT controls (Fig. 4.1). A series of incremental depolarising current injections revealed no changes in intrinsic firing in *Syngap*$^{+/-}$ nor in *Syngap*$^{+/\Delta GAP}$ (Fig. 4.2). As expected from the normal intrinsic excitability, no changes were observed in action potential properties between either groups (Fig. 4.3), nor were any post action potential currents altered in LA from neither *Syngap*$^{+/-}$ or *Syngap*$^{+/\Delta GAP}$ at p14 (Fig. 4.4).

Similarly to LA, no changes were found in passive membrane properties in p14 BA principal neurons in *Syngap*$^{+/-}$ or in *Syngap*$^{+/\Delta GAP}$ (Fig. 4.5). *Syngap*$^{+/-}$ displayed comparable intrinsic excitability and rheobase to *Syngap*$^{+/+}$ (Fig. 4.6). The voltage threshold for AP initiation was found to be significantly different in *Syngap*$^{+/-}$ compared

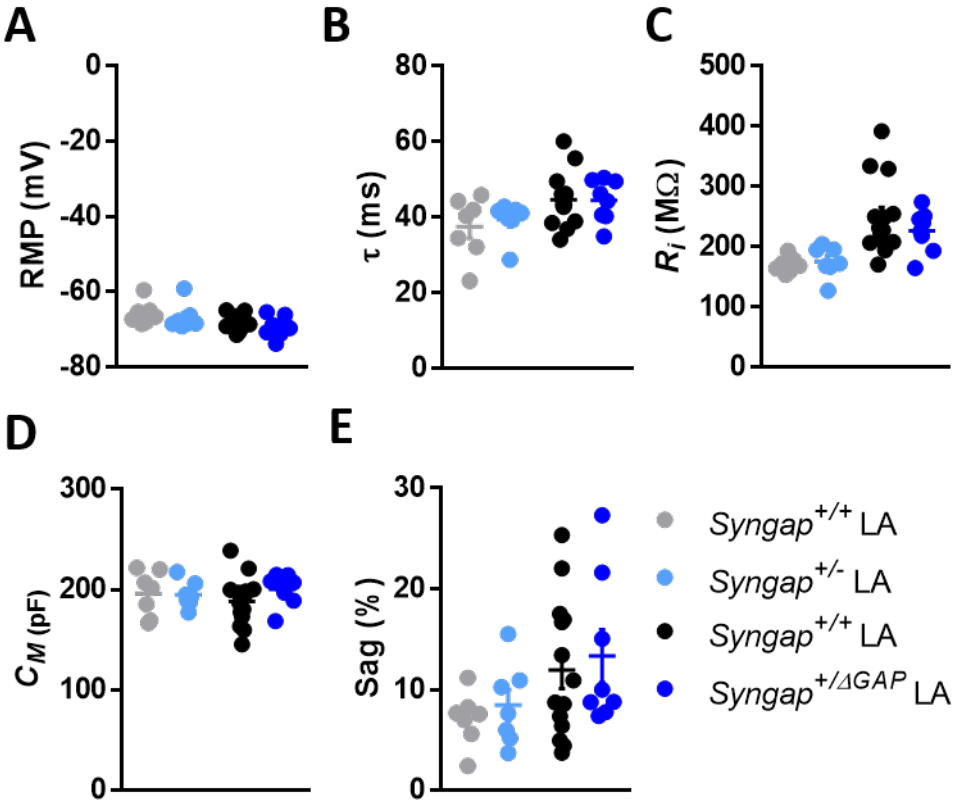

Figure 4.1: Passive membrane properties were not affected by a decrease in SynGAP or lack of the GAP domain in LA principal neurons at p14. (A) Resting membrane potential measured during 1 min of I=0 shows that *Syngap*$^{+/-}$ LA neurons have a comparable RPM to *Syngap*$^{+/+}$ (WT: -65.72 ± 1.14 mV, n=17 cells/7 animals; *Syngap*$^{+/-}$: -66.78 ± 1.33 mV, n=16 cells/7 animals; p=0.56, Student's unpaired *t*-test), as were the case between *Syngap*$^{+/\Delta GAP}$ and their WT littermates (*Syngap*$^{+/+}$: -68.01 ± 0.54 mV, n=32 cells/14 animals; *Syngap*$^{+/\Delta GAP}$: -69.19 ± 0.98 mV, n=20 cells/8 animals; p=0.26, Student's unpaired *t*-test). (B) The membrane time constant, τ, was not significantly different between the genotypes (*Syngap*$^{+/+}$: 37.50 ± 3.04 ms, n=17 cells/7 animals; *Syngap*$^{+/-}$: 39.33 ± 1.82 ms, n=16 cells/7 animals; p=0.61, Student's unpaired *t*-test; *Syngap*$^{+/+}$: 44.73 ± 1.87 ms, n=32 cells/14 animals; *Syngap*$^{+/\Delta GAP}$: 44.53 ± 1.97 ms, n=20 cells/8 animals; p=0.95, Student's Student's unpaired *t*-test.) (C) The input resistance was comparable between genotypes (*Syngap*$^{+/+}$: 169.9 ± 4.99 MΩ, n=17 cells/7 animals; *Syngap*$^{+/-}$: 175.3 ± 9.91 MΩ, n=16 cells/7 animals; p=0.63, Student's unpaired *t*-test; *Syngap*$^{+/+}$: 248.5 ± 16.51 MΩ, n=32 cells/14 animals; *Syngap*$^{+/\Delta GAP}$: 226.4 ± 12.27 MΩ, n=20 cells/8 animals; p=0.37, Student's unpaired *t*-test.) (D) Membrane capacitance was not significantly different in *Syngap*$^{+/-}$ or *Syngap*$^{+/\Delta GAP}$ compared to their respective WT littermates (*Syngap*$^{+/+}$: 195.9 ± 8.57 pF, n=17 cells/7 animals; *Syngap*$^{+/-}$: 195.0 ± 5.02 pF, n=16 cells/7 animals; p=0.92, Student's unpaired *t*-test; *Syngap*$^{+/+}$: 188.2 ± 6.55 pF, n=32 cells/14 animals; *Syngap*$^{+/\Delta GAP}$: 200.5 ± 5.49 pF, n=20 cells/8 animals; p=0.22, Student's unpaired *t*-test.) (E) Sag, a measure of Ih, was similar between genotypes (*Syngap*$^{+/+}$: 7.1 ± 1.01%, n=17 cells/7 animals; *Syngap*$^{+/-}$: 8.45 ± 1.54%, n=16 cells/7 animals; p=0.48, Student's unpaired *t*-test; *Syngap*$^{+/+}$: 11.94 ± 1.83%, n=32 cells/14 animals; *Syngap*$^{+/\Delta GAP}$: 13.33 ± 2.63%, n=20 cells/8 animals; p=0.66, Student's unpaired *t*-test.)

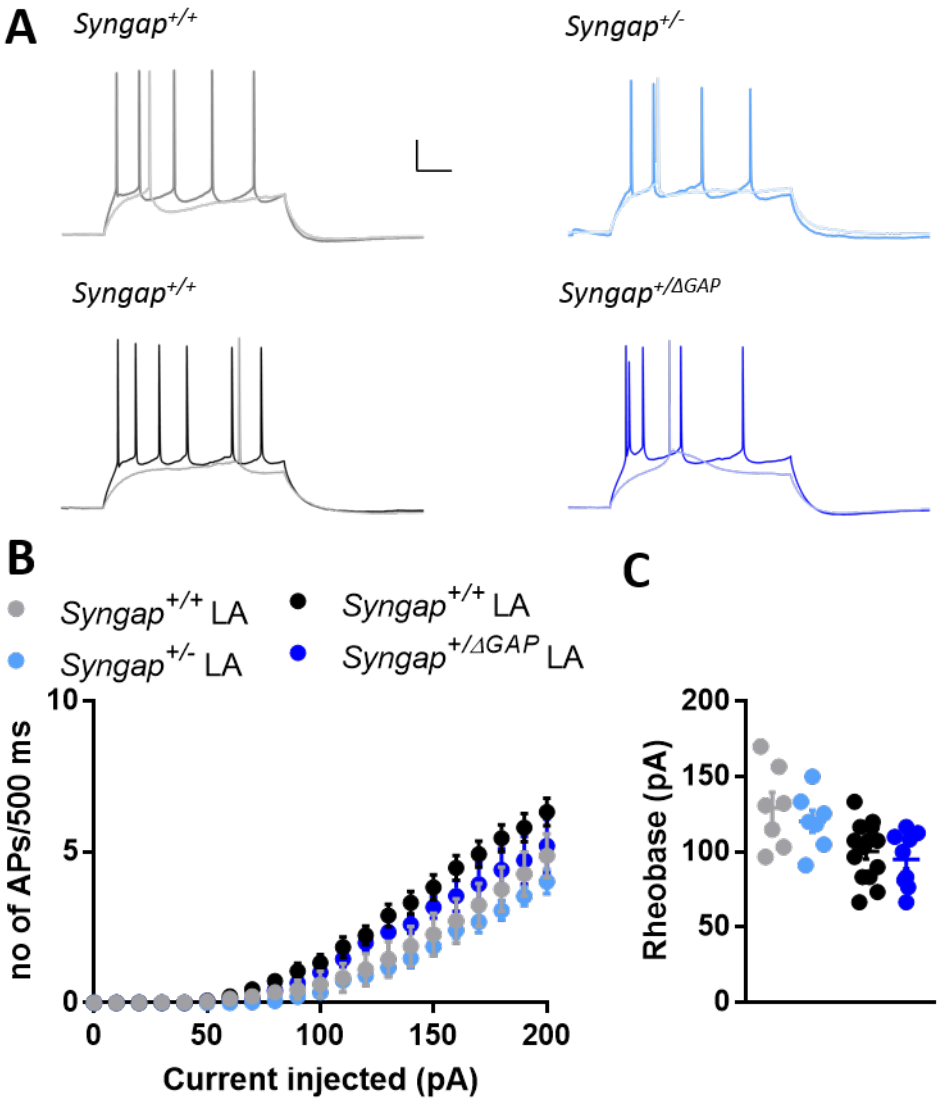

Figure 4.2: *SynGAP*$^{+/-}$ and *SynGAP*$^{+/\Delta GAP}$ LA principal neurons at p14 exhibit a comparable firing rate to WT littermates. (A) Example traces of *Syngap*$^{+/-}$ and *Syngap*$^{+/\Delta GAP}$ and their respective WT littermates, *Syngap*$^{+/+}$ voltage responses to rheobase and +200 pA current steps. Scale 100 ms, 20 mV. (B) *Syngap*$^{+/-}$ and *Syngap*$^{+/\Delta GAP}$ LA neurons firing frequencies to a series of depolarising current injections (0-200pA) are comparable to that of WT (*Syngap*$^{+/+}$/ *Syngap*$^{+/-}$: F(1,12)=0.48; p=0.50, 2-way RM-ANOVA; *Syngap*$^{+/+}$/ Syngap+/ GAP: F(1,15)=1.41; p=0.25, 2way RM-ANOVA)). (C) Rheobase was not significantly changed in either genotype (*Syngap*$^{+/+}$: 129.2 ± 10.19 pA, n=17 cells/7 animals; *Syngap*$^{+/-}$: 120.5 ±7.19 pA, n=16 cells/7 animals; p=0.50, Student's unpaired *t*-test; *Syngap*$^{+/+}$: 100.4 ± 5.1 pA, n=32 cells/14 animals; Syngap+/ GAP: 95.05 ±6.09 pA, n=20 cells/9 animals; p=0.51, Student's unpaired *t*-test).

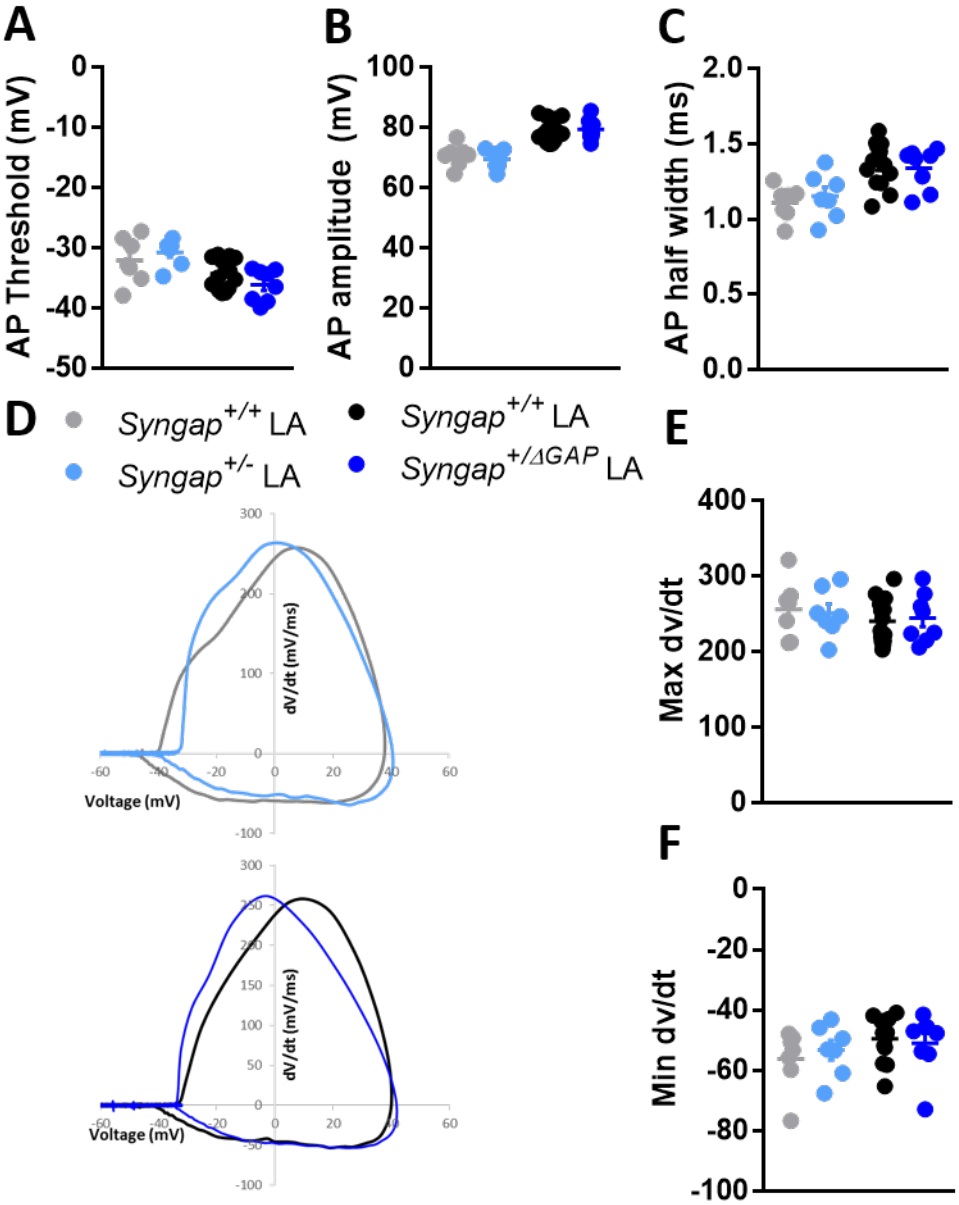

Figure 4.3: Action potential properties in *SynGAP*$^{+/-}$ and *SynGAP*$^{+/\Delta GAP}$ LA principal neurons at p14 are comparable to their WT littermates. (*continued on next page*)

Figure 4.3: (*contiued*) (A) AP threshold was comparable between genotypes (*Syngap*$^{+/+}$: -32.02 ± 1.44 mV, n=17 cells/7 animals; *Syngap*$^{+/-}$: -30.69 ± 0.82 mV, n=16 cells/7 animals; p=0.44, Student's unpaired *t*-test; *Syngap*$^{+/+}$: -34.23 ± 0.65 mV, n=32 cells/14 animals; *Syngap*$^{+/\Delta GAP}$: -36.09 ± 0.93 mV, n=20 cells/8 animals; p=0.11, Student's unpaired *t*-test). (B) AP amplitude measured from threshold was not different to WT littermates in neither *Syngap*$^{+/-}$ nor *Syngap*$^{+/\Delta GAP}$ (*Syngap*$^{+/+}$: 70.74 ± 1.41 mV, n=17 cells/7 animals; *Syngap*$^{+/-}$: 69.51 ± 1.19 mV, n=16 cells/7 animals; p=0.52, Student's unpaired *t*-test; *Syngap*$^{+/+}$: 79.12 ± 0.96 mV, n=32 cells/14 animals; *Syngap*$^{+/\Delta GAP}$: 79.55 ± 1.21 mV, n=20 cells/8 animals; p=0.79, Student's unpaired *t*-test). (C) AP half width at half AP height was similar between genotypes (*Syngap*$^{+/+}$: 1.11 ± 0.04 ms, n=17 cells/7 animals; *Syngap*$^{+/-}$: 1.16 ± 0.06 ms, n=16 cells/7 animals; p=0.54, unpaired Student's unpaired *t*-test; *Syngap*$^{+/+}$: 1.36 ± 0.04 ms, n=32 cells/14 animals; *Syngap*$^{+/\Delta GAP}$: 1.34 ± 0.05 ms, n=20 cells/8 animals; p=0.73, Student's unpaired *t*-test). (D) TOP: Phase plot of action potential in *Syngap*$^{+/+}$ (grey) and *Syngap*$^{+/-}$ (light blue) LA neuron. BOTTOM: Phase plot of action potential in *Syngap*$^{+/+}$ (black) and *Syngap*$^{+/-}$ (dark blue) LA neuron. (E) Max dv/dt was comparable between genotypes (*Syngap*$^{+/+}$: 256.6 ± 14.55 mV/ms, n=17 cells/7 animals; *Syngap*$^{+/-}$: 251.6 ± 12.04 mV/ms, n=16 cells/7 animals; p=0.80, Student's unpaired *t*-test; *Syngap*$^{+/+}$: 241.0 ± 7.80 mV/ms, n=32 cells/14 animals; *Syngap*$^{+/\Delta GAP}$: 244.9 ± 11.36 mV/ms, n=20 cells/8 animals; p=0.77, Student's unpaired *t*-test), as was min dv/dt (F) (*Syngap*$^{+/+}$: -56.15 ± 3.74 mV/ms, n=17 cells/7 animals; *Syngap*$^{+/-}$: -53.28 ± 3.22 mV/ms, n=16 cells/7 animals; p=0.57, Student's unpaired *t*-test; *Syngap*$^{+/+}$: -49.53 ± 1.86 mV/ms, n=32 cells/14 animals; *Syngap*$^{+/\Delta GAP}$: -51.03 ± 3.50 mV/ms, n=20 cells/8 animals; p=0.68, Student's unpaired *t*-test).

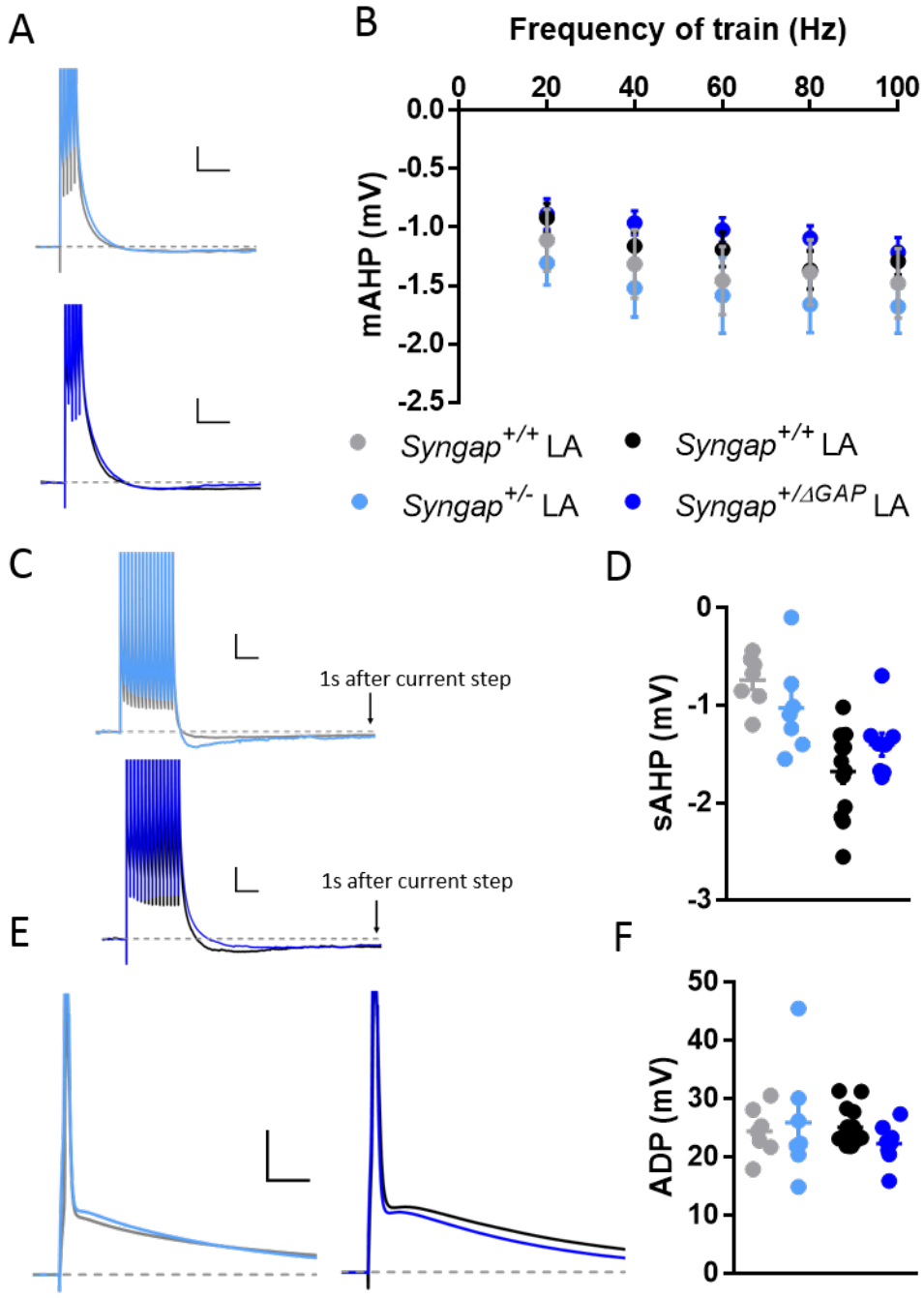

Figure 4.4: Post AP currents are not changed in *SynGAP*$^{+/-}$ or *SynGAP*$^{+/\Delta GAP}$ LA principal neurons at p14. (*continued on next page*)

Figure 4.4: (*continued*) (A) Example traces of the maximum AHP evoked by a train of 5 pulses at 100 Hz in (TOP) *Syngap*$^{+/+}$ (grey) and *Syngap*$^{+/-}$ (light blue) LA neurons, and (BOTTOM) *Syngap*$^{+/+}$ (black) and *Syngap*$^{+/\Delta GAP}$ (dark blue). Scale 100 ms, 5 mV. (B) Average mAHP after a train of 5 pulses at varying frequencies (20–100Hz) shows no significant differences between genotypes (*Syngap*$^{+/+}$/ *Syngap*$^{+/-}$: F(1,11)=0.28; p=0.60, 2way RM-ANOVA; *Syngap*$^{+/+}$/ Syngap+/ GAP: F(1,20)=0.66; p=0.43, 2way RM-ANOVA). (C) Example traces of sAHP after a train of 15 action potentials at 50 Hz in (TOP) *Syngap*$^{+/+}$ (grey) and *Syngap*$^{+/-}$ (light blue), and (BOTTOM) *Syngap*$^{+/+}$ (black) and *Syngap*$^{+/\Delta GAP}$ (dark blue) LA neurons. Scale 100ms, 5mV. (D) No significant difference was observed between either genotypes in sAHP (*Syngap*$^{+/+}$: -0.74 ± 0.10mV, n=17 cells/7 animals; *Syngap*$^{+/-}$: -1.02 ± 0.18ms, n=16 cells/7 animals; p=0.19, Student's unpaired *t*-test; *Syngap*$^{+/+}$: -1.68 ± 0.12mV, n=28 cells/13 animals; *Syngap*$^{+/\Delta GAP}$: -1.40 ± 0.12mV, n=20 cells/8 animals; p=0.14, Student's unpaired *t*-test). (E) Example traces of ADP following a single action potential in (TOP) *Syngap*$^{+/+}$ (grey) and *Syngap*$^{+/-}$ (light blue), and (BOTTOM) *Syngap*$^{+/+}$ (black) and *Syngap*$^{+/\Delta GAP}$ (dark blue) LA neurons. Scale bar 10ms, 20mV. (F) ADP after a single action potential was similar between genotypes *Syngap*$^{+/+}$: 24.43 ± 1.57mV, n=17 cells/7 animals; *Syngap*$^{+/-}$: 25.93 ± 3.72ms, n=16 cells/7 animals; p=0.72, Student's unpaired *t*-test; *Syngap*$^{+/+}$: 25.14 ± 0.88mV, n=32 cells/14 animals; *Syngap*$^{+/\Delta GAP}$: 22.30 ± 1.20mV, n=20 cells/8 animals; p=0.07, Student's unpaired *t*-test).

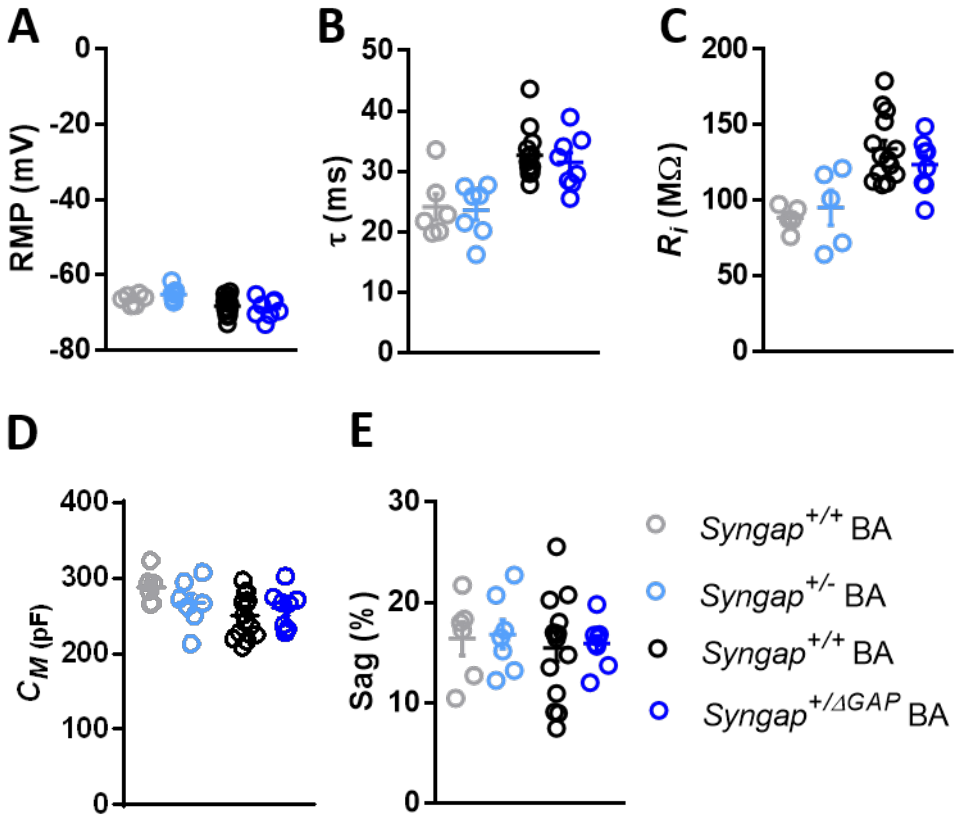

Figure 4.5: Passive membrane properties were not affected by a decrease in SynGAP or lack of the GAP domain in BA principal neurons at p14. (A) Resting membrane potential measured during 1 min of I=0 shows that *Syngap*$^{+/-}$ BA neurons have a comparable RPM to *Syngap*$^{+/+}$ (WT: -66.42 ± 0.56 mV, n=13 cells/6 animals; *Syngap*$^{+/-}$: -65.13 ± 0.74 mV, n=18 cells/7 animals; p=0.20, Student's unpaired *t*-test), as were the case between *Syngap*$^{+/\Delta GAP}$ and their WT littermates (*Syngap*$^{+/+}$: -68.16 ± 0.70 mV, n=34 cells/14 animals; *Syngap*$^{+/\Delta GAP}$: -68.79 ± 0.90 mV, n=17 cells/8 animals; p=0.59, Student's unpaired *t*-test). (B) The membrane time constant, τ, was not significantly different between the genotypes (*Syngap*$^{+/+}$: 24.11 ± 2.13 ms, n=13 cells/6 animals; *Syngap*$^{+/-}$: 23.62 ± 1.64 ms, n=16 cells/7 animals; p=0.86, Student's unpaired *t*-test; *Syngap*$^{+/+}$: 32.70 ± 1.07 ms, n=34 cells/14 animals; *Syngap*$^{+/\Delta GAP}$: 31.56 ± 1.57 ms, n=17 cells/8 animals; p=0.54, Student's unpaired *t*-test.) (C) The input resistance was comparable between genotypes (*Syngap*$^{+/+}$: 88.51 ± 3.67 MΩ, n=13 cells/6 animals; *Syngap*$^{+/-}$: 95.15 ± 11.6 MΩ, n=18 cells/7 animals; p=0.61, Student's unpaired *t*-test with Welch's correction; *Syngap*$^{+/+}$: 134.0 ± 5.80 MΩ, n=34 cells/14 animals; *Syngap*$^{+/\Delta GAP}$: 123.5 ± 6.27 MΩ, n=17 cells/8 animals; p=0.26, Student's unpaired *t*-test). (D) Membrane Capacitance was not significantly different in *Syngap*$^{+/-}$ or *Syngap*$^{+/\Delta GAP}$ compared to their respective WT littermates (*Syngap*$^{+/+}$: 288.0 ± 8.75 pF, n=13 cells/6 animals; *Syngap*$^{+/-}$: 266.8 ± 11.64 pF, n=18 cells/7 animals; p=0.19, Student's unpaired *t*-test; *Syngap*$^{+/+}$: 249.7 ± 7.54 pF, n=34 cells/14 animals; *Syngap*$^{+/\Delta GAP}$: 260.2 ± 9.01 pF, n=17 cells/8 animals; p=0.40, Student's unpaired *t*-test.) (E) Sag, a measure of Ih, was similar between genotypes (*Syngap*$^{+/+}$: 16.41 ± 1.67%, n=13 cells/6 animals; *Syngap*$^{+/-}$: 16.84 ± 1.44%, n=18 cells/7 animals; p=0.85, Student's unpaired *t*-test; *Syngap*$^{+/+}$: 15.47 ± 1.36%, n=34 cells/14 animals; *Syngap*$^{+/\Delta GAP}$: 15.9 ± 0.81%, n=17 cells/8 animals; p=0.79, Student's unpaired *t*-test with Welch's correction).

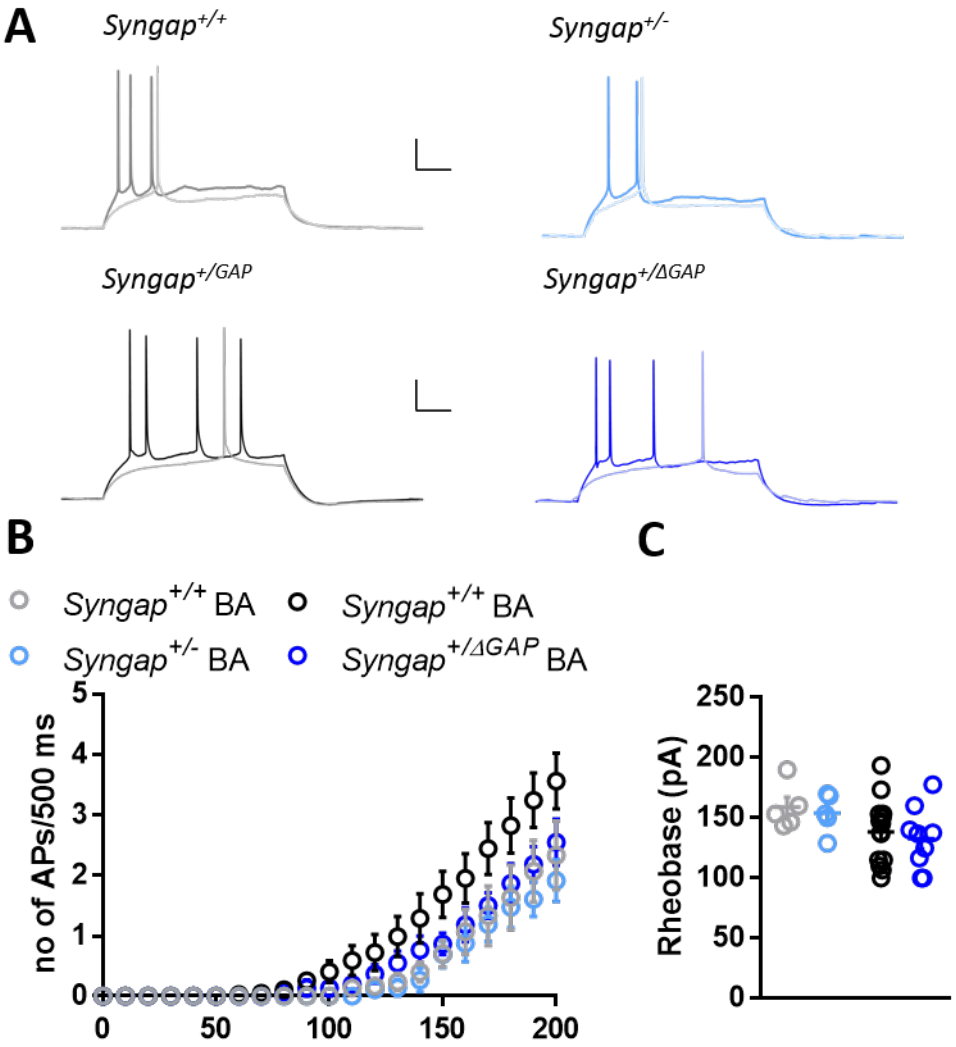

Figure 4.6: *SynGAP*$^{+/-}$ and *SynGAP*$^{+/\Delta GAP}$ BA principal neurons at p14 exhibit a comparable firing rate to WT littermates. (A) Example traces of *Syngap*$^{+/-}$ and *Syngap*$^{+/\Delta GAP}$ and their respective WT littermates, *Syngap*$^{+/+}$, voltage responses to rheobase and +200 pA current steps. Scale 100 ms, 20 mV. (B) *Syngap*$^{+/-}$ and *Syngap*$^{+/\Delta GAP}$ BA neurons firing frequencies to a series of depolarising current injections (0–200pA) are comparable to that of WT (*Syngap*$^{+/+}$/ *Syngap*$^{+/-}$: F(1,8)=0.27; p=0.62, 2-way RM-ANOVA; *Syngap*$^{+/+}$/*Syngap*$^{+/\Delta GAP}$: F(1,15)=1.39; p=0.26, 2way RM-ANOVA)). (C) Rheobase was not significantly changed in either genotype (*Syngap*$^{+/+}$: 158.7 ± 8.34 pA, n=8 cells/5 animals; *Syngap*$^{+/-}$: 154.1 ±7.47 pA, n=7 cells/5 animals; p=0.50, Student's unpaired *t*-test; *Syngap*$^{+/+}$: 138.3 ± 7.16 pA, n=34 cells/14 animals; *Syngap*$^{+/\Delta GAP}$: 132.5 ±8.58 pA, n=20 cells/9 animals; p=0.62, Student's unpaired *t*-test).

to *Syngap*$^{+/+}$, however all other action potential properties were found to be comparable (Fig. 4.7). Since no other changes to intrinsic properties were found, the significant differences in voltage threshold was considered to be a false positive.

Similar post action potential currents were found to *Syngap*$^{+/-}$ compared to its WT control (Fig. 4.8). *Syngap*$^{+/\Delta GAP}$ BA principal neurons showed a decrease in number of action potentials fired, though this was not significantly different (Fig. 4.6). Action potential properties were not affected in *Syngap*$^{+/\Delta GAP}$ BA principal neurons at p14 (Fig. 4.7), and no significant changes were observed in post action potential currents between *Syngap*$^{+/\Delta GAP}$ and *Syngap*$^{+/+}$ (Fig. 4.8).

Taken together, this data suggests that a reduction of whole SynGAP or loss of its GAP domain has little to no consequences on intrinsic properties in LA and BA principal neurons at p14.

4.2.2 *SynGAP*$^{+/-}$ display an increase in firing in LA principal neurons at p28

SynGAP expression peaks between p4 and p14, followed by a decrease in expression with age (Porter et al. (2005)). You might therefore expect to see physiological changes emerge at an early post natal age, but development of phenotypes later in development has also been observed (Ozkan et al. (2014)). The latter could be compensatory to correct for more direct effects following SynGAP reduction.

Similarly to p14 LA principal neurons, no significant changes were found in passive membrane properties in LA principal neurons from p28 animals between *Syngap*$^{+/-}$, *Syngap*$^{+/\Delta GAP}$, and their respective WT controls (Fig. 4.9). In response to depolarising current steps, *Syngap*$^{+/\Delta GAP}$ demonstrated a similar rate of firing to *Syngap*$^{+/+}$ in LA (Fig. 4.10). However, *Syngap*$^{+/-}$ showed a significant increase in firing at increasing depolarising current steps (Fig. 4.10B; effect of interaction: $F(16,192)=6.15$; $p<0.001$, 2way RM-ANOVA). A decrease in rheobase was seen in *Syngap*$^{+/-}$ compared to *Syngap*$^{+/+}$, albeit this was not significant (Fig. 4.10C). Measuring the action potential waveform and kinetics revealed no significant differences in either model (Fig. 4.11), suggesting that the active cation currents underlying APs are not causing the changes observed in firing rate in *Syngap*$^{+/-}$ LA principal neurons. The post action potential currents (mAHP, sAHP, and ADP) were all found to be comparable between *Syngap*$^{+/-}$, *Syngap*$^{+/\Delta GAP}$, and their respective WT controls (Fig. 4.12), hence these

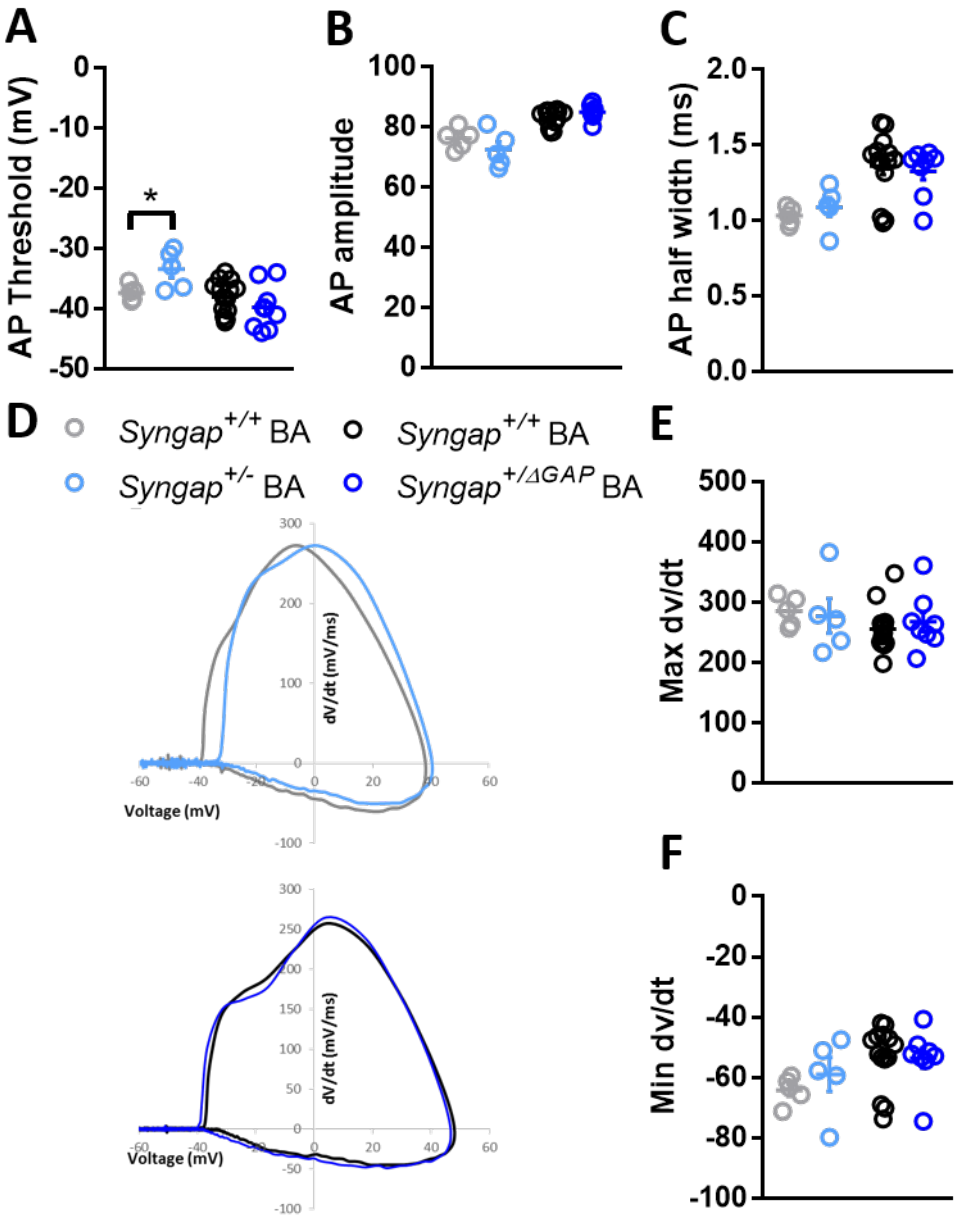

Figure 4.7: Action potential properties in *SynGAP*$^{+/-}$ and *SynGAP*$^{+/\Delta GAP}$ BA principal neurons at p14 are comparable to their WT littermates. (*continued on next page*)

Figure 4.7: (*continued*) (A) AP threshold was significantly different between *Syngap*$^{+/-}$ and *Syngap*$^{+/+}$ (*Syngap*$^{+/+}$: -37.3 ± 0.59 mV, n=8 cells/5 animals; *Syngap*$^{+/-}$: -33.39 ± 1.42 mV, n=7 cells/5 animals; p=0.04, Student's unpaired *t*-test), but comparable between *Syngap*$^{+/-}$ and *Syngap*$^{+/+}$ *Syngap*$^{+/+}$: -37.99 ± 0.73 mV, n=34 cells/14 animals; *Syngap*$^{+/\Delta GAP}$: -39.77 ± 1.22 mV, n=20 cells/8 animals; p=0.19, Student's unpaired *t*-test). (B) AP amplitude measured from threshold was not different to WT littermates in neither *Syngap*$^{+/-}$ nor *Syngap*$^{+/\Delta GAP}$ (*Syngap*$^{+/+}$: 76.3 ± 1.58 mV, n=7 cells/5 animals; *Syngap*$^{+/-}$: 72.54 ± 2.66 mV, n=7 cells/5 animals; p=0.26, Student's unpaired *t*-test; *Syngap*$^{+/+}$: 83.24 ± 0.74 mV, n=34 cells/14 animals; *Syngap*$^{+/\Delta GAP}$: 85.04 ± 0.88 mV, n=20 cells/8 animals; p=0.14, Student's unpaired *t*-test). (C) AP half width at half AP height was similar between genotypes (*Syngap*$^{+/+}$: 1.03 ± 0.03 ms, n=8 cells/5 animals; *Syngap*$^{+/-}$: 1.09 ± 0.06 ms, n=7 cells/5 animals; p=0.42, Student's unpaired *t*-test; *Syngap*$^{+/+}$: 1.36 ± 0.06ms, n=34 cells/14 animals; *Syngap*$^{+/\Delta GAP}$: 1.33 ± 0.06ms, n=20 cells/8 animals; p=0.70, Student's unpaired *t*-test). (D) Phase plot of action potential in (TOP) *Syngap*$^{+/+}$ (grey), *Syngap*$^{+/-}$ (light blue), (BOTTOM) *Syngap*$^{+/+}$ (black), and *Syngap*$^{+/-}$ (dark blue) BA neurons. (E) Max dv/dt was comparable between genotypes (*Syngap*$^{+/+}$: 286.2 ± 11.3mV/ms, n=8 cells/5 animals; *Syngap*$^{+/-}$: 278.1 ± 28.76mV/ms, n=7 cells/5 animals; p=0.80, Student's unpaired *t*-test; *Syngap*$^{+/+}$: 255.9 ± 9.88mV/ms, n=34 cells/14 animals; *Syngap*$^{+/\Delta GAP}$: 268.1 ± 16.23mV/ms, n=20 cells/8 animals; p=0.50, Student's unpaired *t*-test), as was min dv/dt (F) (*Syngap*$^{+/+}$: -64.13 ± 2.04mV/ms, n=8 cells/5 animals; *Syngap*$^{+/-}$: -59.0 ± 5.61mV/ms, n=7 cells/5 animals; p=0.42, Student's unpaired *t*-test; *Syngap*$^{+/+}$: -53.22 ± 2.76mV/ms, n=34 cells/14 animals; *Syngap*$^{+/\Delta GAP}$: -53.52 ± 3.36mV/ms, n=20 cells/8 animals; p=0.95, Student's unpaired *t*-test).

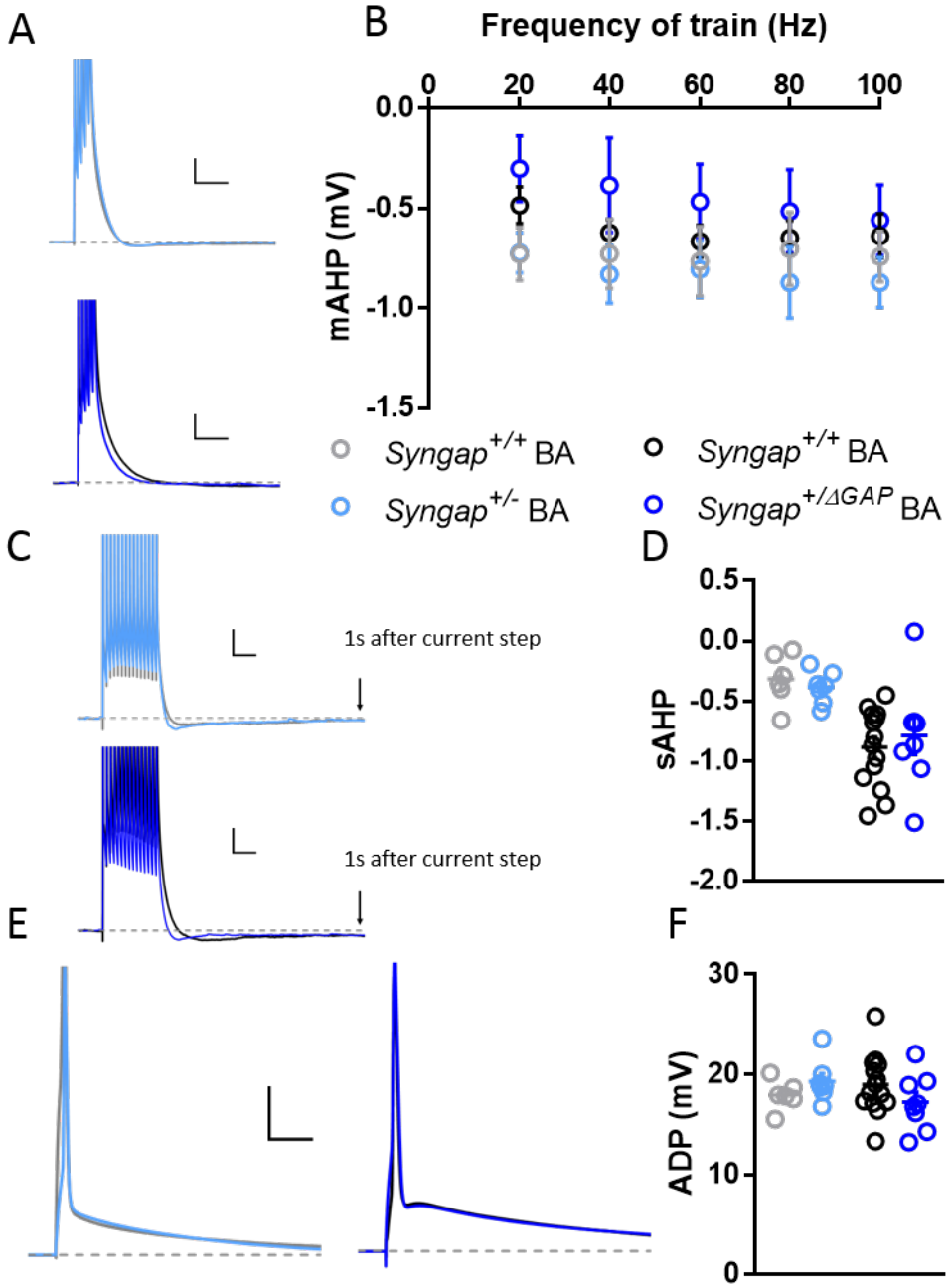

Figure 4.8: Post AP currents are not changed in $SynGAP^{+/-}$ or $SynGAP^{+/\Delta GAP}$ BA principal neurons at p14. (*continued on next page*)

Figure 4.8: (*continued*) (A) Example traces of the maximum AHP evoked by a train of 5 pulses at 100 Hz in (TOP) *Syngap*$^{+/+}$ (grey), *Syngap*$^{+/-}$ (light blue), (BOTTOM) *Syngap*$^{+/+}$ (black), and *Syngap*$^{+/\Delta GAP}$ (dark blue) BA neurons. Scale 100 ms, 5 mV. (B) Average mAHP after a train of 5 pulses at varying frequencies (20–100Hz) shows no significant differences between genotypes (*Syngap*$^{+/+}$/ *Syngap*$^{+/-}$: F(1,11)=0.18; p=0.68, 2way RM-ANOVA; *Syngap*$^{+/+}$/ Syngap+/ GAP: F(1,20)=0.90; p=0.35, 2way RM-ANOVA). (C) Example traces of sAHP after a train of 15 action potentials at 50 Hz in (TOP) *Syngap*$^{+/+}$ (grey), *Syngap*$^{+/-}$ (light blue), (BOTTOM) *Syngap*$^{+/+}$ (black), and *Syngap*$^{+/\Delta GAP}$ (dark blue) BA neurons. Scale 100 ms, 5 mV. (D) No significant difference was observed between either genotypes in sAHP (*Syngap*$^{+/+}$: -0.31 ± 0.09 mV, n=13 cells/6 animals; *Syngap*$^{+/-}$: -0.38 ± 0.05 ms, n=18 cells/7 animals; p=0.49, Student's unpaired *t*-test; *Syngap*$^{+/+}$: -0.89 ± 0.09 mV, n=30 cells/13 animals; *Syngap*$^{+/\Delta GAP}$: -0.79 ± 0.15 mV, n=16 cells/8 animals; p=0.56, Student's unpaired *t*-test). (E) Example traces of ADP following a single action potential in (TOP) *Syngap*$^{+/+}$ (grey), *Syngap*$^{+/-}$ (light blue), (BOTTOM) *Syngap*$^{+/+}$ (black), and *Syngap*$^{+/\Delta GAP}$ (dark blue) BA neurons. Scale bar 10 ms, 20 mV. (F) ADP after a single action potential was similar between genotypes *Syngap*$^{+/+}$: 17.95 ± 0.62 mV, n=13 cells/6 animals; *Syngap*$^{+/-}$: 19.32 ± 0.80 ms, n=18 cells/7 animals; p=0.21, Student's unpaired *t*-test; *Syngap*$^{+/+}$: 18.99 ± 0.79 mV, n=31 cells/14 animals; *Syngap*$^{+/\Delta GAP}$: 17.23 ± 1.00 mV, n=17 cells/8 animals; p=0.07, Student's unpaired *t*-test).

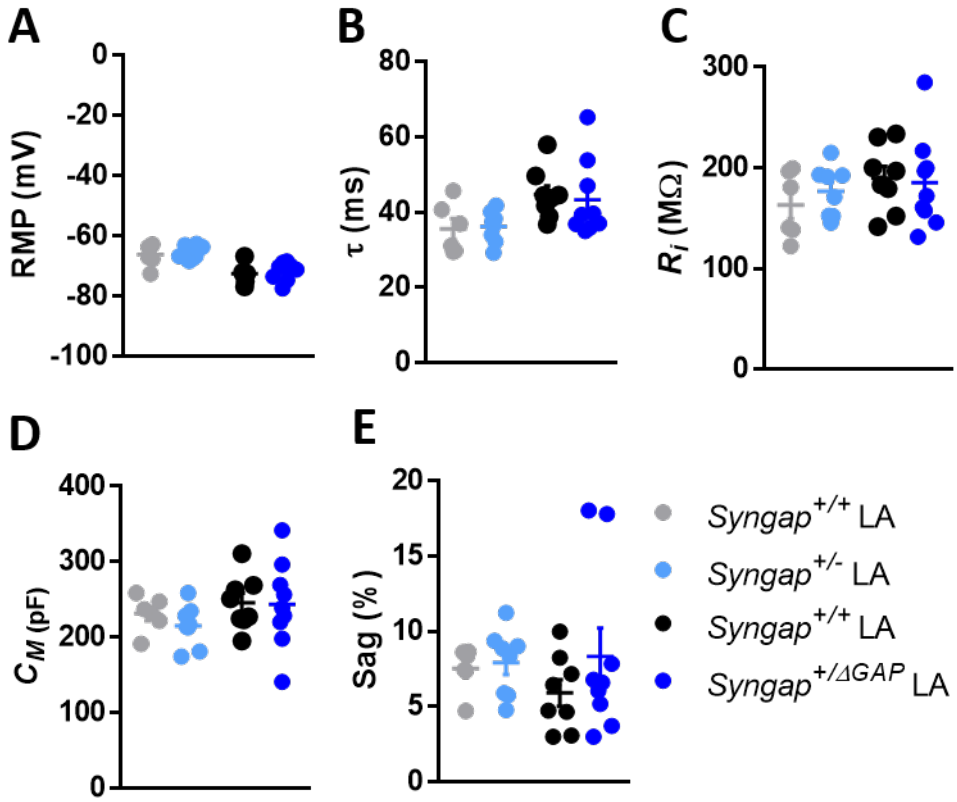

Figure 4.9: Passive membrane properties were not affected by a decrease in SynGAP or lack of the GAP domain in LA principal neurons at p28 (A) Resting membrane potential measured during 1 min of I=0 shows that both *Syngap*$^{+/-}$ and *Syngap*$^{+/\Delta GAP}$ LA neurons have a comparable RPM to their WT littermates (*Syngap*$^{+/+}$: -66.19 ± 1.51 mV, n=22 cells/6 animals; *Syngap*$^{+/-}$: -65.72 ± 0.81 mV, n=29 cells/8 animals; p=0.77, Student's unpaired *t*-test; *Syngap*$^{+/+}$: -72.56 ± 1.04 mV, n=24 cells/8 animals; *Syngap*$^{+/\Delta GAP}$: -71.43 ± 1.02 mV, n=24 cells/9 animals; p=0.45, Student's unpaired *t*-test). (B) The membrane time constant, τ, was not significantly different between the genotypes (*Syngap*$^{+/+}$: 35.65 ± 2.72 ms, n=22 cells/6 animals; *Syngap*$^{+/-}$: 36.22 ± 1.48 ms, n=29 cells/8 animals; p=0.85, Student's unpaired *t*-test; *Syngap*$^{+/+}$: 44.77 ± 2.34 ms, n=24 cells/8 animals; *Syngap*$^{+/\Delta GAP}$: 43.36 ± 3.41 ms, n=24 cells/9 animals; p=0.74, Student's unpaired *t*-test.) (C) The input resistance was comparable between genotypes (*Syngap*$^{+/+}$: 163.0 ± 13.57 MΩ, n=22 cells/6 animals; *Syngap*$^{+/-}$: 176.5 ± 8.87 MΩ, n=29 cells/8 animals; p=0.40, Student's unpaired *t*-test; *Syngap*$^{+/+}$: 189.7 ± 11.66 MΩ, n=24 cells/8 animals; *Syngap*$^{+/\Delta GAP}$: 185.1 ± 15.5 MΩ, n=24 cells/9 animals; p=0.82, Student's unpaired *t*-test.) (D) Membrane Capacitance was not significantly different in *Syngap*$^{+/-}$ or *Syngap*$^{+/\Delta GAP}$ compared to their respective WT littermates (*Syngap*$^{+/+}$: 231.4 ± 9.55 pF, n=22 cells/6 animals; *Syngap*$^{+/-}$: 215.2 ± 9.74 pF, n=29 cells/8 animals; p=0.27, Student's unpaired *t*-test; *Syngap*$^{+/+}$: 245.5 ± 12.63 pF, n=24 cells/8 animals; *Syngap*$^{+/\Delta GAP}$: 243.4 ± 19.26 pF, n=24 cells/9 animals; p=0.93, Student's unpaired *t*-test.) (E) Sag, a measure of Ih, was similar between genotypes (*Syngap*$^{+/+}$: 7.53 ± 0.61%, n=22 cells/6 animals; *Syngap*$^{+/-}$: 7.91 ± 0.78%, n=29 cells/8 animals; p=0.72, Student's unpaired *t*-test; *Syngap*$^{+/+}$: 5.92 ± 0.88%, n=24 cells/8 animals; *Syngap*$^{+/\Delta GAP}$: 8.33 ± 1.88%, n=24 cells/9 animals; p=0.28, Student's unpaired *t*-test.)

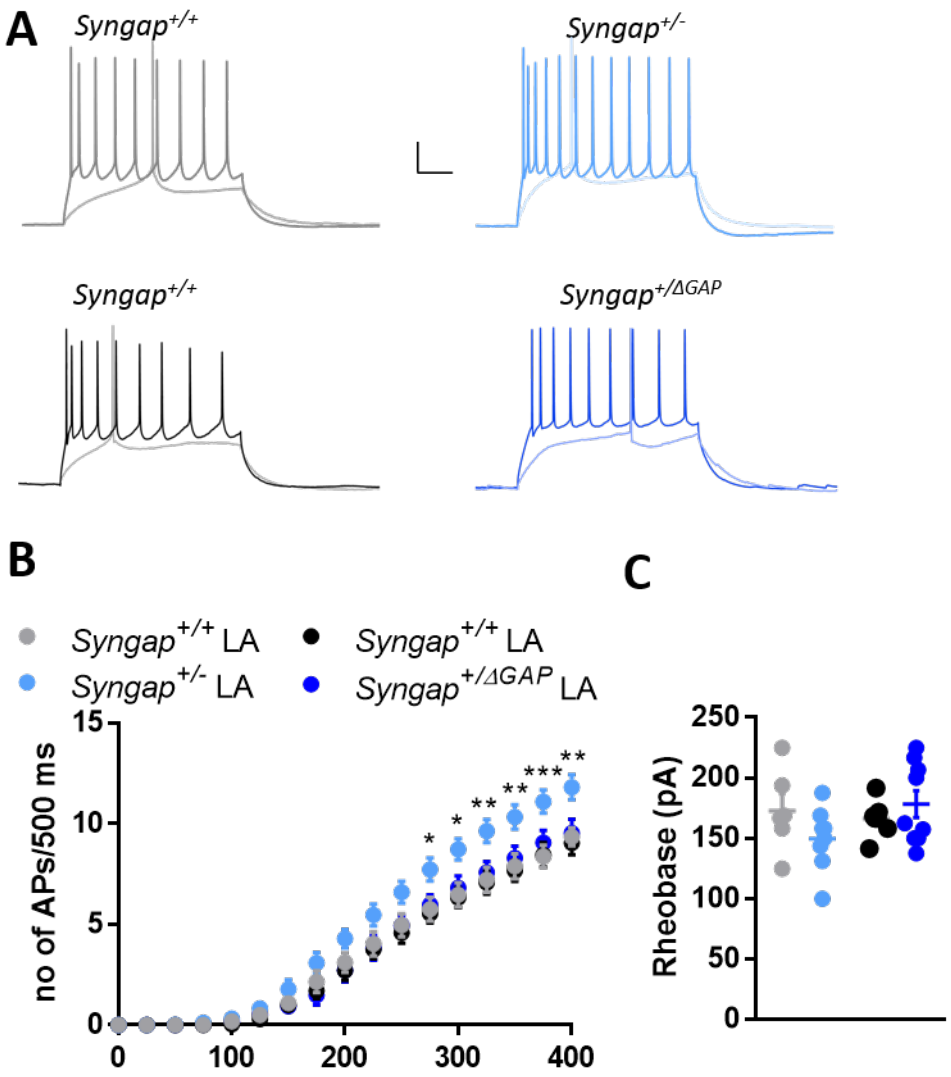

Figure 4.10: *SynGAP*$^{+/-}$ p28 LA principal neurons have an increase in firing rate compared to WT littermates. (A) Example traces of *Syngap*$^{+/-}$ and *Syngap*$^{+/\Delta GAP}$ and their respective WT littermates, *Syngap*$^{+/+}$, voltage responses to rheobase and +400 pA current steps. Scale 100 ms, 20 mV. (B) *Syngap*$^{+/-}$ p28 LA principal neurons show an increase in firing rate compared to *Syngap*$^{+/+}$ ($F(16,192)=6.15$; $p<0.0001$, 2way RM-ANOVA with Sidak post hoc correction), whereas *Syngap*$^{+/\Delta GAP}$ LA neurons firing rates are comparable to that of WT ($F(1,15)=0.22$; $p=0.65$, 2-way RM-ANOVA). (C) Rheobase was not significantly changed in either genotype (*Syngap*$^{+/+}$: 172.9 ± 13.80 pA, n=22 cells/6 animals; *Syngap*$^{+/-}$: 149.7 ± 9.26 pA, n=29 cells/8 animals; p=0.17, Student's unpaired *t*-test; *Syngap*$^{+/+}$: 166.5 ± 4.9 pA, n=24 cells/8 animals; Syngap+/ GAP: 178.4 ±11.1 pA, n=24 cells/9 animals; p=0.35, Student's unpaired *t*-test).

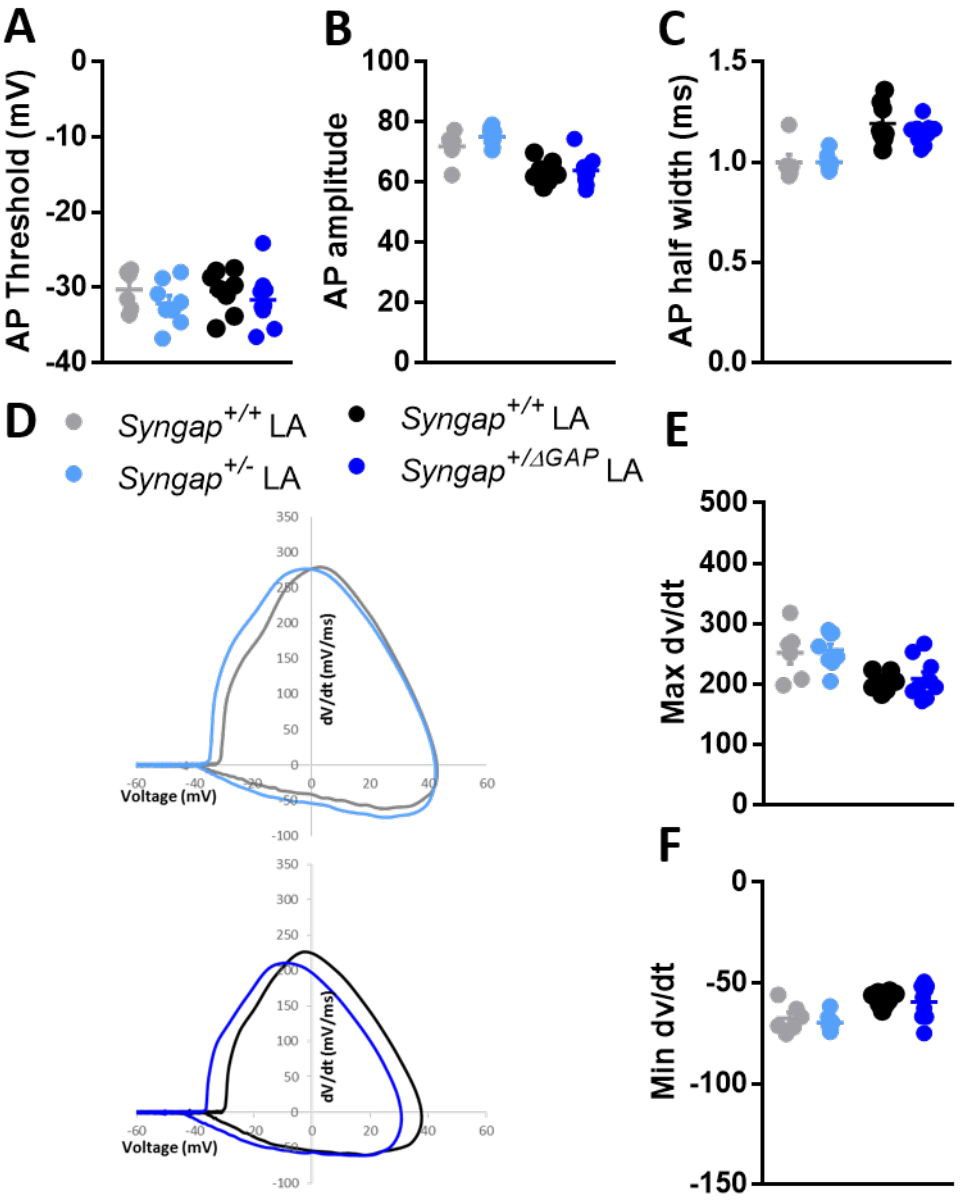

Figure 4.11: Action potential properties in *SynGAP*$^{+/-}$ and *SynGAP*$^{+/\Delta GAP}$ LA principal neurons at p28 are comparable to their WT littermates. (*continued on next page*)

Figure 4.11: (*continued*) (A) AP threshold was comparable between genotypes (*Syngap*$^{+/+}$: -30.28 ± 1.09 mV, n=22 cells/6 animals; *Syngap*$^{+/-}$: -32.1 ± 1.03 mV, n=29 cells/8 animals; p=0.26, Student's unpaired *t*-test; *Syngap*$^{+/+}$: -30.49 ± 1.00 mV, n=24 cells/8 animals; *Syngap*$^{+/\Delta GAP}$: -31.63 ± 1.21 mV, n=24 cells/9 animals; p=0.49, Student's unpaired *t*-test). (B) AP amplitude measured from threshold was not different to WT littermates in neither *Syngap*$^{+/-}$ nor *Syngap*$^{+/\Delta GAP}$ (*Syngap*$^{+/+}$: 71.9 ± 2.08mV, n=22 cells/6 animals; *Syngap*$^{+/-}$: 75.08 ± 1.06mV, n=29 cells/8 animals; p=0.17, Student's unpaired *t*-test; *Syngap*$^{+/+}$: 63.62 ± 1.30mV, n=24 cells/8 animals; *Syngap*$^{+/\Delta GAP}$: 63.9 ± 1.65mV, n=24 cells/9 animals; p=0.90, Student's unpaired *t*-test). (C) AP half width at half AP height was similar between genotypes (*Syngap*$^{+/+}$: 0.99 ± 0.04ms, n=22 cells/6 animals; *Syngap*$^{+/-}$: 1.00 ± 0.01ms, n=29 cells/8 animals; p=0.97, Welch's unpaired *t*-test with; *Syngap*$^{+/+}$: 1.19 ± 0.04ms, n=24 cells/8 animals; *Syngap*$^{+/\Delta GAP}$: 1.15 ± 0.02ms, n=24 cells/9 animals; p=0.26, unpaired *t*-test). (D) (TOP) Phase plot of action potential in *Syngap*$^{+/+}$ (grey), *Syngap*$^{+/-}$ (light blue), (BOTTOM) *Syngap*$^{+/+}$ (black), and *Syngap*$^{+/-}$ (dark blue) LA neurons. (E) Max dv/dt was comparable between genotypes (*Syngap*$^{+/+}$: 252.0 ± 17.95 mV/ms, n=22 cells/6 animals; *Syngap*$^{+/-}$: 256.0 ± 10.46 mV/ms, n=29 cells/8 animals; p=0.84, Student's unpaired *t*-test; *Syngap*$^{+/+}$: 204.0 ± 5.09 mV/ms, n=24 cells/8 animals; *Syngap*$^{+/\Delta GAP}$: 209.1 ± 11.16 mV/ms, n=24 cells/9 animals; p=0.69, Student's unpaired *t*-test), as was min dv/dt (F) (*Syngap*$^{+/+}$: -67.38 ± 2.91 mV/ms, n=22 cells/6 animals; *Syngap*$^{+/-}$: -69.75 ± 1.43 mV/ms, n=29 cells/8 animals; p=0.44, Student's unpaired *t*-test; *Syngap*$^{+/+}$: -57.91 ± 1.25 mV/ms, n=24 cells/8 animals; *Syngap*$^{+/\Delta GAP}$: -59.29 ± 2.94 mV/ms, n=24 cells/9 animals; p=0.68, Student's unpaired *t*-test).

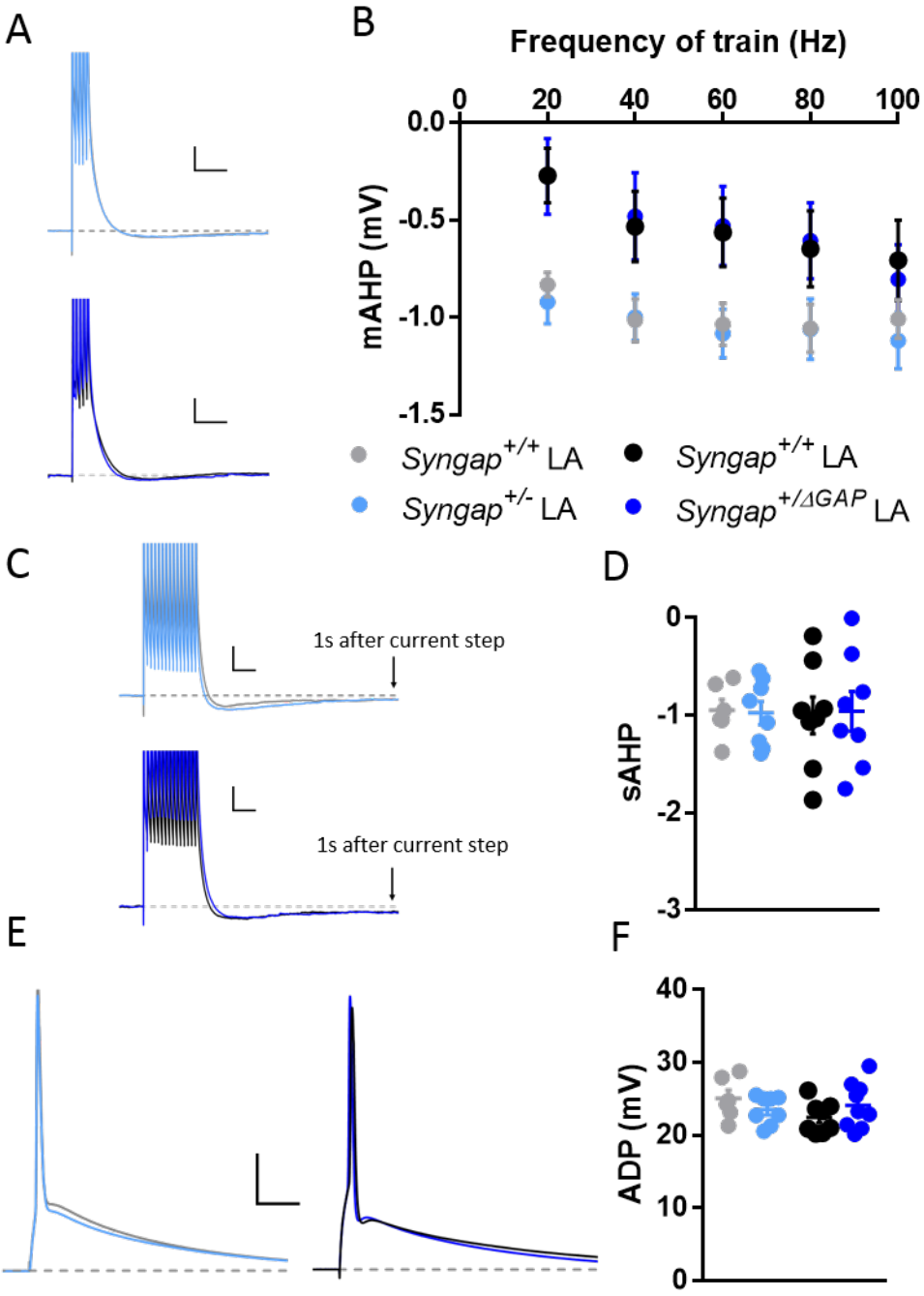

Figure 4.12: Post AP currents are not changed in *SynGAP*$^{+/-}$ or *SynGAP*$^{+/\Delta GAP}$ LA principal neurons at p28 (*continued on next page*)

Figure 4.12: (*continued*) (A) Example traces of the maximum AHP evoked by a train of 5 pulses at 100 Hz in (TOP) *Syngap*$^{+/+}$ (grey), *Syngap*$^{+/-}$ (light blue), (BOTTOM) *Syngap*$^{+/+}$ (black), and *Syngap*$^{+/\Delta GAP}$ (dark blue). Scale 100 ms, 5 mV. (B) Average mAHP after a train of 5 pulses at varying frequencies (20-100Hz) shows no significant differences between genotypes (*Syngap*$^{+/+}$/ *Syngap*$^{+/-}$: F(1,12)=0.08; p=0.78, 2way RM-ANOVA; *Syngap*$^{+/+}$/ Syngap+/ GAP: F(1,15)=0.0003; p=0.99, 2way RM-ANOVA). (C) Example traces of sAHP after a train of 15 action potentials at 50 Hz in (TOP) *Syngap*$^{+/+}$ (grey), *Syngap*$^{+/-}$ (light blue), (BOTTOM) *Syngap*$^{+/+}$ (black), and *Syngap*$^{+/\Delta GAP}$ (dark blue) LA neurons. Scale 100ms, 5mV. (D) No significant difference was observed between either genotypes in sAHP (*Syngap*$^{+/+}$: -0.95 ± 0.11 mV, n=22 cells/6 animals; *Syngap*$^{+/-}$: -0.98 ± 0.12 mV, n=29 cells/8 animals; p=0.88, Student's unpaired *t*-test; *Syngap*$^{+/+}$: -1.00 ± 0.19 mV, n=24 cells/8 animals; *Syngap*$^{+/\Delta GAP}$: -0.96 ± 0.21 mV, n=24 cells/9 animals; p=0.88, Student's unpaired *t*-test). (E) Example traces of ADP following a single action potential in (TOP) *Syngap*$^{+/+}$ (grey), *Syngap*$^{+/-}$ (light blue), (BOTTOM) *Syngap*$^{+/+}$ (black), and *Syngap*$^{+/\Delta GAP}$ (dark blue) LA neurons. Scale bar 10 ms, 20 mV. (F) ADP after a single action potential was similar between genotypes *Syngap*$^{+/+}$: 25.05 ± 1.16 mV, n=22 cells/6 animals; *Syngap*$^{+/-}$: 23.52 ± 0.68 mV, n=29 cells/8 animals; p=0.25, Student's unpaired *t*-test; *Syngap*$^{+/+}$: 22.46 ± 0.76 mV, n=24 cells/8 animals; *Syngap*$^{+/\Delta GAP}$: 24.12 ± 1.05 mV, n=24 cells/9 animals; p=0.23, Student's unpaired *t*-test).

do not contribute to the changes in excitability in *Syngap*$^{+/-}$ LA principal neurons.

In the BA, *Syngap*$^{+/-}$ principal neurons at p28 presented with similar passive membrane properties to *Syngap*$^{+/+}$ (Fig. 4.13). *Syngap*$^{+/\Delta GAP}$ BA principal neurons displayed no significant changes in passive membrane properties, though both the membrane time constant and the input resistance were trending to a decrease compared to *Syngap*$^{+/+}$. Whereas *Syngap*$^{+/-}$ principal neurons in the LA displayed an increase in firing, BA principal neurons from *Syngap*$^{+/-}$ had a comparable firing rate to that of *Syngap*$^{+/+}$ (Fig. 4.14). *Syngap*$^{+/\Delta GAP}$ BA principal neurons, on the other hand, were hypoexcitable compared to *Syngap*$^{+/+}$ (Fig. 4.14B; effect of interaction $F(16, 256)=6.75$; $p<0.001$, 2way RM-ANOVA), which was associated with a significant increase in rheobase (Fig. 4.14C; *Syngap*$^{+/+}$: 205.1 ± 8.7 pA, n=24 cells/8 animals; *Syngap*$^{+/\Delta GAP}$: 240.4 ±12.36 pA, n=29 cells/10 animals; $p=0.04$, Student's unpaired *t*-test).

The decrease in firing in *Syngap*$^{+/\Delta GAP}$ BA principal neurons could not be explained by changes to action potential waveforms or kinetics, as these were all comparable to *Syngap*$^{+/+}$ (Fig. 4.15). Additionally, post action potential currents were not altered in *Syngap*$^{+/\Delta GAP}$ (Fig. 4.16), and thus does not underlie the hypoexcitability. *Syngap*$^{+/-}$ displayed comparable action potential properties and kinetics to *Syngap*$^{+/+}$ (Fig. 4.15), as well as similar post AP currents in BA principal neurons at p28 (Fig. 4.16).

In sum, divergent *Syngap* model and nuclei distinct alterations to intrinsic excitability was detected after longer term reduction in SynGAP and its GAP domain, supporting the theory of several functionally important domain in SynGAP.

4.2.3 No effects on mEPSC amplitudes or frequencies were associated with loss of SynGAP or its GAP domain

SynGAP has been shown to regulate AMPAR trafficking (Kim et al. (2003); Vazquez et al. (2004)). As a result of this, changes to AMPAR expression levels and excitatory synaptic transmission is generally seen in SynGAP KO or haploinsufficiency models (Clement et al. (2012, 2013); Wang et al. (2013); Ozkan et al. (2014)). Given this, I therefore expected to see an increase in mEPSC amplitude/frequency in both *Syngap*$^{+/-}$ and *Syngap*$^{+/\Delta GAP}$.

Basal excitatory synaptic transmission was examined by recording of mEPSCs from principal neurons in the LA and BA. In the LA, contrary to what was expected, neither

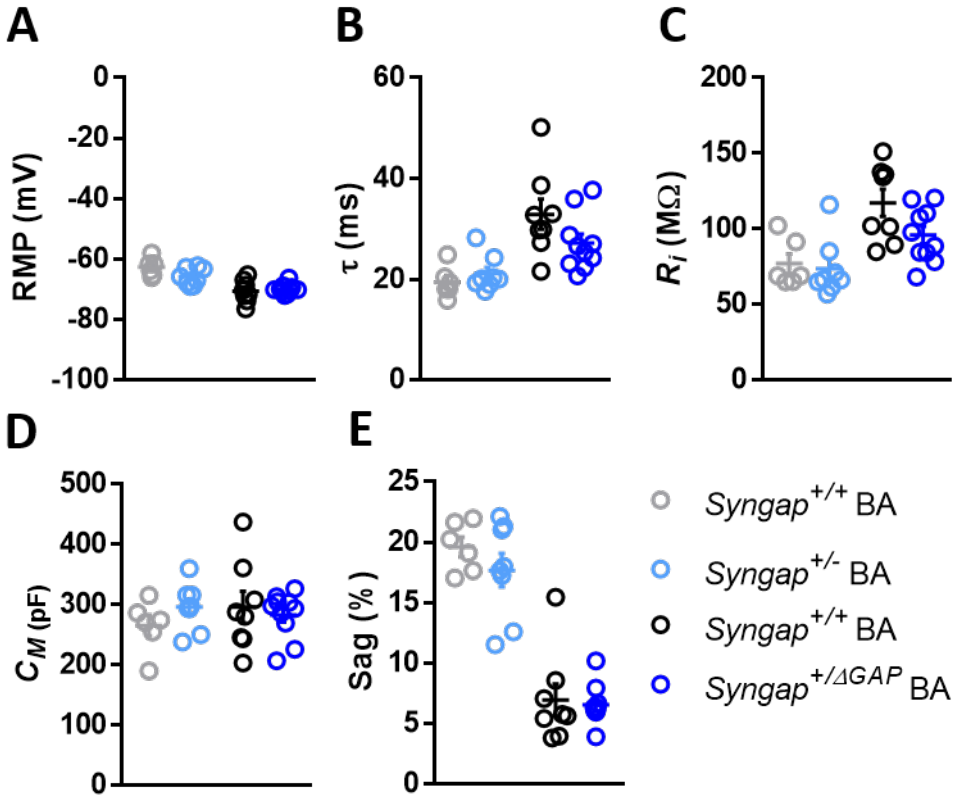

Figure 4.13: Passive membrane properties were not affected by a decrease in SynGAP or lack of the GAP domain in BA principal neurons at p28 (A) Resting membrane potential measured during 1 min of I=0 shows that both *Syngap*$^{+/-}$ and *Syngap*$^{+/\Delta GAP}$ BA neurons have a comparable RPM to their WT littermates (*Syngap*$^{+/+}$: -62.71 ± 1.21 mV, n=20 cells/6 animals; *Syngap*$^{+/-}$: -65.81 ± 0.98 mV, n=28 cells/8 animals; p=0.07, Student's unpaired *t*-test; *Syngap*$^{+/+}$: -70.61 ± 1.30 mV, n=24 cells/8 animals; *Syngap*$^{+/\Delta GAP}$: -69.93 ± 0.50 mV, n=29 cells/10 animals; p=0.64, Welch's Student's unpaired *t*-test). (B) The membrane time constant, τ, was not significantly different between the genotypes (*Syngap*$^{+/+}$: 19.44 ± 1.26 ms, n=20 cells/6 animals; *Syngap*$^{+/-}$: 21.12 ± 1.22 ms, n=28 cells/8 animals; p=0.36, Student's unpaired *t*-test; *Syngap*$^{+/+}$: 32.9 ± 3.02 ms, n=24 cells/8 animals; *Syngap*$^{+/\Delta GAP}$: 27.18 ± 1.78 ms, n=29 cells/10 animals; p=0.11, Student's unpaired *t*-test.). (C) The input resistance was comparable between genotypes (*Syngap*$^{+/+}$: 76.96 ± 6.50 MΩ, n=20 cells/6 animals; *Syngap*$^{+/-}$: 73.54 ± 6.73 MΩ, n=28 cells/8 animals; p=0.73, Student's unpaired *t*-test; *Syngap*$^{+/+}$: 117.1 ± 8.98 MΩ, n=24 cells/8 animals; *Syngap*$^{+/\Delta GAP}$: 95.92 ± 5.69 MΩ, n=29 cells/10 animals; p=0.05, Student's unpaired *t*-test.) (D) Membrane Capacitance was not significantly different in *Syngap*$^{+/-}$ or *Syngap*$^{+/\Delta GAP}$ compared to their respective WT littermates (*Syngap*$^{+/+}$: 265.3 ± 17.19 pF, n=20 cells/6 animals; *Syngap*$^{+/-}$: 295.6 ± 13.56 pF, n=28 cells/8 animals; p=0.19, Student's unpaired *t*-test; *Syngap*$^{+/+}$: 295.8 ± 26.25 pF, n=24 cells/8 animals; *Syngap*$^{+/\Delta GAP}$: 282.8 ± 12.16 pF, n=29 cells/10 animals; p=0.64, Student's unpaired *t*-test.) (E) Sag, a measure of Ih, was similar between genotypes (*Syngap*$^{+/+}$: 19.61 ± 0.83%, n=20 cells/6 animals; *Syngap*$^{+/-}$: 17.68 ± 1.39%, n=28 cells/8 animals; p=0.30, Student's unpaired *t*-test; *Syngap*$^{+/+}$: 6.95 ± 1.33%, n=24 cells/8 animals; *Syngap*$^{+/\Delta GAP}$: 6.55 ± 0.51%, n=29 cells/10 animals; p=0.78, Student's unpaired *t*-test.)

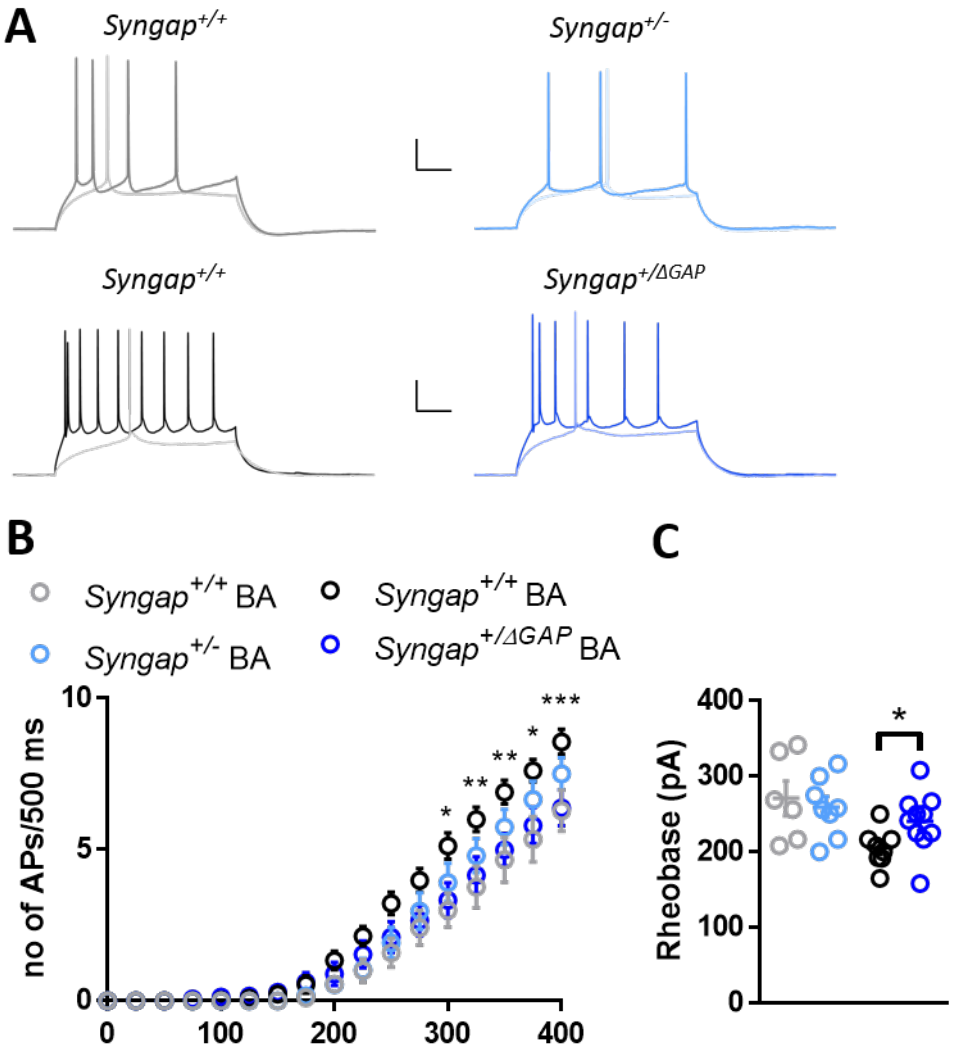

Figure 4.14: *SynGAP*$^{+/\Delta GAP}$ p28 BA principal neurons have a decrease in firing rate compared to WT littermates. (A) Example traces of *Syngap*$^{+/-}$ and *Syngap*$^{+/\Delta GAP}$ and their respective WT littermates, *Syngap*$^{+/+}$, voltage responses to rheobase and +400 pA current steps. Scale 100 ms, 20 mV. (B) *Syngap*$^{+/-}$ and p28 BA principal neurons show a comparable firing rate to WT littermates (Genotype: F(1,12)=0.90; p=0.36, 2way RM-ANOVA), whereas *Syngap*$^{+/\Delta GAP}$ show a decrease in firing in response to current injections compared to *Syngap*$^{+/+}$ (Interaction: F(16, 256)=6.75; p<0.0001, 2-way RM-ANOVA with Sidak post hoc correction). (C) Rheobase in *Syngap*$^{+/-}$ BA neurons was similar to WT (*Syngap*$^{+/+}$: 270.8 ± 23.08 pA, n=20 cells/6 animals; *Syngap*$^{+/-}$: 259.1 ± 13.77 pA, n=28 cells/8 animals; p=0.65, Student's unpaired *t*-test), whereas in Syngap+/ GAP rheobase was significantly higher compared to WT (*Syngap*$^{+/+}$: 205.1 ± 8.7 pA, n=24 cells/8 animals; *Syngap*$^{+/\Delta GAP}$: 240.4 ±12.36 pA, n=29 cells/10 animals; p=0.04, Student's unpaired *t*-test).

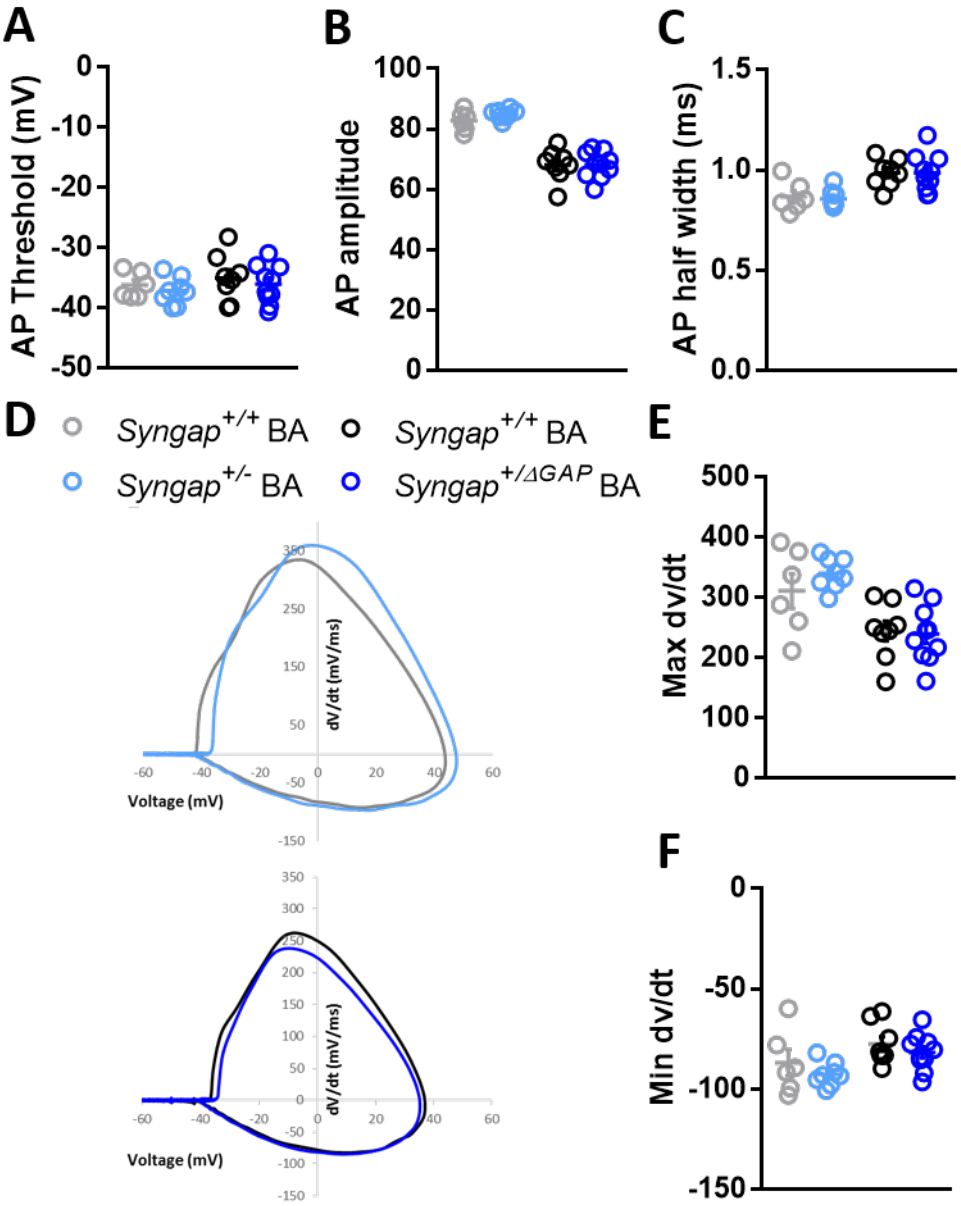

Figure 4.15: Action potential properties in *SynGAP*$^{+/-}$ and *SynGAP*$^{+/\Delta GAP}$ BA principal neurons at p28 are comparable to their WT littermates. (*continued on next page*)

Figure 4.15: (*continued*) (A) AP threshold was comparable between genotypes ($Syngap^{+/+}$: -36.22 ± 0.89 mV, n=20 cells/6 animals; $Syngap^{+/-}$: -37.16 ± 0.81 mV, n=28 cells/8 animals; p=0.45, Student's unpaired *t*-test; $Syngap^{+/+}$: -35.01 ± 1.38 mV, n=24 cells/8 animals; $Syngap^{+/\Delta GAP}$: -36.05 ± 1.00 mV, n=29 cells/10 animals; p=0.54, Student's unpaired *t*-test). (B) AP amplitude measured from threshold was not different to WT littermates in neither $Syngap^{+/-}$ nor $Syngap^{+/\Delta GAP}$ ($Syngap^{+/+}$: 82.76 ± 1.35 mV, n=20 cells/6 animals; $Syngap^{+/-}$: 84.99 ± 0.55 mV, n=28 cells/8 animals; p=0.12, Student's unpaired *t*-test; $Syngap^{+/+}$: 68.19 ± 1.87 mV, n=24 cells/8 animals; $Syngap^{+/\Delta GAP}$: 68.24 ± 1.40 mV, n=29 cells/10 animals; p=0.98, Student's unpaired *t*-test). (C) AP half width at half AP height was similar between genotypes ($Syngap^{+/+}$: 0.87 ± 0.03 ms, n=20 cells/6 animals; $Syngap^{+/-}$: 0.86 ± 0.02 ms, n=28 cells/8 animals; p=0.73, Student's unpaired *t*-test; $Syngap^{+/+}$: 0.99 ± 0.02 ms, n=24 cells/8 animals; $Syngap^{+/\Delta GAP}$: 0.99 ± 0.03 ms, n=29 cells/10 animals; p=0.99, Student's unpaired *t*-test). (D) (TOP) Phase plot of action potential in $Syngap^{+/+}$ (grey), $Syngap^{+/-}$ (light blue), (BOTTOM) $Syngap^{+/+}$ (black), and $Syngap^{+/-}$ (dark blue) LA neurons. (E) Max dv/dt was comparable between genotypes ($Syngap^{+/+}$: 311.1 ± 28.61 mV/ms, n=20 cells/6 animals; $Syngap^{+/-}$: 340.2 ± 9.2 mV/ms, n=28 cells/8 animals; p=0.37, Welch's unpaired *t*-test; $Syngap^{+/+}$: 244.5 ± 16.63 mV/ms, n=24 cells/8 animals; $Syngap^{+/\Delta GAP}$: 239.6 ± 15.01 mV/ms, n=29 cells/10 animals; p=0.83, Student's unpaired *t*-test), as was min dv/dt (F) ($Syngap^{+/+}$: -86.85 ± 6.48 mV/ms, n=20 cells/6 animals; $Syngap^{+/-}$: -92.56 ± 2.12 mV/ms, n=28 cells/8 animals; p=0.43, Student's unpaired *t*-test; $Syngap^{+/+}$: -77.52 ± 3.6 mV/ms, n=24 cells/8 animals; $Syngap^{+/\Delta GAP}$: -81.7 ± 2.84 mV/ms, n=29 cells/10 animals; p=0.37, Student's unpaired *t*-test).

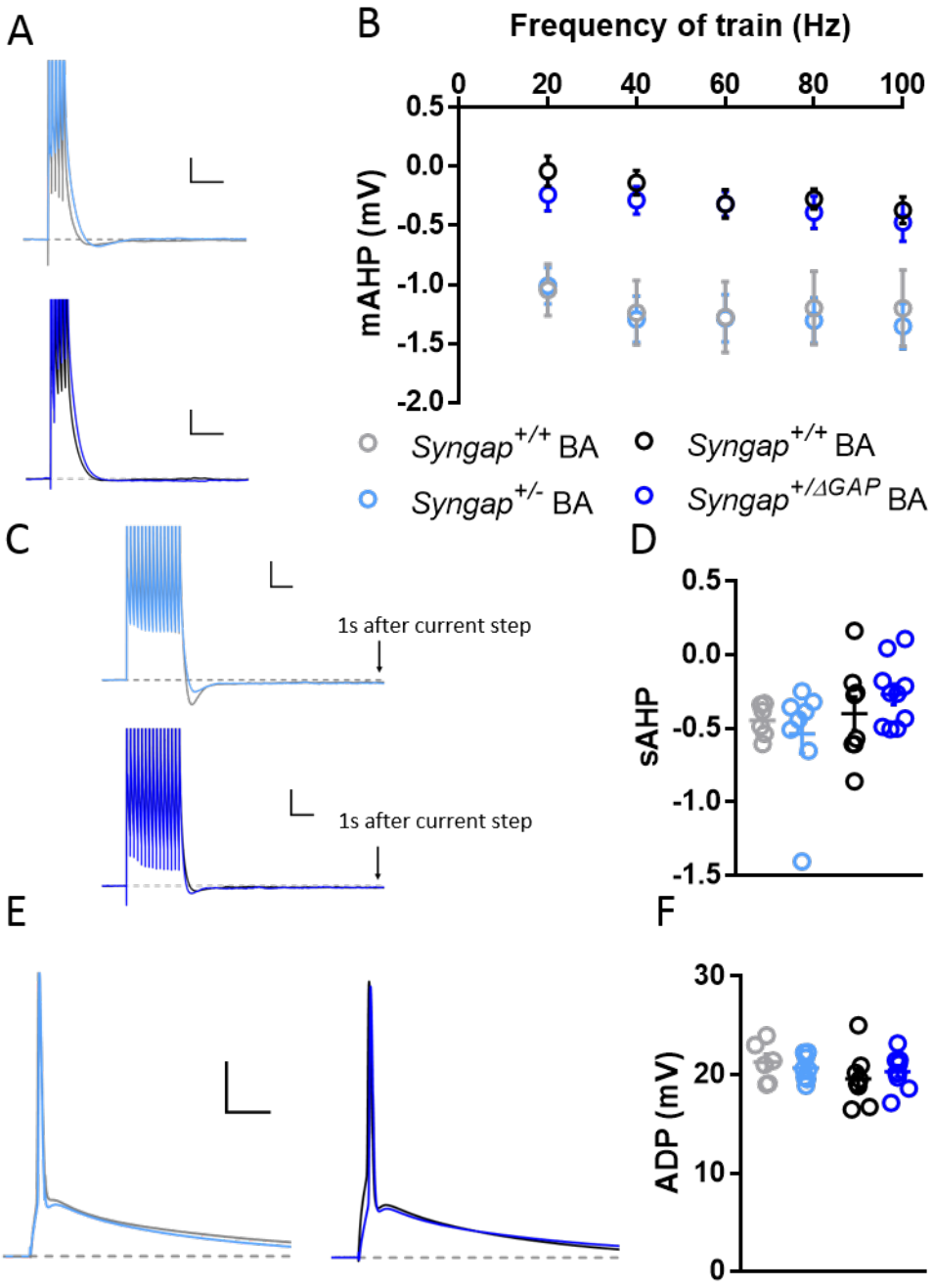

Figure 4.16: Post AP currents are not changed in *SynGAP*$^{+/-}$ or *SynGAP*$^{+/\Delta GAP}$ BA principal neurons at p28 (*continued on next page*)

Figure 4.16: (*continued*) (A) Example traces of the maximum AHP evoked by a train of 5 pulses at 100 Hz in (TOP) *Syngap*$^{+/+}$ (grey), *Syngap*$^{+/-}$ (light blue), (BOTTOM) *Syngap*$^{+/+}$ (black), and *Syngap*$^{+/\Delta GAP}$ (dark blue). Scale 100 ms, 5 mV. (B) Average mAHP after a train of 5 pulses at varying frequencies (20-100Hz) shows no significant differences between genotypes (*Syngap*$^{+/+}$/ *Syngap*$^{+/-}$: F(1,12)=0.03; p=0.86, 2way RM-ANOVA; *Syngap*$^{+/+}$/ Syngap+/ GAP: F(1,16)=0.48; p=0.50, 2way RM-ANOVA). (C) Example traces of sAHP after a train of 15 action potentials at 50 Hz in (TOP) *Syngap*$^{+/+}$ (grey), *Syngap*$^{+/-}$ (light blue), (BOTTOM) *Syngap*$^{+/+}$ (black), and *Syngap*$^{+/\Delta GAP}$ (dark blue) BA neurons. Scale 100 ms, 5 mV. (D) No significant difference was observed between either genotypes in sAHP (*Syngap*$^{+/+}$: -0.45 ± 0.05 mV, n=20 cells/6 animals; *Syngap*$^{+/-}$: -0.54 ± 0.13 ms, n=28 cells/8 animals; p=0.52, Welch's Student's unpaired *t*-test; *Syngap*$^{+/+}$: -0.40 ± 0.11 mV, n=24 cells/8 animals; *Syngap*$^{+/\Delta GAP}$: -0.26 ± 0.07 mV, n=29 cells/10 animals; p=0.32, Student's unpaired *t*-test). (E) Example traces of ADP following a single action potential in (TOP) *Syngap*$^{+/+}$ (grey), *Syngap*$^{+/-}$ (light blue), (BOTTOM) *Syngap*$^{+/+}$ (black), and *Syngap*$^{+/\Delta GAP}$ (dark blue) BA neurons. Scale bar 10 ms, 20 mV. (F) ADP after a single action potential was similar between genotypes (*Syngap*$^{+/+}$: 21.27 ± 0.82 mV, n=20 cells/6 animals; *Syngap*$^{+/-}$: 20.71 ± 0.45 mV, n=28 cells/8 animals; p=0.54, Student's unpaired *t*-test; *Syngap*$^{+/+}$: 19.6 ± 0.95 mV, n=24 cells/8 animals; *Syngap*$^{+/\Delta GAP}$: 20.33 ± 0.53 mV, n=29 cells/10 animals; p=0.49, Student's unpaired *t*-test).

Syngap$^{+/-}$ or *Syngap*$^{+/\Delta GAP}$ p14 principal neurons presented with shifts in mEPSC amplitudes or frequency (Fig. 4.17). Similarly in the BA, mEPCS amplitudes in *Syngap*$^{+/-}$ and *Syngap*$^{+/\Delta GAP}$ were comparable to their respective WTs (Fig. 4.18B). *Syngap*$^{+/-}$ presented with an increase in mEPSC frequency, however due to a small *Syngap*$^{+/-}$ sample size this was not significant (Fig. 4.18C). Power analysis showed that 15 *Syngap*$^{+/+}$/6 *Syngap*$^{+/-}$ are needed to reach significance.

Examining the longer term effects of the reduction of whole SynGAP levels or its GAP-domain revealed no changes to basal excitatory synaptic transmission in LA principal neurons. *Syngap*$^{+/-}$ and *Syngap*$^{+/\Delta GAP}$ both showed comparable mEPSC amplitude and frequency to their respective WTs (Fig. 4.19). In BA, mEPSC amplitude was similar in both *Syngap*$^{+/-}$ and *Syngap*$^{+/\Delta GAP}$ compared to WT (Fig. 4.20B). Whereas *Syngap*$^{+/-}$ showed no changes in mEPSC frequency (Fig. 4.20C), *Syngap*$^{+/\Delta GAP}$ showed an increase in mEPSC frequency, although not significant. Power analysis determined that 12 animals/genotype is needed for significance.

This data would suggest that, contrary to hypothesised SynGAP does not regulate the basal excitatory synaptic strength in the BLA at any of the time points investigated here.

4.2.4 SynGAP does not regulate basal inhibitory synaptic transmission in LA or BA

SynGAP is expressed mainly in excitatory synapses (Chen et al. (1998); Kim et al. (1998); Moon et al. (2008)), but also localises to inhibitory synapses (Zhang et al. (1999); Moon et al. (2008)). In interneurons SynGAP appears to promote formation of inhibitory synapses onto glutamatergic neurons (Berryer et al. (2016)). It is therefore possible that inhibitory synaptic transmission is affected in *Syngap* haploinsufficiency. Opposing changes in inhibitory transmission has been observed in *Syngap*$^{+/-}$ mice; mIPSC frequency and amplitude was increased in hippocampus (Clement et al. (2012)), whereas a decrease was reported in mIPSC amplitude in mPFC L2/3 neurons (Ozkan et al. (2014)). This could indicate that SynGAP exerts distinct functions depending on its location.

I therefore hypothesised to find changes to inhibitory synaptic transmission in the BLA. Basal inhibitory synaptic transmission was assessed by recording mIPSC in LA and BA principal neurons from p14 *Syngap*$^{+/-}$ and *Syngap*$^{+/\Delta GAP}$. Contrary to

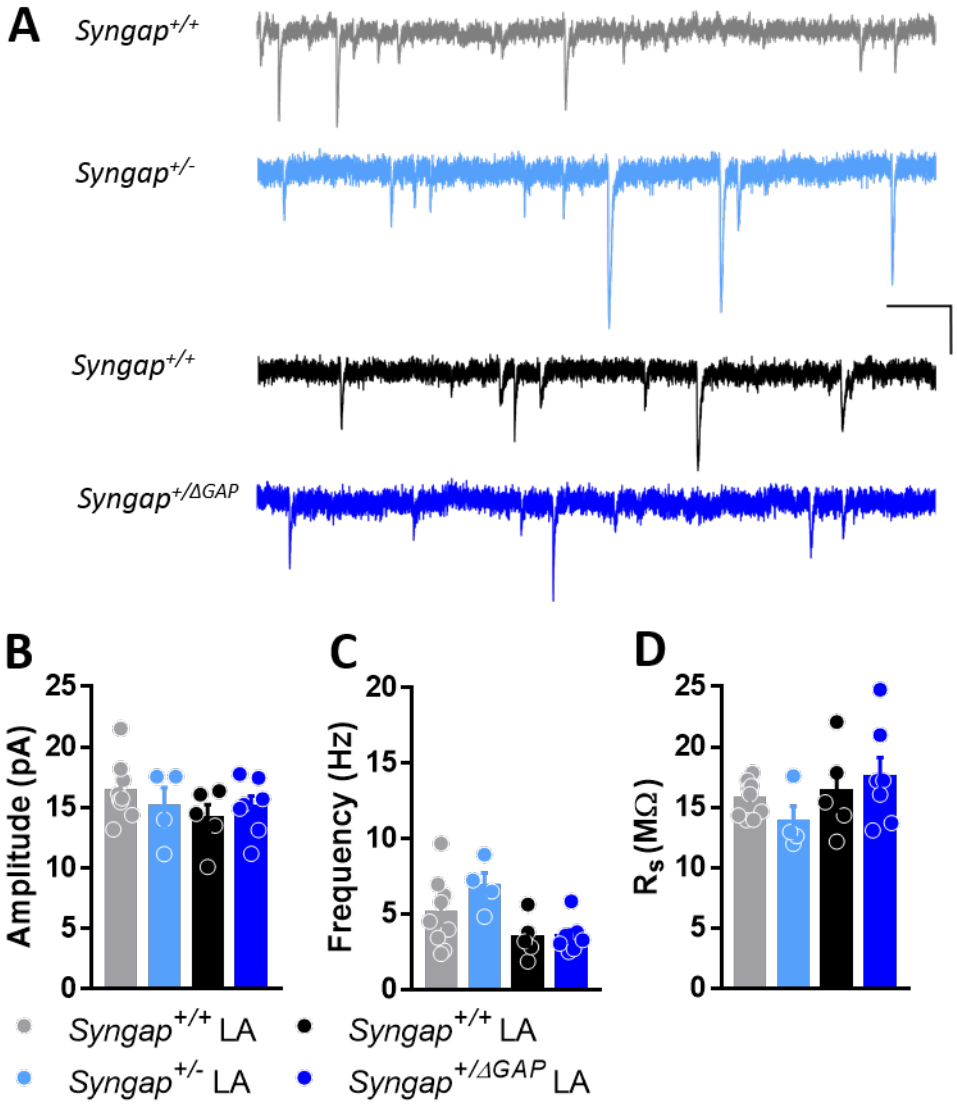

Figure 4.17: mEPSCs amplitude and frequency are unaltered in *SynGAP*$^{+/-}$ and *SynGAP*$^{+/\Delta GAP}$ LA principal neurons at p14. (A) Example traces of mEPSCs in (TOP) *Syngap*$^{+/+}$ (grey), *Syngap*$^{+/-}$ (light blue), (BOTTOM) *Syngap*$^{+/+}$ (black), and *Syngap*$^{+/\Delta GAP}$ (dark blue). Scale 200 ms, 20 pA. (B) LA neuron mEPSC amplitude in *Syngap*$^{+/-}$ and *Syngap*$^{+/\Delta GAP}$ is comparable to their WT littermates (*Syngap*$^{+/+}$: 16.40 ± 0.81 pA, n=20 cells/9 animals; *Syngap*$^{+/-}$: 15.08± 1.55 pA, n=10 cells/4 animals; p=0.42, Student's unpaired *t*-test; *Syngap*$^{+/+}$: 14.11 ± 1.13 pA, n=14 cells/5 animals; *Syngap*$^{+/\Delta GAP}$: 15.07± 0.87 pA, n=19 cells/7 animals; p=0.51, Student's unpaired *t*-test). (C) mEPSC frequency is not significantly different between genotypes (*Syngap*$^{+/+}$: 5.07 ± 0.79 Hz, n=20 cells/9 animals; *Syngap*$^{+/-}$: 6.89 ± 0.85 Hz, n=10 cells/4 animals; p=0.20, Student's unpaired *t*-test; *Syngap*$^{+/+}$: 3.47 ± 0.63 Hz, n=14 cells/5 animals; *Syngap*$^{+/\Delta GAP}$: 3.55± 0.42 Hz, n=19 cells/7 animals; p=0.92, Student's unpaired *t*-test). (D) Series resistance was comparable between genotypes (*Syngap*$^{+/+}$: 15.72 ± 0.50 MΩ, n=20 cells/9 animals; *Syngap*$^{+/-}$: 13.79 ± 1.29 MΩ, n=10 cells/4 animals; p=0.11, Student's unpaired *t*-test; *Syngap*$^{+/+}$: 16.37 ± 1.70 MΩ, n=14 cells/5 animals; *Syngap*$^{+/\Delta GAP}$: 17.57 ± 1.55 MΩ, n=19 cells/7 animals; p=0.62, Student's unpaired *t*-test).

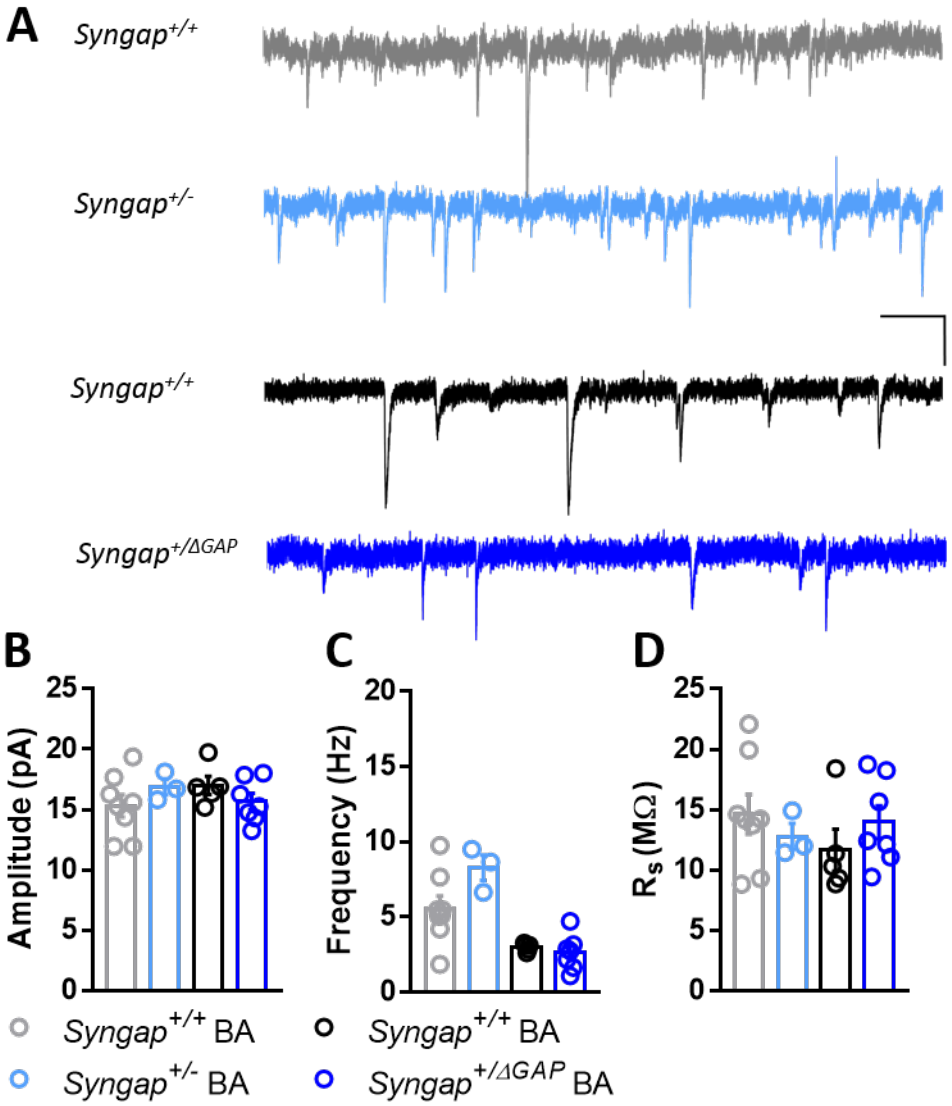

Figure 4.18: mEPSCs amplitude and frequency are unaltered in *SynGAP*$^{+/-}$ and *SynGAP*$^{+/\Delta GAP}$ BA principal neurons at p14. (A) Example traces of mEPSCs in (TOP) *Syngap*$^{+/+}$ (grey), *Syngap*$^{+/-}$ (light blue), (BOTTOM) *Syngap*$^{+/+}$ (black), and *Syngap*$^{+/\Delta GAP}$ (dark blue). Scale 200 ms, 20 pA. (B) BA neuron mEPSC amplitude in *Syngap*$^{+/-}$ and *Syngap*$^{+/\Delta GAP}$ is comparable to their WT littermates (*Syngap*$^{+/+}$: 15.31 ± 0.91 pA, n=18 cells/8 animals; *Syngap*$^{+/-}$: 16.89± 0.66 pA, n=8 cells/3 animals; p=0.34, Student's unpaired *t*-test; *Syngap*$^{+/+}$: 17.01 ± 0.75 pA, n=13 cells/5 animals; *Syngap*$^{+/\Delta GAP}$: 15.69± 0.68 pA, n=19 cells/7 animals; p=0.23, Student's unpaired *t*-test). (C) mEPSC frequency is not significantly different between genotypes (*Syngap*$^{+/+}$: 5.57 ± 0.83 Hz, n=18 cells/8 animals; *Syngap*$^{+/-}$: 8.27 ± 0.85 Hz, n=8 cells/3 animals; p=0.10, Student's unpaired *t*-test; *Syngap*$^{+/+}$: 3.00 ± 0.12 Hz, n=13 cells/5 animals; *Syngap*$^{+/\Delta GAP}$: 2.63± 0.44 Hz, n=19 cells/7 animals; p=0.45, Student's unpaired *t*-test). (D) Series resistance was comparable between genotypes (*Syngap*$^{+/+}$: 14.62 ± 1.62 MΩ, n=18 cells/8 animals; *Syngap*$^{+/-}$: 12.79 ± 1.08 MΩ, n=8 cells/3 animals; p=0.53, Student's unpaired *t*-test; *Syngap*$^{+/+}$: 11.66 ± 1.70 MΩ, n=13 cells/5 animals; *Syngap*$^{+/\Delta GAP}$: 13.96 ± 1.37 MΩ, n=19 cells/7 animals; p=0.32, Student's unpaired *t*-test).

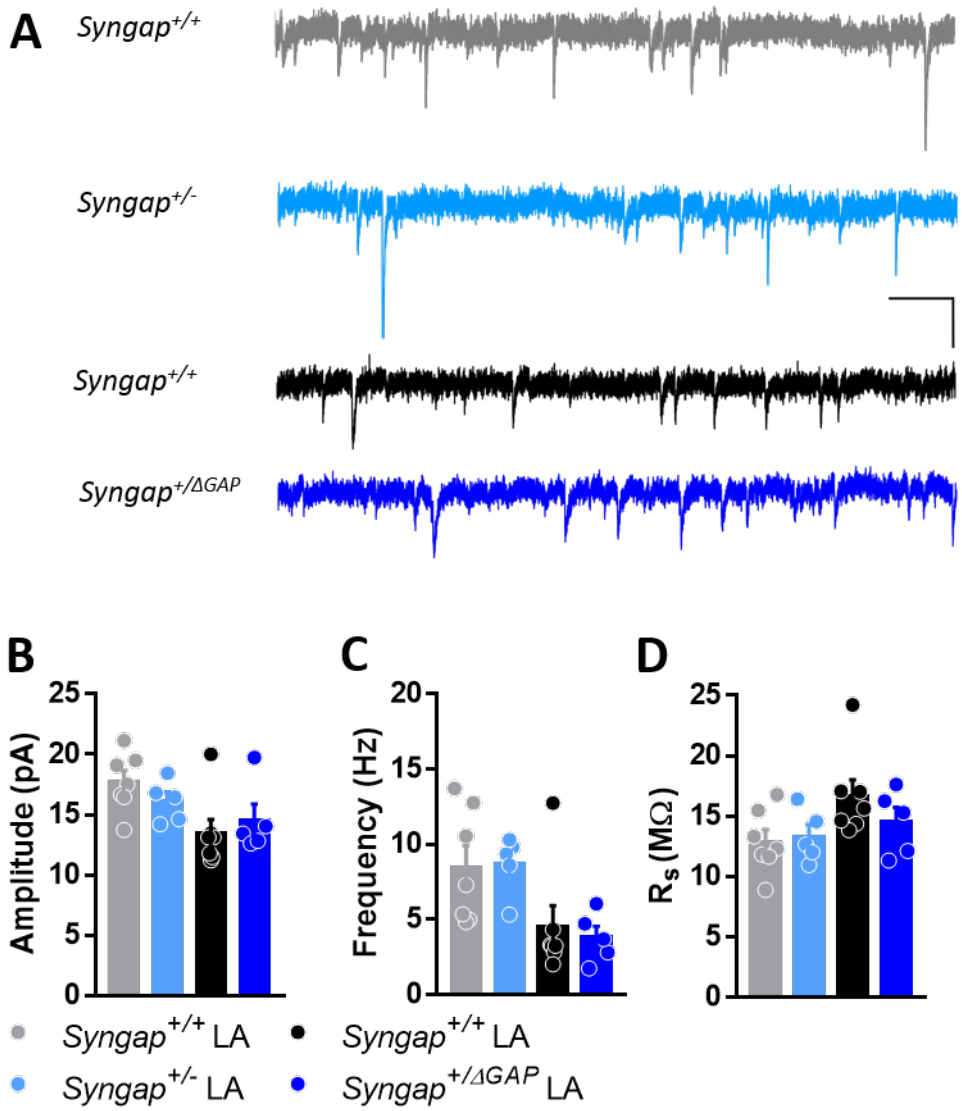

Figure 4.19: mEPSCs amplitude and frequency are unaltered in *SynGAP*$^{+/-}$ and *SynGAP*$^{+/\Delta GAP}$ LA principal neurons at p28. (A) Example traces of mEPSCs in (TOP) *Syngap*$^{+/+}$ (grey), *Syngap*$^{+/-}$ (light blue), (BOTTOM) *Syngap*$^{+/+}$ (black), and *Syngap*$^{+/\Delta GAP}$ (dark blue). Scale 200 ms, 20 pA. (B) LA neuron mEPSC amplitude in *Syngap*$^{+/-}$ and *Syngap*$^{+/\Delta GAP}$ is comparable to their WT littermates (*Syngap*$^{+/+}$: 17.73 ± 0.92 pA, n=17 cells/7 animals; *Syngap*$^{+/-}$: 16.11± 0.77 pA, n=10 cells/5 animals; p=0.23, Student's unpaired *t*-test; *Syngap*$^{+/+}$: 13.45 ± 1.14 pA, n=14 cells/7 animals; Syngap+/ GAP: 14.54± 1.32 pA, n=13 cells/5 animals; p=0.55, Student's unpaired *t*-test). (C) mEPSC frequency is not significantly different between genotypes (*Syngap*$^{+/+}$: 8.49 ± 1.44 Hz, n=17 cells/7 animals; *Syngap*$^{+/-}$: 8.68 ± 0.89 Hz, n=10 cells/5 animals; p=0.92, Student's unpaired *t*-test; *Syngap*$^{+/+}$: 4.53 ± 1.39 Hz, n=14 cells/7 animals; *Syngap*$^{+/\Delta GAP}$: 3.81± 0.75 Hz, n=13 cells/5 animals; p=0.69, Student's unpaired *t*-test). (D) Series resistance was comparable between genotypes (*Syngap*$^{+/+}$: 12.89 ± 0.99 MΩ, n=17 cells/7 animals; *Syngap*$^{+/-}$: 13.32 ± 0.97 MΩ, n=10 cells/5 animals; p=0.77, Student's unpaired *t*-test; *Syngap*$^{+/+}$: 16.68 ± 1.34 MΩ, n=14 cells/7 animals; *Syngap*$^{+/\Delta GAP}$: 14.52 ± 1.21 MΩ, n=13 cells/5 animals; p=0.28, Student's unpaired *t*-test).

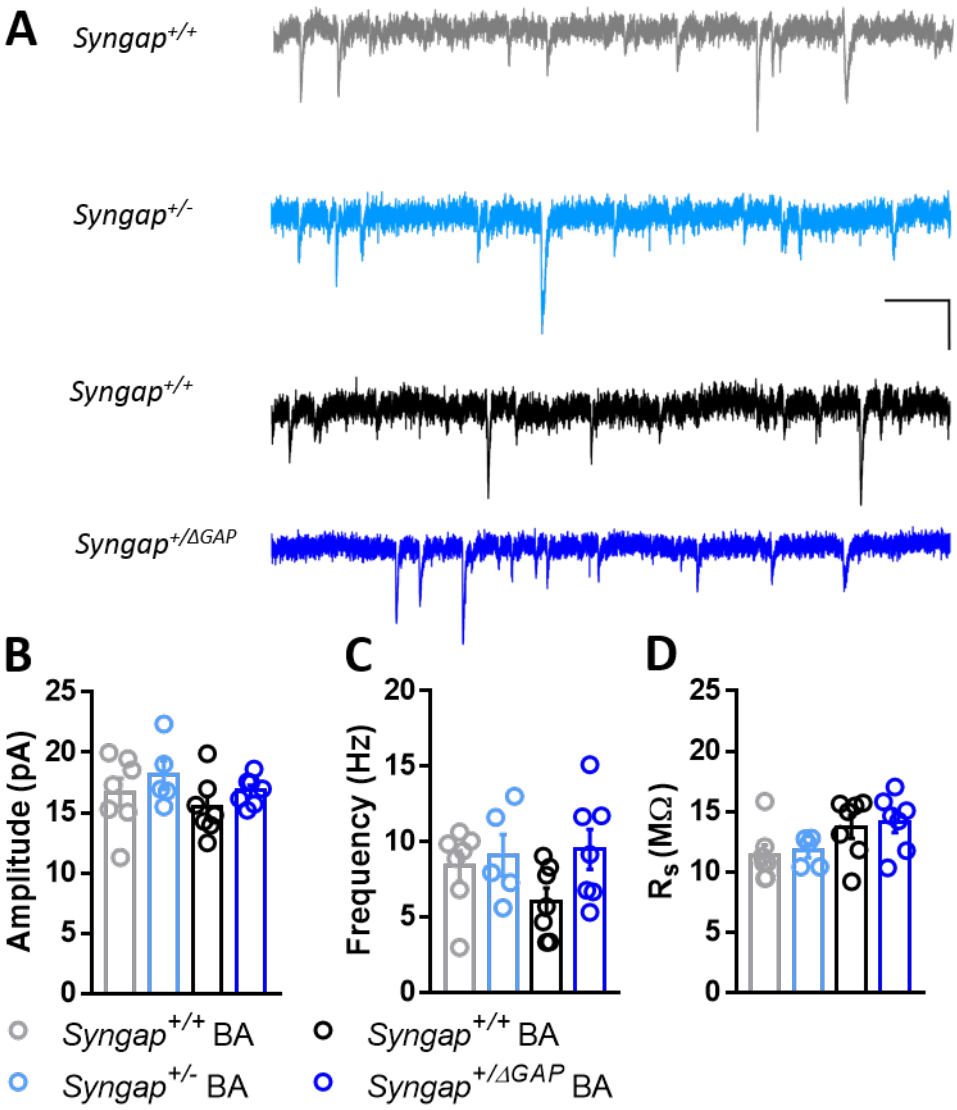

Figure 4.20: mEPSCs amplitude and frequency are unaltered in *SynGAP*$^{+/-}$ and *SynGAP*$^{+/\Delta GAP}$ BA principal neurons at p28. (A) Example traces of mEPSCs in (TOP) *Syngap*$^{+/+}$ (grey), *Syngap*$^{+/-}$ (light blue), (BOTTOM) *Syngap*$^{+/+}$ (black), and *Syngap*$^{+/\Delta GAP}$ (dark blue). Scale 200 ms, 20 pA. (B) BA neuron mEPSC amplitude in *Syngap*$^{+/-}$ and *Syngap*$^{+/\Delta GAP}$ is comparable to their WT littermates (*Syngap*$^{+/+}$: 16.71 ± 1.16 pA, n=18 cells/7 animals; *Syngap*$^{+/-}$: 18.13± 1.20 pA, n=12 cells/5 animals; p=0.42, Student's unpaired *t*-test; *Syngap*$^{+/+}$: 15.44 ± 0.91 pA, n=22 cells/7 animals; *Syngap*$^{+/\Delta GAP}$: 16.83± 0.45 pA, n=23 cells/7 animals; p=0.20, Student's unpaired *t*-test). (C) mEPSC frequency is not significantly different between genotypes (*Syngap*$^{+/+}$: 8.39 ± 1.01 Hz, n=18 cells/7 animals; *Syngap*$^{+/-}$: 9.10 ± 1.38 Hz, n=12 cells/5 animals; p=0.68, Student's unpaired *t*-test; *Syngap*$^{+/+}$: 6.04 ± 0.90 Hz, n=22 cells/7 animals; *Syngap*$^{+/\Delta GAP}$: 9.50± 1.33 Hz, n=23 cells/7 animals; p=0.05, Student's unpaired *t*-test). (D) Series resistance was comparable between genotypes (*Syngap*$^{+/+}$: 11.39 ± 0.82 MΩ, n=18 cells/7 animals; *Syngap*$^{+/-}$: 11.75 ± 0.55 MΩ, n=12 cells/5 animals; p=0.75, Student's unpaired *t*-test; *Syngap*$^{+/+}$: 13.71 ± 0.94 MΩ, n=22 cells/7 animals; *Syngap*$^{+/\Delta GAP}$: 14.13 ± 0.88 MΩ, n=23 cells/7 animals; p=0.75, Student's unpaired *t*-test).

hypothesised, LA principal neurons from neither *Syngap*$^{+/-}$ or *Syngap*$^{+/\Delta GAP}$ showed any changes in mIPSC amplitudes or frequency compared to WT (Fig. 4.21). Similarly in p14 BA principal neurons, mIPSCs of comparable size and frequencies were observed in both *Syngap*$^{+/-}$ and *Syngap*$^{+/\Delta GAP}$ compared to WT (Fig. 4.22).

Additionally, SynGAP was found not to be required for normal basal inhibitory synaptic transmission in LA or BA principal neurons at p28, as no changes were observed in mIPSC amplitude or frequency in *Syngap*$^{+/-}$ nor *Syngap*$^{+/\Delta GAP}$ compared to their respective WTs (Fig. 4.23 and Fig. 4.24).

4.2.5 Thalamo-amygdala LTP in LA is impaired in *Syngap*$^{+/-}$ and *Syngap*$^{+/\Delta GAP}$

The visual input to the LA comes from the visual cortical areas through cortico-amygdaloid afferents (Turner and Herkenham (1991); Mcdonald (1998)) and from visual thalamic nuclei through thalamo-amygdala afferents (Doron and LeDoux (1999)). The visual input from the thalamus is a fast, direct visual route that is thought to be essential for visual cued fear conditioning (Doron and LeDoux (1999)). Work done in the lab show that both *Syngap*$^{+/-}$ and *Syngap*$^{+/\Delta GAP}$ show enhanced fear recall and fear extinction deficits in response to visually cued fear conditioning (Sup. Fig. S3).

I therefore expected to see changes in the ability of thalamo-amygdala synapses to undergo synaptic plasticity. The same protocol used to assess thalamic LTP in LA in *Nlgn3*$^{-/y}$ was employed here. Two trains of 100 pulses at 30 Hz were delivered to the thalamic afferents in the internal capsule to elicit LTP at thalamo-amygdala synapses in the LA from p35–p45. This protocol elicited little to no LTP in LA principal neurons from *Syngap*$^{+/-}$, which was significantly different to *Syngap*$^{+/+}$ (Fig. 4.25; *Syngap*$^{+/+}$: 1.85 ± 0.21, n=7 cells/6 animals; *Syngap*$^{+/-}$: 1.13 ± 0.05, n=13 cells/7 animals; $p<0.01$, Welsch's *t*-test). Similarly, the protocol failed to induce LTP in *Syngap*$^{+/\Delta GAP}$ LA principal neurons (Fig. 4.26; *Syngap*$^{+/+}$: 1.76 ± 0.17, n=9 cells/7 animals; *Syngap*$^{+/\Delta GAP}$: 1.11 ± 0.10, n=13 cells/6 animals; $p<0.01$, Student's unpaired *t*-test). This would suggest that the GAP domain of SynGAP is important for regulating synaptic plasticity at thalamo-amygdala synapses.

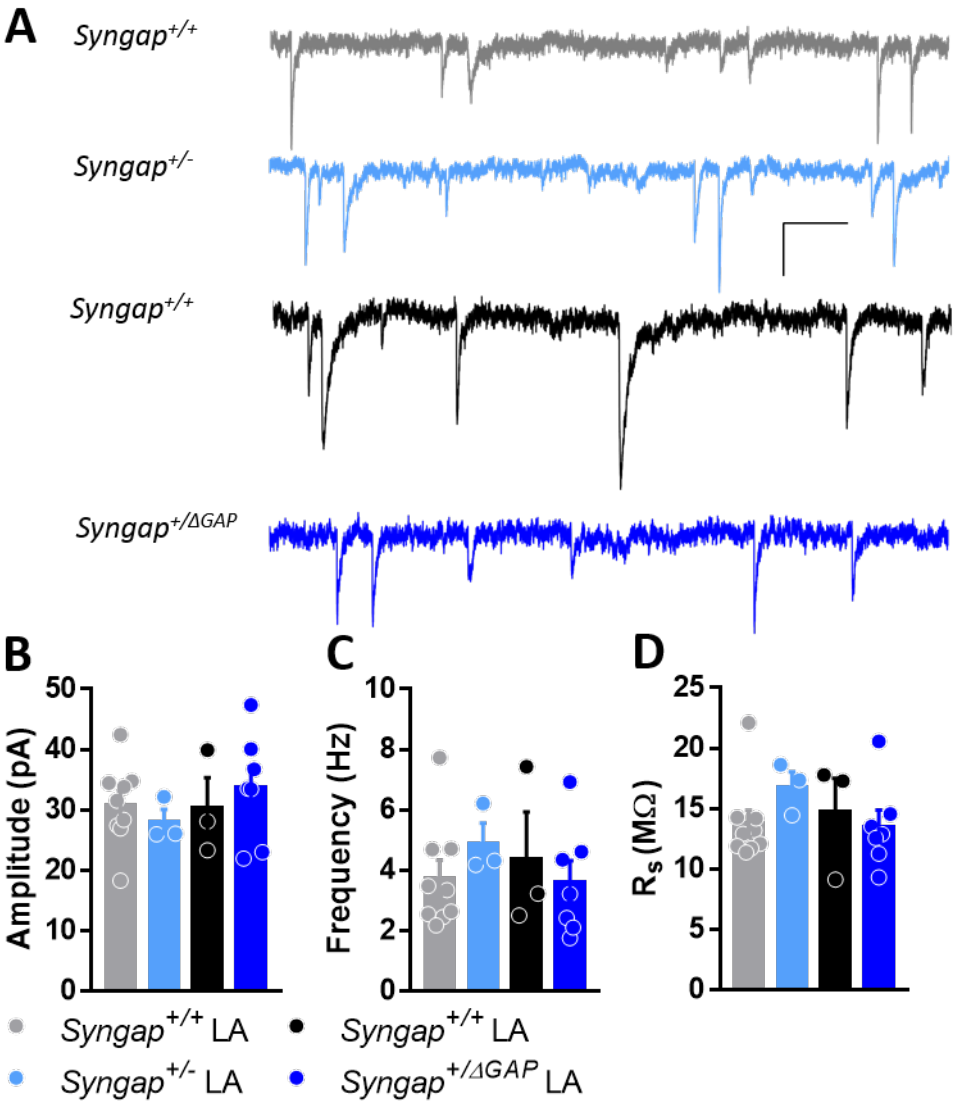

Figure 4.21: mIPSCs amplitude and frequency are unaltered in *SynGAP*$^{+/-}$ and *SynGAP*$^{+/\Delta GAP}$ LA principal neurons at p14. (A) Example traces of mIPSCs in (TOP) *Syngap*$^{+/+}$ (grey), *Syngap*$^{+/-}$ (light blue), (BOTTOM) *Syngap*$^{+/+}$ (black), and *Syngap*$^{+/\Delta GAP}$ (dark blue). Scale 200 ms, 40 pA. (B) LA neuron mIPSC amplitude in *Syngap*$^{+/-}$ and *Syngap*$^{+/\Delta GAP}$ is comparable to their WT littermates (*Syngap*$^{+/+}$: 30.89 ± 2.24 pA, n=18 cells/9 animals; *Syngap*$^{+/-}$: 28.07± 2.05 pA, n=6 cells/3 animals; p=0.51, Student's unpaired *t*-test; *Syngap*$^{+/+}$: 30.44 ± 4.93 pA, n=7 cells/3 animals; *Syngap*$^{+/\Delta GAP}$: 33.74± 3.42 pA, n=18 cells/7 animals; p=0.61, Student's unpaired *t*-test). (C) mIPSC frequency is not significantly different between genotypes (*Syngap*$^{+/+}$: 3.75 ± 0.59 Hz, n=18 cells/9 animals; *Syngap*$^{+/-}$: 4.9 ± 0.66 Hz, n=6 cells/3 animals; p=0.32, Student's unpaired *t*-test; *Syngap*$^{+/+}$: 4.39 ± 1.43 Hz, n=7 cells/3 animals; *Syngap*$^{+/\Delta GAP}$: 3.63± 0.69 Hz, n=18 cells/7 animals; p=0.61, Student's unpaired *t*-test). (D) Series resistance was comparable between genotypes (*Syngap*$^{+/+}$: 13.75 ± 1.10 MΩ, n=18 cells/9 animals; *Syngap*$^{+/-}$: 16.81 ± 1.24 MΩ, n= 6 cells/3 animals; p=0.17, Student's unpaired *t*-test; *Syngap*$^{+/+}$: 14.73 ± 2.80 MΩ, n=7 cells/3 animals; *Syngap*$^{+/\Delta GAP}$: 13.52 ± 1.33 MΩ, n=18 cells/7 animals; p=0.67, Student's unpaired *t*-test).

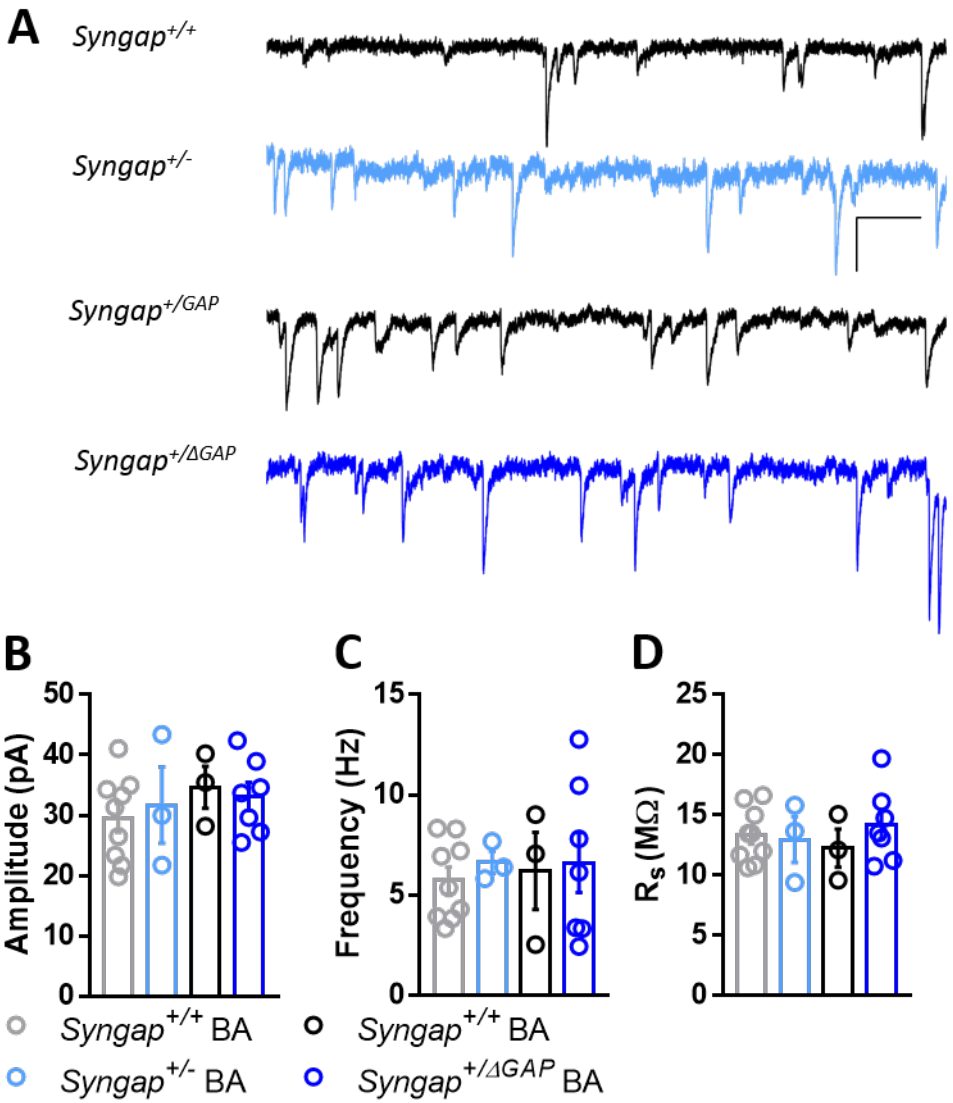

Figure 4.22: mIPSCs amplitude and frequency are unaltered in *SynGAP*$^{+/-}$ and *SynGAP*$^{+/\Delta GAP}$ BA principal neurons at p14 (A) Example traces of mIPSCs in (TOP) *Syngap*$^{+/+}$ (grey), *Syngap*$^{+/-}$ (light blue), (BOTTOM) *Syngap*$^{+/+}$ (black), and *Syngap*$^{+/\Delta GAP}$ (dark blue). Scale 200 ms, 40 pA. (B) BA neuron mIPSC amplitude in *Syngap*$^{+/-}$ and *Syngap*$^{+/\Delta GAP}$ is comparable to their WT littermates (*Syngap*$^{+/+}$: 29.6 ± 2.37 pA, n=20 cells/9 animals; *Syngap*$^{+/-}$: 31.72± 6.31 pA, n=7 cells/3 animals; p=0.70, Student's unpaired *t*-test; *Syngap*$^{+/+}$: 34.64 ± 3.49 pA, n=6 cells/3 animals; *Syngap*$^{+/\Delta GAP}$: 33.14± 2.33 pA, n=17 cells/7 animals; p=0.73, Student's unpaired *t*-test). (C) mIPSC frequency is not significantly different between genotypes (*Syngap*$^{+/+}$: 5.73 ± 0.66 Hz, n=20 cells/9 animals; *Syngap*$^{+/-}$: 6.63 ± 0.55 Hz, n=7 cells/3 animals; p=0.47, Student's unpaired *t*-test; *Syngap*$^{+/+}$: 6.20 ± 1.92 Hz, n=6 cells/3 animals; *Syngap*$^{+/\Delta GAP}$: 6.62± 1.49 Hz, n=17 cells/7 animals; p=0.88, Student's unpaired *t*-test). (D) Series resistance was comparable between genotypes (*Syngap*$^{+/+}$: 13.32 ± 0.75 MΩ, n=20 cells/9 animals; *Syngap*$^{+/-}$: 12.95 ± 1.89 MΩ, n= 7 cells/3 animals; p=0.83, Student's unpaired *t*-test; *Syngap*$^{+/+}$: 12.24 ± 1.58 MΩ, n=6 cells/3 animals; *Syngap*$^{+/\Delta GAP}$: 14.15 ± 1.16 MΩ, n=17 cells/7 animals; p=0.38, Student's unpaired *t*-test).

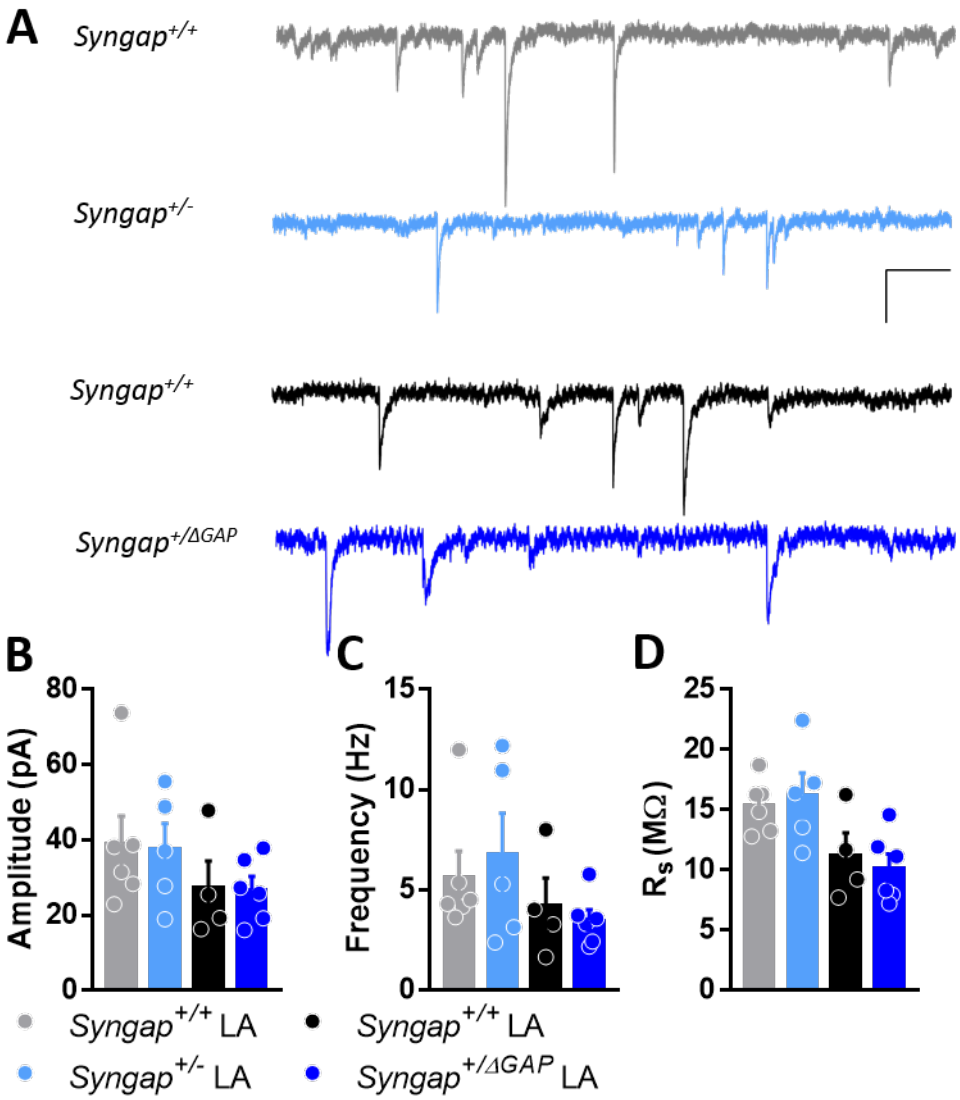

Figure 4.23: mIPSCs amplitude and frequency are unaltered in *SynGAP*$^{+/-}$ and *SynGAP*$^{+/\Delta GAP}$ LA principal neurons at p28. (A) Example traces of mIPSCs in (TOP) *Syngap*$^{+/+}$ (grey), *Syngap*$^{+/-}$ (light blue), (BOTTOM) *Syngap*$^{+/+}$ (black), and *Syngap*$^{+/\Delta GAP}$ (dark blue). Scale 200 ms, 40 pA. (B) LA neuron mIPSC amplitude in *Syngap*$^{+/-}$ and *Syngap*$^{+/\Delta GAP}$ is comparable to their WT littermates (*Syngap*$^{+/+}$: 38.91 ± 7.38 pA, n=14 cells/6 animals; *Syngap*$^{+/-}$: 37.65± 6.69 pA, n=10 cells/5 animals; p=0.90, Student's unpaired *t*-test; *Syngap*$^{+/+}$: 27.23 ± 7.14 pA, n=10 cells/4 animals; *Syngap*$^{+/\Delta GAP}$: 26.83± 3.46 pA, n=12 cells/6 animals; p=0.96, Student's unpaired *t*-test). (C) mIPSC frequency is not significantly different between genotypes (*Syngap*$^{+/+}$: 5.65 ± 1.29 Hz, n=14 cells/6 animals; *Syngap*$^{+/-}$: 6.79 ± 2.02 Hz, n=10 cells/5 animals; p=0.63, Student's unpaired *t*-test; *Syngap*$^{+/+}$: 4.24 ± 1.34 Hz, n=10 cells/4 animals; *Syngap*$^{+/\Delta GAP}$: 3.49± 0.52 Hz, n=12 cells/6 animals; p=0.57, Student's unpaired *t*-test). (D) Series resistance was comparable between genotypes (*Syngap*$^{+/+}$: 15.34 ± 0.90 MΩ, n=10 cells/4 animals; *Syngap*$^{+/-}$: 16.19 ± 1.86 MΩ, n=12 cells/6 animals; p=0.68, Student's unpaired *t*-test; *Syngap*$^{+/+}$: 11.2 ± 1.87 MΩ, n=10 cells/5 animals; *Syngap*$^{+/\Delta GAP}$: 10.17 ± 1.17 MΩ, n= 14 cells/6 animals; p=0.63, Student's unpaired *t*-test).

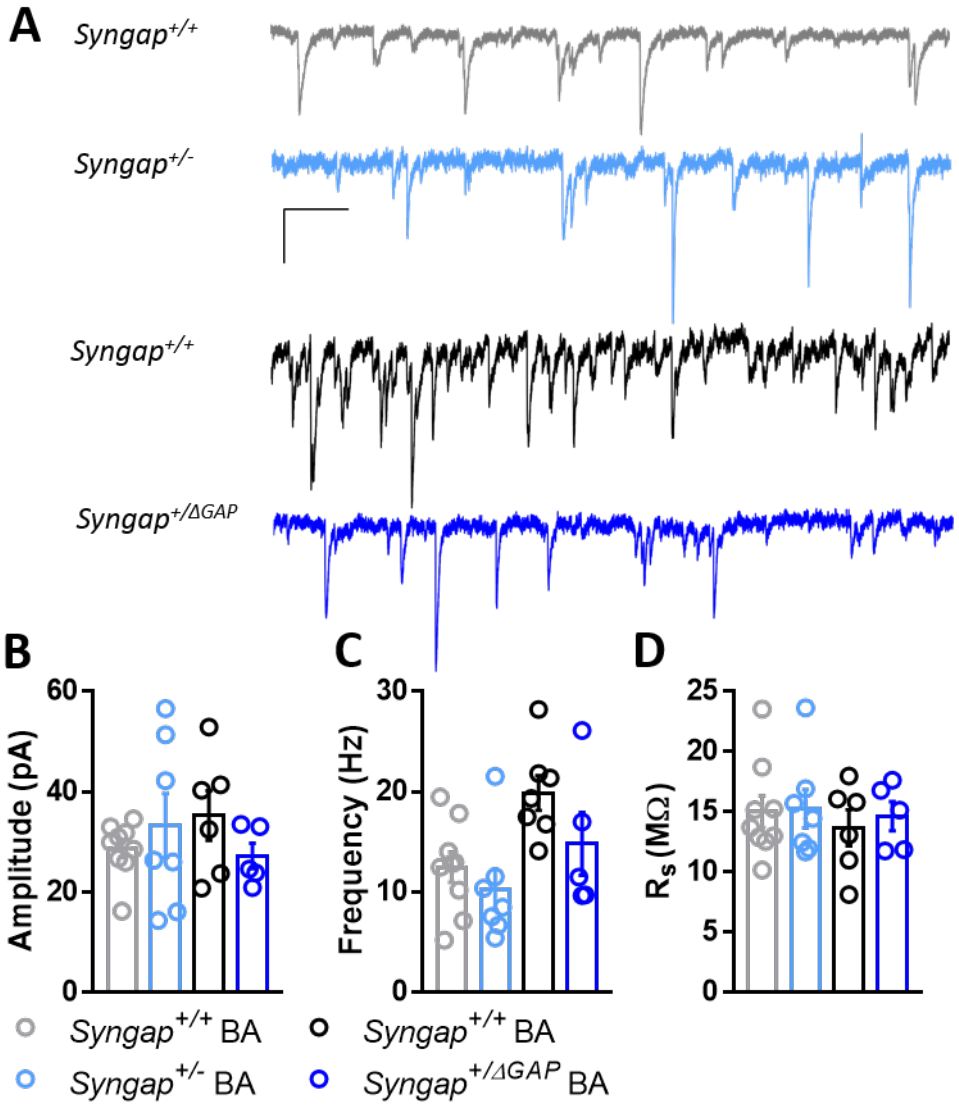

Figure 4.24: mIPSCs amplitude and frequency are unaltered in *SynGAP*$^{+/-}$ and *SynGAP*$^{+/\Delta GAP}$ BA principal neurons at p28. (A) Example traces of mIPSCs in (TOP) *Syngap*$^{+/+}$ (grey), *Syngap*$^{+/-}$ (light blue), (BOTTOM) *Syngap*$^{+/+}$ (black), and *SynGAP*$^{+/\Delta GAP}$ (dark blue). Scale 200 ms, 40 pA. (B) BA neuron mIPSC amplitude in *Syngap*$^{+/-}$ and *SynGAP*$^{+/\Delta GAP}$ is comparable to their WT littermates (*Syngap*$^{+/+}$: 28.66 ± 1.82 pA, n=21 cells/9 animals; *Syngap*$^{+/-}$: 33.29± 6.37 pA, n=16 cells/7 animals; p=0.45, Unpaired *t*-test; *Syngap*$^{+/+}$: 35.29 ± 4.91 pA, n=15 cells/6 animals; *SynGAP*$^{+/\Delta GAP}$: 27.22± 2.56 pA, n=12 cells/5 animals; p=0.20, Unpaired *t*-test). (C) mIPSC frequency is not significantly different between genotypes (*Syngap*$^{+/+}$: 12.45 ± 1.52 Hz, n=21 cells/9 animals; *Syngap*$^{+/-}$: 10.22 ± 2.04 Hz, n=16 cells/7 animals; p=0.39, Unpaired *t*-test; *Syngap*$^{+/+}$: 18.48 ± 1.20 Hz, n=15 cells/6 animals; *SynGAP*$^{+/\Delta GAP}$: 14.79± 3.13 Hz, n=12 cells/5 animals; p=0.27, Unpaired *t*-test). (D) Series resistance was comparable between genotypes (*Syngap*$^{+/+}$: 14.99 ± 1.33 MΩ, n=21 cells/9 animals; *Syngap*$^{+/-}$: 15.25 ± 1.59 MΩ, n= 16 cells/7 animals; p=0.90, Student's unpaired *t*-test; *Syngap*$^{+/+}$: 13.66 ± 1.50 MΩ, n=15 cells/6 animals; *Syngap*$^{+/\Delta GAP}$: 14.63 ± 1.22 MΩ, n=12 cells/5 animals; p=0.64, Student's unpaired *t*-test).

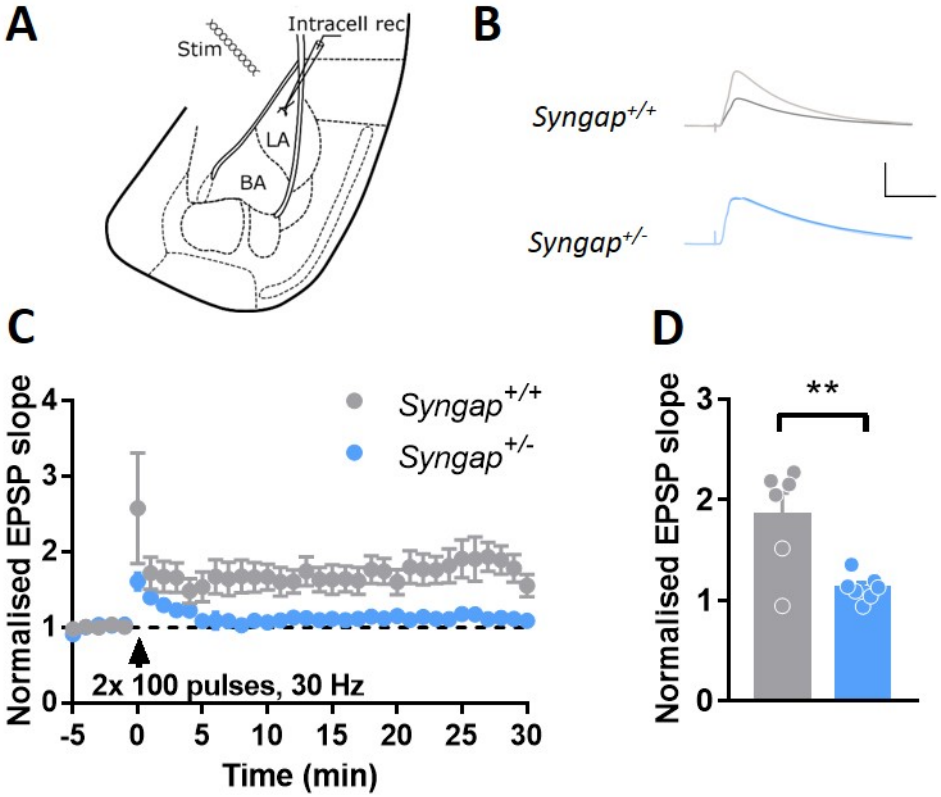

Figure 4.25: Long term potentiation at thalamic input to the LA is impaired at 30 Hz in *SynGAP*$^{+/-}$. (A) Schematic of the placement of stimulating electrode (Stim) and the intracellular recording electrode (Intracell rec). (B) Example traces of *Syngap*$^{+/+}$ (grey/light grey) and *Syngap*$^{+/-}$ (blue/light blue) LA neuron EPSPs at baseline and 30 min after induction. Scale 50 ms, 5 mV. (C) LA *Syngap*$^{+/-}$ neurons LTP time course show impaired thalamic LTP with two trains of 100 pulses at 30 Hz. (D) Bar graph of the last 5 min of recording. EPSP is normalised to the baseline preceding induction. *Syngap*$^{+/-}$ have significantly less LTP compared to WT littermates (*Syngap*$^{+/+}$: 1.85 $\pm$ 0.21, n=7 cells/6 animals; *Syngap*$^{+/-}$: 1.13 $\pm$ 0.05, n=13 cells/7 animals; $p<0.01$, Welsch's *t*-test).

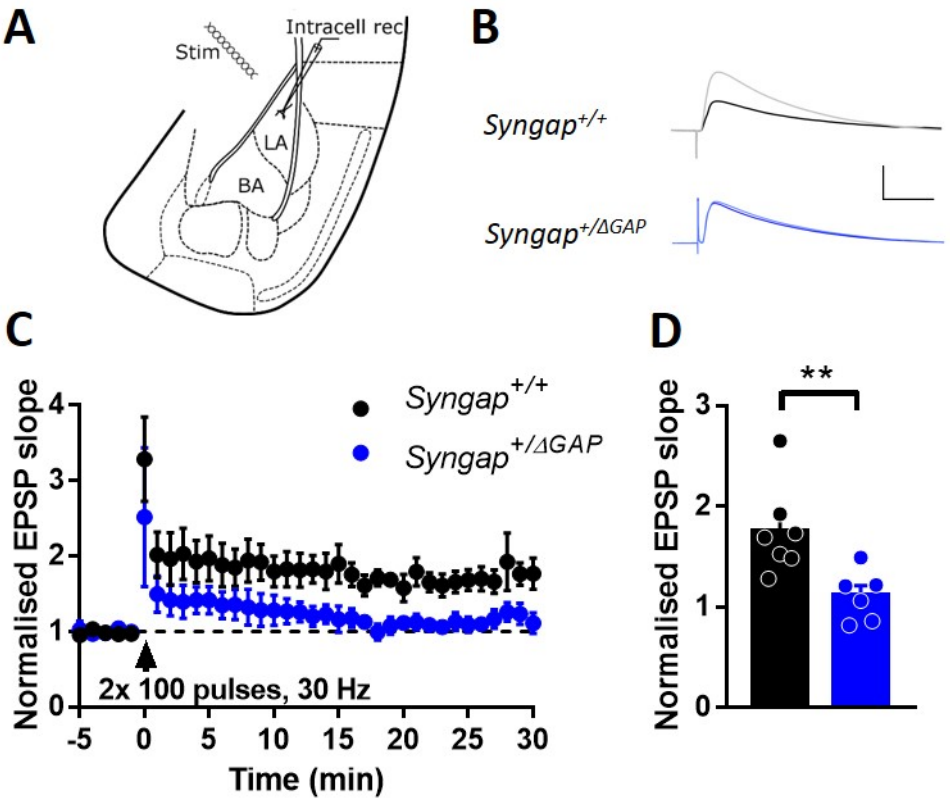

Figure 4.26: Long term potentiation at thalamic input to the LA is impaired at 30Hz in *SynGAP*$^{+/\Delta GAP}$. (A) Schematic of the placement of stimulating electrode (Stim) and the intracellular recording electrode (Intracell rec). (B) Example traces of *Syngap*$^{+/+}$ (black/grey) and *Syngap*$^{+/\Delta GAP}$ (blue/light blue) LA neuron EPSPs at baseline and 30 min after induction. Scale 50ms, 5mV. (C) LA *Syngap*$^{+/\Delta GAP}$ neurons LTP timecourse show impaired thalamic LTP with two trains of 100 pulses at 30 Hz. (D) Bar graph of the last 5 min of recording. EPSP is normalised to the baseline preceding induction. *Syngap*$^{+/\Delta GAP}$ have significantly less LTP compared to WT littermates (*Syngap*$^{+/+}$: 1.76 $\pm$ 0.17, n=9 cells/7 animals; *Syngap*$^{+/\Delta GAP}$: 1.11 $\pm$ 0.10, n=13 cells/6 animals; $p<0.01$, Student's unpaired t-test).

4.2.6 PPR at thalamo-amygdala synapses is decreased in *SynGAP*$^{+/-}$

Since the mEPSC amplitude and frequency were found to be comparable in both *Syngap*$^{+/-}$ and *Syngap*$^{+/\Delta GAP}$ to WT (Fig. 4.17–4.24), suggesting normal basic synaptic transmission, I therefore wanted to investigate the strength of activity-dependent synaptic transmission to clarify if this was underlying the deficits in synaptic plasticity. This was assessed by examining the AMPA/NMDA receptor ratio at thalamo-amygdala synapses in LA principal neurons at p35–p45. Neither *Syngap*$^{+/-}$ or *Syngap*$^{+/\Delta GAP}$ exhibited any changes in AMPA/NMDA receptor ratios compared to their WT controls (Fig. 4.27), suggesting that the postsynaptic strength is unaffected by the absence of SynGAP or its GAP domain.

In addition, presynaptic release probability was examined at thalamo-amygdala synapses by measuring the paired-pulse ratio (PPR). The PPR was found to be significantly decreased in *Syngap*$^{+/-}$ compared to *Syngap*$^{+/+}$ (Fig. 4.28; *Syngap*$^{+/+}$: 1.71 $\pm$ 0.13, n=14 cells/7 animals; *Syngap*$^{+/-}$: 1.35 $\pm$ 0.06, n=22 cells/7 animals; $p<0.05$, Student's unpaired *t*-test), indicating dysfunctional presynaptic release at these synapses. *Syngap*$^{+/\Delta GAP}$, however, showed a comparable PPR to *Syngap*$^{+/+}$ (Fig. 4.28). This could suggest that abberant presynaptic function is an underlying cause of the impairment in LTP in *Syngap*$^{+/-}$, however not in *Syngap*$^{+/\Delta GAP}$.

4.3 Discussion

In this chapter, I sought to decipher how the different functional domains of SynGAP contribute to the amygdala pathophysiology of *Syngap* haploinsufficiency. Increased intrinsic excitability was observed in LA of *Syngap*$^{+/-}$, whereas *Syngap*$^{+/\Delta GAP}$ showed a decrease in excitability in BA. Unexpectedly, no changes were detected in basal excitatory or inhibitory synaptic transmission in either *Syngap* model. Both *Syngap*$^{+/-}$ and *Syngap*$^{+/\Delta GAP}$ showed a deficit in thalamo-amygdala LTP, while only *Syngap*$^{+/-}$ displayed a decrease in presynaptic release probability (Table 4.1).

4.3.1 Differences between WTs

The two different *Syngap* models were bred in separate colonies, and thus were compared to WT controls from within that colony. If you compare the two WTs with each other, there are clear differences in intrinsic and synaptic properties. The

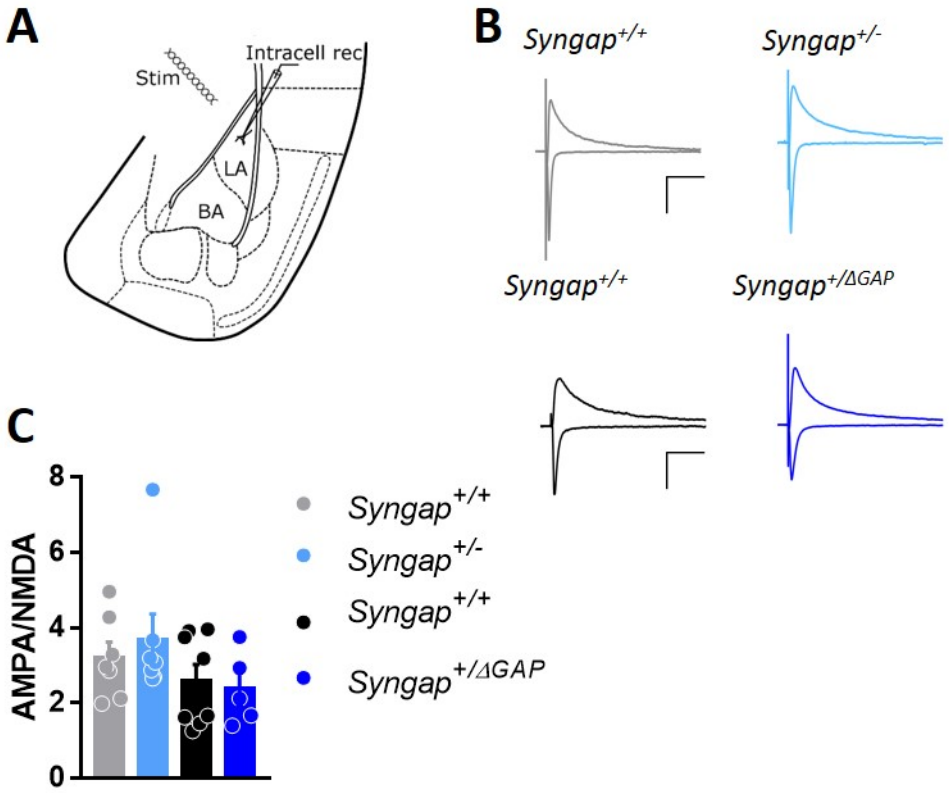

Figure 4.27: AMPA/NMDA ratios in thalamic input to LA neurons in *SynGAP*$^{+/-}$ and *SynGAP*$^{+/\Delta GAP}$ were comparable to that of their WT littermates. (A) Schematic of the placement of stimulating electrode (Stim) and the intracellular recording electrode (Intracell rec). (B) Example traces of *Syngap*$^{+/+}$ (grey/light grey) and *Syngap*$^{+/-}$ (blue/light blue) LA neuron showing AMPAR currents measured at -70 mV and NMDAR currents measured at +40 mV. Scale 200 ms, 100 pA. (C) Neither *Syngap*$^{+/-}$ or *Syngap*$^{+/\Delta GAP}$ neurons show a difference in AMPA/NMDA ratios compared to their WT littermates (*Syngap*$^{+/+}$: 3.21 ± 0.41, n=14 cells/7 animals; *Syngap*$^{+/-}$: 3.70 ± 0.68, n=19 cells/7 animals; p=0.55, Student's unpaired *t*-test; *Syngap*$^{+/+}$: 2.60 ± 0.43, n=16 cells/8 animals; Syngap+/ GAP: 2.38 ± 0.43, n=11 cells/5 animals; p=0.73, Student's unpaired *t*-test).

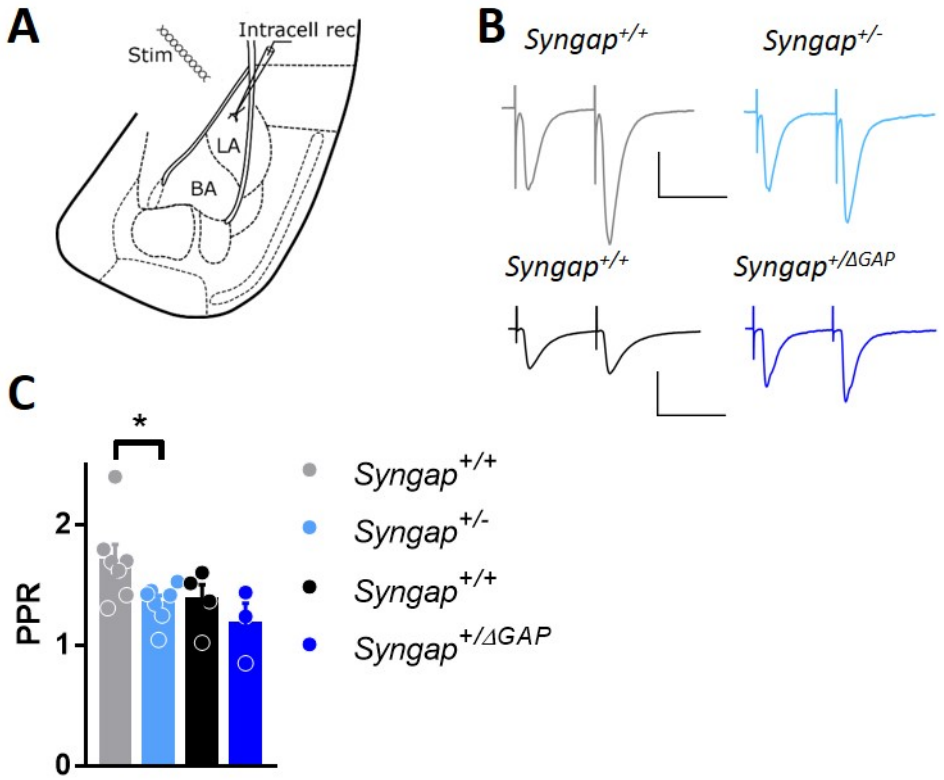

Figure 4.28: Presynaptic release probability at thalamic input to LA neurons in *SynGAP*$^{+/-}$ is reduced compared to WT littermates. (A) Schematic of the placement of stimulating electrode (Stim) and the intracellular recording electrode (Intracell rec). (B) Example traces of *Syngap*$^{+/+}$ (grey/light grey) and *Syngap*$^{+/-}$ (blue/light blue) LA neuron paired pulse EPSCs at 50 ms interpulse intervals measured at -70 mV. Scale 200 ms, 100 pA. (C) Paired-pulse ratio, measured as second pulse over first, is significantly reduced in *Syngap*$^{+/-}$, but normal in *Syngap*$^{+/\Delta GAP}$ neurons (*Syngap*$^{+/+}$: 1.71 ± 0.13, n=14 cells/7 animals; *Syngap*$^{+/-}$: 1.35 ± 0.06, n=22 cells/7 animals; $p<0.05$, Student's unpaired *t*-test; *Syngap*$^{+/+}$: 1.38 ± 0.13, n=9 cells/4 animals; *Syngap*$^{+/\Delta GAP}$: 1.18 ± 0.17, n=8 cells/3 animals; p=0.38, Student's unpaired *t*-test).

Table 4.1: *Summary of intrinsic and synaptic properties in SynGAP$^{+/-}$ and SynGAP$^{+/\Delta GAP}$*

	***Syngap*$^{+/-}$**				*vs.*	***Syngap*$^{+/\Delta GAP}$**			
	LA		**BA**			**LA**		**BA**	
	p14	p28	p14	p28		p14	p28	p14	p28
Intrinsic properties									
Passive membrane properties	–	–	–	–		–	–	–	–
Excitability	–	↑↑↑	–	–		–	–	–	↓↓↓
AP properties	–	–	–	–		–	–	–	–
Post AP currents	–	–	–	–		–	–	–	–
Synaptic properties									
mEPSC amplitude	–	–	–	–		–	–	–	–
mEPSC frequency	–	–	(↑)	–		–	–	–	(↑)
mIPSC amplitude	–	–	–	–		–	–	–	–
mIPSC frequency	–	–	–	–		–	–	–	–
AMPA/NMDA	–	–	–	–		–	–	–	–
PPR	ND	↓	ND	ND		ND	–	ND	ND
LTP	ND	↓↓	ND	ND		ND	↓↓	–	–

ND: not determined, ↑: p<0.05, ↑↑: p<0.01, ↑↑↑: p<0.001.

experiments were not done simultaneously, though experimental conditions were kept the same for both group of experiments. The most parsimonious explanation for the WT differences is genetic variance. Both colonies are outbred on a LEH background, but even though the background is the same, the outbreeding or genetic drift can genetically differentiate the colonies. This can cause animals from the same original outbred stock to respond very differently to experiments if they come from different isolated colonies (Brekke et al. (2018)).

The differences between the WTs could act as a confounding factor, leading to confounding bias, and hence over- or underestimating the effect size. To eliminate this, the two lines are now being cross bred, and future experiments will be performed using the cross line. For the sake of this discussion, it is assumed that the WT differences is not a confounding variable, and the observed effects are true.

4.3.2 Changes to intrinsic excitability

Action potential generation is one of the most fundamental processes in neuronal activity, and modulation of intrinsic excitability can therefore have significant impact. An increase in intrinsic excitability has previously been reported from p8–9 hippocampus in *Syngap*$^{+/-}$ mice (Clement et al. (2012)) — around the time SynGAP expression peaks (Porter et al. (2005)) — suggesting that SynGAP expression can alter the excitability of

these neurons. By the age of p14 and >6 weeks this phenotype had resolved (Clement et al. (2012)). Based on these findings, I expected to find an increase in excitability in the youngest age group, and that this change might be resolved with development.

Instead, a decrease was observed in the number of action potentials fired in p14 BA principal neurons, though this was not statistically significant (Fig. 4.6). The protocol that was initially used to examining intrinsic excitability in p14 was the same as the protocol used at p28 with depolarising currents going from 0–400 pA (data not shown). The first handful of animals would go into depolarising block using this protocol, and the protocol was therefore revised to go from 0–200 pA when recording from p14 neurons. This protocol generated fewer action potentials, particularly in BA principal neurons, where the WTs fire less than 5 APs during the largest depolarising current steps (Fig. 4.6). This makes it difficult to detect any potential differences there might be in intrinsic excitability, when the effect sizes are of smaller scale. Using a different protocol to examine the intrinsic firing in these neurons might reveal if a true decrease in firing is present in $Syngap^{+/\Delta GAP}$ BA principal neurons at p14.

LA principal neurons from $Syngap^{+/-}$ rats exhibit increased excitability, whereas $Syngap^{+/\Delta GAP}$ BA neurons displayed a decrease in excitability. Both these phenotypes emerged in the p28 age group, in contrast to the observation by Clement et al. (2012). This would suggest that the changes in excitability observed here are not the direct result of SynGAP reduction, but rather a compensatory mechanism to another more direct consequence.

To determine the cellular mechanism underlying the change in excitability, proxies for underlying currents can be measured through passive membrane properties, AP kinetics, and post-AP currents. However, none of these were measurably different in $Syngap^{+/-}$ or $Syngap^{+/\Delta GAP}$. The changes in excitability are observed at higher current injections, which could indicate that conductances activated at higher voltages are abnormal. Examples of such are those mediated by voltage gated calcium channels (VGCCs), such as T-type Ca^{2+} currents and high-voltage activated (HVA) calcium currents. These currents are important for regulating excitability (Iftinca (2011); Simms and Zamponi (2014)). VGCCs have been shown to be involved in fear associative learning (Chen et al. (2012); Temme and Murphy (2017)), and changes in T-type Ca^{2+} channels and other VGCCs are associated with different types of epilepsy (Kim et al. (2001);

Eckle et al. (2014); Casillas-Espinosa et al. (2015)). Furthermore, there is a high prevalence of epilepsy in people with MRD5 (Weldon et al. (2018)), making VGCCs candidates for contributing to the change in intrinsic excitability. Interestingly, deletion of L-type VGCCs results in enhanced excitability, but impaired long term potentiation within the amygdala (McKinney et al. (2009)). Moreover, L-type VGCCs mediate fear extinction, and $Ca_{v1.2}$ knockout mice are incapable of extinction learning (Temme and Murphy (2017)). These phenotypes are very similar to those observed in the *Syngap*$^{+/-}$, both cellularly and behaviourally. This could suggest that L-type VGCCs are reduced in *Syngap*$^{+/-}$. Measuring L-type VGCCs protein expression levels in the amygdala, and directly measuring their currents through pharmacological isolation would clarify if this hypothesis is true.

4.3.3 No changes observed in mPSCs

SynGAP has been shown to regulate excitatory synaptic strength by regulating AMPAR trafficking (Kim et al. (2003); Rumbaugh et al. (2006); Vazquez et al. (2004); Carlisle et al. (2008); Araki et al. (2015)). I therefore hypothesised an increase in excitatory synaptic strength in BLA as a result of heterozygous deletion of SynGAP. The two SynGAP mechanisms believed to be involved in regulating synaptic strength are (1) the control of Ras/Rap activation in the PSD by SynGAP's GAP domain; and (2) the association/disassociation of SynGAP with PSD-95 through its C-terminal PDZ motif. If SynGAP's GTPase activity is necessary for regulating synaptic strength, and SynGAP–PSD-95 dissociation is only sufficient, you would expect to see a change in synaptic transmission in the *Syngap*$^{+/\Delta GAP}$ model. If SynGAP–PSD-95 dissociation is a required factor as well, you would not expect to see a change in *Syngap*$^{+/\Delta GAP}$, but you would see changes in synaptic strength in *Syngap*$^{+/-}$.

Unexpectedly, basal synaptic transmission was not found to be different in BLA in either *Syngap*$^{+/-}$ or *Syngap*$^{+/\Delta GAP}$ (Fig. 4.17-4.24). SynGAP is expressed as several different isoforms (Li et al. (2001); Moon et al. (2008); McMahon et al. (2012)) that have been shown to have opposing effects on synaptic functions (McMahon et al. (2012)) with SynGAP Aα2 showing minimal regulation of synaptic strength. The absence of changes in synaptic strength in *Syngap*$^{+/-}$ and *Syngap*$^{+/\Delta GAP}$ could be explained by isoform specific expression profiles in the BLA. If SynGAP Aα2 is the main isoform being expressed in the BLA, reducing its expression would not lead to alterations in the

AMPAR levels, and thus no observable changes in mEPSCs. No thorough investigation has been done into the N- and C-terminal isoform expression profiles, though the C-terminal isoforms $\alpha 1$ and β have been shown to differentially distribute between brain regions, as well as subcellularly (Moon et al. (2008)). It is therefore possible that SynGAP display a differential isoform expression pattern, which would then give rise to distinct phenotypes upon its reduction. Investigation the SynGAP isoform expression profile in the amygdala would help explain the observed results, in addition to increasing our understanding of their distinct role in cellular physiology.

4.3.4 SynGAP regulates thalamo-amygdala LTP in LA

SynGAP is part of the NMDAR-complex through its direct association with the PDZ domains of PSD-95 (Chen et al. (1998); Kim et al. (1998)) and is in a position to regulate synaptic transmission and plasticity, and thereby the encoding of new memories. Thalamo-amygdala LTP was impaired in both $Syngap^{+/-}$ and $Syngap^{+/\Delta GAP}$. This is consistent with other findings, that show impairment of hippocampal LTP in $Syngap^{+/-}$ (Komiyama et al. (2002); Kim et al. (2003); Carlisle et al. (2008); Ozkan et al. (2014)). The presence of this phenotype in both *Syngap* models would indicate that this form of plasticity is regulated by the GAP domain in SynGAP. The LTP deficits occurred in the absence of any clear changes in basal synaptic transmission and NMDAR function. Furthermore, the experiments were completed in the presence of picrotoxin, eliminating any contribution of inhibitory synaptic transmission in LTP induction.

SynGAP can control protein synthesis (Wang et al. (2013)) which in turn can regulate mGluR-dependent signalling in a Ras/ERK dependent manner (Barnes et al. (2015)). Furthermore, altered mGluR-dependent signalling was observed in the hippocampus of $Syngap^{+/-}$ mice (Barnes et al. (2015)), implicating SynGAP as an effector of the mGluR downstream signalling pathway. Thalamo-amygdala LTP in LA is dependent on both NMDARs and mGluRs (Bauer et al. (2002); Rodrigues et al. (2002)), and since no changes were observed in basal synaptic transmission in LA principal neurons, it is possible that the LTP deficit is partly caused by abnormal mGluR-dependent signalling in these neurons. The $Syngap^{+/-}$ mice have been shown to have convergent exaggerated hippocampal mGluR-dependent LTD with $Fmr1^{-/y}$ mice (Barnes et al. (2015)). It is therefore possible that $Syngap^{+/-}$ will share other phenotypes with FXS. $Fmr1^{-/y}$ rats display a deficit in thalamo-amygdala LTP, like $Syngap^{+/-}$ rats, but they also exhibit

impaired mGluR-LTP at cortico-amygdala synapses (Dr. Adam Jackson, University of Edinburgh, unpublished). It is therefore likely that *Syngap*$^{+/-}$ could be replicating the mGluR-dysfunction seen in FXS. To confirm if this is true, investigation of other mGluR-dependent forms of synaptic plasticity, like mGluR-LTP and mGluR-LTD at cortico-amygdala synapses is needed. This would confirm if there is convergence of the cellular pathophysiology between FXS and MRD5, and could give an insight into the functional interplay of mGluRs and SynGAP.

An decrease in paired pulse ratio was observed in *Syngap*$^{+/-}$, which would indicate an increase in transmitter release probabilities at the presynaptic site. Since this was not observed in *Syngap*$^{+/\Delta GAP}$, this would indicate that this change is a consequence of SynGAP–PSD-95 disassociation, rather than an effect mediated by a reduction of GAP GTPase activity. No evidence supports a presynaptic presence of SynGAP, suggesting a retrograde mechanism for the observed change in PPR. The reduction of SynGAP associated with PSD-95 seen in *Syngap*$^{+/-}$ mice (Walkup et al. (2016)) allows for other postsynaptic proteins to bind to PSD-95, like LRRTM, Cadherins, NGLs, and NLGNs, changing the composition of the PSD. Changing the levels of these proteins at the synapse can have a retrograde effect on the presynaptic release probability (Futai et al. (2007); Sylwestrak and Ghosh (2012); Blackman et al. (2013); Matsukawa et al. (2014); Um et al. (2016)). For example, overexpression of NLGNs reduces paired-pulse ratio in hippocampal slice cultures (Futai et al. (2007)). Measuring the protein expression levels of common PSD proteins in the BLA in the *Syngap*$^{+/-}$ and WT would confirm if this was true, and which proteins are upregulated specifically in the amygdala. The decrease in paired pulse ratio could have an impact on LTP, since presynaptic mechanisms for LTP at these synapses exists (Shin et al. (2010)), however since a similar deficit is observed in *Syngap*$^{+/\Delta GAP}$ without the accompaniment of a decrease in PPR another mechanism is likely to play a major role.

The Ras family GTPases and their downstream signalling pathways, ERK, JNK, p38MAPK, and PI3K, control a range of physiological processes, including synaptic plasticity (Thomas and Huganir (2004)). Both hypo- and hyperactivity of small GTPase can impair the capacity of synaptic plasticity (Stornetta and Zhu (2011)). Several Rasopathies — conditions caused by mutations in genes of the Ras-MAPK pathway — display hyperactive Ras pathway activity that leads to deficits in synaptic plasticity

(Costa et al. (2002); Denayer et al. (2008); Lee et al. (2014); Schreiber et al. (2017)). Similarly, increased levels of active ERK has been observed in hippocampus of *Syngap*$^{+/-}$ mice (Komiyama et al. (2002); Carlisle et al. (2008); Ozkan et al. (2014); Barnes et al. (2015)), as well as impaired LTP in the hippocampus (Komiyama et al. (2002); Kim et al. (2003); Carlisle et al. (2008); Ozkan et al. (2014)), suggesting that hyperactivity of the Ras pathways could underlie the impairments in synaptic plasticity in *Syngap* haploinsufficiency. It is unknown whether the Ras-ERK-MAPK pathway is overactive in the BLA in *Syngap*$^{+/-}$ and *Syngap*$^{+/\Delta GAP}$. However, the ERK/MAPK signalling pathway is required for thalamo-amygdala LTP in the LA and for LTP in BA, as well as for fear memory consolidation (Brambilla et al. (1997); Schafe et al. (2000)), making it likely that hyperactive Ras underlies the impairment in LTP in LA observed in both *Syngap* rat models.

Downregulation of hyperactive Ras pathways with inhibitors of this cascade, such as lovastatin, has been shown to be effective for restoring multiple cellular phenotypes, like impaired synaptic plasticity and elevated protein synthesis, but also for restoring learning and attention deficits (Costa et al. (2002); Li et al. (2005); Lee et al. (2014); Barnes et al. (2015); Schreiber et al. (2017)). If the thalamo-amygdala LTP deficit in *Syngap* is caused by hyperactive Ras pathways, then genetic or pharmacologic disruption of the Ras-ERK-MAPK signalling pathway should rescue the phenotype. If so, the Ras pathway could prove to be a suitable therapeutical target for treating individuals with MRD5.

4.3.5 Consequences on behaviour

A panoply of molecular mechanisms in the LA mediate the acquisition and consolidation of fear memories (Puzzo et al. (2016)). This include NMDAR-dependent signalling (Miserendino et al. (1990); Kim et al. (1991)) and the ERK/MAPK kinase pathways (Schafe et al. (2000)) — both cascades that can involve SynGAP. It is therefore expected that *Syngap*$^{+/-}$ and *Syngap*$^{+/\Delta GAP}$ rats will display abnormal fear behaviour. Given that thalamo-amygdala LTP is thought to be the cellular correlate of fear conditioning, the predicted outcome on fear behaviour based on the findings shown in this chapter would be attenuation in fear acquisition and fear recall. However, both *Syngap*$^{+/-}$ and *Syngap*$^{+/\Delta GAP}$ rats present with normal fear acquisition, but enhanced fear recall and slower extinction (Sup. Fig. S3).

Two major pathways carry CS information to the LA: the thalamic pathway entering LA through the internal capsule, and the cortical pathway entering the LA through the external capsule. Either pathway alone is sufficient in the acquisition of fear memory (Romanski and Ledoux (1992)). However, post-training lesions of the cortical input leads to loss of fear memory, while fear memory remains after lesions of the thalamic pathway. This suggests that the cortical pathway performs a more dominant role in fear conditioning (Campeau and Davis (1995); Boatman and Kim (2006)), however this is not uncontested: more rapid plastic changes in thalamic afferents during fear conditioning suggest that the thalamic pathway plays the primary role (Quirk et al. (1997)). The electrophysiological data here together with the behavioural data, would suggest that the cortical pathway is sufficient to overcome the failure to induce thalamo-amygdala synaptic potentiation and acquire the fear memory. Testing the ability of cortico-amygdala synapses to potentiate would clarify if plasticity in this pathway is intact, and if it is compensating for the thalamo-amygdala synapses.

Another possibility is that the deficit in thalamo-amygdala LTP prevents the animals from acquiring fear extinction. The circuit involved in fear extinction is similar but distinct from fear acquisition and recall (Duvarci and Pare (2014)). Extinction of fear is considered a new type of learning rather than forgetting (Pape and Pare (2010)), and as with fear acquisition, synaptic plasticity in the BLA is necessary for its learning (Falls et al. (1992); Walker et al. (2002); Herry et al. (2006); Sotres-Bayon et al. (2007)). Particularly, NMDAR-dependent synaptic plasticity via the ERK/MAPK pathway in the LA has been proposed as the likely mechanism underlying extinction learning (Sotres-Bayon et al. (2007)) — a signalling pathway involving SynGAP, and which is necessary for thalamo-amygdala LTP (Schafe et al. (2000); Bauer et al. (2002)). It is therefore possible that this form of synaptic plasticity is contributing more to fear extinction learning rather than the initial fear memory acquisition. The inability for *Syngap*$^{+/-}$ and *Syngap*$^{+/\Delta GAP}$ rats to induce synaptic plasticity at thalamo-amygdala synapses could therefore result in failure to extinguish the fear memory during the fear recall protocol, and thus enhance freezing during recall and extinction (Sup. Fig. S3B).

In addition to enhanced recall, *Syngap*$^{+/-}$ and *Syngap*$^{+/\Delta GAP}$ rats show increased freezing during pre-tone (Sup. Fig. S3B), and are unable to discriminate CS from no CS (data not shown). This could be an indication that the animals are prone to generalise

fear, though this has not been confirmed with a generalised fear protocol. During fear conditioning, distinct neuronal populations in the LA are recruited to the CS^+ and CS^- (Ghosh and Chattarji (2015)). The total number of LA principal neurons recruited to the CS^+ signifies the strength of the fear memory, whereas the ratio of CS^+ to CS^- recruited neurons determines the animals ability to distinguish between CS^+ and CS^-. Animals with fear generalisation show relatively enhanced firing to the CS^- and are therefore unable to discriminate (Ghosh and Chattarji (2015)). LA principal neurons in *Syngap*$^{+/-}$ display an increase in excitability. Neurons with greater excitability are more likely to get recruited in new memory traces (Zelcer et al. (2006); Kim et al. (2013)). Therefore, the enhanced excitability could lead to more neurons being recruited to the CS^-, leaving the animals unable to fear discriminate, and longer to extinguish.

Increased intrinsic excitability was only observed in LA neurons in *Syngap*$^{+/-}$ and not in *Syngap*$^{+/\Delta GAP}$. This would mean that *Syngap*$^{+/\Delta GAP}$'s inability to extinguish is due to something else, or that the increased excitability in *Syngap*$^{+/-}$ is unrelated to this phenotype. To confirm that the two *Syngap* models truly show divergent excitability phenotypes, their intrinsic excitability would have to be confirmed in the *Syngap*$^{+/-}$ $\times$ *Syngap*$^{+/\Delta GAP}$ cross line, thereby eliminating the possible confounding bias of colony differences.

4.4 Summary

The findings in this chapter has expanded our knowledge of SynGAP protein function and amygdala pathophysiology associated with *Syngap* haploinsufficiency. Distinct changes were observed in excitability of BLA principal neurons in the two *Syngap* models. This would suggest that SynGAP has an important role in regulating neuronal function through both GAP-dependent and -independent mechanisms. Moreover, these changes were nucleus specific indicating that SynGAP have distinct functions depending on its location, even in closely associated brain areas. Unexpectedly, SynGAP reduction did not affect basal excitatory or inhibitory synaptic transmission. *Syngap*$^{+/-}$ showed a decrease in paired-pulse ratio, indicating that the SynGAP–PSD-95 association, and not the GAP domain, controls short-term presynaptic plasticity. However, LTP at thalamo-amygdala synapses was impaired in both models, suggesting a major regulatory role by the GAP domain in this form of plasticity.

Chapter 5

Establishing methodology to study circuit function in amygdala

5.1 Introduction

The value of single cell electrophysiological recordings contributes more than just increasing our understanding of how neurons process information and how the brain works. It also gives insight into neurological disorders, the underlying pathology, and potential use of therapeutical compounds. The most important limitation to single cell physiology is that the brain functions in an orchestrated fashion by a large ensemble of cells. Networks of cells exhibit diverse activity patterns, such as oscillations, waves, avalanches, and songs (Engel et al. (2001); Ermentrout and Kleinfeld (2001); Beggs and Plenz (2003); Ikegaya et al. (2004)), which cannot be understood from the activity of single neurons. Thus, to get a complete understanding of higher brain function we must also look beyond the individual cell, and look at how they work together in a circuit.

In the previous chapter, I showed that *Syngap* heterozygous animals display changes in their intrinsic excitability and are unable to induce LTP at thalamo-amygdala synapses. I wanted to determine how this would affect excitability at the amygdala circuit level. Altered circuit excitability has been found in other brain regions of *Syngap*$^{+/-}$ mice. Signal propagation in the hippocampus was dramatically amplified in young *Syngap*$^{+/-}$ mice (Clement et al. (2012)). Similar results were found in adult mPFC, where significantly larger signals were observed in response to stimulation (Ozkan et al. (2014)). Furthermore, altered amygdala circuits have been detected in another model of autism. Mice lacking Pcdh10 show a specific reduction in gamma band coherence in

the BA in response to high frequency LA stimulations (Schoch et al. (2017)). Taken together, I would therefore predict nuclei distinct changes in circuit activity that could translate into changes in signal propagation.

As described earlier, the amygdala microcircuit has a crucial role in regulating acquisition, specificity, and extinction of conditioned fear, and also for regulating anxiety. In addition to investigating basal amygdala circuit activity in *Syngap* haploinsufficient animals, I want to determine how the circuit responds to fear conditioning and to a fear generalisation paradigm. Work done in the lab by colleagues have shown that *Syngap* heterozygous animals display increased freezing during fear recall (Sup. Fig. S3). In addition, the animals are unable to discriminate between CS and no CS presentations, suggesting that these animals might display generalised fear. In animals with generalised fear, more neurons in the LA show responses to CS^- presentations and consequently are unable to discriminate between CS^+ and CS^- (Ghosh and Chattarji (2015)). Furthermore, changes in tonic activity in the CeA microcircuit is seen in animals with generalised fear (Ciocchi et al. (2010)). Similarly, a study in trait anxiety found a positive correlation between increasing levels of anxiety and increased activity in CeA compared to LA (Avrabos et al. (2013)).

Based on this, I therefore hypothesize that *Syngap* haploinsufficient animals will display an increased response in the LA to auditory evoked stimuli after fear conditioning with altered propagation of the signal from BLA to CeA, and changes in the tonic activity in the CeA. To investigate this, I will use imaging to determine the spatial and temporal pattern of the propagation of membrane potential change when electrically stimulating thalamic input in the internal capsule, as well as determine the level of activity in the circuitry. To examine how fear conditioning would alter this circuit, these experiments would be carried out pre and post fear conditioning.

In order to do this, I needed to establish an *in vitro* optical imaging assay in the lab. The purpose of this chapter will be to describe the optical imaging techniques considered, the advantages and limitations of these, and the process of establishing the methodology. Moreover, a preliminary data set is presented from the *Syngap* haploinsufficiency rat model, as well as a discussion of how the optical imaging assay can be improved.

5.2 Optical imaging of neuronal activity

There are several ways to look at circuit function, one being conversion of the neuronal physiological signal into an optical signal by using a molecular probe. These probes can be sensitive to the fluctuations of the membrane potential, i.e. voltage-sensitive, or sensitve to changes in ion concentrations such as Ca^{2+}, i.e. calcium-sensitive. Both probes are available as organic dyes and genetically encoded, but this chapter will mainly be discussing the organic dyes. These two types of molecular probes, voltage-sensitive dyes and calcium-indicator dyes, measure neuronal activity in a direct and indirect way, respectively. Voltage-sensitive dyes create a signal that is directly related to the membrane potential changes, whereas calcium-indicator dyes are an indirect measure of neuronal activity by reporting on changes in intracellular $[Ca^{2+}]$. These two complementary methodologies each has their limitations and advantages as discussed below.

5.2.1 Voltage-sensitive Dye Imaging

VSDs bind to the external membrane of a cell, presumably without disrupting normal cellular function (as discussed below, this is not always true). VSDs have a hydrophobic element embedded in the membrane that senses changes in trans-membrane potential. Fluctuations in membrane potential causes subtle conformational or electronic rearrangements leading to a shift in the excitation or emission spectrum of the dye, in turn altering the intensity of the fluorescence/absorption at a particular wavelength (Stuart and Palmer (2006)).

The changes in voltage are expressed as fractional intensity change ($\Delta I/I$ or $\Delta F/F$). Stimulus evoked normalised fractional intensity changes in brain slice preparations have been shown to reflect neuronal action potentials as well as EPSPs (Ross et al. (1977); Zecevic (1996); Tominaga et al. (2000)). From the data obtained from VSD imaging, it is possible to visualise where activity occurs, how large the events are, and how they move through the slice in time.

Voltage-sensitive dyes

The two most commonly used types of voltage-sensitive dyes are absorption dyes and fluorescent dyes. **Absorption dyes** require light at the wavelength that is maximally

absorbed by the dye, and usually require trans-illumination. Alterations in membrane potential is measured as a change in light absorption (Jin et al. (2002); Hochman (2009)).

Fluorescence dyes are excited at one wavelength of light and fluoresce at a distinctly different wavelength. Changes in emission fluorescence correspond to membrane potential fluctuations. Fluorescent dyes can be further divided into 'fast' and 'slow' dyes. **Fast dyes**, such as the hemicyanine/styryl dyes, respond to changes in membrane potential by intramolecular redistribution of electrical charge changing their fluorescent properties (Yan et al. (2012)). This gives them rapid optical responses allowing for measurements in a timescale of miliseconds. **The slow dyes**, such as the rhodamine, merocyanine, and oxonol dyes, are subjected to voltage-dependent changes in their intramembrane distribution giving rise to fluorescent changes, which is signicanlty slower than the fast dyes. However, the fast dyes have smaller changes in fluorescence compared to the slow dyes (Hochman (2009); Loew (2015)). FRET-pair membrane potential sensors also belong to the slow-response dyes, but their mechanism of responding to membrane potential changes is through fluorescence resonance energy transfer (FRET) from a lipophilic anion in the membrane interior and static donor fluorphore on the membrane surface. The fluorescence change in FRET-pair voltage-sensitive dyes is superior to any of the other, showing >25% increase per 100 mV, but because of their slow response time, they are still not widely used.

Comparing fluorescent and absorption dyes, fluorescent dyes have larger fractional changes than absorption dyes, but absorption dyes can give a better signal-to-noise ratio (Jin et al. (2002)). Whereas, the absorption dyes are not easily obtainable, both fast and slow voltage-sensitive dyes are commercially available, including hemicyanine dyes (di-4-ANEPPS, di-8-ANEPPS, RH237, RH795) and oxonol dyes (Oxonol V, DiBAC^4(3)). Voltage-sensitive dyes can be measured either ratiometrically or non-ratiometrically.

5.2.2 Calcium-sensitive Imaging

Intracellular calcium is integral to a range of physiological processes, including neurotransmitter release, ion channel gating, and second messenger pathways. In neurons, electrical activity is linked to intracellular signalling through calcium, thus changes in calcium concentrations can act as an indirect measure of electrical activity (Grienberger and Konnerth (2012)).

As opposed to voltage-sensitive dyes, calcium-dyes function intracellularly in the axoplasm, where they report the presence of freely diffusible Ca^{2+} through a direct binding-induced change in fluorescence. Like VSDs, calcium-imaging is reported as fractional changes in fluorescence intensity/ratio of fluorescence intensity.

Calcium indicator dyes

Organic calcium indicator dyes can be categorised into ratiometric dyes or non-ratiometric dyes. **Ratiometric dyes** have different excitation or emission wavelengths depending on whether they have Ca^{2+} bound or not. Data is obtained by alternating excitation between two distinct wavelengths, and taking the ratio of the measurements. Ratiometric dyes can be used quantitatively with a calibration curve. Measurements are dye-concentration independent, and are unaffected by illumination intensity, probe loading, bleaching, or optical path length. Drawbacks are more complicated data acquisition and manipulation. Additionally, UV/near UV-wavelengths needed for ratiometric dyes can lead to production of reactive oxygen species, which can lead to non-physiological effects (Paredes et al. (2008)).

Non-ratiometric dyes show a large change in either excitation or emission fluorescence intensity upon direct binding to Ca^{2+}. Non-ratiometric dyes are mainly used for qualitative imaging, since a quantitative measure is unreliable. Non-ratiometric dyes are prone to detect changes to fluorescence intensity based on dye concentration and experiment specific conditions that are unrelated to $[Ca^{2+}]$ (Paredes et al. (2008)).

Three types of Ca^{2+} indicator dyes are commercially available: salts, dextran conjugates, and acetoxymethyl (AM) esters. **Salts** are the simplest, but are membrane impermeable because of their hydrophilic nature, and therefore need invasive loading procedures. **Dextran conjugates** of Ca^{2+} indicators have high solubility, low toxicity, and are less prone to compartmentalization. Like salts, dextran conjugated dyes are membrane impermeable. **AM ester dyes** were made to enable loading of hydrophilic dyes into cells, and can be passively loaded. Once inside, the AM group is cleaved by esterases and the dye is trapped inside the cell. Because of the AM group, the dyes have low solubility, and therefore need DMSO and F-127 Pluronic to dissolve. (Paredes et al. (2008))

5.2.3 Advantages and limitations to optical imaging

General Advantages

Using optical imaging to measure neuronal activity can offer advantages over other methods looking at populations or small circuits of neurons. Voltage- and Calcium-sensitive dyes allow measurements of activity in a large population of neurons at once, and from several areas at once. Multisite recordings combined with the high spatial resolution achieved with these methodologies can offer information about action potential initiation and propagation, including velocity and direction (Baker et al. (2005)).

In addition, optical imaging is principally noninvasive. This leaves the intracellular milieu intact, including signal transduction pathways underlying synaptic plasticity, which are normally lost during whole-cell patch recordings.

Furthermore, simultaneous electrophysiological recordings from neurons can facilitate the correlation of optical signals from a population of cells to activity in a single cell (Carlson and Coulter (2008)).

General limitations

For the purpose of this study, the dyes would be extracellularly applied to stain the whole slice. Extracellularly applied dyes stain all cells indiscriminately, including glial and vasculature. This can result in high background signals, lowering the signal-to-noise ratio, and masking the optical signals originating from neurons (Konnerth et al. (1987); Kriegler and Chiu (1993)). In addition, the optical signal is weighted towards dendritic potentials, since the area of dendritic membranes exceeds that of soma and axon.

Most current setups for wide-field optical imaging uses CCD or CMOS cameras. CCD and CMOS cameras have relatively high individual pixel noise, and it can therefore be necessary to average over a number of pixels in 10-14 trials to achieve good signal-to-noise ratios.

Light scattering or other intrinsic signals can cause changes in wavelength signals, that are wavelength independent. Ratiometric dyes can control for this, and for non-ratiometric dyes signals can be distinguised from this by measuring illumination at a minimum signal wavelength (Yuste and Katz (1991); Jin et al. (2002)).

Furthermore, dye bleaching and phototoxicity can be a limiting factor in optical imaging. After long exposure, or exposure at high intentisty, dye bleaching can occur,

which is the reduction of optical signal, while electrical activity remains unchanged. Bleaching can be corrected for by subtracting an area unaffected by the stimulation or a trial with no electrical stimulation. Phototoxicity is irreversible damage to the stained tissue caused by exposure to light, and causes a decrease in both optical and electrical activity (Ross et al. (1977); Jin et al. (2002)). Recording a field EPSP simultaneously with your optical recording can act as a control for slice health and the phototoxicity effect. Both bleaching and phototoxicity can be reduced by limited and intermittent exposure to light.

Both VSDs and calcium-indicators have dyes that have low solubility in aqueous solutions, because of hydrophobic groups in their structure (Paredes et al. (2008); Canepari and Zecevic (2010)), which can render them less practical in use. This can be circumvented by using a DMSO and the non-ionic surfactant F-127 Pluronic, however these are not entirely harmless to cells (Cavaletti et al. (2000); Brunet-Maheu et al. (2008); Yuan et al. (2014)), and their concentrations should be kept as low as possible.

There are two kinds of noise in optical measurements that can cause complications: Shot noise (the statistical fluctuation of the photon flow), which is irreducible and inherent to the measurement of light; and extrinsic noise resulting from mechanical vibrations, disturbances in the optical path, instability of the light source, and dark noise/dark currents in the measurement system. Dark noise/dark currents can be reduced by choice of equipment, but if it is smaller than the shot noise, it is not the limiting factor. Several measures can be taken to reduce mechanical vibrations and other disturbances like bolting the microscope and amplifiers to a vibration isolation table; avoiding air bubbles in the solution; and minimising vibrations at the saline-air interface.

Shot noise is proportional to the square root of light intensity reaching the detector, and is the physical limit for the signal-to-noise ratio. The relative size of the shot noise can be reduced by improving the light collection efficacy.

Advantages of Voltage senstitive dyes

The strength of VSD imaging is its ability to measure fast electrical signals at high spatial and temporal resolution, which allows for analysis of synaptic integration in circuits (Jin et al. (2002)). Under the presumption that neurons are evenly stained by

Table 5.1: ***Comparison between voltage-sensitive dyes and calcium-indicators***

Voltage-sensitive dyes	*vs.*	**Calcium-indicators**
Direct measure of neuronal activity		Indirect measure of neuronal activity
Small optical signal with fractional changes of 0.1–10% per 100mV		Large optical signal with fractional changes of 10-20% per AP
AP driven activity & Subthreshold potential detection		AP driven activity
Differentiation between excitatory and inhibitory transmission		Indistinguishable excitatory and inhibitory transmission
Narrow dynamic range		Large dynamic range
Sensitive to noise/Limited signal-to-noise		High signal-to-noise ratio
Internalisation of dyes decreases signal		Leakage of dye decreases signal
Pharmacological side effects		Acts as Ca^{2+} buffer

the VSD, the amplitude of the signal should be linear to the synchrony of the activity, and the area under the waveform linear to the number of spikes during an event. In addition to measuring spiking activity, it is possible with VSD imaging to detect subthreshold synaptic potentials (Jin et al. (2002)).

Another strength of VSDs is their ability to measure both excitatory and inhibitory synaptic transmission (Carlson and Coulter (2008)). The decrease and increase in the fluorescent intensity from the preparation corresponds to membrane depolarisation and hyperpolarisation, respectively. In fact, VSD imaging has proven very useful in examining responses with large inhibitory elements (Fujieda et al. (2015); Colavita et al. (2016); Nixima et al. (2017)). This is particularly useful when investigating circuit function in the amygdala, as inhibitory circuits within the amygdala control the strength of sensory input and can exert a gating action over neural activity during fear acquisition, expression and extinction (Ehrlich et al. (2009); Pape and Pare (2010); Fujieda et al. (2015)).

Limitations of Voltage sensitive dyes

VSDs are limited by their sensitivity to changes in voltage, and produce only small fractional changes in absorption or fluoresence. The fractional intensity change ($\Delta I/I$ or $\Delta F/F$) is in the range of 10^{-2}–10^{-5} of the resting light intensity per 100 mV. That being said, with good signal-to-noise ratio, the small fractional change in light intensity does not have to be limiting, and it is possible to achieve a decent signal-to-noise in a single recording trial (Momose-Sato et al. (1999); Jin et al. (2002)). It is therefore vital to limit noise to reliably detect a signal, and increase the signal as much as possible.

Given that the amplitude of the VSD signal is proportional to the light intensity, and the shot noise is proportional to the square root of the light intensity, the signal-to-noise ratio is proportional to the square root of the light intensity, hence higher light intensity levels can increase the sensitivity of the measurement. The light intensity cannot be increased without limitations. While shot noise is proportional to the square root of the light intensity, vibration noise is proportional to the light intensity. Therefore, at increasing light intensity vibration noise starts to become dominant.

Furthermore, the dyes can be prone to internalisation of dyes, which causes rapid degradation of the signal-to-noise ratio.

A premise for using voltage sensitive dyes is that they do not interfere with the parameters they are meant to measure, whether in a direct or indirect manner. Several commonly used VSDs were shown to have potentiating effects on $GABA_A$ receptors *in vitro* and *ex vivo* (Mennerick et al. (2010)), and some to have pharmacological side effects *in vivo* (Grandy et al. (2012)), though the *ex vivo* and *in vivo* pharmacological effects were shown to be transient for some of the dyes. This indicates that caution is needed when choosing dyes and designing experiments to avoid modulation of network activity by your dye.

Advantages to calcium-sensitive dyes

The major strength of calcium-indicators, and the reason they are more commonly used for optical imaging, is the generation of large optical signals of between 10–20% per AP. Because of their large signal, they can provide large signal-to-noise ratios, making calcium-indicators easier to implement.

Given that Ca^{2+} concentrations can vary >100 fold during physiological activity (Muri and Knöpfel (1994)) coupled with high sensitivity of calcium-indicators, Calcium-imaging can have a much larger dynamic range compared to VSDs. The dynamic range of the calcium-indicator, Fluo-3, can be seen in Fig. 5.1A.

Limitations to calcium-indicator dyes

The major limitation to using calcium-indicator dyes is their speed. Calcium-indicator dyes are limited by calcium ion dynamics in the neurons, which are significantly slower than membrane voltage changes and are usually too slow to follow oscillations at frequencies above 10 Hz (Antic et al. (2016)). Fig. 5.1B shows a comparison of the

time course of voltage- and calcium-imaging signals, and the slower dynamics of the calcium-signal is indisputable.

A caveat of calcium-indicators is that the signal is an indirect measure of neuronal activity, and only of that which triggers a large enough change in calcium concentration, unlike sub-threshold synaptic currents, which are not measurable with calcium-indicators (Mao et al. (2001)).

Another caution with using calcium-sensitive dyes is that, because they bind to Ca^{2+}, they contribute to the buffering of intracellular Ca^{2+} and homeostasis. This will limit the magnitude of changes in $[Ca^{2+}]$ and slow down the dynamics of this. This can disrupt Ca^{2+}-dependent signalling and cellular function, and alter the pattern of neuronal activity they are meant to study (McMahon and Jackson (2018)). A compromise must be made between the strength of the indicator signal and the problems associated with increasing calcium-indicator concentrations.

Opposite to VSDs, where dyes can get internalised and decrease signal-to-noise, calcium-indicators can leak out of the cell. This will lead to a decrease in excitation, and hence a decrease in signal-to-noise. Ratiometric dyes allow you to correct for, or at least detect, dye leakage, since it will be visible as a decrease at both excitations wavelengths. In addition, some dyes get compartmentalised, which degrades the Ca^{2+} measurements within the cytosol. For shorter recordings of 30 min to an hour, this is generally not an issue.

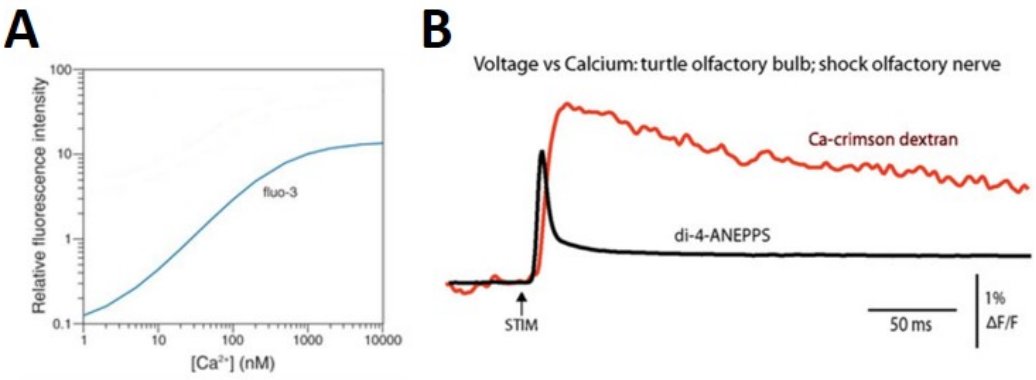

Figure 5.1: Properties of calcium-indicator dyes(A) Fluorescence intensity with increasing $[Ca^{2+}]$ shows a high relative change in intensity with increasing concentrations, indicative of its large dynamic range. (B) Time course comparison of the voltage and calcium dye signal from the same location in the olfactory bulb in response to electric stimulation shows that the voltage-sensitive dye signal is much faster compared to the calcium-indicator signal. Figure adapted from Canepari and Zecevic (2010).

5.2.4 Choice of methodology

I wanted to use optical imaging to study the spatiotemporal dynamics of the intranuclear circuitry of the amygdala. Given that inhibitory synaptic transmission plays a vital role in this microcircuit (Ehrlich et al. (2009); Pape and Pare (2010); Fujieda et al. (2015)), my first approach was to use VSD imaging, as this method enables the investigator to distinguish between excitatory and inhibitory synaptic transmission, unlike calcium-imaging. VSD imaging also has a far superior temporal resolution, albeit it suffers from small optical signals, making it a tougher methodology to implement. As is evident below, a VSD optical imaging assay proved harder to establish, hence a calcium-indicator dye was used to get an initial protocol up and running.

5.3 Methods

5.3.1 Animals

The two *Syngap* rat lines used in chapter 4, *Syngap*$^{+/\Delta GAP}$ and *Syngap*$^{+/-}$, were crossed to get one colony generating both models as well as WT littermate controls. Any weak/runt pups suspected to be homozygotes were culled before postnatal day 6, because *Syngap* homozygosity is lethal. *Syngap*$^{+/\Delta GAP}$, *Syngap*$^{+/-}$, and WT were maintained for experiments, and only male animals were used for experiments.

5.3.2 Staining protocol

Acute slice preparation

Acute coronal slices were prepared as described in Chapter 2. After cutting, slices were allowed to recover at 34°C for 30 min and then stored at room temperature for 30 min before staining commenced.

Staining with the voltage-sensitive dye, di-8-ANEPPS

A di-8-ANEPPS (Invitrogen, Fisher Scientific UK) stock was prepared by dissolving 5 mg of dye in 1686 μL DMSO to achieve a 5 mM stock concentration. The stock was stored at 4°C, and when needed, was warmed slightly and vortexed to dissolve crystals.

Loading solution was prepared by diluting 60 μL di-8-ANEPPS stock into 30 mL of ACSF to achieve a final concentration of 10 μM (0.2% DMSO). As di-8-ANEPPS is

highly lipophilic, F-127 pluronic acid (0.05%) was added to the loading solution to aid with solubilisation of the dye. The loading solution was added to the staining chamber and continuously carbogenated, and was placed on a shaking table during staining. Slices were staining between 15 min and 2 hrs, and were shielded from light while staining.

After staining, slices were washed in recording ACSF for 2×15 min to remove excess dye, and imaging would follow.

Staining with the calcium-indicator dye, Fluo-4

50 μg of Fluo-4 was dissolved in 8 μL DMSO and 2 μL F-127 pluronic acid (5% in DMSO) and vortexed for 15–20 min. Any dye left over was kept in the fridge, and used within a couple of days.

For calcium-indicator dye staining, an interface staining chamber (Fig.5.2) was assembled using instructions from Dawitz et al. (2011). 2.5 mL ACSF was added to the chamber with continuous carbogenation. Slices were transfered to the interface dish in the staining chamber and 5 μL dye was pipetted directly over the amygdala divided between 2 or 3 slices. This resulted in a high initial concentration over the slices, but achieved a final concentration of 10 μM Fluo-4 (0.2% DMSO, 0.02% F-127 Pluronic). The staining chamber was incubated at 34°C protected from light, and slices were stained for 10 min + postnatal age in min, i.e. a slice from a p40 rat would get stained for 50 min, as recommended by MacLean and Yuste (2009). After staining, slices were transferred back to a holding chamber for at least 30 min before imaging commenced.

5.3.3 Imaging setup

Fluorescence images were acquired using an upright Leica DM LFS microscope equipped with a 1.25x (NA=0.05; Leica) objective and a CMOS camera (OptiMOS, QImaging) with LED-based illumination (pE300,CoolLED). Turning the LEDs on/off was used in place of a shutter, which would help minimise mechanical noise.

A filter cube was used to separate excitation and emission. For di-8-ANEPPS, a cube containing an excitation band-pass filter centred at 470nm and 40nm wide and emission filter centred at 630nm and 75nm wide (ET470/40x, ET630/75m; Chroma). For Fluo-4, a single band filter set with an excitation filter centred at 470nm with 40nm bandwidth and emission filter centred at 525nm with 50nm bandwidth (FITC/Cy2, Chroma). ImageJ was used for the optical image data acquisition. The frame rate was

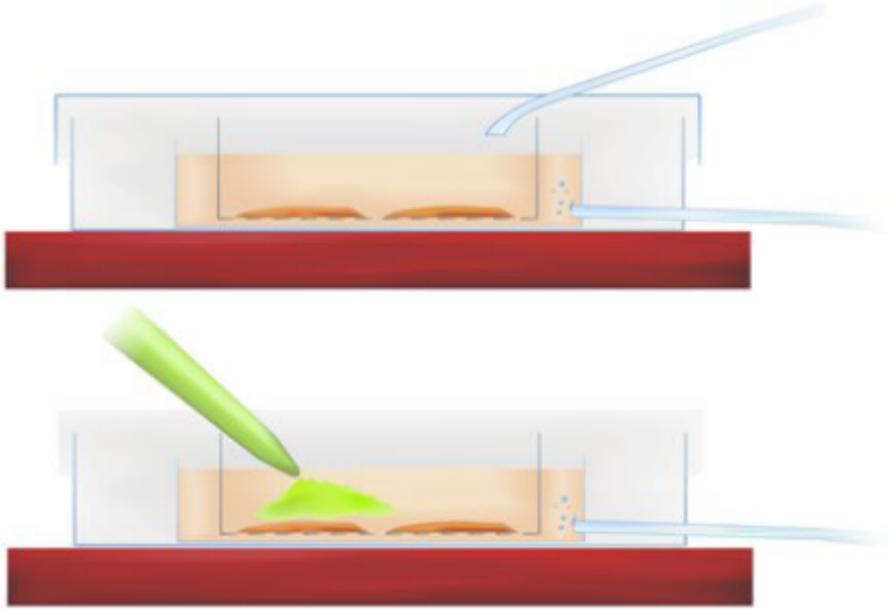

Figure 5.2: Cross-section of Calcium-indicator dye staining chamber. Staining chamber was made from instruction given in Dawitz et al. (2011). Top section shows slice incubation with carbogen coming in at the bottom to carbogenate the ACSF, as well as through a hole in the lid. Bottom section shows how application of dye is done over the region of interest on each slice. Figure from Dawitz et al. (2011).

100 frames per second with an exposure time of 10 ms. Each time lapse recording was 1.5 sec.

5.3.4 Recording

Slices were transferred to a submerged recording chamber of an upright microscope, and was continuously perfused with carbogenated recording ACSF at a rate of 3–5mL/min using a peristaltic pump. The temperature was kept at 27–29°C using an inline heater.

Field EPSPs (fEPSPs) were recorded with a micropipette filled with ACSF (1-3 MΩ) made from borosilicate glass capillaries (OD 1.5 mm, ID 0.86 mm, Harvard apparatus, UK) using a horizontal puller (P-97 Flaming Brown, Sutter Instrument, US). Test pulses were delivered at thalamic or cortical inputs to the LA using a bipolar stimulating electrode placed in the internal or external capsule, respectively. A single pulse or a train of 5 pulses at 20 Hz were used to elicit synaptic responses. Stimulations were elicited every 20 secs.

Onset of electrical stimulation would trigger the light to go on, and imaging to commence. For some experiments, stimulations trials were interleaved with non-stimulation

trials. For each experiment, between 7-25 trials were done.

5.3.5 Confocal Imaging

Confocal imaging was used to assess the level of di-8-ANEPPS dye staining at high magnification. Slices were put into 4% PFA for 1 hr at RT immediately after the staining wash cycles or after VSD imaging was completed. The slices were washed in PBS (Phosphate-buffered saline: 0.025M PB, 0.9% NaCl) for 3×15 min, and mounted on glass slides using Fluoromount (Sigma-Aldrich, UK) and sealed with varnish. Images were acquired using a Zeiss Axiovert LSM 510 inverted confocal microscope with a 63× objective (1.5 NA) in 1 μm steps.

5.3.6 Analysis

The optical data format was a 150 frame-long time lapse sequence of TIFF images, which was analysed on ImageJ and MATLAB R2017b. As noise and bleaching are inherent parts of fluorescence imaging, a background of averaged pixels from an area not affected by the stimulation was subtracted from each other pixel. Because the fluorescence signals are small and to reduce noise, particularly for VSD imaging, 7–25 trials were averaged together. The averaged image was then filtered with a digital 2D Gaussian kernel (5 × 5; x × y; σ=1.5)

The fluorescence intensity emitted by the slice prior to stimulation (50–100 ms prior) was averaged and used as the reference intensity (F_0).

The change in fluorescence ($\Delta F = F_t - F_0$) was normalised by the reference to obtain the fractional fluorescence ($\Delta F/F$), which was used as the optical signal. The normalised fractional fluorescence intensities were analysed using a MATLAB VSD analysis toolbox developed by and described in (Bourgeois et al. (2014)). This toolbox allows the user to visualise and statistically compare activity across the full spatiotemporal range of the fluorescence dataset.

The three-dimensional optical data (x × y × time) is first geometrically transformed into a two-dimensional spatiotemporal rasterised image of activity (anatomical position× time; Fig. 5.7A), guided by user-defined anatomical regions of interest in the slice. The anatomical boundaries of the LA, BA, and CeA are clearly visible in an acute coronal slice, and can be used to draw region boundaries (Fig. 5.3). For the purpose of establishing the methodology, only the LA was used for raster

plot construction, as this region was expected to elicit the strongest optical signal. The toolbox automatically divides the regions into fixed-width polygonal segments (Fig. 5.8A), and the average fractional fluorescence signal within each segment is calculated. The signal from each segment is depicted as a row in the raster.

To allow for direct comparison between slices, the toolbox interpolates rasters along the y-axis to a standard number of polygonal segments and stretches or compresses each raster to be the same size. Within a group, rasters are then averaged. From here, statistical tests can be performed between groups at each spatiotemporal site using a non-parametric permutation test (t = 1000) giving you a two-dimensional heatmap of spatiotemporally significant differences (Fig. 5.12D). The toolbox can also measure the velocity of the spread of activity and test for anatomical differences, but these measurements were not carried out on this dataset.

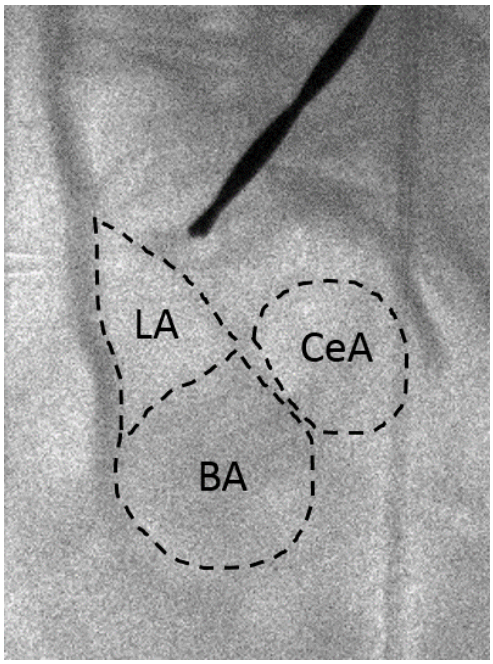

Figure 5.3: Amygdala anatomical boundaries. Grey scale image of an acute coronal slice with clear anatomical boundaries of the LA, BA, and CeA.

5.4 Preliminary findings

5.4.1 Optimizing staining protocol

I selected a fast-response voltage-sensitive dye to fully exploit the advantages of VSD imaging. Amongst the fast VSDs, the ANEPPS are the most commonly used, with di-4-ANEPPS being the most common. Furthermore, they are some of the most sensitive of the fast-response dyes exhibiting around 10% per 100 mV changes in fluorescence intensity. I chose the di-8-ANEPPS over di-4-ANEPPS due to its higher resistance to internalisation, better photo stability, and lower phototoxicity.

When examining staining protocols from other studies using ANEPPS dyes, I found no clear consensus on dye concentration, staining time, or conditions for staining. Concentrations could vary from 0.2 μM–200 μM; duration of staining was from 10 s to 90

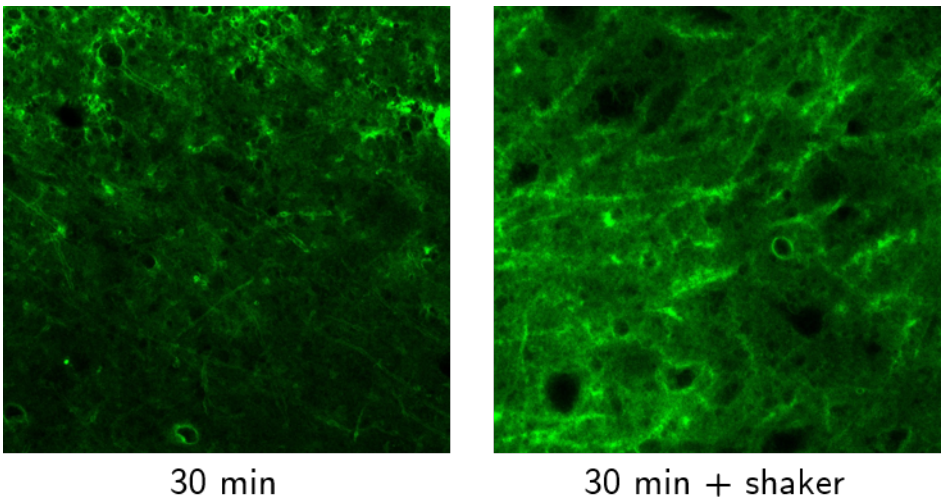

Figure 5.4: Dye staining was improved by incubation on shaker The image to the left shows a z-stack average from 5–11 μm from the surface of a slice stained for 30 min at RT. Little to no dye was observable at depths beyond 11 μm from the surface. The right image shows a slice stained for 30 min on a shaking table. The z-stack is from 18–26 μm average from the surface, but dye could be seen down to 31 μm from the surface.

min; and temperature ranged from 10–30°C, but most commonly room temperature was used for dye incubation (Bedlack et al. (1992); Bourgeois et al. (2014); Fujieda et al. (2015); Colavita et al. (2016); Nixima et al. (2017); Takesian et al. (2018)). I decided to use a concentration of 10 μM di-8-ANEPPS, and staining at room temperature at varying lengths of time (15 min–2 hrs). I opted for a lower dye concentration to minimise pharmacological side effects (Mennerick et al. (2010)), and because more even staining is associated with lower concentrations and longer staining time (Baker et al. (2015)). I found that longer staining time allowed for the dye to perfuse deeper into the tissue, but the staining was still superficial. To get better penetration of the dye into the tissue, the slices were stained while on a shaking table, which greatly improved the staining (Fig. 5.4).

As evident in Fig. 5.5A, only sparse staining was seen after 15 min. Deeper penetration of the dye was observed after 30 min of staining (Fig. 5.5B), but the fluorescence intensity appeared to decrease slightly with staining of 1 and 2 hours (Fig. 5.5C+D). The decrease in staining seen at longer incubation times could be caused by internalisation of the dye, or variability in efficiency of staining. As will follow below, the optical imaging was mostly unsuccessful, so how staining time and optical signal amplitude correlate is unknown.

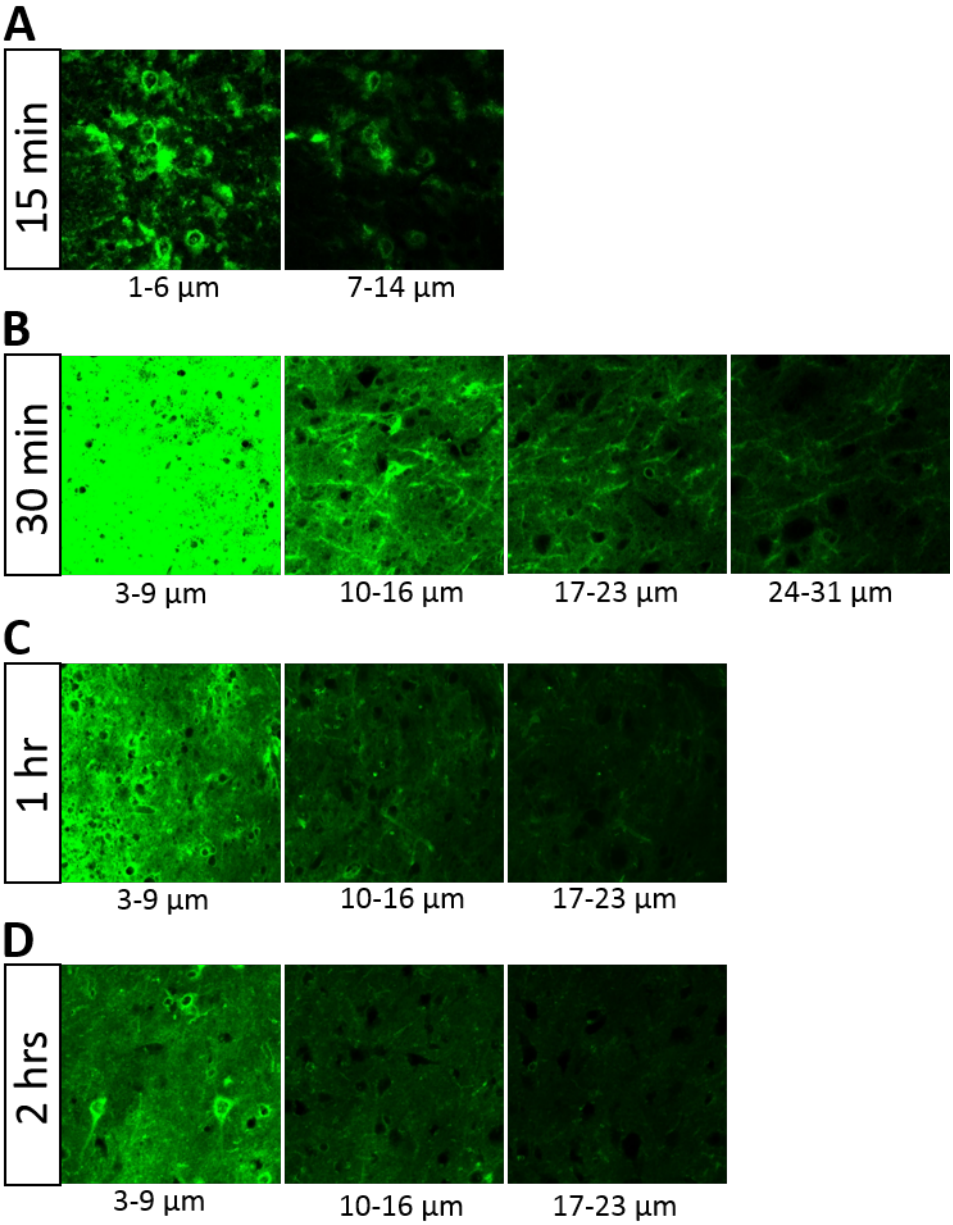

Figure 5.5: The effect of time on dye staining. (A) 15 min of staining resulted in staining down to 14 μm from the surface. (B) 30 min of staining improved the diffusion of the dye. Dye was detectable down to 31 μm. (C)+(D) 1 hr and 2hrs of dye incubated resulted in a similar staining of the dye. The images are average z-projections from the indicated depths below the images. Brightness and contrast levels were adjusted to be the same between z-projections from the same staining time duration.

5.4.2 Autofluorescence

When doing optical imaging, autofluorescence can interfere with your signal, particularly green tissue autofluorescence (Shibuki et al. (2003); Coutinho et al. (2004); Reinert et al. (2004)). To investigate how much autofluorescence contributed to the total fluorescence signal, imaging was done on an acute brain slice that had not undergone staining with a fluorescence dye. Comparison of fluorescence measured in tissue with no dye to tissue stained with Di-8-ANEPPS demonstrated that tissue autofluorescence levels accounts for less than 17% of the fluorescence measured in stained tissue. Furthermore, the autofluorescence show no activity dependent changes in fluorescence (Fig. 5.6).

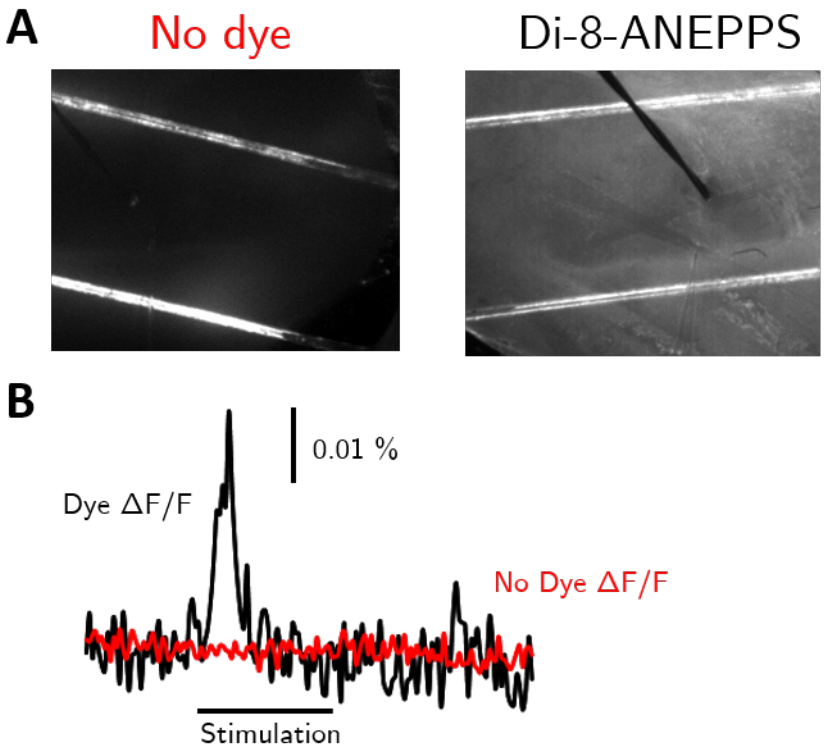

Figure 5.6: Contribution of autofluorescence to the fluorescence intensity (A) Very little autofluorescence was measured from the slice when illuminating with blue light with no dye present (Average intensity from a 50x50 pixel ROI in the LA: No dye=317.20, Di-8-ANEPPS=1917.59). (B) Time course of changes in $\Delta F/F$ after electrical stimulation illuminated with blue light shows that autofluorescence does not contribute to the stimulated signal.

5.4.3 VSD imaging

The majority of the VSD imaging experiments that were performed had no obvious VSD signal upon stimulation (Fig. 5.7). Neither a single pulse or a train of 5 pulses at 10 Hz elicited a detectable change in fluorescence intensity, nor did a longer staining time. Apart from an undetectable change in fluorescence upon stimulation, some experiments showed artefacts (see Fig. 5.7A+B+F). These were possibly caused by uneven staining, extraneous noise, or physical effects from handling the slice, which partly obscured the optical signal. Some of the slices were fixed after imaging to assess the staining by confocal microscopy, and as seen in Fig. 5.7C+E+G dye is present in the tissue, but whether the amount of staining is enough to cause a detectable change in fluorescence is not clear. Most likely a VSD signal was undetectable because of poor signal-to-noise ratio.

One experiment appeared to be successful (Fig. 5.8). Fig. 5.8A shows the polygonal segmentations of the LA. Each segment corresponds to a line in the raster plot in fig. 5.8A. The raster plot is an average of 7 trials, and shows a decrease in membrane potential following electrical stimulation. The stimulation protocol was a train of 5 pulses at 10 Hz, but it is only the first pulse in the train, that is detected as a change in $\Delta F/F$. Seeing that the amplitude of the fEPSP is decreasing in the subsequent pulses in the train (Fig. 5.8B), this is likely because the evoked responses are not large enough to be differentiated by the noise. From the detectable signal, the maximal signal-to-noise ratio was calculated to be 10.7 (Maximum signal amplitude divided by root mean square of the baseline), which is in the lower range of what has been reported by others (Momose-Sato et al. (1999); Preuss and Stein (2013)).

The lack of a detectable optical signal made it difficult to optimise the assay. I therefore decided to attempt calcium-imaging to see if a protocol could be established using a calcium-indicator, before returning to VSD imaging.

5.4.4 Calcium imaging

The calcium-indicator Fluo-4 was chosen because it shows minimal fluorescence at resting Ca^{2+} levels, and an increase in fluorescence intensity >100-fold with increasing Ca^{2+} concentration. In addition, Fluo-4 is available with an AM ester, making it cell permeant and easy to apply to acute slices.

As the age of the animal can influence the uptake of the dye (MacLean and Yuste

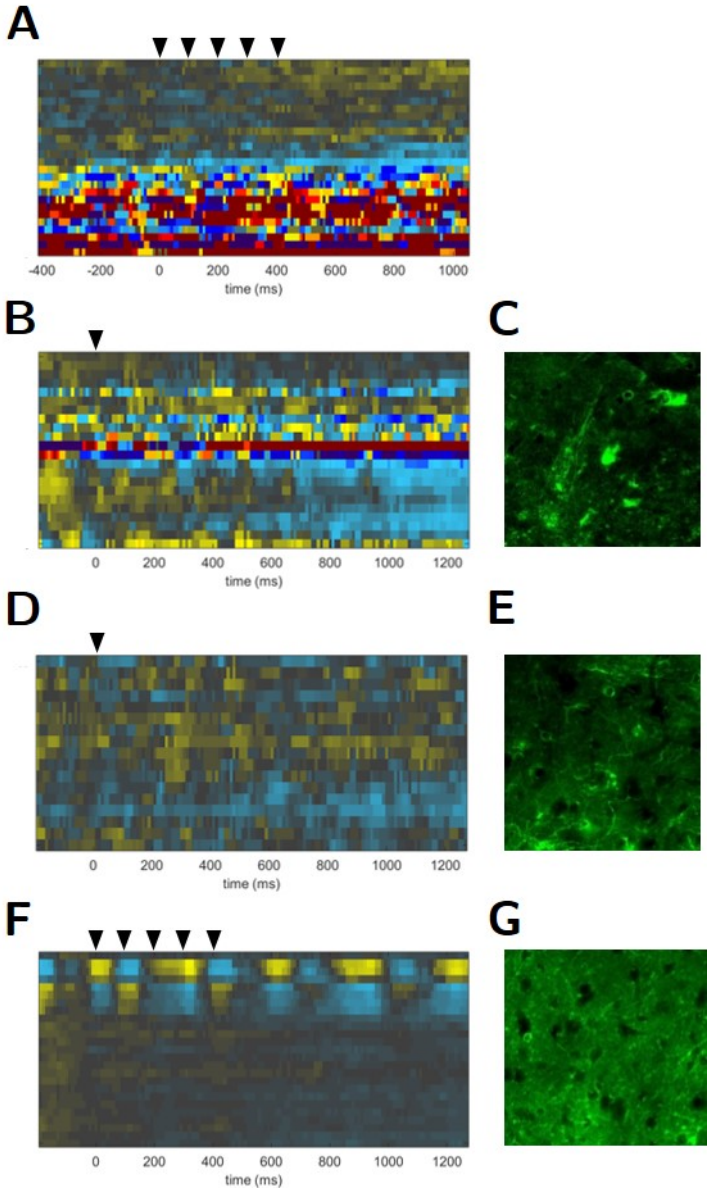

Figure 5.7: Absence of stimulation induced optical signal. (A+B+D+F) Slices were stained with Di-8-ANEPPS for 1 hr (B) or 2 hrs (A+D+F). Either a single pulse was delivered to the thalamic input to the LA (B+D) or a train of 5 pulses at 10 Hz (A+F). (C+E+G) After optical imaging slices were fixed and imaged under a confocal microscope.

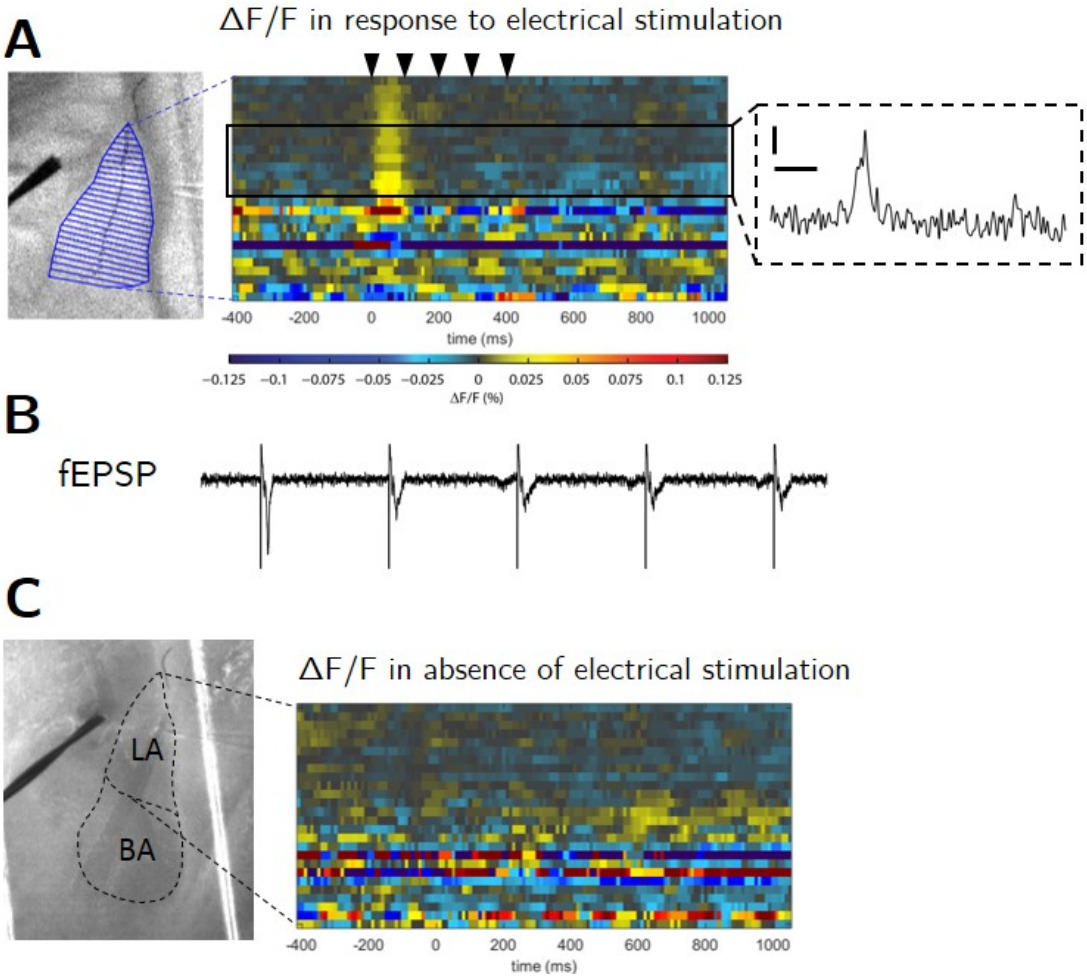

Figure 5.8: Depolarisation in the LA following stimulation of thalamic input (A) Grey scale image of the LA overlaid with polygonal segments, each corresponding to a row in the raster. The raster displays the spatiotemporal change in $\Delta F/F$ in response to a train of 5 pulses at 10Hz with the pseudocolour key below. To the right of the raster is an average time course of the area within the box. Scale bar: 0.01%; 200 ms. (B) Simultaneous recording of field EPSP recorded from the dorsal LA. Scale bar: 0.5 mV; 50 ms. (C) Grey scale fluorescence image with the anatomical boundaries drawn on top. The raster shows the spatiotemporal changes in $\Delta F/F$ in the absence of electrical stimulation.

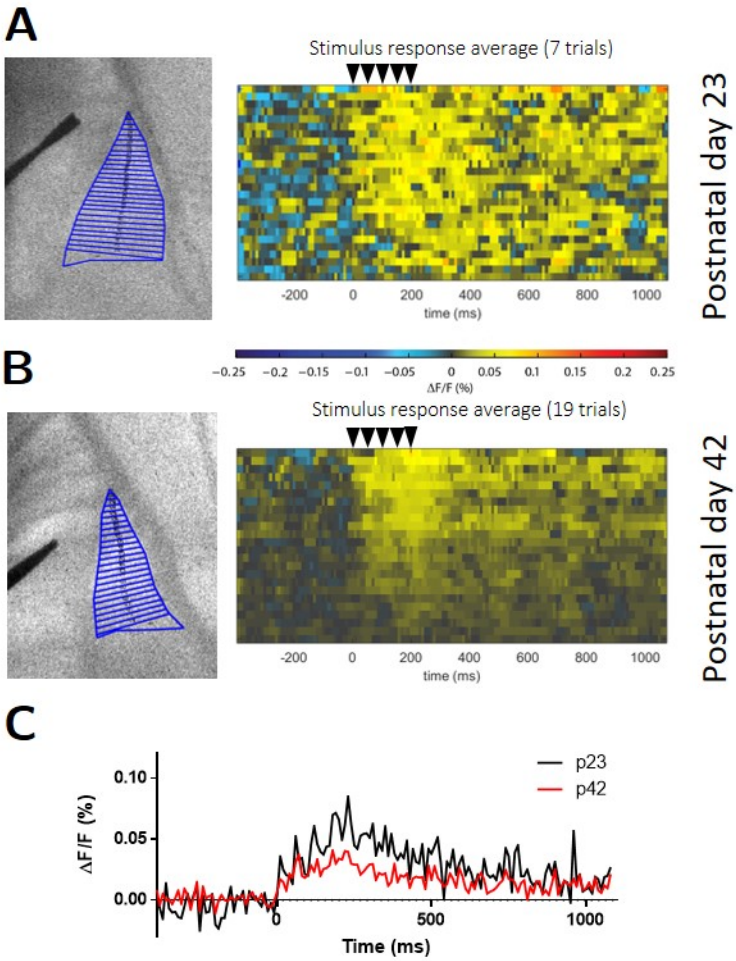

Figure 5.9: Fluorescence intensity decreases with age (A) Left: Grey scale image with polygonal segment overlay corresponding to the rows in the raster plot. The raster plots shows the spatiotemporal response to a train of 5 pulses at 20 Hz in an acute slice from a p23 rat. (B) Raster of the $\Delta F/F$ in response to a 5x20 Hz stimulation in a p42 rat. (C) Comparison of the timecourse of the $\Delta F/F$ between p23 and p42 show a larger change in fluorescence in response to stimulation in p23. The pseudocolour code is the same for both raster plots.

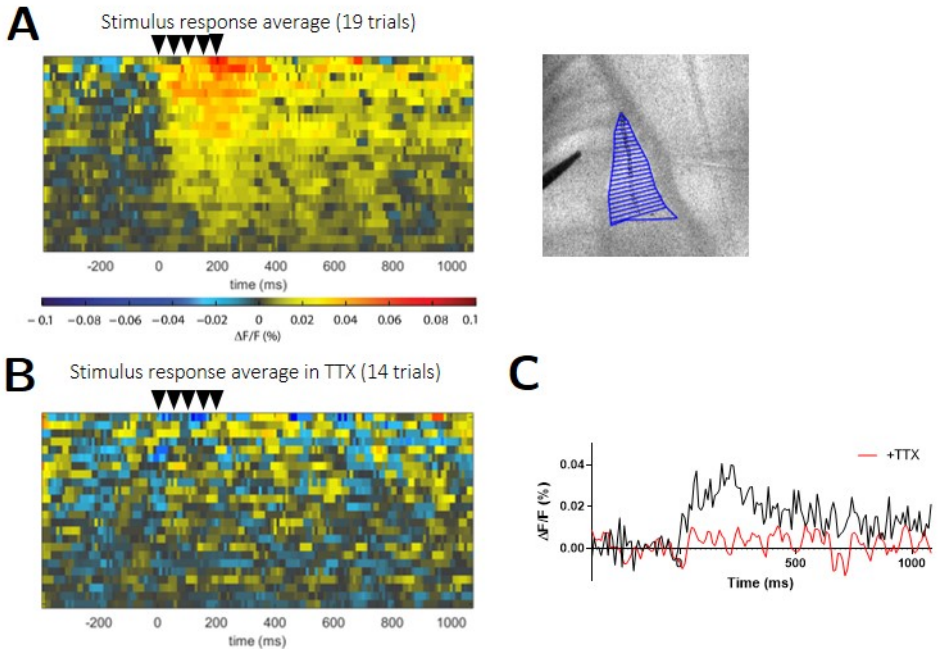

Figure 5.10: Fluorescence signal driven by action potential firing (A) The raster plots shows the spatiotemporal response to a train of 5 pulses at 20 Hz in an acute slice. Right: Grey scale image with polygonal segment overlay corresponding to the rows in the raster plot. (B) Raster of the $\Delta F/F$ in response to a 5x20 Hz stimulation in the same slice as in (A) after a 10 min wash-in of TTX (300 nM). (C) Comparison of the timecourse of the $\Delta F/F$ with and without TTX show an abolishment of the fluorescence in response to stimulation. The pseudocolour code is the same for both raster plots.

(2009); Hamad et al. (2015)), I first tested out Fluo-4 on a p23 animal. Upon stimulation a clear rise in fluorescence intensity was seen followed by a slow decay back towards baseline intensity. Next, I repeated the experiment at the intended experimental age p42. Here I observed a similar increase in fluorescence intensity following electrical stimulation, though the amplitude of the signal was lower compared to that of p23 (Fig. 5.9).

To confirm that the rise in fluorescence intensity was caused by activity-induced changes in $[Ca^{2+}]$, 300 nM TTX was washed onto the slice. This abolished the stimulus induced change in fluorescence, confirming that the signal was driven by AP firing (Fig. 5.10).

Different types of stimulation protocols were tried to gauge which protocol would work better. Fig. 5.11 shows the change in fluorescence following a single pulse and the change following a train of 5 pulses at 20 Hz. The single pulse only elicited a small change in fluorescence, whereas the train evoked a larger signal that spread further in the LA (Fig. 5.11). Since the 5x20 Hz stimulation protocol produced a relatively

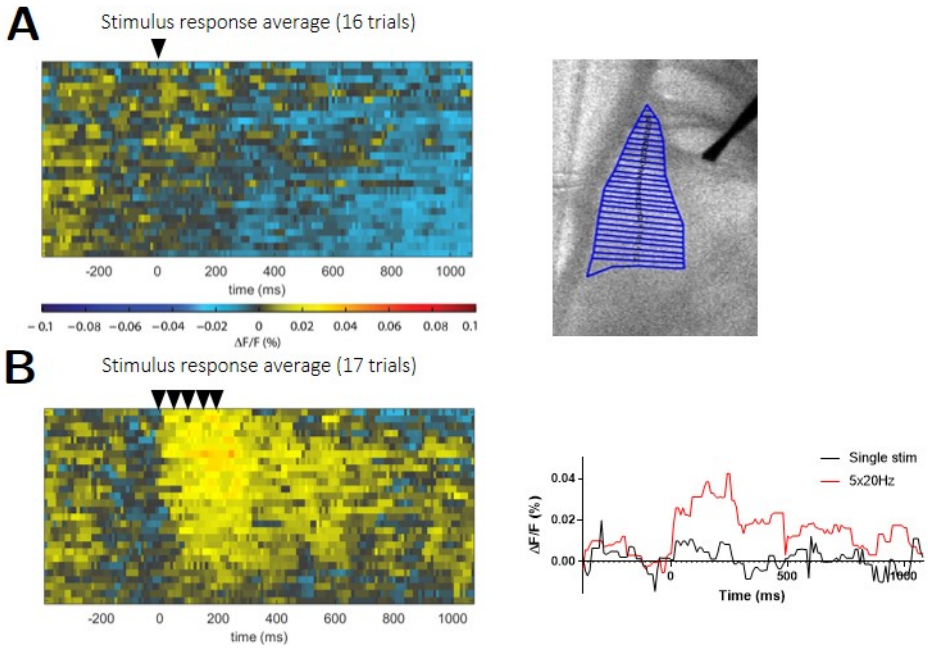

Figure 5.11: Comparison of different stimulation protocols (A) Raster plot of ΔF/F in response to a single stimulation protocol. Right: Grey scale image with polygonal segment overlay. (B) Raster plot displaying the change in ΔF/F evoked by a train of 5 pulses at 20 Hz. To the right is a time course comparison of the ΔF/F responses between the two stimulation protocols.

good optical response, this was chosen to acquire a preliminary dataset from WT and *Syngap*$^{+/-}$.

Fig. 5.12A and B show the average responses from 3 WT and *Syngap*$^{+/-}$ animals, respectively, at 5-6 weeks old. Imaging was also done in *Syngap*$^{+/\Delta GAP}$ animals, but these were mostly unsuccessful. Statistical analysis was performed using a permutation test in two steps. First, an empirical null distribution was generated for each site in the spatiotemporal domain. Then, a two-sample t-test was performed between WT and *Syngap*$^{+/-}$ at each spatiotemporal site, which is seen as a heatmap of p-values (Fig. 5.12C). Finally, the T-statistic for each site was compared to the empirical null distribution, and a map was generated showing only the sites where the null hypothesis was rejected (Fig. 5.12D). The number of sites identified as significantly different in recordings of thalamic evoked activity in LA (0.76%) is lower than the expected difference by chance (5% for α=0.05). Therefore, this preliminary dataset indicates that there is no difference in thalamic input evoked activity between WT and *Syngap*$^{+/-}$.

The preliminary dataset between WT and *Syngap*$^{+/-}$ did not reveal a difference in activity in response to stimulation of the thalamic input into the amygdala. However, given the low sample size and that this data was acquired with an non-optimised protocol,

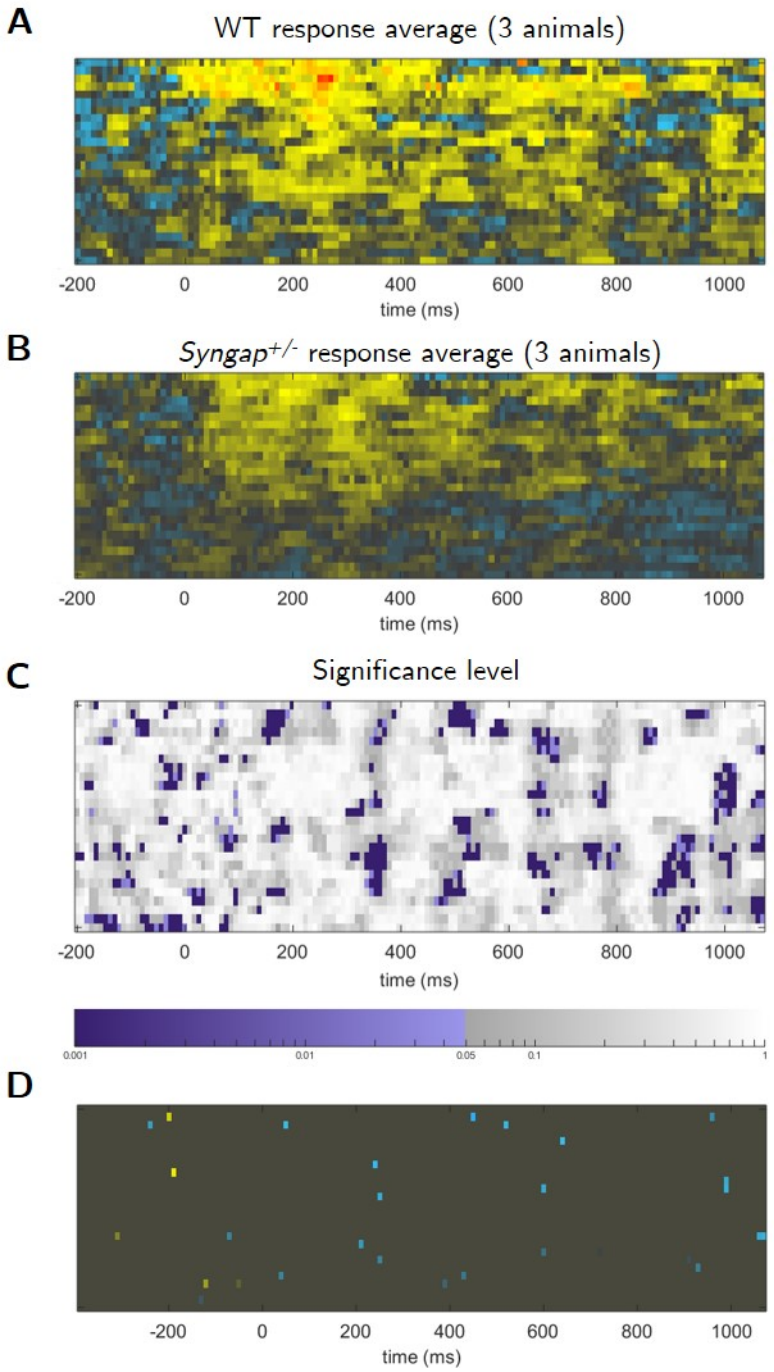

Figure 5.12: Statistical analysis of responses to thalamic stimulation to the LA (A)+(B) Rasters from multiple recordings show overall trends in activity in the WT (A) and *Syngap*$^{+/-}$ (B). Visual inspection could suggest a potential difference in activity between the two groups. (C) A two-sample t-test was done between WT and *Syngap*$^{+/-}$ at each spatiotemporal site, the result of which is shown in the heatmap. Statistically different values ($p<0.05$) are shaded purple. The T-statistics for each site is then compared to an empirical null distribution, and only the sites where the null hypothesis gets rejected is shown (D). Significant difference was measured at 29 sites out of 3819 (0.76%).

it would therefore need repeating. Moreover, the Ca-indicator dye is not discriminative between excitatory and inhibitory transmission. Hence, possible changes in inhibitory transmission could be missed, or could mask potential changes in excitatory transmission.

5.5 Future Directions

5.5.1 Improvements on the optical imaging assay

The major issue that needs improvement for this technique to work is the signal-to-noise ratio, i.e. increase the signal and decrease the noise. There are several ways to potentially increase the intensity of the fluorescence signal:

Improving the staining of the cells

Both DMSO and F127 Pluronic are essential for dye loading, but their concentration can also influence the efficacy of loading. A gradual decrease in fluorescence intensity is seen with increasing F-127 Pluronic concentrations, and increasing DMSO concentrations can affect loading efficacy and tissue penetration depth (Hamad et al. (2015)). This study was done on calcium-indicators, but it is possible that DMSO and F-127 Pluronic has the same effect on loading efficacy of voltage-sensitive dyes. Increasing the DMSO concentration slightly to 0.25–0.5%, and decreasing the F-127 Pluronic concentration to 0.0025% could possibly increase the effectiveness of dye staining, and hence the fluorescence intensity. I also noticed a tendency for foam to form on the ACSF caused by the F-127 Pluronic. Dyes are prone to concentrate on the air-water interface, and thus the foaming could decrease the actual concentration of the dye in solution. Lowering the F-127 Pluronic concentration would help address that issue as well.

As mentioned above, there is no real consensus on the optimal staining conditions for VSDs. I chose to stain the slices at RT, since this seemed to be the most prevalent temperature used, but it is possible that better staining could be obtained with either higher or lower incubation temperatures. Calcium-indicator dyes tend to be incubated at higher temperatures (MacLean and Yuste (2009); Dawitz et al. (2011); Hamad et al. (2015); Cameron et al. (2016)), suggesting that higher temperatures might be more optimal.

Another factor that influences the efficacy of staining is age. The age of the animal influences how well the tissue takes on the dye (Fig. 5.9, Peterlin et al. (2002); MacLean

and Yuste (2009); Hamad et al. (2015)). Performing the experiments at a younger age would increase the intensity of the fluorescence signal, aiding in protocol optimisation. Once optical imaging is consistently obtained, the experimental age could be increased.

Increasing signal amplitude

Given that the signal-to-noise ratio is proportional to the square root of the light intensity, increasing the intensity of light could increase the sensitivity of the recording. Increasing the light intensity will also exacerbate any vibration noise, thus finding the optimal light intensity will require some adjusting.

Some dyes show time-dependent changes in the optical signal after staining, i.e. there is an enlargement of signal obtained in the 60 min after staining (Momose-Sato et al. (1999)). This suggests that leaving more time after the staining and before imaging begins could increase the amplitude of the fluorescence signal.

Di-8-ANEPPS is a ratiometric dye. Signal-to-noise ratio could be improved by using a different excitation/emission wavelength where the signal amplitude is larger, or by implementing a dual-wavelength ratio detection scheme. The primary advantage of ratiometric measurements is that the sensitivity of the ratio is approximately equal to the additive absolute sensitivities at each wavelength, though this does require a more complicated image acquisition setup.

Trying a different dye is also an option. In solution di-8-ANEPPS and di-4-ANEPPS display similar fluorescence, but the cellular accumulation between di-4-ANEPPS and di-8-ANEPPS is significantly different. A retention assay showed that di-4-ANEPPS displayed a >5-fold higher fluorescence in the plasma membrane than di-8-ANEPPS, though di-4-ANEPPS was also strongly internalized (Mennerick et al. (2010)). Trying di-4-ANEPPS instead of di-8-ANEPPS could yield better results. Alternatively, using a genetically encoded voltage sensor would improve the signal-to-noise ratio, but this would add increased complexity and cost to the experimental design.

Finally, the signal-to-noise ratio could be improved by using a higher power objective with a better numerical aperture.

Decrease the noise

The signal-to-noise ratio can also be improved by minimising the level of noise. The current setup uses a submerged recording chamber, which is more sensitive to noise

introduced by the water flow. It also scatters the light more, decreasing the quantal yield. Changing the recording chamber to an interfase chamber will reduce the mechanical noise from the water flow, and decrease the amount of light scattering.

Chapter 6

Discussion

6.1 Concluding Remarks

An immense genetic heterogeneity is associated with ID and ASD, yet individuals with these disorders can display similar behavioural features. This raises the question whether ID/ASD are caused by a spectrum of pathologies or a single common one. The convergence on common molecular pathways can help explain why a group of genetically heterogeneous individuals, can display similar behavioural outcomes. Understanding of the neuropathology is critical for identifying potential therapeutic targets. Great effort has gone into answering this question, through genetic investigations, transcriptomic analysis, and by modelling these disorders in animals. These studies have highlighted synaptic function as a point of convergence in ID/ASD (Zoghbi and Bear (2012); Quesnel-Vallières et al. (2019)).

6.1.1 Convergence and divergence of amygdala phenotypes

One thing to consider when studying ID/ASD is the different roles specific brain regions play. Not all brain regions are strongly associated with the ID/ASD, and the most frequently associated are the cerebellum, cortex, and the amygdala (Amaral et al. (2008)). A wealth of human studies continuously implicate the amygdala as one of the major brain regions impacted in ASD (Pierce et al. (2001); Baron-Cohen (2004); Amaral et al. (2008); Kleinhans et al. (2009); Shen et al. (2016); Hrybouski et al. (2016); Weir et al. (2018); Ibrahim et al. (2019)). Whereas amygdala related behavioural deficits are commonly observed in ID/ASD models, the role ID/ASD associated genes has on synaptic function and plasticity in the amygdala is scantily investigated. In order

to bridge the gap between the findings of amygdala dysfunction in humans, and the observed amygdala-dependent behavioural abnormalities in rodent models, we need to get a better understanding of the molecular, cellular, and circuit dysfunction of this key brain area.

When examining what is known about the amygdala pathophysiology in ID/ASD models a complex picture emerges. Starting with the data presented in this thesis, convergence and divergence of cellular phenotypes were found between $Nlgn3^{-/y}$ and the two *Syngap* models (Table 6.1). Intrinsic excitability of LA neurons was enhanced in both $Nlgn3^{-/y}$ and $Syngap^{+/-}$, but not in $Syngap^{+/\Delta GAP}$. Basal synaptic transmission was similar to controls in all three, whereas basal inhibitory synaptic transmission was increased in $Nlgn3^{-/y}$.

Most notably, all three models shared a deficit in thalamo-amygdala LTP. Interestingly, the rat model of FXS, $Fmr1^{-/y}$, shows a similar deficit in thalamo-amygdala LTP in the LA (Dr. Adam Jackson, University of Edinburgh, unpublished data) — a deficit also observed in the $Fmr1^{-/y}$ mouse model (Suvrathan et al. (2010)). Moreover, the reduction of NLGN1 also results in impaired thalamo-amygdala LTP (Kim et al. (2008); Jung et al. (2010)), making this a highly convergent amygdala phenotype in ASD models, supporting the idea of pathological pathway convergence. However, some ID/ASD models report no impairments in thalamo-amygdala LTP (Houbaert et al. (2013); Jayachandran et al. (2014)), but display deficits in cortico-amygdala LTP instead (Jayachandran et al. (2014)). This indicates that synaptic plasticity at major sensory input associated with the formation of fear memories is impaired and could be a convergent pathway for amygdala pathology in ID/ASD.

Synaptic plasticity at these synapses is important for fear memory consolidation. However, while the cellular phenotypes for fear conditioning appear to show convergence in a subset of ID/ASD models, the behavioural phenotypes seem more complicated. All three rats models investigated in our lab display distinct fear responses during fear recall: $Nlgn3^{-/y}$ exhibit normal acquisition of fear during conditioning, but need both cue and contextual input to recall the fear association. Furthermore, $Nlgn3^{-/y}$ express their fear behaviour through flight, rather than freezing (Natasha Anstey, University of Edinburgh); $Syngap^{+/-}$ show normal acquisition of fear memory but increased freezing during recall and slower acquisition of extinction. Additionally, these animals show little

discrimination between CS and no CS; while *Fmr1*$^{-/y}$ display normal acquisition but impaired fear recall (Dr. Sally Till, University of Edinburgh, unpublished).

The complexity of behavioural outcomes in these rat models highlight the need for better phenotyping and reporting of these. Most papers studying fear conditioning report either a decrease or increase in freezing without dissecting the finer behavioural expression patterns of the animals, thereby missing a lot of valuable information about the cellular and circuit dysfunction underlying it.

Table 6.1 shows a comparison of a range of ID/ASD models, where amygdala dysfunction has been examined. This shows that while some deficits are shared amongst models of ASD, such as impaired synaptic plasticity, other phenotypes manifest in different ways. The heterogeneity of behavioural outcomes challenges the idea of cellular convergence leading to similar behavioural outcomes in ASD. More importantly, it highlights the necessity of integrative physiology and looking at these disorders from a range of perspectives to be able to connect all the dots — especially in order to find possible convergence between models.

One neglected area of study is local network and circuit activity, particularly for the amygdala. ID/ASD are generally considered as circuit syndromes (Belger et al. (2011); Fernández et al. (2018)), and abnormal circuit function is commonly observed in models of these disorders. Increased hyperexcitability is observed in hippocampal and cortical circuit in *Syngap*$^{+/-}$ mice (Clement et al. (2012); Ozkan et al. (2014)), and studies from *Fmr1*$^{-/y}$ mice display increased neuronal hyperactivity and network synchrony in cortical areas (Hays et al. (2011); Gonçalves et al. (2013)). Similarly, cortical hyperactivity was reported in *Shank3*$^{-/-}$ mice (Peixoto et al. (2016)), whereas *Pcdh*10$^{+/-}$ mice exhibit a reduction in gamma band activity in the BLA (Schoch et al. (2017)).

The local amygdala network excitability has not been examined in any of the models from Table 6.1. An important next step will be to determine how the changes in cellular excitability and synaptic plasticity translate to network excitability in these models of ID/ASD, and how this correlates with the amygdala-dependent behaviours.

Table 6.1: *Amygdala phenotypes in ID/ASD*

Model	FC	Cued Fear Recall	TA-LTP	CO-LTP	mEPSC	mIPSC	Intrinsic excitability	Reference
Nlgn3$^{-/y}$ rat	↔	↓/↔	↓	–	↔	↑	↑	[1] [2]
Syngap$^{+/-}$ rat	↔	↑	↓	–	↔	↔	↑	[1] [3]
Fmr1$^{-/y}$ rat	↔	↓	↓	↓	Freq ↓	↔	↔	[3] [4]
Fmr1$^{-/y}$ mouse	–	↔/↓	↓	–	↓	Amp+Freq↓	↑	[5] [6] [7]
Nlgn1 KO mouse	↔	↓	↓	↔	↔	–	–	[8] [9]
NL3-R451C mouse	–	–	–	–	Amp ↑	Amp ↓	–	[10]
Coronin 1 KO mouse	–	↓	↔	↓	–	–	–	[11]
il1rapl1 KO mouse	↓	↓	↔	–	↔	–	↓	[12]
Mecp2$^{-/y}$ mouse	–	↓	–	↔	↔	–	–	[13] [14]
Tsc2$^{+/-}$ mouse	↔	↔	–	–	–	–	–	[15]

–: unknown; ↑: increased compared to control; ↓: decreased compared to control; ↔: comparable to control

[1]: This thesis; [2]: Ms Natasha Anstey, University of Edinburgh; [3]: Dr. Sally Till, University of Edinburgh; [4]: Dr. Adam Jackson, University of Edinburgh;
[5]: Suvrathan et al. (2010); [6]: Spencer et al. (2006); [7]: Olmos-Serrano et al. (2010); [8]: Kim et al. (2008); [9]:Jung et al. (2010);[10]:Hosie et al. (2018)
[11]: Jayachandran et al. (2014); [12]: Houbaert et al. (2013); [13]: Stearns et al. (2007); [14]: Gambino et al. (2010); [15]: Waltereit et al. (2011)

6.2 Future directions

The work in this thesis has shown the existence of cellular deficits in the amygdala in a basic physiological state. However, how these deficits affect the cellular and circuit responses to changes in emotional states in $Nlgn3^{-/y}$ and $Syngap^{+/-}$ is unknown. Understanding how the neurons and the circuit will respond to emotional changes is particularly important to gain a complete understanding of the pathology of ID/ASD, since ASD patients in particular have difficulty with social intelligence.

Fear conditioning and extinction has been shown to modify the intrinsic excitability of neurons in the prefrontal cortex, hippocampus, and amygdala (Santini et al. (2008); McKay et al. (2009); Sehgal et al. (2014)). Given the changes in excitability and alterations in fear response behaviour in $Nlgn3^{-/y}$ and $Syngap^{+/-}$, you would therefore expect to see different modifications to intrinsic excitability in these models compared to controls. To determine whether the intrinsic excitability is enhanced differently in LA neurons in $Nlgn3^{-/y}$ and $Syngap^{+/-}$ by fear conditioning and extinction, whole-cell patch-clamp recordings of the intrinsic excitability would be done from naive, conditioned, and conditioned-extinguished rats. This would help dissect how the different forms of associative learning during fear conditioning modulate the intrinsic plasticity. The behavioural data would indicate that the differences between genotypes for both models would be found during extinction rather than during initial fear conditioning. Moreover, once the optical imaging protocol is fully optimised, examining the inter-amygdala circuit function in basal emotional states and in response to fear conditioning and extinction would follow.

The work presented in this thesis has had an amygdala-centric viewpoint. The amygdala is a key brain structure in emotional processing, but it is also part of a bigger team and the interplay between players in this circuit is as crucial as the individual players themselves. Several studies of ASD patients have revealed hypo-connectivity between the amygdala and cortical areas, particularly the prefrontal cortex (Shen et al. (2016); Gibbard et al. (2018); Ibrahim et al. (2019); Iidaka et al. (2019)). The mPFC is reciprocally connected with the BLA, in particular to the prelimbic (PL) and infralimbic (IL) area (Sah et al. (2003)). Whereas the PL area supports fear expression and receives projection from BA 'fear' neurons, the IL is involved in extinction and receives projections specifically from 'extinction' neurons (Duvarci and Pare (2014)).

Furthermore, inactivation of the IL hinders the acquisition of extinction (Sierra-Mercado et al. (2011)). The possibility therefore exists that hypo-connectivity between the BLA and the IL is contributing to the impaired acquisition of extinction seen in $Syngap^{+/-}$. This could be investigated in several ways: one could be to inject retrobeads into the BLA–IL and record the intrinsic and synaptic properties from IL projection neurons in the BLA, and vice versa; another approach is to optogenetically stimulate IL projections in the BLA coupled with VSD imaging to record the inter-amygdala circuit response.

In conclusion, my findings encourage further experiments, especially with the aim to elucidate amygdala circuit function in models of ID and ASD. Furthermore, understanding the neuronal activity and circuitry in response to changes in emotional states is important for our understanding of these disorders. From this we will gain a more comprehensive understanding of how genetic changes lead to abnormal behavioural outcomes, and with that, hopefully, the insight needed to develop target pharmacological treatment options for these debilitating disorders.

Appendix A

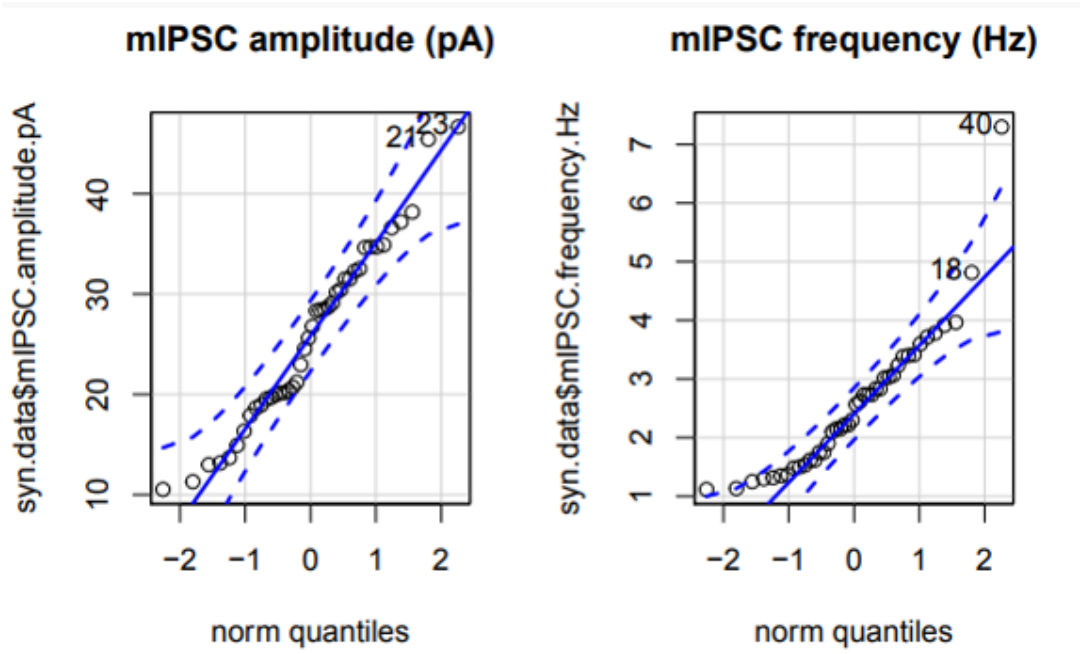

Figure S1: QQ plot show normal distribution. To perform a GLMM, the data needs to follow a normal distribution. A quantile-quantile (QQ) plot shows that both mIPSC amplitude and frequency follow a normal distribution, meaning a GLMM can be used. Data analysis performed by Zrinko Kozic, University of Edinburgh.

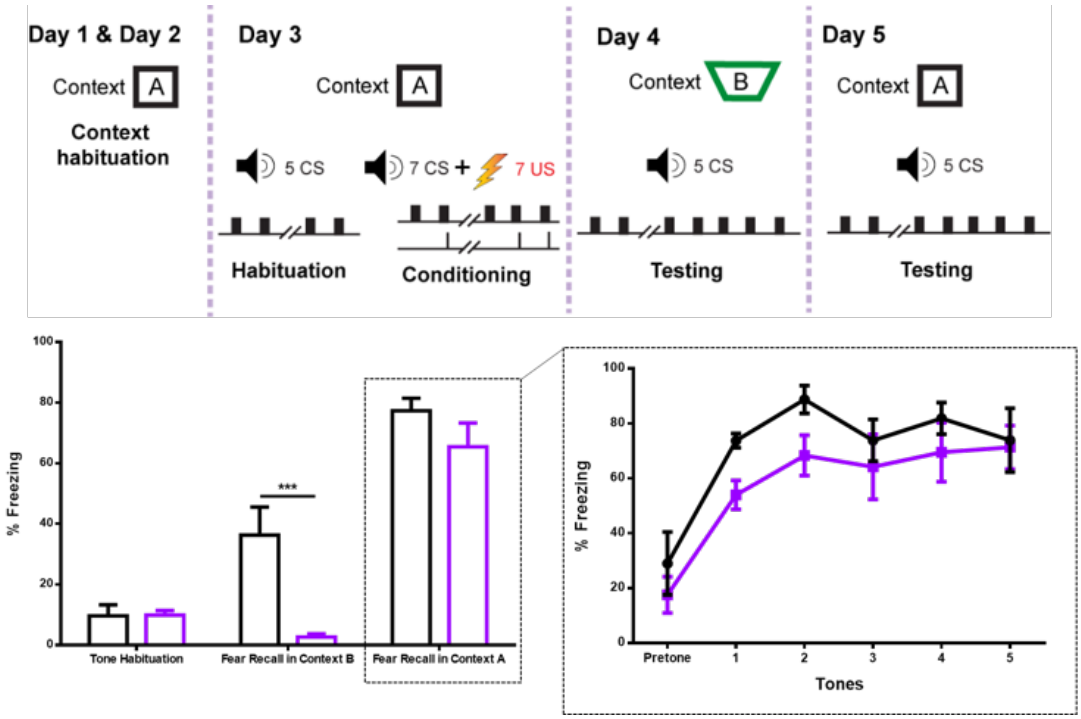

Figure S2: *Nlgn3*$^{-/y}$ rats exhibit freezing behaviour when presented with both tone and context. On day 1 and 2 rats were habituated to context A. This context was where tone habituation and conditioning was performed on day 3. On day 4 the rats were tested for cued fear recall in a different context B, and on day 5 fear recall was tested in the context of conditioning. *Nlgn3*$^{-/y}$ rats show an impairment in freezing when presented to cue alone during recall, but when presented with both cue and context *Nlgn3*$^{-/y}$ rats exhibit comparable freezing behaviour to WT controls. Figures supplied by Natasha Anstey, University of Edinburgh

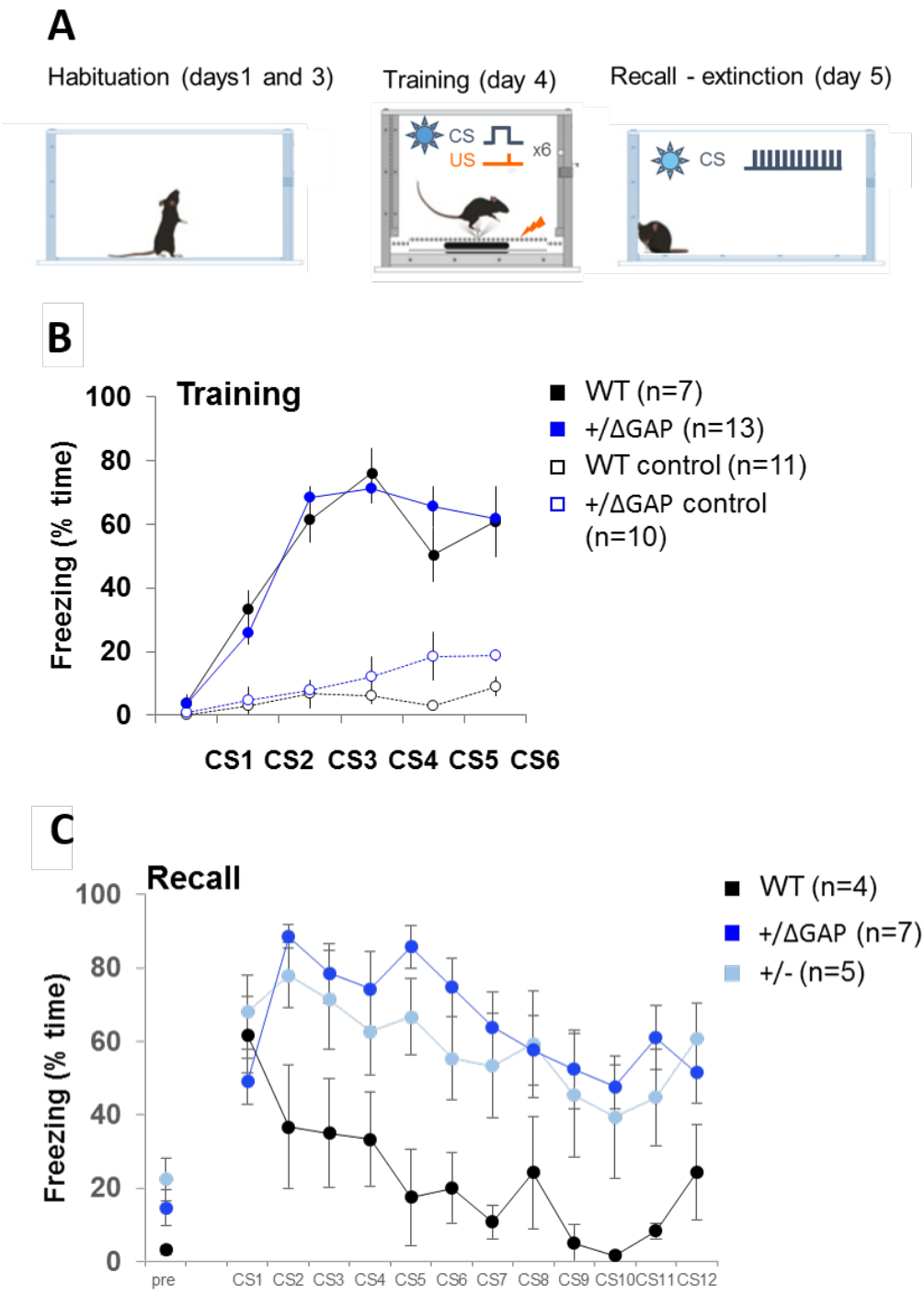

Figure S3: Enhanced fear recall in rat models of *SYNGAP* haploinsufficiency. (A) The visual cued conditioning paradigm consisted of initial habituation, followed by fear conditioning training in a different context to the habituation. The conditioning consisted of 6 CS–US pairings. On day 5 fear recall was tested in the original context with 12 CSs. (B) *Syngap*$^{+/\Delta GAP}$ exhibit normal fear acquisition during fear conditioning training. (C) *Syngap*$^{+/-}$ and *Syngap*$^{+/\Delta GAP}$ show enhanced freezing during before CS presentation during recall testing, and enhanced freezing during CS presentations. Furthermore, *Syngap*$^{+/-}$ and *Syngap*$^{+/\Delta GAP}$ are unable to distinguish between CS and no CS, i.e. rats continue to freeze between CS presentations (data not shown). Figures supplied by Dr. Sally Till, University of Edinburgh

Bibliography

Abel HJ, Lee J, Callaway JC, Foehring RC (2004) Relationships Between Intracellular Calcium and Afterhyperpolarizations in Neocortical Pyramidal Neurons. *Journal of Neurophysiology* 91:324–335.

Adolphs R (2010) What does the amygdala contribute to social cognition? *Annals of the New York Academy of Sciences* 1191:42–61.

Alger B, Nicoll RA (1980) Epileptiform Burst Afterhyperpolarization: Calcium-Dependent Potassium Potential in Hippocampal CA1 Pyramidal Cells. *Science* 210:1122–1124.

Amano T, Duvarci S, Popa D, Pare D (2011) The Fear Circuit Revisited: Contributions of the Basal Amygdala Nuclei to Conditioned Fear. *Journal of Neuroscience* 31:15481–15489.

Amaral DG, Schumann CM, Nordahl CW (2008) Neuroanatomy of autism. *Trends in Neurosciences* 31:137–145.

American Psychiatric Association (2013) *Diagnostic and statistical manual of mental disorders* Americann Psychiatric association, 5th edition.

Antic SD, Empson RM, Knöpfel T (2016) Voltage imaging to understand connections and functions of neuronal circuits. *Journal of Neurophysiology* 116:135–152.

Antonelli R, Pizzarelli R, Pedroni A, Fritschy Jm, Sal GD, Cherubini E, Zacchi P (2014) Pin1-dependent signalling negatively affects GABAergic transmission by modulating neuroligin2/gephyrin interaction. *Nature Communications* 5:1–14.

Araç D, Boucard AA, Özkan E, Strop P, Newell E, Südhof TC, Brunger AT (2007) Structures of Neuroligin-1 and the Neuroligin-1/Neurexin-1β Complex Reveal Specific Protein-Protein and Protein-Ca2+ Interactions. *Neuron* 56:992–1003.

Araki Y, Zeng M, Zhang M, Huganir R (2015) Rapid Dispersion of SynGAP from Synaptic Spines Triggers AMPA Receptor Insertion and Spine Enlargement during LTP. *Neuron* 85:173–189.

Avrabos C, Sotnikov SV, Dine J, Markt PO, Holsboer F, Landgraf R, Eder M (2013) Real-Time Imaging of Amygdalar Network Dynamics In Vitro Reveals a Neurophysiological Link to Behavior in a Mouse Model of Extremes in Trait Anxiety. *Journal of Neuroscience* 33:16262–16267.

Babaev O, Botta P, Meyer E, Müller C, Ehrenreich H, Brose N, Lüthi A, Krueger-burg D (2016) Neuroligin 2 deletion alters inhibitory synapse function and anxiety-associated neuronal activation in the amygdala. *Neuropharmacology* 100:56–65.

Baker B, Gao X, Wolff BS, Jin L, Cohen LB, Bleau CX, Wu JY (2015) Voltage-sensitive dye imaging of population signals in brain slices. *Cold Spring Harbor Protocols* 2015:995–999.

Baker BJ, Kosmidis EK, Vucinic D, Falk CX, Cohen LB, Djurisic M, Zecevic D (2005) Imaging brain activity with voltage- and calcium-sensitive dyes. *Cellular and Molecular Neurobiology* 25:245–282.

Baldwin KT, Eroglu C (2017) Molecular mechanisms of astrocyte-induced synaptogenesis. *Current Opinion in Neurobiology* 45:113–120.

Barnes SA, Wijetunge LS, Jackson AD, Katsanevaki D, Osterweil EK, Komiyama NH, Grant SGN, Bear MF, Nagerl UV, Kind PC, Wyllie DJA (2015) Convergence of Hippocampal Pathophysiology in Syngap+/- and Fmr1-/y Mice. *Journal of Neuroscience* 35:15073–15081.

Barnett MW, Watson RF, Vitalis T, Porter K, Komiyama NH, Stoney PN, Gillingwater TH, Grant SGN, Kind PC (2006) Synaptic Ras GTPase activating protein regulates pattern formation in the trigeminal system of mice. *The Journal of neuroscience : the official journal of the Society for Neuroscience* 26:1355–1365.

Baron-Cohen S (2004) The cognitive neuroscience of autism. *Journal of Neurology, Neurosurgery and Psychiatry* 75:945–948.

Baron-Cohen S, Ring Ha, Bullmore ET, Wheelwright S, Ashwin C, Williams SCR (2000) The amygdala theory of autism. *Neuroscience and Biobehavioral Reviews* 24:355–364.

Baudouin S, Gaudias J, Gerharz S, Hatstatt L, Zhou K, Punnakkal P, Tanaka KF, Spooren W, Hen R, De Zeeuw CI, Vogt KE, Scheiffele P (2012) Shared Synaptic Pathophysiology in Syndromic and Nonsyndromic Rodent Models of Autism. *Science* 338:128–132.

Bauer EP, Schafe GE, LeDoux JE (2002) NMDA receptors and L-type voltage-gated calcium channels contribute to long-term potentiation and different components of fear memory formation in the lateral amygdala. *The Journal of neuroscience* 22:5239–5249.

Bedlack RS, Wei Md, Loew LM (1992) Localized membrane depolarizations and localized calcium influx during electric field-guided neurite growth. *Neuron* 9:393–403.

Beggs JM, Plenz D (2003) Neuronal Avalanches in Neocortical Circuits. *The Journal of neuroscience* 23:11167–11177.

Belger A, Carpenter KL, Yucel GH, Cleary KM, Donkers FC (2011) The neural circuitry of autism. *Neurotoxicity Research* 20:201–214.

Bemben MA, Nguyen QA, Wang T, Li Y, Nicoll RA, Roche KW (2015a) Autism-associated mutation inhibits protein kinase C-mediated neuroligin-4X enhancement of excitatory synapses. *Proceedings of the National Academy of Sciences* 112:2551–2556.

Bemben MA, Shipman SL, Nicoll RA, Roche KW (2015b) The cellular and molecular landscape of neuroligins. *Trends in Neurosciences* 38:496–505.

Berryer MH, Chattopadhyaya B, Xing P, Riebe I, Bosoi C, Sanon N, Antoine-Bertrand J, Lévesque M, Avoli M, Hamdan FF, Carmant L, Lamarche-Vane N, Lacaille JC,

Michaud JL, Di Cristo G (2016) Decrease of SYNGAP1 in GABAergic cells impairs inhibitory synapse connectivity, synaptic inhibition and cognitive function. *Nature Communications* 7:13340.

Berryer MH, Hamdan FF, Klitten LL, Møller RS, Carmant L, Schwartzentruber J, Patry L, Dobrzeniecka S, Rochefort D, Neugnot-Cerioli M, Lacaille JC, Niu Z, Eng CM, Yang Y, Palardy S, Belhumeur C, Rouleau Ga, Tommerup N, Immken L, Beauchamp MH, Patel GS, Majewski J, Tarnopolsky Ma, Scheffzek K, Hjalgrim H, Michaud JL, Di Cristo G (2013) Mutations in SYNGAP1 Cause Intellectual Disability, Autism, and a Specific Form of Epilepsy by Inducing Haploinsufficiency. *Human Mutation* 34:385–394.

Blackman AV, Abrahamsson T, Costa RP, Lalanne T, Sjöström PJ (2013) Target-cell-specific short-term plasticity in local circuits. *Frontiers in Synaptic Neuroscience* 5:1–13.

Blundell J, Blaiss CA, Etherton MR, Espinosa F, Tabuchi K, Walz C, Bolliger MF, Südhof TC, Powell CM (2010) Neuroligin-1 Deletion Results in Impaired Spatial Memory and Increased Repetitive Behavior. *Journal of Neuroscience* 30:2115–2129.

Boatman JA, Kim JJ (2006) A thalamo-cortico-amygdala pathway mediates auditory fear conditioning in the intact brain. *European Journal of Neuroscience* 24:894–900.

Bolliger MF, Pei J, Maxeiner S, Boucard AA, Grishin NV, Sudhof TC (2008) Unusually rapid evolution of Neuroligin-4 in mice. *Proceedings of the National Academy of Sciences* 105:6421–6426.

Bolliger MF, Frei K, Winterhalter KH, GloorLOOR SM (2001) Identification of a novel neuroligin in humans which binds to PSD-95 and has a widespread expression. *Biochemical Journal* 356:581–588.

Boucard AA, Chubykin AA, Comoletti D, Taylor P, Südhof TC (2005) A splice code for trans-synaptic cell adhesion mediated by binding of neuroligin 1 to α- and β-neurexins. *Neuron* 48:229–236.

Bourgeois EB, Johnson BN, McCoy AJ, Trippa L, Cohen AS, Marsh ED (2014) A toolbox for spatiotemporal analysis of voltage-sensitive dye imaging data in brain slices. *PLoS ONE* 9.

Bourgeron T (2015) From the genetic architecture to synaptic plasticity in autism spectrum disorder. *Nature Reviews Neuroscience* 16:551–563.

Bowden JB, Abraham WC, Harris KM (2012) Differential effects of strain, circadian cycle, and stimulation pattern on LTP and concurrent LTD in the dentate gyrus of freely moving rats. *Hippocampus* 22:1363–1370.

Brambilla R, Gnesutta N, Minichiello L, White G, Roylance AJ, Herron CE, Ramsey M, Wolfer DP, Cestari V, Rossi-Arnaud C, Grant SGN, Chapman PF, Lipp HP, Sturani E, Klein R (1997) A role for the Ras signalling pathway in synaptic transmission and long- term memory. *Nature* 390:284–286.

Brekke TD, Steele KA, Mulley JF (2018) Inbred or Outbred? Genetic Diversity in Laboratory Rodent Colonies. *G3 Genes Genomes Genetics* 8:679–686.

Brunet-Maheu JM, Fernandes JC, De Lacerda CAV, Shi Q, Benderdour M, Lavigne P (2008) Pluronic F-127 as a Cell Carrier for Bone Tissue Engineering. *Journal of Biomaterials Applications* 24:275–287.

Budreck EC, Kwon Ob, Jung JH, Baudouin S, Thommen A, Kim Hs, Fukazawa Y, Harada H, Tabuchi K, Shigemoto R, Scheiffele P, Kim JH (2013) Neuroligin-1 controls synaptic abundance of NMDA-type glutamate receptors through extracellular coupling. *Pnas* 110:725–730.

Budreck EC, Scheiffele P (2007) Neuroligin-3 is a neuronal adhesion protein at GABAergic and glutamatergic synapses. *European Journal of Neuroscience* 26:1738–1748.

Burden SJ, Scheiffele P (2013) Chapter 17 - Synapse Formation In *Fundamental Neuroscience*, pp. 385–403. Elsevier Inc., fourth edi edition.

Cai H, Haubensak W, Anthony TE, Anderson DJ (2014) Central amygdala PKC-δ+ neurons mediate the influence of multiple anorexigenic signals. *Nature Neuroscience* 17:1240–1248.

Cameron M, Kekesi O, Morley JW, Tapson J, Breen PP, Van Schaik A, Buskila Y (2016) Calcium imaging of am dyes following prolonged incubation in acute neuronal tissue. *PLoS ONE* 11:1–13.

Campeau S, Davis M (1995) Involvement of subcortical and cortical afferents to the lateral nucleus of the amygdala in fear conditioning measured with fear-potentiated startle in rats trained concurrently with auditory and visual conditioned stimuli. *The Journal of neuroscience : the official journal of the Society for Neuroscience* 15:2312–27.

Canepari M, Zecevic D (2010) *Membrane Potential Imaging in the Nervous System* Number 2. Springer US.

Cao G, Harris KM (2014) Augmenting saturated LTP by broadly spaced episodes of theta-burst stimulation in hippocampal area CA1 of adult rats and mice. *Journal of Neurophysiology* 112:1916–1924.

Carlier Mf, Laurent V, Santolini J, Melki R, Didry D, Xia Gx, Hong Y, Chua Nh, Pantaloni D (1997) Actin Depolymerizing Factor (ADF/Cofilin) Enhances the Rate of Filament Turnover: Implication in Actin-based Motility. *The Journal of Cell Biology* 136:1307–1322.

Carlisle HJ, Manzerra P, Marcora E, Kennedy MB (2008) SynGAP regulates steady-state and activity-dependent phosphorylation of cofilin. *The Journal of neuroscience : the official journal of the Society for Neuroscience* 28:13673–13683.

Carlson GC, Coulter DA (2008) In vitro functional imaging in brain slices using fast voltage-sensitive dye imaging combined with whole-cell patch recording. *Nature protocols* 3:249–55.

Carrasquillo Y, Burkhalter A, Nerbonne JM (2012) A-type K+ channels encoded by Kv4.2, Kv4.3 and Kv1.4 differentially regulate intrinsic excitability of cortical pyramidal neurons. *Journal of Physiology* 590:3877–3890.

Carvill GL, Heavin SB, Yendle SC, Mcmahon JM, Roak BJO, Cook J, Khan A, Dorschner MO, Weaver M, Calvert S, Malone S, Wallace G, Stanley T, Bye AME,

Bleasel A, Howell KB, Kivity S, Mackay MT, Lerman-sagie T, Lev D, Møller RS, Gill D, Andrade DM, Freeman JL, Sadleir LG, Shendure J, Berkovic SF, Scheffer IE, Mefford HC (2013) Targeted resequencing in epileptic encephalopathies identifies de novo mutations in CHD2 and SYNGAP1. *Nature genetics* 45:825–830.

Casillas-Espinosa PM, Hicks A, Jeffreys A, Snutch TP, O'Brien TJ, Powell KL, Spafford JD (2015) Z944, a novel selective t-type calcium channel antagonist delays the progression of seizures in the amygdala kindling model. *PLoS ONE* 10:1–12.

Cavaletti G, Oggioni N, Sala F, Pezzoni G, Cavalletti E, Marmiroli P, Petruccioli MG, Frattola L, Tredici G (2000) Effect on the peripheral nervous system of systemically administered dimethylsulfoxide in the rat: A neurophysiological and pathological study. *Toxicology Letters* 118:103–107.

CDC (2018) Prevalence of Autism Spectrum Disorder Among Children Aged 8 Years — Autism and Developmental Disabilities Monitoring Network , 11 Sites , United States , 2014. *Morbidity and Mortality Weekly Report* 67.

Chadman KK, Gong S, Scattoni ML, Boltuck SE, Gandhy SU, Heintz N, Crawley JN (2008) Minimal aberrant behavioral phenotypes of neuroligin-3 R451C knockin mice. *Autism Research* 1:147–158.

Chanda S, Aoto J, Lee SJ, Wernig M, Südhof TC (2016) Pathogenic mechanism of an autism-associated neuroligin mutation involves altered AMPA-receptor trafficking. *Molecular Psychiatry* 21:169–177.

Chanda S, Hale WD, Zhang B, Wernig M, Südhof TC (2017) Unique versus Redundant Functions of Neuroligin Genes in Shaping Excitatory and Inhibitory Synapse Properties. *The Journal of Neuroscience* 37:6816–6836.

Chanda S, Marro S, Wernig M, Südhof TC (2013) Neurons generated by direct conversion of fibroblasts reproduce synaptic phenotype caused by autism-associated neuroligin-3 mutation. *Proceedings of the National Academy of Sciences of the United States of America* 110:16622–7.

Chechlacz M, Gleeson JG (2003) Is Mental Retardation a Defect of Synapse Structure and Function ? *Pediatric Neurology* 29:11–17.

Chen A, Hu WW, Jiang XL, Potegal M, Li H (2017) Molecular mechanisms of group I metabotropic glutamate receptor mediated LTP and LTD in basolateral amygdala in vitro. *Psychopharmacology* 234:681–694.

Chen CC, Shen JW, Chung NC, Min MY, Cheng SJ, Liu IY (2012) Retrieval of Context-Associated Memory is Dependent on the Cav3.2 T-Type Calcium Channel. *PLOS ONE* 7:e29384.

Chen HJ, Rojas-Soto M, Oguni A, Kennedy MB (1998) A synaptic Ras-GTPase activating protein (p135 SynGAP) inhibited by CaM kinase II. *Neuron* 20:895–904.

Chen LY, Jiang M, Zhang B, Gokce O, Südhof TC (2017) Conditional Deletion of All Neurexins Defines Diversity of Essential Synaptic Organizer Functions for Neurexins. *Neuron* 94:611–625.e4.

Cherry KE, Matson JL, Paclawskyj TR (1997) Psychopathology in older adults with severe and profound mental retardation. *American Journal on Mental Retardation* 101:445–458.

Chih B, Engelman H, Scheiffele P (2005) Control of Excitatory and Inhibitory Synapse Formation by Neuroligins. *Science* 307:1324–1328.

Chih B, Afridi SK, Clark L, Scheiffele P (2004) Disorder-associated mutations lead to functional inactivation of neuroligins. *Human Molecular Genetics* 13:1471–1477.

Chih B, Gollan L, Scheiffele P (2006) Alternative Splicing Controls Selective Trans-Synaptic Interactions of the Neuroligin-Neurexin Complex. *Neuron* 51:171–178.

Cho JH, Bayazitov IT, Meloni EG, Myers KM, Carlezon WA, Zakharenko SS, Bolshakov VY (2012) Coactivation of thalamic and cortical pathways induces input timing-dependent plasticity in amygdala. *Nature Neuroscience* 15:113–122.

Chubykin AA, Atasoy D, Etherton MR, Brose N, Kavalali ET, Gibson JR, Südhof TC (2007) Activity-Dependent Validation of Excitatory versus Inhibitory Synapses by Neuroligin-1 versus Neuroligin-2. *Neuron* 54:919–931.

Ciocchi S, Herry C, Grenier F, Wolff SB, Letzkus JJ, Vlachos I, Ehrlich I, Sprengel R, Deisseroth K, Stadler MB, Müller C, Lüthi A (2010) Encoding of conditioned fear in central amygdala inhibitory circuits. *Nature* 468:277–282.

Clayton AJ, Begbie J, Regan MC, Savas JN, Vennekens KM, Cvetkovska V, de Wit J, Aricescu AR, Elegheert J, Craig AM, Furukawa H, Heroven C, Jia W, Smukowski SN, Smith AC (2017) Structural Mechanism for Modulation of Synaptic Neuroligin-Neurexin Signaling by MDGA Proteins. *Neuron* 95:896–913.e10.

Clement JP, Ozkan ED, Aceti M, Miller Ca, Rumbaugh G (2013) SYNGAP1 Links the Maturation Rate of Excitatory Synapses to the Duration of Critical-Period Synaptic Plasticity. *Journal of Neuroscience* 33:10447–10452.

Clement JP, Aceti M, Creson TK, Ozkan ED, Shi Y, Reish NJ, Almonte AG, Miller BH, Wiltgen BJ, Miller Ca, Xu X, Rumbaugh G (2012) Pathogenic SYNGAP1 mutations impair cognitive development by disrupting maturation of dendritic spine synapses. *Cell* 151:709–723.

Colavita M, Terral G, Lemercier CE, Drago F, Marsicano G, Massa F (2016) Layer-specific potentiation of network GABAergic inhibition in the CA1 area of the hippocampus. *Scientific Reports* 6:1–14.

Comoletti D, Flynn R, Jennings LL, Chubykin A, Matsumura T, Hasegawa H, Südhof TC, Taylor P (2003) Characterization of the Interaction of a Recombinant Soluble Neuroligin-1 with Neurexin-1β. *Journal of Biological Chemistry* 278:50497–50505.

Comoletti D, Grishaev A, Whitten AE, Tsigelny I, Taylor P, Trewhella J (2007) Synaptic Arrangement of the Neuroligin/β-Neurexin Complex Revealed by X-Ray and Neutron Scattering. *Structure* 15:693–705.

Connor SA, Ammendrup-Johnsen I, Chan AW, Kishimoto Y, Murayama C, Kurihara N, Tada A, Ge Y, Lu H, Yan R, LeDue JM, Matsumoto H, Kiyonari H, Kirino Y, Matsuzaki F, Suzuki T, Murphy TH, Wang YT, Yamamoto T, Craig AM (2016)

Altered Cortical Dynamics and Cognitive Function upon Haploinsufficiency of the Autism-Linked Excitatory Synaptic Suppressor MDGA2. *Neuron* 91:1052–1068.

Cooper SA, Van Der Speck R (2009) Epidemiology of mental ill health in adults with intellectual disabilities. *Current Opinion in Psychiatry* 22:431–436.

Costa RM, Federov NB, Kogan JH, Murphy GG, Stern J, Ohno M, Kucherlapati R, Jacks T, Silva AJ (2002) Mechanism for the learning deficits in a mouse model of neurofibromatosis type 1. *Nature* 415:526–530.

Coutinho V, Mutoh H, Knöpfel T (2004) Functional topology of the mossy fibre-granule cell-Purkinje cell system revealed by imaging of intrinsic fluorescence in mouse cerebellum. *European Journal of Neuroscience* 20:740–748.

Dahlhaus R, Hines RM, Eadie BD, Kannangara TS, Hines DJ, Brown CE, Christie BR, El-Hussefini A (2010) Overexpression of the cell adhesion protein neuroligin-1 induces learning deficits and impairs synaptic plasticity by altering the ratio of excitation to inhibition in the hippocampus. *Hippocampus* 20:305–322.

Dalton KM, Nacewicz BM, Johnstone T, Schaefer HS, Gernsbacher MA, Goldsmith HH, Alexander AL, Davidson RJ (2005) Gaze fixation and the neural circuitry of face processing in autism. *Nature Neuroscience* 8:519–526.

Dalzell L, Connor S, Penner M, Saari MJ, Leboutillier JC, Weeks ACW (2011) Fear Conditioning is Associated With Synaptogenesis in the Lateral Amygdala. *Synapse* 65:513–519.

Dang R, Qi J, Liu A, Ren Q, Lv D, Han L, Zhou Z, Cao F, Xie W, Jia Z (2018) Regulation of hippocampal long term depression by Neuroligin 1. *Neuropharmacology* 143:205–216.

Davis M (1993) Pharmacological analysis of fear-potentiated startle. *Brazilian journal of medical and biological research* 26:235–260.

Dawitz J, Kroon T, Hjorth JJ, Meredith RM (2011) Functional Calcium Imaging in Developing Cortical Networks. *Journal of Visualized Experiments* pp. 1–8.

De Rubeis S, He X, Goldberg A, Poultney C, Samocha K, Cicek A, Al. E (2014) Synaptic, transcriptional, and chromatin genes disrupted in autism. *Nature* 515:209–215.

Dean C, Dresbach T (2006) Neuroligins and neurexins: linking cell adhesion , synapse formation and cognitive function. *Trends in neurosciences* 29.

Dean C, Scholl FG, Choih J, DeMaria S, Berger J, Isacoff E, Scheiffele P (2003) Neurexin mediates the assembly of presynaptic terminals. *Nature neuroscience* 6:708–716.

Deciphering Developmental Disorders S (2015) Large-scale discovery of novel genetic causes of developmental disorders. *Nature* 519:223–228.

Deciphering Developmental Disorders S (2017) Prevalence and architecture of de novo mutations in developmental disorders. *Nature* 542:433–438.

Denayer E, Ahmed T, Brems H, Van Woerden G, Borgesius NZ, Callaerts-Vegh Z, Yoshimura A, Hartmann D, Elgersma Y, D'Hooge R, Legius E, Balschun D (2008) Spred1 Is Required for Synaptic Plasticity and Hippocampus-Dependent Learning. *Journal of Neuroscience* 28:14443–14449.

Doron NN, LeDoux JE (1999) Organization of Projections to the Lateral Amygdala From Auditory and Visual Areas of the Thalamus in the Rat. *The Journal of comparative neurology* 412:383–409.

Duvarci S, Pare D (2014) Amygdala microcircuits controlling learned fear. *Neuron* 82:966–980.

Eckle VS, Shcheglovitov A, Vitko I, Dey D, Yap CC, Winckler B, Perez-Reyes E (2014) Mechanisms by which a CACNA1H mutation in epilepsy patients increases seizure susceptibility. *Journal of Physiology* 592:795–809.

Ehrlich I, Humeau Y, Grenier F, Ciocchi S, Herry C, Lüthi A (2009) Amygdala Inhibitory Circuits and the Control of Fear Memory. *Neuron* 62:757–771.

Ehrlich I, Klein M, Rumpel S, Malinow R (2007) PSD-95 is required for activity-driven synapse stabilization. *Pnas* 104:4176–4181.

Elegheert J, Cvetkovska V, Clayton AJ, Heroven C, Vennekens KM, Smukowski SN, Regan MC, Jia W, Smith AC, Furukawa H, Savas JN, de Wit J, Begbie J, Craig AM, Aricescu AR (2017) Structural Mechanism for Modulation of Synaptic Neuroligin-Neurexin Signaling by MDGA Proteins. *Neuron* 95:896–913.e10.

Engel AK, Fries P, Singer W (2001) DYNAMIC PREDICTIONS: OSCILLATIONS AND SYNCHRONY IN TOP – DOWN PROCESSING. *Nature Reviews Neuroscience* 2:704–716.

Ermentrout BG, Kleinfeld D (2001) Traveling Electrical Waves in Cortex: Insight from Phase Dynamics and Speculation on a Computational Role. *Neuron* 29:33–44.

Etherton M, Földy C, Sharma M, Tabuchi K, Liu X, Shamloo M (2011a) Autism-linked neuroligin-3 R451C mutation differentially alters hippocampal and cortical synaptic function. *Pnas* 108:13764–13769.

Etherton MR, Tabuchi K, Sharma M, Ko J, Südhof TC (2011b) An autism-associated point mutation in the neuroligin cytoplasmic tail selectively impairs AMPA receptor-mediated synaptic transmission in hippocampus. *The EMBO journal* 30:2908–2919.

Faber ES, Callister RJ, Sah P (2001) Morphological and electrophysiological properties of principal neurons in the rat lateral amygdala in vitro. *Journal of neurophysiology* 85:714–723.

Falls WA, Miserendino MJ, Davis M (1992) Extinction of fear-potentiated startle: blockade by infusion of an NMDA antagonist into the amygdala. *The Journal of neuroscience : the official journal of the Society for Neuroscience* 12:854–63.

Fernández M, Mollinedo-Gajate I, Peñagarikano O (2018) Neural Circuits for Social Cognition: Implications for Autism. *Neuroscience* 370:148–162.

Földy C, Malenka RC, Südhof TC (2013) Autism-associated neuroligin-3 mutations commonly disrupt tonic endocannabinoid signaling. *Neuron* 78:498–509.

Frank RA, Komiyama NH, Ryan TJ, Zhu F, O'Dell TJ, Grant SG (2016) NMDA receptors are selectively partitioned into complexes and supercomplexes during synapse maturation. *Nature Communications* 7.

Frank RA, Zhu F, Komiyama NH, Grant SG (2017) Hierarchical organization and genetically separable subfamilies of PSD95 postsynaptic supercomplexes. *Journal of Neurochemistry* 142:504–511.

Fu Z, Washbourne P, Ortinski P, Vicini S (2003) Functional Excitatory Synapses in HEK293 Cells Expressing Neuroligin and Glutamate Receptors. *Journal of Neurophysiology* 90:3950–3957.

Fujieda T, Koganezawa N, Ide Y, Shirao T, Sekino Y (2015) An inhibitory pathway controlling the gating mechanism of the mouse lateral amygdala revealed by voltage-sensitive dye imaging. *Neuroscience Letters* 590:126–131.

Futai K, Kim MJ, Hashikawa T, Scheiffele P, Sheng M, Hayashi Y (2007) Retrograde modulation of presynaptic release probability through signaling mediated by PSD-95 – neuroligin. *Nature neuroscience* 10.

Gambino F, Khelfaoui M, Poulain B, Bienvenu H, Chelly J, Humeau Y (2010) Synaptic maturation at cortical projections to the lateral amygdala in a mouse model of rett syndrome. *PLoS ONE* 5.

Garner CC, Zhai RG, Gundelfinger ED, Ziv NE (2002) Molecular mechanisms of CNS synaptogenesis. *Trends in neurosciences* 25:243–250.

Ghosh S, Chattarji S (2015) Neuronal encoding of the switch from specific to generalized fear. *Nature Neuroscience* 18:112–120.

Giannone G, Mondin M, Grillo-Bosch D, Tessier B, Saint-michel E, Czondor K, Sainlos M, Choquet D, Thoumine O (2013) Neurexin-1 b Binding to Neuroligin-1 Triggers the Preferential Recruitment of PSD-95 versus Gephyrin through Tyrosine Phosphorylation of Neuroligin-1. *Cell reports* 3:1996–2007.

Gibbard CR, Ren J, Skuse DH, Clayden JD, Clark CA (2018) Structural connectivity of the amygdala in young adults with autism spectrum disorder. *Human Brain Mapping* 39:1270–1282.

Gökçek-Saraç Ç, Wesierska M, Jakubowska-Doğru E (2015) Comparison of spatial learning in the partially baited radial-arm maze task between commonly used rat strains: Wistar, Spargue-Dawley, Long-Evans, and outcrossed Wistar/Sprague-Dawley. *Learning and Behavior* 43:83–94.

Gonçalves JT, Anstey JE, Golshani P, Portera-Cailliau C (2013) Circuit level defects in the developing neocortex of Fragile X mice. *Nature Neuroscience* 16:903–909.

Graf ER, Zhang X, Jin SX, Linhoff MW, Craig AM (2004) Neurexins induce differentiation of GABA and glutamate postsynaptic specializations via neuroligins. *Cell* 119:1013–1026.

Grandy TH, Greenfield SA, Devonshire IM (2012) An evaluation of in vivo voltage-sensitive dyes: pharmacological side effects and signal-to-noise ratios after effective removal of brain-pulsation artifacts. *Journal of Neurophysiology* 108:2931–2945.

Grienberger C, Konnerth A (2012) Imaging Calcium in Neurons. *Neuron* 73:862–885.

Gu N, Vervaeke K, Hu H, Storm JF (2005) Kv7/KCNQ/M and HCN/h, but not KCa2/SK channels, contribute to the somatic medium after-hyperpolarization and excitability control in CA1 hippocampal pyramidal cells. *Journal of Physiology* 566:689–715.

Gumus E (2019) A Hemizygous 370 Kilobase Microduplication at Xq13.1 in a Three-Year-Old Boy With Autism and Speech Delay. *Fetal and Pediatric Pathology* 0:1–6.

Guo X, Hamilton PJ, Reish NJ, Sweatt JD, Miller Ca, Rumbaugh G (2009) Reduced expression of the NMDA receptor-interacting protein SynGAP causes behavioral abnormalities that model symptoms of Schizophrenia. *Neuropsychopharmacology : official publication of the American College of Neuropsychopharmacology* 34:1659–1672.

Guzman SJ, Schlögl A, Schmidt-Hieber C (2014) Stimfit: quantifying electrophysiological data with Python. *Frontiers in neuroinformatics* 8:16.

Haas KT, Compans B, Letellier M, Bartol TM, Grillo-Bosch D, Sejnowski TJ, Sainlos M, Choquet D, Thoumine O, Hosy E (2018) Pre-post synaptic alignment through neuroligin-1 tunes synaptic transmission efficiency. *eLife* 7:1–22.

Hamad MIK, Krause M, Wahle P (2015) Improving AM ester calcium dye loading efficiency. *Journal of Neuroscience Methods* 240:48–60.

Hamdan FF, Daoud H, Piton A, Gauthier J, Dobrzeniecka S, Krebs MO, Joober R, Lacaille JC, Nadeau A, Milunsky JM, Wang Z, Carmant L, Mottron L, Beauchamp MH, Rouleau GA, Michaud JL (2011) De novo syngap1 mutations in nonsyndromic intellectual disability and autism. *Biological Psychiatry* 69:898–901.

Hamdan FF, Gauthier J, Spiegelman D, Noreau A, Yang Y, Pellerin S, Dobrzeniecka S, Côté M, Perreau-linck E, Carmant L, Anjou GD, Fombonne É, Addington AM, Rapoport JL, Delisi LE, Krebs Mo, Mouaffak F, Joober R, Mottron L, Drapeau P, Marineau C, Lafreniere RG, Lacaille JC, Rouleau Ga, Michaud JL (2009) Mutations in SYNGAP1 in Autosomal Nonsyndromic Mental Retardation. *New England Journal of Medicine* 360:599–605.

Hamilton SM, Green JR, Veeraragavan S, Yuva L, McCoy A, Wu Y, Warren J, Little L, Ji D, Cui X, Weinstein E, Paylor R (2014) Fmr1 and Nlgn3 knockout rats: novel tools for investigating autism spectrum disorders. *Behavioral neuroscience* 128:103–109.

Han Jh, Kushner Sa, Yiu AP, Cole CJ, Matynia A, Brown Ra, Neve RL, Guzowski JF, Silva AJ, Josselyn Sa (2007) Neural Competition during memory formation. *Science* 316:457–460.

Han Jh, Kushner SA, Yiu AP, Hsiang Hl, Buch T, Waisman A, Bontempi B, Neve RL, Frankland PW, Josselyn Sa (2009) Selective Erasure of a Fear Memory. *Science* 323:1492–1496.

Harris KM, Stevens JK (1989) Dendritic Spines of CA1 pyramidal Cells in the Rat Hippocampus: Serial Electron Microscope with Reference to their Biophysical Characteristics. *The Journal of Neuroscience* 9:2982–2997.

Hays SA, Huber KM, Gibson JR (2011) Altered Neocortical Rhythmic Activity States in Fmr1 KO Mice Are Due to Enhanced mGluR5 Signaling and Involve Changes in Excitatory Circuitry. *Journal of Neuroscience* 31:14223–14234.

Herry C, Ciocchi S, Senn V, Demmou L, Müller C, Lüthi A (2008) Switching on and off fear by distinct neuronal circuits. *Nature* 454:600–606.

Herry C, Trifilieff P, Micheau J, Lüthi A, Mons N (2006) Extinction of auditory fear conditioning requires MAPK/ERK activation in the basolateral amygdala. *European Journal of Neuroscience* 24:261–269.

Hochman DW (2009) IMAGING | Optical Imaging in Epilepsy Research: Overview of Methods and Applications pp. 545–551. Academic Press, Oxford.

Hölscher C (2002) Different strains of rats show different sensitivity to block of long-term potentiation by nitric oxide synthase inhibitors. *European Journal of Pharmacology* 457:99–106.

Hoon M, Soykan T, Falkenburger B, Hammer M, Patrizi A, Schmidt KF, Sassoe-Pognetto M, Lowel S, Moser T, Taschenberger H, Brose N, Varoqueaux F (2011) Neuroligin-4 is localized to glycinergic postsynapses and regulates inhibition in the retina. *Proceedings of the National Academy of Sciences* 108:3053–3058.

Hosie S, Malone DT, Liu S, Glass M, Adlard PA, Hannan AJ, Hill-Yardin EL (2018) Altered Amygdala Excitation and CB1 Receptor Modulation of Aggressive Behavior in the Neuroligin-3R451C Mouse Model of Autism. *Frontiers in Cellular Neuroscience* 12:1–10.

Hotson JR, Prince DA (1980) A calcium-activated hyperpolarization follows repetitive firing in hippocampal neurons. *Journal of Neurophysiology* 43:409–419.

Houbaert X, Zhang CL, Gambino F, Lepleux M, Deshors M, Normand E, Levet F, Ramos M, Billuart P, Chelly J, Herzog E, Humeau Y (2013) Target-Specific Vulnerability of Excitatory Synapses Leads to Deficits in Associative Memory in a Model of Intellectual Disorder. *Journal of Neuroscience* 33:13805–13819.

Hrybouski S, Aghamohammadi-Sereshki A, Madan CR, Shafer AT, Baron CA, Seres P, Beaulieu C, Olsen F, Malykhin NV (2016) Amygdala subnuclei response and connectivity during emotional processing. *NeuroImage* 133:98–110.

Huang YY, Kandel ER (1998) Postsynaptic Induction and PKA-Dependent Expression of LTP in the Lateral Amygdala. *Neuron* 21:169–178.

Humeau Y, Herry C, Kemp N, Shaban H, Fourcaudot E, Bissière S, Lüthi A (2005) Dendritic spine heterogeneity determines afferent-specific Hebbian plasticity in the amygdala. *Neuron* 45:119–131.

Ibrahim K, Eilbott JA, Ventola P, He G, Pelphrey KA, McCarthy G, Sukhodolsky DG (2019) Reduced Amygdala-Prefrontal Functional Connectivity in Children with Autism Spectrum Disorder and Co-Occurring Disruptive Behavior. *Biological Psychiatry: Cognitive Neuroscience and Neuroimaging* pp. 1–11.

Ichtchenko K, Hata Y, Nguyen T, Ullrich B, Missler M, Moomaw C, Südhof TC (1995) Neuroligin 1: A splice site-specific ligand for β-neurexins. *Cell* 81:435–443.

Ichtchenko K, Nguyen T, Südhof TC (1996) Structures, alternative splicing, and neurexin binding of multiple neuroligins. *Journal of Biological Chemistry* 271:2676–2682.

Iftinca M (2011) Neuronal T-type calcium channels : What's new ? *Journal of Medicine and Life* 4:126–138.

Iida J, Hirabayashi S, Sato Y, Hata Y (2004) Synaptic scaffolding molecule is involved in the synaptic clustering of neuroligin. *Molecular and Cellular Neuroscience* 27:497–508.

Iidaka T, Kogata T, Mano Y, Komeda H (2019) Thalamocortical Hyperconnectivity and Amygdala-Cortical Hypoconnectivity in Male Patients With Autism Spectrum Disorder. *Frontiers in Psychiatry* 10:1–11.

Ikegaya Y, Aaron G, Cossart R, Aronov D, Lampl I, Ferster D, Yuste R (2004) Synfire Chains and Cortical Songs: Temporal Modules of Cortical activity. *Science* 304:559–565.

Iossifov I, Roak BJO, Sanders SJ, Ronemus M, Krumm N, Levy D, Stessman HA, Witherspoon KT, Vives L, Patterson KE, Smith JD, Paeper B, Nickerson DA, Dea J, Dong S, Gonzalez LE, Mandell JD, Mane SM, Murtha MT, Sullivan CA, Walker MF, Waqar Z, Wei L, Willsey AJ, Yamrom B, Lee Yh, Grabowska E, Dalkic E, Wang Z, Marks S, Andrews P, Leotta A, Kendall J, Hakker I, Rosenbaum J, Ma B, Rodgers L, Troge J, Narzisi G, Yoon S, Schatz MC, Ye K, Mccombie WR, Shendure J, Eichler EE, State MW, Wigler MH (2014) The contribution of de novo coding mutations to autism spectrum disorder. *Nature* 515:216–221.

Irie M, Hata Y, Takeuchi M, Ichtchenko K, Toyoda A, Hirao K, Takai Y, Rosahl TW, Südhof TC (1997) Binding of Neuroligins to PSD-95. *Science* 277:1511–1516.

Jamain S, Radyushkin K, Hammerschmidt K, Granon S, Boretius S, Varoqueaux F, Ramanantsoa N, Gallego J, Ronnenberg A, Winter D, Frahm J, Fischer J, Bourgeron T, Ehrenreich H, Brose N (2008) Reduced social interaction and ultrasonic communication in a mouse model of monogenic heritable autism. *Proceedings of the National Academy of Sciences* 105:1710–1715.

Jamain S, Quach H, Betancur C, Råstam M, Colineaux C, Gillberg IC, Soderstrom H, Giros B, Leboyer M, Gillberg C, Bourgeron T (2003) Mutations of the X-linked genes encoding neuroligins NLGN3 and NLGN4 are associated with autism. *Nature genetics* 34:27–29.

Jayachandran R, Liu X, BoseDasgupta S, Müller P, Zhang CL, Moshous D, Studer V, Schneider J, Genoud C, Fossoud C, Gambino F, Khelfaoui M, Müller C, Bartholdi D, Rossez H, Stiess M, Houbaert X, Jaussi R, Frey D, Kammerer RA, Deupi X, de Villartay JP, Lüthi A, Humeau Y, Pieters J (2014) Coronin 1 Regulates Cognition and Behavior through Modulation of cAMP/Protein Kinase A Signaling. *PLoS Biology* 12.

Jiang DY, Wu Z, Forsyth CT, Hu Y, Yee SP, Chen G (2018) GABAergic deficits and schizophrenia-like behaviors in a mouse model carrying patient-derived neuroligin-2 R215H mutation. *Molecular Brain* 11:1–11.

Jiang M, Polepalli J, Chen LY, Zhang B, Südhof TC, Malenka RC (2016) Conditional ablation of neuroligin-1 in CA1 pyramidal neurons blocks LTP by a cell-autonomous NMDA receptor-independent mechanism. *Molecular Psychiatry* pp. 1–9.

Jin W, Zhang RJ, Wu JY (2002) Voltage-sensitive dye imaging of population neuronal activity in cortical tissue. *Journal of Neuroscience Methods* 115:13–27.

Johansen JP, Hamanaka H, Monfils MH, Behnia R, Deisseroth K, Blair HT, LeDoux JE (2010) Optical activation of lateral amygdala pyramidal cells instructs associative fear learning. *Proceedings of the National Academy of Sciences* 107:12692–12697.

Jung SY, Kim J, Kwon OB, Jung JH, An K, Jeong AY, Lee CJ, Choi YB, Bailey CH, Kandel ER, Jung SY, Kim JH (2010) Input-specific synaptic plasticity in the amygdala is regulated by neuroligin-1 via postsynaptic NMDA receptors. *Proceedings of the National Academy of Sciences* 107:4710–4715.

Kennedy MB (1997) The postsynaptic density at glutamatergic synapses. *TINS* 20:264–68.

Kennedy MB (2016) Synaptic Signaling in Learning and Memory. *Cold Spring Harbor perspectives in biology* 8.

Kennedy MB (2018) The Protein Biochemistry of the Postsynaptic Density in Glutamatergic Synapses Mediates Learning in Neural Networks. *Biochemistry* 57:4005–4009.

Kennedy MB, Beale HC, Carlisle HJ, Washburn LR (2005) Integration of biochemical signalling in spines. *Nature reviews. Neuroscience* 6:423–434.

Kilinc M, Creson T, Rojas C, Aceti M, Ellegood J, Vaissiere T, Lerch JP, Rumbaugh G (2018) Species-conserved SYNGAP1 phenotypes associated with neurodevelopmental disorders. *Molecular and Cellular Neuroscience* 91:140–150.

Kim D, Pare D, Nair SS (2013) Assignment of Model Amygdala Neurons to the Fear Memory Trace Depends on Competitive Synaptic Interactions. *Journal of Neuroscience* 33:14354–14358.

Kim D, Song I, Keum S, Lee T, Jeong MJ, Kim SS, McEnery MW, Shin HS (2001) Lack of the burst firing of thalamocortical relay neurons and resistance to absence seizures in mice lacking α1G T-type Ca2+ channels. *Neuron* 31:35–45.

Kim JJ, Decola JP, Landeira-Fernandez J, Fanselow MS (1991) N-Methyl-D-Aspartate Receptor Antagonist APV Blocks Acquisition but Not Expression of Fear Conditioning. *Behavioral neuroscience* 105:126–133.

Kim JH, Lee HK, Takamiya K, Huganir RL (2003) The role of synaptic GTPase-activating protein in neuronal development and synaptic plasticity. *The Journal of neuroscience : the official journal of the Society for Neuroscience* 23:1119–1124.

Kim JH, Liao D, Lau LF, Huganir RL (1998) SynGAP: A synaptic RasGAP that associates with the PSD-95/SAP90 protein family. *Neuron* 20:683–691.

Kim J, Jung SY, Lee YK, Park S, Choi JS, Lee CJ, Kim HS, Choi YB, Scheiffele P, Bailey CH, Kandel ER, Kim JH (2008) Neuroligin-1 is required for normal expression of LTP and associative fear memory in the amygdala of adult animals. *Pnas* 105:9087–9092.

Kleinhans NM, Johnson LC, Richards T, Mahurin R, Greenson J, Dawson G, Aylward E (2009) Reduced neural habituation in the amygdala and social impairments in autism spectrum disorders. *American Journal of Psychiatry* 166:467–475.

Klenowski PM, Fogarty MJ, Belmer A, Noakes PG, Bellingham MC, Bartlett SE (2015) Structural and functional characterization of dendritic arbors and GABAergic synaptic inputs on interneurons and principal cells in the rat basolateral amygdala. *Journal of Neurophysiology* 114:942–957.

Kling AS, Brothers LA (1992) The amygdala and social behavior In Aggleton J, editor, *Neurobiological aspects of emotion, memory, and mental dysfunction.* Wiley-Liss, Inc.

Kneussel M, Betz H (2000) Clustering of inhibitory neurotransmitter receptors at developing postsynaptic sites: the membrane activation model. *TINS* 23:429–435.

Ko J, Zhang C, Arac D, Boucard AA, Brunger AT, Südhof TC (2009) Neuroligin-1 performs neurexin-dependent and neurexin-independent functions in synapse validation. *EMBO Journal* 28:3244–3255.

Komiyama NH, Watabe AM, Carlisle HJ, Porter K, Charlesworth P, Monti J, Strathdee DJC, O'Carroll CM, Martin SJ, Morris RGM, O'Dell TJ, Grant SGN (2002) SynGAP regulates ERK/MAPK signaling, synaptic plasticity, and learning in the complex with postsynaptic density 95 and NMDA receptor. *The Journal of neuroscience : the official journal of the Society for Neuroscience* 22:9721–9732.

Konnerth A, Obaid AL, Salzberg BM (1987) Optical recording of electrical activity from parallel fibres and other cell types in skate cerebellar slices in vitro. *The Journal of Physiology* 393:681–702.

Krapivinsky G, Medina I, Krapivinsky L, Gapon S, Clapham DE (2004) SynGAP-MUPP1-CaMKII synaptic complexes regulate p38 MAP kinase activity and NMDA receptor- dependent synaptic AMPA receptor potentiation. *Neuron* 43:563–574.

Kriegler S, Chiu S (1993) Calcium signaling of glial cells along mammalian axons. *The Journal of Neuroscience* 13:4229–4245.

Kroon T, Sierksma MC, Meredith RM (2013) Investigating mechanisms underlying neurodevelopmental phenotypes of autistic and intellectual disability disorders: a perspective. *Frontiers in systems neuroscience* 7:75.

Kurshan PT, Merrill SA, Dong Y, Ding C, Hammarlund M, Bai J, Jorgensen EM, Shen K (2018) γ-Neurexin and Frizzled Mediate Parallel Synapse Assembly Pathways Antagonized by Receptor Endocytosis. *Neuron* 100:150–166.e4.

Kurshan PT, Shen K (2019) Synaptogenic pathways. *Current Opinion in Neurobiology* 57:156–162.

Kwon HB, Kozorovitskiy Y, Oh WJ, Peixoto RT, Akhtar N, Saulnier JL, Gu C, Sabatini BL (2012) Neuroligin-1-dependent competition regulates cortical synaptogenesis and synapse number. *Nature Neuroscience* 15:1667–1674.

Lai MC, Lombardo M, Baron-Cohen S (2014) Autism. *The Lancet* 383:896–910.

Laumonnier F, Bonnet-Brilhault F, Gomot M, Blanc R, David A, Moizard MP, Raynaud M, Ronce N, Lemonnier E, Calvas P, Laudier B, Chelly J, Fryns JP, Ropers HH, Hamel BC, Andres C, Barthélémy C, Moraine C, Briault S (2004) X-Linked Mental Retardation and Autism Are Associated with a Mutation in the NLGN4 Gene, a Member of the Neuroligin Family. *The American Journal of Human Genetics* 74:552–557.

Lautz JD, Brown EA, Van W, Schoiack AA, Smith SE (2018) Synaptic activity induces input-specific rearrangements in a targeted synaptic protein interaction network. *Journal of Neurochemistry* 146:540–559.

LeDoux J (2003) The emotional brain, fear, and the amygdala. *Cellular and Molecular Neurobiology* 23:727–738.

LeDoux JE (1993) Emotional Memory: In search of Systems and Synapses. *Ann NY Acad Sci* 702:149–157.

Lee YS, Ehninger D, Zhou M, Oh JY, Kang M, Kwak C, Ryu HH, Butz D, Araki T, Cai Y, Balaji J, Sano Y, I Nam C, Kim HK, Kaang BK, Burger C, Neel BG, Silva AJ (2014) Mechanism and treatment for learning and memory deficits in mouse models of Noonan syndrome. *Nature Neuroscience* 17:1736–1743.

Lemmon MA (2008) Membrane recognition by phospholipid-binding domains. *Nature Reviews Molecular Cell Biology* 9:99–111.

Letellier M, Szíber Z, Chamma I, Saphy C, Papasideri I, Tessier B, Sainlos M, Czöndör K, Thoumine O (2018) A unique intracellular tyrosine in neuroligin-1 regulates AMPA receptor recruitment during synapse differentiation and potentiation. *Nature Communications* 9.

Li W, Cui Y, Kushner SA, Brown RA, Jentsch JD, Frankland PW, Cannon TD, Silva AJ (2005) The HMG-CoA reductase inhibitor lovastatin reverses the learning and attention deficits in a mouse model of Neurofibromatosis Type 1. *Current Biology* 15:1961–1967.

Li W, Okano A, Tian QB, Nakayama K, Furihata T, Nawa H, Suzuki T (2001) Characterization of a Novel synGAP Isoform, synGAP-β. *Journal of Biological Chemistry* 276:21417–21424.

Liang J, Xu W, Hsu YT, Yee AX, Chen L, Südhof TC (2015) Conditional neuroligin-2 knockout in adult medial prefrontal cortex links chronic changes in synaptic inhibition to cognitive impairments. *Molecular Psychiatry* 20:850–859.

Lin Yc, Koleske AJ (2010) Mechanisms of Synapse and Dendrite Maintenance and Their Disruption in Psychiatric and Neurodegenerative Disorders. *Annu. Rev. Neurosci.* 33:349–78.

Liu D, Ejikeme T, Ramirez J, Baldwin KT, Enustun E, Eroglu C, Kim YH, Stogsdill JA, Ji RR (2017) Astrocytic neuroligins control astrocyte morphogenesis and synaptogenesis. *Nature* 551:192–197.

Loew LM (2015) Design and Use of Organic Voltage Sensitive Dyes In Canepari M, Zecevic D, Bernus , editors, *Membrane Potential Imaging in the Nervous System and Heart. Advances in Experimental Medicine and Biology.* Springer, Cham.

Lüscher C, Nicoll RA, Malenka RC, Muller D (2000) Synaptic plasticity and dynamic modulation of the postsynaptic membrane. *Nature Neuroscience* 3:545–550.

MacLean J, Yuste R (2009) Imaging action potentials with calcium indicators. *Cold Spring Harbor Protocols* 4:1–4.

Mahanty NK, Sah P (1999) Excitatory synaptic inputs to pyramidal neurons of the lateral amygdala. *European Journal of Neuroscience* 11:1217–1222.

Makino H, Malinow R (2009) Article AMPA Receptor Incorporation into Synapses during LTP : The Role of Lateral Movement. *Neuron* 64:381–390.

Malenka RC, Nicoll RA (1997) Silent Synapses Speak Up. *Neuron* 19:473–476.

Maletic-Savatic M, Malinow R, Svoboda K (1999) Rapid Dendritic Morphogenesis in CA1 Hippocampal Dendrites Induced by Synaptic Activity. *Science* 283:1923–1928.

Malinow R, Malenka RC (2002) AMPA Receptor Trafficking and Synaptic Plasticity. *Annu. Rev. Neurosci.* 25:103–26.

Manassero E, Renna A, Milano L, Sacchetti B (2018) Lateral and Basal Amygdala Account for Opposite Behavioral Responses during the Long-Term Expression of Fearful Memories. *Scientific Reports* 8:1–12.

Mao Bq, Hamzei-sichani F, Aronov D, Froemke RC, Yuste R (2001) Dynamics of Spontaneous Activity in Neocortical Slices. *Neuron* 32:883–898.

Martin BS, Corbin JG, Huntsman MM (2014) Deficient tonic GABAergic conductance and synaptic balance in the Fragile-X Syndrome Amygdala. *Journal of neurophysiology* 3:890–902.

Matson JL, Shoemaker M (2009) Intellectual disability and its relationship to autism spectrum disorders. *Research in Developmental Disabilities* 30:1107–1114.

Matson JL, Smiroldo BB, Hamilton M, Baglio CS (1997) Do anxiety disorders exist in persons with severe and profound mental retardation? *Research in Developmental Disabilities* 18:39–44.

Matsukawa H, Akiyoshi-Nishimura S, Zhang Q, Lujan R, Yamaguchi K, Goto H, Yaguchi K, Hashikawa T, Sano C, Shigemoto R, Nakashiba T, Itohara S (2014) Netrin-G/NGL Complexes Encode Functional Synaptic Diversification. *Journal of Neuroscience* 34:15779–15792.

Matsuzaki M, Ellis-Davies GC, Nemoto T, Miyashita Y, Iino M, Kasai H (2001) Dendritic spine geometry is critical for AMPA receptor expression in hippocampal CA1 pyramidal neurons. *Nature Neuroscience* 4:1086–1092.

Matsuzaki M, Honkaru N, Ellis-Davies GC, Kasai H (2004) Structural basis of long-term potentiation in single dendritic spines. *Nature* 429.

Maulik PK, Mascarenhas MN, Mathers CD, Dua T, Saxena S (2011) Prevalence of intellectual disability: A meta-analysis of population-based studies. *Research in Developmental Disabilities* 32:419–436.

McCarthy J (2007) Children with autism spectrum disorders and intellectual disability. *Current Opinion in Psychiatry* 20:472–476.

McDonald AJ, Augustine JR (1993) Localization of GABA-like immunoreactivity in the monkey amygdala. *Neuroscience* 52:281–294.

Mcdonald AJ (1998) Cortical Pathways To the Mammalian Amygdala. *progress in Neurobiology* 55.

McGillivray JA, McCabe MP, Kershaw MM (2008) Depression in people with intellectual disability: An evaluation of a staff-administered treatment program. *Research in Developmental Disabilities* 29:524–536.

McKay BM, Matthews EA, Oliveira FA, Disterhoft JF (2009) Intrinsic Neuronal Excitability Is Reversibly Altered by a Single Experience in Fear Conditioning. *Journal of Neurophysiology* 102:2763–2770.

McKernan MG, Shinnick-Gallagher P (1997) Fear conditioning induces a lasting potentiation of synaptic currents in vitro. *Nature* 390:607–611.

McKinney BC, Sze W, Lee B, Murphy GG (2009) Impaired Long-term Potentiation and Enhanced Neuronal Excitability in the Amygdala of CaV 1.3 Knockout Mice. *Neurobiology of Learning and Memory* 92:519–528.

McMahon A, Barnett M, O'Leary T, Stoney P, Collins M, Papadia S, Choudhary J, Komiyama N, Grant S, Hardingham G, Wyllie D, Kind P (2012) SynGAP isoforms exert opposing effects on synaptic strength. *Nature Communications* 3:900.

McMahon SM, Jackson MB (2018) An Inconvenient Truth: Calcium Sensors Are Calcium Buffers. *Trends in Neurosciences* 41:880–884.

Mennerick S, Chisari M, Shu Hj, Taylor A, Eisenman LN, Zorumski CF (2010) Diverse voltage-sensitive dyes modulate GABAA receptor function. *J Neurosci* 30:2871–2879.

Meyer G, Varoqueaux F, Neeb A, Oschlies M, Brose N (2004) The complexity of PDZ domain-mediated interactions at glutamatergic synapses: A case study on neuroligin. *Neuropharmacology* 47:724–733.

Mignot C, Stülpnagel CV, Nava C, Ville D, Sanlaville D, Lesca G, Rastetter A, Gachet B, Marie Y, Korenke GC, Borggraefe I, Hoffmann-zacharska D, Rudzka-dyba M, Yi U, Ça H, Isapof A, Marey I, Panagiotakaki E, Korff C, Rossier E, Riess A, Beckwoedl S, Rauch A, Zweier C, Hoyer J, Reis A, Mironov M, Bobylova M, Mukhin K, Hernandez-hernandez L, Maher B, Sisodiya S, Kuhn M, Glaeser D, Wechuysen S, Myers CT, Mefford HC, Hörtnagel K, Biskup S, Mae Er, Lemke JR, Héron D, Kluger G, Depienne C (2016) Genetic and neurodevelopmental spectrum of SYNGAP1 -associated intellectual disability and epilepsy. *J Med Gen* pp. 1–12.

Miserendino MJD, Sananes CB, Melia KR, Davis M (1990) Blocking of acquisition but not expression of conditioned fear-potentiated startle by NMDA antagonists in the amygdala. *Nature* 345:1988–1990.

Missler M, Zhang W, Rohlmann A, Kattenstroth G, Hammer RE, Gottmann K, Südhof TC (2003) α-neurexins couple Ca 2+ channels to synaptic vesicle exocytosis. *Nature* 423:939–948.

Momose-Sato Y, Sato K, Arai Y, Yazawa I, Mochida H, Kamino K (1999) Evaluation of voltage-sensitive dyes for long-term recording of neural activity in the hippocampus. *Journal of Membrane Biology* 172:145–157.

Moon IS, Sakagami H, Nakayama J, Suzuki T (2008) Differential distribution of synGAP α1 and synGAP β isoforms in rat neurons. *Brain research* 1241:62–75.

Muhia M, Yee BK, Feldon J, Markopoulos F, Knuesel I (2010) Disruption of hippocampus-regulated behavioural and cognitive processes by heterozygous constitutive deletion of SynGAP. *European Journal of Neuroscience* 31:529–543.

Muri R, Knöpfel T (1994) Activity Induced Elevations of Intracellular Calcium Concentration Neurons of the Deep Cerebellar Nuclei. *Journal of neurophysiology* 7:420–428.

Murphy CM, Wilson CE, Robertson DM, Ecker C, Daly EM, Hammond N, Galanopoulos A, Dud I, Murphy DG, McAlonan GM (2016) Autism spectrum disorder in adults : diagnosis , management , and health services development. *Neuropsychiatric Disease and Treatment* 12:1669–1686.

Murthy VN, Schikorski T, Stevens CF, Zhu Y (2001) Inactivity Produces Increases in Neurotransmitter Release and Synapse Size. *Neuron* 32:673–682.

Nacewicz BM, Dalton KM, Johnstone T, Long MT, McAuliff EM, Oakes TR, Alexander AL, Davidson RJ (2006) Amygdala Volume and Nonverbal Social Impairment in Adolescent and Adult Males With Autism. *Archives of General Psychiatry* 63:1417–1428.

Nakanishi M, Nomura J, Ji X, Tamada K, Arai T, Takahashi E, Bućan M, Takumi T (2017) Functional significance of rare neuroligin 1 variants found in autism. *PLoS Genetics* 13:1–28.

Nixima K, Okanoya K, Ichinohe N, Kurotani T (2017) Fast Voltage-Sensitive Dye Imaging of Excitatory and Inhibitory Synaptic Transmission in the Rat Granular Retrosplenial Cortex. *Journal of Neurophysiology* p. jn.00734.2016.

Ogden KK, Ozkan ED, Rumbaugh G (2016) Prioritizing the development of mouse models for childhood brain disorders. *Neuropharmacology* 100:2–16.

Oh JS, Manzerra P, Kennedy MB (2004) Regulation of the Neuron-specific Ras GTPase-activating Protein, synGAP, by Ca2+/Calmodulin-dependent Protein Kinase II. *Journal of Biological Chemistry* 279:17980–17988.

Olmos-Serrano JL, Paluszkiewicz SM, Martin BS, Kaufmann WE, Corbin JG, Huntsman MM (2010) Defective GABAergic neurotransmission and pharmacological rescue of neuronal hyperexcitability in the amygdala in a mouse model of fragile X syndrome. *The Journal of neuroscience* 30:9929–38.

Opazo P, Choquet D (2011) A three-step model for the synaptic recruitment of AMPA receptors. *Molecular and Cellular Neuroscience* 46:1–8.

Opazo P, Sainlos M, Choquet D (2012) Regulation of AMPA receptor surface diffusion by PSD-95 slots. *Current Opinion in Neurobiology* 22:453–460.

Oswald MJ, Oorschot DE, Schulz JM, Lipski J, Reynolds JN (2009) IH current generates the afterhyperpolarisation following activation of subthreshold cortical synaptic inputs to striatal cholinergic interneurons. *Journal of Physiology* 587:5879–5897.

Ozkan ED, Creson TK, Kramár EA, Rojas C, Seese RR, Babyan AH, Shi Y, Lucero R, Xu X, Noebels JL, Miller CA, Lynch G, Rumbaugh G (2014) Reduced cognition in Syngap1 mutants is caused by isolated damage within developing forebrain excitatory neurons. *Neuron* 82:1317–1333.

Pape HC, Pare D (2010) Plastic Synaptic Networks of the Amygdala for the Acquisition, Expression, and Extinction of Conditioned Fear. *Physiological reviews* 90:419–463.

Pare D, Duvarci S (2012) Amygdala microcircuits mediating fear expression and extinction. *Current Opinion in Neurobiology* 22:717–723.

Paredes RM, Etzler JC, Watts LT, Zheng W, Lechleiter JD (2008) Chemical calcium indicators. *Methods* 46:143–151.

Parente DJ, Garriga C, Baskin B, Douglas G, Cho MT, Araujo GC, Shinawi M (2017) Neuroligin 2 Nonsense Variant Associated with Anxiety, Autism, Intellectual Disability, Hyperphagia, and Obesity. *Am J Med Genet Part A* 173A:213–216.

Park K, Lee S, Kang SJ, Choi S, Shin KS (2007) Hyperpolarization-activated currents control the excitability of principal neurons in the basolateral amygdala. *Biochemical and Biophysical Research Communications* 361:718–724.

Parker MJ, Fryer AE, Shears DJ, Lachlan KL, McKee Sa, Magee AC, Mohammed S, Vasudevan PC, Park SM, Benoit V, Lederer D, Maystadt I, Study D, FitzPatrick DR (2015) De novo, heterozygous, loss-of-function mutations in SYNGAP1 cause a syndromic form of intellectual disability. *American Journal of Medical Genetics Part A* pp. n/a–n/a.

Peixoto RT, Wang W, Croney DM, Kozorovitskiy Y, Sabatini BL (2016) Early hyperactivity and precocious maturation of corticostriatal circuits in Shank3B â '/â ' mice. *Nature Neuroscience* 19:716–724.

Pena V, Hothorn M, Eberth A, Kaschau N, Parret A, Gremer L, Bonneau F, Ahmadian MR, Scheffzek K (2008) The C2 domain of SynGAP is essential for stimulation of the Rap GTPase reaction. *EMBO reports* 9:350–355.

Peterlin ZA, Kozloski J, Mao BQ, Tsiola A, Yuste R (2002) Optical probing of neuronal circuits with calcium indicators. *Proceedings of the National Academy of Sciences* 97:3619–3624.

Pettem KL, Yokomaku D, Takahashi H, Ge Y, Craig AM (2013) Interaction between autism-linked MDGAs and neuroligins suppresses inhibitory synapse development. *The Journal of Cell Biology* 200:321–336.

Pierce K, Muller RA, Ambrose J, Allen G, Courchesne E (2001) Face processing occurs outside the fusiform 'face area' in autism: evidence from functional MRI. *Brain* 124:2059–2073.

Pinto D, Pagnamenta AT, Klei L, Anney R, Merico D, Conroy J, al. E (2010) Functional impact of global rare copy number variation in autism spectrum disorders. *Nature* 466:368–372.

Pizzarelli R, Cherubini E (2013) Developmental regulation of GABAergic signalling in the hippocampus of neuroligin 3 R451C knock-in mice: an animal model of Autism. *Frontiers in cellular neuroscience* 7:1–11.

Popescu AT, Paré D (2011) Synaptic Interactions Underlying Synchronized Inhibition in the Basal Amygdala: Evidence for Existence of Two Types of Projection Cells. *Journal of Neurophysiology* 105:687–696.

Porter K, Komiyama NH, Vitalis T, Kind PC, Grant SGN (2005) Differential expression of two NMDA receptor interacting proteins, PSD-95 and SynGAP during mouse development. *European Journal of Neuroscience* 21:351–362.

Poulopoulos A, Aramuni G, Meyer G, Soykan T, Hoon M, Harvey K, Jedlicka P, Papadopoulos T, Zhang M, Paarmann I, Schwarzacher SW, Betz H, Harvey RJ, Brose N, Zhang W (2009) Neuroligin 2 Drives Postsynaptic Assembly at Perisomatic Inhibitory Synapses through Gephyrin and Collybistin. *Neuron* 63:628–642.

Poulopoulos A, Soykan T, Tuffy LP, Hammer M, Varoqueaux F, Brose N (2012) Homodimerization and isoform-specific heterodimerization of neuroligins. *Biochemical Journal* 446:321–330.

Preuss S, Stein W (2013) Comparison of Two Voltage-Sensitive Dyes and Their Suitability for Long-Term Imaging of Neuronal Activity. *PLoS ONE* 8.

Purcell SM, Moran JL, Fromer M, Ruderfer D, Solovieff N, Roussos P, O'Dushlaine C, Chambert K, Bergen SE, Kähler A, Duncan L, Stahl E, Genovese G, Fernández E, Collins MO, Komiyama NH, Choudhary JS, Magnusson PK, Banks E, Shakir K, Garimella K, Fennell T, Depristo M, Grant SG, Haggarty SJ, Gabriel S, Scolnick EM, Lander ES, Hultman CM, Sullivan PF, McCarroll SA, Sklar P (2014) A polygenic burden of rare disruptive mutations in schizophrenia. *Nature* 506:185–190.

Puzzo D, Fiorito J, Purgatorio R, Gulisano W, Palmeri A, Arancio O, Nicholls R (2016) Molecular Mechanisms of Learning and Memory. *Genes, Environment and Alzheimer's Disease* 147:1–27.

Quesnel-Vallières M, Weatheritt RJ, Cordes SP, Blencowe BJ (2019) Autism spectrum disorder: insights into convergent mechanisms from transcriptomics. *Nature Reviews Genetics* 20:51–63.

Quirk GJ, Armony JL, Ledoux JE (1997) Fear conditioning enhances different temporal components of tone-evoked spike trains in auditory cortex and lateral amygdala. *Neuron* 19:613–624.

Quirk GJ, Repa JC, LeDoux JE (1995) Fear conditioning enhances short-latency auditory responses of lateral amygdala neurons: Parallel recordings in the freely behaving rat. *Neuron* 15:1029–1039.

Radyushkin K, Hammerschmidt K, Boretius S, Varoqueaux F, El-Kordi A, Ronnenberg A, Winter D, Frahm J, Fischer J, Brose N, Ehrenreich H (2009) Neuroligin-3-deficient mice: model of a monogenic heritable form of autism with an olfactory deficit. *Genes, Brain and Behavior* 8:416–425.

Rainnie DG, Asprodini EK, Shinnick-Gallagher P (1993) Intracellular recordings from morphologically identified neurons of the basolateral amygdala. *Journal of neurophysiology* 69:1350–62.

Reinert KC, Dunbar RL, Gao W, Chen G, Ebner TJ (2004) Flavoprotein Autofluorescence Imaging of Neuronal Activation in the Cerebellar Cortex In Vivo. *Journal of Neurophysiology* 92:199–211.

Repa JC, Muller J, Apergis J, Desrochers TM, Zhou Y, LeDoux JE (2001) Two different lateral amygdala cell populations contribute to the initiation and storage of memory. *Nature Neuroscience* 4:724.

Rodrigues SM, Bauer EP, Farb CR, Schafe GE, LeDoux JE (2002) The group I metabotropic glutamate receptor mGluR5 is required for fear memory formation and long-term potentiation in the lateral amygdala. *The Journal of neuroscience* 22:5219–5229.

Rogan MT, LeDoux JE (1995) LTP is accompanied by commensurate enhancement of auditory-evoked responses in a fear conditioning circuit. *Neuron* 15:127–136.

Rogan MT, Staubli UV, LeDoux JE (1997) Fear conditioning induces associative long-term potentiation in the amygdala. *Nature* 390:604–607.

Romanski LM, Clugnet MC, Bordi F, LeDoux JE (1993) Somatosensory and auditory convergence in the LA.pdf.

Romanski L, Ledoux J (1992) Equipotentiality of thalamo-amygdala and thalamo-cortico-amygdala circuits in auditory fear conditioning. *Journal of Neuroscience* 12:4501–4509.

Ross WN, Salzberg BM, Cohen LB, Grinvald A, Davila HV, Waggoner AS, Wang CH (1977) Changes in absorption, fluorescence, dichroism, and birefringence in stained giant axons: Optical measurement of membrane potential. *The Journal of Membrane Biology* 33:141–183.

Rothwell PE, Fuccillo MV, Maxeiner S, Hayton SJ, Gokce O, Lim BK, Fowler SC, Malenka RC, Südhof TC (2014) Autism-Associated Neuroligin-3 Mutations Commonly Impair Striatal Circuits to Boost Repetitive Behaviors. *Cell* 158:198–212.

Rumbaugh G, Adams JP, Kim JH, Huganir RL (2006) SynGAP regulates synaptic strength and mitogen-activated protein kinases in cultured neurons. *Proceedings of the National Academy of Sciences of the United States of America* 103:4344–4351.

Saar D, Grossman Y, Barkai E (1998) Reduced after-hyperpolarization in rat piriform cortex pyramidal neurons is associated with increased learning capability during operant conditioning. *European Journal of Neuroscience* 10:1518–1523.

Sah P, Faber ESL, Lopez De Armentia M, Power J (2003) The amygdaloid complex: anatomy and physiology. *Physiological reviews* 83:803–834.

Sah P, Faber ES (2002) Channels underlying neuronal calcium-activated potassium currents. *Progress in Neurobiology* 66:345–353.

Sanders SJ, Ercan-Sencicek AG, Hus V, Luo R, Murtha MT, Moreno-De-Luca D, Chu SH, Moreau MP, Gupta AR, Thomson SA, Mason CE, Bilguvar K, Celestino-Soper PB, Choi M, Crawford EL, Davis L, Davis Wright NR, Dhodapkar RM, DiCola M, DiLullo NM, Fernandez TV, Fielding-Singh V, Fishman DO, Frahm S, Garagaloyan R, Goh GS, Kammela S, Klei L, Lowe JK, Lund SC, McGrew AD, Meyer KA, Moffat WJ, Murdoch JD, O'Roak BJ, Ober GT, Pottenger RS, Raubeson MJ, Song Y, Wang Q, Yaspan BL, Yu TW, Yurkiewicz IR, Beaudet AL, Cantor RM, Curland M, Grice DE, Günel M, Lifton RP, Mane SM, Martin DM, Shaw CA, Sheldon M, Tischfield JA, Walsh CA, Morrow EM, Ledbetter DH, Fombonne E, Lord C, Martin CL, Brooks AI, Sutcliffe JS, Cook EH, Geschwind D, Roeder K, Devlin B, State MW (2011) Multiple Recurrent De Novo CNVs, Including Duplications of the 7q11.23 Williams Syndrome Region, Are Strongly Associated with Autism. *Neuron* 70:863–885.

Sanders SJ, He X, Willsey AJ, Devlin B, Roeder K, State MW, Sanders SJ, He X, Willsey AJ, Ercan-sencicek AG, Samocha KE, Al. E (2015) Insights into Autism Spectrum Disorder Genomic Architecture and Biology from 71 Risk Loci. *Neuron* 87:1215–1233.

Santini E, Quirk GJ, Porter JT (2008) Fear Conditioning and Extinction Differentially Modify the Intrinsic Excitability of Infralimbic Neurons. *Journal of Neuroscience* 28:4028–4036.

Schafe GE, Atkins CM, Swank MW, Bauer EP, Sweatt JD, LeDoux JE (2000) Activation of ERK/MAP kinase in the amygdala is required for memory consolidation of pavlovian fear conditioning. *The Journal of neuroscience : the official journal of the Society for Neuroscience* 20:8177–87.

Scheiffele P, Fan J, Choih J, Fetter R, Serafini T (2000) Neuroligin expressed in non-neuronal cells triggers presynaptic development in contacting axons. *Cell* 101:657–69.

Schoch H, Kreibich AS, Ferri SL, White RS, Bohorquez D, Banerjee A, Port RG, Dow HC, Cordero L, Pallathra AA, Kim H, Li H, Bilker WB, Hirano S, Schultz RT, Borgmann-Winter K, Hahn CG, Feldmeyer D, Carlson GC, Abel T, Brodkin ES (2017) Sociability Deficits and Altered Amygdala Circuits in Mice Lacking Pcdh10, an Autism Associated Gene. *Biological Psychiatry* 81:193–202.

Schreiber J, Grimbergen LA, Overwater I, Van Der Vaart T, Stedehouder J, Schuhmacher AJ, Guerra C, Kushner SA, Jaarsma D, Elgersma Y (2017) Mechanisms underlying cognitive deficits in a mouse model for Costello Syndrome are distinct from other RASopathy mouse models. *Scientific Reports* 7:1–19.

Schroeder BW, Shinnick-Gallagher P (2004) Fear memories induce a switch in stimulus response and signaling mechanisms for long-term potentiation in the lateral amygdala. *European Journal of Neuroscience* 20:549–556.

Schumann CM, Bauman MD, Amaral DG (2011) Abnormal structure or function of the amygdala is a common component of neurodevelopmental disorders. *Neuropsychologia* 49:745–759.

Sehgal M, Ehlers VL, Moyer JR (2014) Learning enhances intrinsic excitability in a subset of lateral amygdala neurons. *Learning and Memory* 21:161–170.

Shah MM (2018) Neuronal HCN channel function and plasticity. *Current Opinion in Physiology* 2:92–97.

Sharp BM (2017) Basolateral amygdala and stress-induced hyperexcitability affect motivated behaviors and addiction. *Translational psychiatry* 7:e1194.

Shen MD, Li DD, Keown CL, Lee A, Johnson RT, Angkustsiri K, Rogers SJ, Müller RA, Amaral DG, Nordahl CW (2016) Functional Connectivity of the Amygdala Is Disrupted in Preschool-Aged Children With Autism Spectrum Disorder. *Journal of the American Academy of Child and Adolescent Psychiatry* 55:817–824.

Sheng M, Hoogenraad CC (2007) The Postsynaptic Architecture of Excitatory Synapses : A More Quantitative View. *Annu. Rev. Biochem.* 76:823–47.

Shibuki K, Hishida R, Murakami H, Kudoh M, Kawaguchi T, Watanabe M, Watanabe S, Kouuchi T, Tanaka R (2003) Dynamic imaging of somatosensory cortical activity in the rat visualized by flavoprotein autofluorescence. *Journal of Physiology* 549:919–927.

Shin LM, Liberzon I (2010) The neurocircuitry of fear, stress, and anxiety disorders. *Neuropsychopharmacology* 35:169–191.

Shin RM, Tully K, Li Y, Cho JH, Higuchi M, Suhara T, Bolshakov VY (2010) Hierarchical order of coexisting pre- and postsynaptic forms of long-term potentiation at synapses in amygdala. *Proceedings of the National Academy of Sciences of the United States of America* 107:19073–19078.

Shipman SL, Nicoll RA (2012a) A Subtype-Specific Function for the Extracellular Domain of Neuroligin 1 in Hippocampal LTP. *Neuron* 76:309–316.

Shipman SL, Nicoll RA (2012b) Dimerization of postsynaptic neuroligin drives synaptic assembly via transsynaptic clustering of neurexin. *Pnas* 109:19432–19437.

Shipman SL, Schnell E, Hirai T, Chen BS, Roche KW, Nicoll RA (2011) Functional dependence of neuroligin on a new non-PDZ intracellular domain. *Nature Neuroscience* 14:718–726.

Sierra-Mercado D, Padilla-Coreano N, Quirk GJ (2011) Dissociable roles of prelimbic and infralimbic cortices, ventral hippocampus, and basolateral amygdala in the expression and extinction of conditioned fear. *Neuropsychopharmacology : official publication of the American College of Neuropsychopharmacology* 36:529–538.

Simms BA, Zamponi GW (2014) Neuronal voltage-gated calcium channels: Structure, function, and dysfunction. *Neuron* 82:24–45.

Simonoff E, Pickles A, Charman T, Chandler S, Loucas T, Baird G (2008) Psychiatric disorders in children with autism spectrum disorders: Prevalence, comorbidity, and associated factors in a population-derived sample. *Journal of the American Academy of Child and Adolescent Psychiatry* 47:921–929.

Song JY, Ichtchenko K, Sudhof TC, Brose N (1999) Neuroligin 1 is a postsynaptic cell-adhesion molecule of excitatory synapses. *Proceedings of the National Academy of Sciences* 96:1100–1105.

Sotres-Bayon F, Bush DEA, LeDoux JE (2007) Acquisition of fear extinction requires activation of NR2B-containing NMDA receptors in the lateral amygdala. *Neuropsychopharmacology* 32:1929–1940.

Soykan T, Schneeberger D, Tria G, Buechner C, Bader N, Svergun D, Tessmer I, Poulopoulos A, Papadopoulos T, Varoqueaux F, Schindelin H, Brose N (2014) A conformational switch in collybistin determines the differentiation of inhibitory postsynapses. *EMBO Journal* 33:2113–2133.

Spampanato J, Polepalli J, Sah P (2011) Interneurons in the basolateral amygdala. *Neuropharmacology* 60:765–773.

Speed HE, Masiulis I, Gibson JR, Powell CM (2015) Increased cortical inhibition in Autism-Linked neuroligin-3R451C mice is due in part to loss of endocannabinoid signaling. *PLoS ONE* 10:1–16.

Spencer CM, Serysheva E, Yuva-Paylor LA, Oostra BA, Nelson DL, Paylor R (2006) Exaggerated behavioral phenotypes in Fmr1/Fxr2 double knockout mice reveal a functional genetic interaction between Fragile X-related proteins. *Human Molecular Genetics* 15:1984–1994.

Srivastava AK, Schwartz CE (2014) Intellectual disability and autism spectrum disorders: Causal genes and molecular mechanisms. *Neuroscience and Biobehavioral Reviews* 46:161–174.

Stearns NA, Schaevitz LR, Bowling H, Nag N, Berger UV, Berger-Sweeney J (2007) Behavioral and anatomical abnormalities in Mecp2 mutant mice: A model for Rett syndrome. *Neuroscience* 146:907–921.

Stornetta RL, Zhu JJ (2011) Ras and Rap signaling in synaptic plasticity and mental disorders. *Neuroscientist* 17:54–78.

Stuart GJ, Palmer LM (2006) Imaging membrane potential in dendrites and axons of single neurons. *Pflugers Archiv European Journal of Physiology* 453:403–410.

Südhof TC (2008) Neuroligins and neurexins link synaptic function to cognitive disease. *Nature* 455:903–911.

Sumita K, Sato Y, Iida J, Kawata A, Hamano M, Hirabayashi S, Ohno K, Peles E, Hata Y (2007) Synaptic scaffolding molecule (S-SCAM) membrane-associated guanylate kinase with inverted organization (MAGI)-2 is associated with cell adhesion molecules at inhibitory synapses in rat hippocampal neurons. *Journal of neurochemistry* 100:154–166.

Suvrathan A, Hoeffer Ca, Wong H, Klann E, Chattarji S (2010) Characterization and reversal of synaptic defects in the amygdala in a mouse model of fragile X syndrome. *Proceedings of the National Academy of Sciences of the United States of America* 107:11591–6.

Sylwestrak EL, Ghosh A (2012) and of the relative affinity of the responding OVA-specific T cells (fig. S15, A and B). These results suggest that CCL-3/4/5 production in the absence of T. *Science* 338:536–540.

Tabuchi K, Blundell J, Etherton MR, Hammer RE, Liu X, Powell CM, Südhof TC (2007) A Neuroligin-3 Mutation Implicated in Autism Increases Inhibitory Synaptic Transmission in Mice. *Science* 318.

Takesian AE, Bogart LJ, Lichtman JW, Hensch T (2018) Inhibitory circuit gating of auditory critical period plasticity. *Nature neuroscience* 21:218–227.

Talebizadeh Z, Lam DY, Theodoro MF, Bittel DC, Lushington GH, Butler MG (2006) Novel splice isoforms for NLGN3 and NLGN4 with possible implications in autism. *Journal of medical genetics* 43:1–8.

Temme SJ, Murphy GG (2017) The L-type voltage-gated calcium channel CaV1.2 mediates fear extinction and modulates synaptic tone in the lateral amygdale. *Learning and Memory* 24:580–588.

Thomas AM, Schwartz MD, Saxe MD, Kilduff TS (2017) Sleep/wake physiology and quantitative electroencephalogram analysis of the neuroligin-3 knockout rat model of autism spectrum disorder. *Sleep* 40.

Thomas GM, Huganir RL (2004) MAPK cascade signalling and synaptic plasticity. *Nature Reviews Neuroscience* 5:173–183.

Tominaga T, Tominaga Y, Yamada H, Matsumoto G, Ichikawa M (2000) Quantification of optical signals with electrophysiological signals in neural activities of Di-4-ANEPPS stained rat hippocampal slices. *Journal of Neuroscience Methods* 102:11–23.

Tovote P, Fadok JP, Lüthi A (2015) Neuronal circuits for fear and anxiety. *Nature Publishing Group* 16:317–331.

Tsvetkov E, Carlezon WA, Benes FM, Kandel ER, Bolshakov VY (2002) Fear conditioning occludes LTP-induced presynaptic enhancement of synaptic transmission in the cortical pathway to the lateral amygdala. *Neuron* 34:289–300.

Tsvetkov E, Shin RM, Bolshakov VY (2004) Glutamate Uptake Determines Pathway Specificity of Long-Term Potentiation in the Neural Circuitry of Fear Conditioning. *Neuron* 41:139–151.

Turner BH, Herkenham M (1991) Thalamoamygdaloid projections in the rat: A test of the amygdala's role in sensory processing. *Journal of Comparative Neurology* 313:295–325.

Turner KM, Burne THJ (2014) Comprehensive behavioural analysis of long Evans and Sprague-Dawley rats reveals differential effects of housing conditions on tests relevant to neuropsychiatric disorders. *PLoS ONE* 9.

Turrigiano GG, Nelson SB (2004) Homeostatic plasticity in the developing nervous system. *Nature Reviews Neuroscience* 5:97–107.

Tye KM, Prakash R, Kim SY, Fenno LE, Grosenick L, Zarabi H, Thompson KR, Gradinaru V, Ramakrishnan C, Deisseroth K (2011) Amygdala circuitry mediating reversible and bidirectional control of anxiety. *Nature* 471:358–362.

Ullrich B, Ushkaryov YA, Südhof TC (1995) Cartography of neurexins: More than 1000 isoforms generated by alternative splicing and expressed in distinct subsets of neurons. *Neuron* 14:497–507.

Um JW, Choi TY, Kang H, Cho YS, Choii G, Uvarov P, Park D, Jeong D, Jeon S, Lee D, Kim H, Lee SH, Bae YC, Choi SY, Airaksinen MS, Ko J (2016) LRRTM3 Regulates Excitatory Synapse Development through Alternative Splicing and Neurexin Binding. *Cell Reports* 14:808–822.

Van Bokhoven H (2011) Genetic and Epigenetic Networks in Intellectual Disabilities. *Annu. Rev. Genet.* 45:81–104.

Varoqueaux F, Aramuni G, Rawson RL, Mohrmann R, Missler M, Gottmann K, Zhang W, Südhof TC, Brose N (2006) Neuroligins Determine Synapse Maturation and Function. *Neuron* 51:741–754.

Varoqueaux F, Jamain S, Brose N (2004) Neuroligin 2 is exclusively localized to inhibitory synapses. *European Journal of Cell Biology* 83:449–456.

Vazquez LE, Chen HJ, Sokolova I, Knuesel I, Kennedy MB (2004) SynGAP regulates spine formation. *The Journal of neuroscience : the official journal of the Society for Neuroscience* 24:8862–8872.

Vissers LELM, Gilissen C, Veltman JA (2016) Genetic studies in intellectual disability and related disorders. *Nature Reviews Genetics* 17:9–18.

Walker DL, Ressler KJ, Lu KT, Davis M (2002) Facilitation of conditioned fear extinction by systemic administration or intra-amygdala infusions of D-cycloserine as assessed with fear-potentiated startle in rats. *The Journal of neuroscience : the official journal of the Society for Neuroscience* 22:2343–51.

Walkup WG, Washburn LR, Sweredoski MJ, Carlisle HJ, Graham RL, Hess S, Kennedy MB (2015) Phosphorylation of Synaptic GTPase Activating Protein (synGAP) by Ca2+/Calmodulin-dependent Protein Kinase II (CaMKII) and Cyclin-dependent Kinase 5 (CDK5) Alters the Ratio of its GAP Activity Toward Ras and Rap GTPases. *Journal of Biological Chemistry* 290:4908–4927.

Walkup WG, Mastro TL, Schenker LT, Vielmetter J, Hu R, Iancu A, Reghunathan M, Bannon BD, Kennedy MB (2016) A model for regulation by syngap-a1 of binding of synaptic proteins to PDZ-domain "slots" in the postsynaptic density. *eLife* 5:1–31.

Walkup WG, Sweredoski MJ, Graham RL, Hess S, Kennedy MB (2018) Phosphorylation of synaptic GTPase-activating protein (synGAP) by polo-like kinase (Plk2) alters the ratio of its GAP activity toward HRas, Rap1 and Rap2 GTPases. *Biochemical and Biophysical Research Communications* 503:1599–1604.

Waltereit R, Japs B, Schneider M, De Vries PJ, Bartsch D (2011) Epilepsy and Tsc2 haploinsufficiency lead to autistic-like social deficit behaviors in rats. *Behavior Genetics* 41:364–372.

Wang CC, Held RG, Hall BJ (2013) SynGAP regulates protein synthesis and homeostatic synaptic plasticity in developing cortical networks. *PLoS ONE* 8.

Weir RK, Bauman MD, Jacobs B, Schumann CM (2018) Protracted dendritic growth in the typically developing human amygdala and increased spine density in young ASD brains. *Journal of Comparative Neurology* 526:262–274.

Weldon M, Kilinc M, Lloyd Holder J, Rumbaugh G (2018) The first international conference on SYNGAP1-related brain disorders: A stakeholder meeting of families, researchers, clinicians, and regulators. *Journal of Neurodevelopmental Disorders* 10:1–6.

Xu X, Hu Z, Zhang L, Liu H, Cheng Y, Xia K, Zhang X (2017) Not all neuroligin 3 and 4X missense variants lead to significant functional inactivation. *Brain and Behavior* 7:1–8.

Yan J, Oliveira G, Coutinho A, Yang C, Feng J, Katz C, Sram J, Bockholt A, Jones IR, Craddock N, Cook EH, Vicente A, Sommer SS (2005) Analysis of the neuroligin 3 and 4 genes in autism and other neuropsychiatric patients. *Molecular Psychiatry* 10:329–332.

Yan P, Acker CD, Zhou WL, Lee P, Bollensdorff C, Negrean A, Lotti J, Sacconi L, Antic SD, Kohl P, Mansvelder HD, Pavone FS, Loew LM (2012) Palette of fluorinated voltage-sensitive hemicyanine dyes. *Proceedings of the National Academy of Sciences* 109:20443–20448.

Yang Y, Tao-Cheng JH, Bayer KU, Reese TS, Dosemeci A (2013) Camkii-Mediated Phosphorylation Regulates Distributions of Syngap-α1 and -α2 at the Postsynaptic Density. *PLoS ONE* 8:6–11.

Yuan C, Gao J, Guo J, Bai L, Marshall C, Cai Z, Wang L, Xiao M (2014) Dimethyl Sulfoxide Damages Mitochondrial Integrity and Membrane Potential in Cultured Astrocytes. *PLOS ONE* 9:e107447.

Yuste R, Katz LC (1991) Control of postsynaptic Ca2+ influx in developing neocortex by excitatory and inhibitory neurotransmitters. *Neuron* 6:333–344.

Zecevic D (1996) Multiple spike-initiation zones in single neurons revealed by voltage-sensitive dyes. *Nature* 381:322–325.

Zelcer I, Cohen H, Richter-Levin G, Lebiosn T, Grossberger T, Barkai E (2006) A Cellular Correlate of Learning-induced Metaplasticity in the Hippocampus. *Cerebral Cortex* 16:460–468.

Zeng M, Bai G, Zhang M (2017) Anchoring high concentrations of SynGAP at postsynaptic densities via liquid-liquid phase separation. *Small GTPases* 0:1–9.

Zeng M, Shang Y, Araki Y, Guo T, Huganir RL, Zhang M (2016) Phase Transition in Postsynaptic Densities Underlies Formation of Synaptic Complexes and Synaptic Plasticity. *Cell* 166:1163–1175.e12.

Zhang B, Chen LY, Liu X, Maxeiner S, Lee SJ, Gokce O, Südhof TC (2015) Neuroligins Sculpt Cerebellar Purkinje-Cell Circuits by Differential Control of Distinct Classes of Synapses. *Neuron* 87:781–796.

Zhang W, Vazquez L, Apperson M, Kennedy MB (1999) Citron binds to PSD-95 at glutamatergic synapses on inhibitory neurons in the hippocampus. *Journal of Neuroscience* 19:96–108.

Zhang W, Linden DJ (2003) The other side of the engram: experience-driven changes in neuronal intrinsic excitability. *Nature reviews. Neuroscience* 4:885–900.

Zhu JJ, Qin Y, Zhao M, Aelst LV, Malinow R (2002) Ras and Rap Control AMPA Receptor Trafficking during Synaptic Plasticity. *Cell* 110:443–455.

Zoghbi HY, Bear MF (2012) Synaptic dysfunction in neurodevelopmental disorders associated with autism and intellectual disabilities. *Cold Spring Harbor perspectives in biology* 4:1–22.